INL/EXT-12-27855

2012 Status Report on Efforts to Enhance Instrumentation to Support Advanced Test Reactor Irradiations

J. Rempe
D. Knudson
J. Daw
T. Unruh
B. Chase
K. Davis
R. Schley
J. Palmer
K. Condie

December 2012

Idaho National Laboratory

The INL is a U.S. Department of Energy National Laboratory operated by Battelle Energy Alliance

INL/EXT-12-27855

2012 Status Report on Efforts to Enhance Instrumentation to Support Advanced Test Reactor Irradiations

J. Rempe, D. Knudson, J. Daw, T. Unruh, B. Chase,
K. Davis, R. Schley, J. Palmer, and K. Condie

December 2012

Idaho National Laboratory
Idaho Falls, Idaho 83415

Prepared for the
U.S. Department of Energy
Office of Nuclear Energy
Under DOE Idaho Operations Office
Contract DE-AC07-05ID14517

ABSTRACT

The Department of Energy (DOE) designated the Advanced Test Reactor (ATR) as a National Scientific User Facility (NSUF) in April 2007 to support U.S. leadership in nuclear science and technology. By attracting new research users - universities, laboratories, and industry - the ATR NSUF facilitates basic and applied nuclear research and development, further advancing the nation's energy security needs. A key component of the ATR NSUF effort at the Idaho National Laboratory (INL) is to design, develop, and deploy new in-pile instrumentation techniques that are capable of providing real-time measurements of key parameters during irradiation. To address this need, an assessment of instrumentation available and under-development at other test reactors was completed. Based on this initial review, recommendations were made with respect to what instrumentation is needed at the ATR, and a strategy was developed for obtaining these sensors. In 2009, a report was issued documenting this program's strategy and initial progress toward accomplishing program objectives. Since 2009, annual reports have been issued to provide updates on the program strategy and the progress made on implementing the strategy. This report provides the 2012 update.

As reported in this document, significant accomplishments occurred in several instrumentation development and deployment areas during 2012. Specialized INL-developed sensors for real-time detection of temperature and thermal conductivity are not only being provided to NSUF reactors at INL and at the Massachusetts Institute of Technology, but are also being provided to the Commissariat à l'Énergie Atomique et aux Energies Alternatives (CEA) in France and to the Institute for Energy Technology/Halden Reactor Project (IFE/HRP) in Norway for evaluation. High Temperature Test Laboratory (HTTL) staff are also involved in expanding options for peak temperature sensors, such as melt wires and silicon carbide temperature monitors, and integral fluence sensors, such as activation foils and flux wires available to our users. On-going tasks to deploy real-time length and flux detection sensors are continuing. A test rig for evaluating creep specimens is now ready for use in the newly reactivated ATR pressurized water loop and efforts have been initiated to develop a crack growth test rig. In addition, several tasks evaluating 'advanced' technologies, such as fiber-optics based length detection and ultrasonic thermometers, were initiated.

During FY13, the HTTL will be relocated to INL's Research and Education Laboratory, a new facility that is being constructed in Idaho Falls. New investments, such as a clean room, that are being incorporated into this facility will ensure that the HTTL continues to play a significant role in ensuring that the NSUF reactors have the instrumentation required at 'world class' facilities.

CONTENTS

FIGURES

TABLES

EXECUTIVE SUMMARY

The Department of Energy (DOE) designated the Advanced Test Reactor (ATR) at the Idaho National Laboratory (INL) as a National Scientific User Facility (NSUF) in April 2007 to support the growth of nuclear science and technology in the U.S. By attracting new researchers - universities, laboratories, and industry - the ATR NSUF facilitates basic and applied nuclear research and development, further advancing the nation's energy security needs. A key component of the ATR NSUF effort is the design, development, and deployment of new in-pile instrumentation to support irradiation testing. In addition to ATR NSUF needs, it is recognized that new in-pile instrumentation enhances the ATR's ability to attract new customers from the commercial power, defense, and manufacturing sectors. In 2008, a strategy was developed for obtaining these sensors. In 2009, a report was issued documenting this program's strategy and initial progress toward accomplishing program objectives. Since 2009, annual reports have been issued to document the program strategy and the progress made to implement the strategy. This report provides the 2012 update. It is anticipated that additional status reports will be issued in future years.

As noted within this document, the ATR is unique with respect to irradiation testing capabilities. The test volumes and flux levels in each of its irradiation locations [Static Capsules, the Hydraulic Shuttle Irradiation System (HSIS), Instrumented Lead Tests, and Pressurized Water Reactor (PWR) loops] are unsurpassed by few, if any, test reactors in the world. Despite its long history for developing highly specialized instrumentation to meet demands of customers conducting unique tests in one-of-a-kind test facilities, INL instrumentation research funding decreased significantly in the 1980s when large nuclear test facility programs ended.

In 2008, the ATR NSUF initiated an effort that allowed INL to restart programs associated with the design and development of world class instrumentation. As part of this effort, a review was first completed to identify instrumentation available to users at other materials and test reactors (MTRs) located in the US and abroad. Table ES-1 summarizes results from this review. The column labeled "Technology Available at ATR" indicates the types of sensors currently available to ATR users. The column "Proposed Advanced Technology" includes two categories: "Available at Other Reactors," which identifies several technologies employed at other test reactors that could be adapted to enhance ATR instrumentation capabilities; and "Developmental," which lists developmental or non-nuclear technologies that could be used in ATR irradiation tests. Technologies listed in this column are considered to be less "ready" for implementation. Blue text in Table ES-1 indicates current instrumentation research efforts, red text indicates demonstrated new or enhanced sensors now available to users as a result of recent instrumentation research, and magenta text indicates new sensors and capabilities that are now ready for deployment as a result of recent instrumentation research. It should be noted that many of these instrumentation development efforts are conducted with, and in many cases, expedited by collaboration with universities and other research organizations.

Table ES-1. Instrumentation available at ATR and proposed advanced technologies.

Parameter	Location			Available Technology at ATR	Proposed Advanced Technology	
	Static Capsule/ Shuttle	Instr. Lead	PWR Loop		Available at Other MTRs	Developmental
Temperature	✔	✔	✔	-Melt wires (peak)[a] -Silicon Carbide (SiC) temperature monitors (range)	-Paint spots (peak) -Thermal Expansion Devices (TEDs)	
		✔	✔	-Thermocouples (Type N, K, C[b], and HTIR-TCs[c])	-Expansion thermometer	- Fiber optics -Noise thermometry -Ultrasonic thermometers (UTs)
Thermal Conductivity		✔	✔	- Transient Hot Wire Method Needle Probe (THWM NP)	-Degradation using signal changes in thermocouples	
Flux/Fluence (neutron)	✔	✔	✔	-Flux wires and foils		
		✔	✔		-Self-Powered Neutron Detectors (SPNDs) -Subminiature / miniature fission chambers	- Moveable SPNDs - Micro-Pocket Fission Detectors (MPFDs)
Gamma Heating / Gamma Flux		✔	✔		-Calorimeters -Gamma thermometers -Self-Powered Gamma Detectors (SPGDs)	
Dimensional		✔	✔	-LVDT-based elongation	-Diameter gauge	-Ultrasonic techniques -Fiber optics
Fission Gas (Amount, Composition)		✔	✔	-On-line Fission Product Sampling -Gas Chromatography -Pressure sensor	-LVDT-based pressure monitors	-Acoustic measurements with high-frequency echography
Loop Pressure			✔	-Differential pressure transmitters -Pressure gauges with impulse lines		
Loop Flowrate			✔	-Flow venturis -Orifice plates	-Turbine flow meters (for individual fuel assemblies	
Loop Water Chemistry			✔	-Off-line sampling / analysis	-Electrical chemical potential probes	
Crud Deposition			✔		- Diameter gauge with neutron detectors, and thermocouples	
Crack Growth Rate			✔		-Direct current potential drop (DCPD) technique	

a. Although melt wires have been used at ATR, recent efforts have expanded the types offered to our users, allowing more accurate estimates of peak temperature with enhanced encapsulation methods.
b. Type C thermocouple use requires a "correction factor" to correct for decalibration during irradiation.
c. High Temperature Irradiation Resistant ThermoCouple (HTIR-TC)

Most of the instrumentation currently being developed was selected based on anticipated user needs and "technology readiness" (to provide ATR users needed instrumentation as soon as possible). For example, other MTRs have sensors available for real-time detection of parameters such as neutron flux (thermal and fast) and geometry changes (length and diameter). As indicated by the blue text in Table ES-1, efforts are underway to explore using these technologies at the ATR. However, as discussed in Section 2, adapting instrumentation used at other test reactors often requires demonstrations because of ATR-specific irradiation conditions (e.g., higher neutron fluxes, higher temperatures, etc.) and test capsule geometries. As indicated by the red and magenta text in Table ES-1, several enhanced sensors are now available to ATR users as a result of this instrumentation development effort. The ultimate goal of this effort is to provide ATR users sensors for detecting all of the parameters listed in Table ES-1.

Section 3 provides detailed information about instrumentation available and under development at other test reactors. As reported within Section 3, several foreign test reactor programs, such as the Institute for Energy Technology at the Halden Reactor Program (IFE/HRP) have maintained their instrumentation development and evaluation research capability. The Japan Atomic Energy Agency (JAEA) in Japan, Studiecentrum voor Kernenergie Centre d'Étude de l'Énergie Nucléaire (SCK•CEN) in Belgium, and the Korea Atomic Energy Research Institute (KAERI) in Korea also offer selected instrumentation to users performing irradiations in their test reactors. Finally, the Commissariat à l'Énergie Atomique et aux Energies Alternatives (CEA), which supports the existing OSIRIS test reactor and the new Jules Horowitz Reactor, not only offer users a suite of instrumentation, but are rapidly trying to increase their capabilities. Clearly, if the ATR is to remain competitive, enhanced instrumentation must be made available to its users.

An instrumentation research and development plan was developed in 2008 by INL so that ATR users will have access to enhanced real-time in-pile sensors, comparable to (and, in some cases, superior to) that available at other MTRs by 2015. Figure ES-1 graphically illustrates the process for developing and demonstrating this instrumentation. There are several major activities identified, "Nearer-Term Instrumentation Development", and "Developmental", and "Expansion". Representative tasks identified in each area are also shown with qualitative judgments with respect to ATR capabilities compared to other test reactors in this figure. As indicated, it is expected to have comparable instrumentation for most parameters during FY13, and "world class" (e.g., comparable, and in some cases, superior) irradiation capabilities by FY15. Nevertheless, the ability to meet such goals is dependent upon allocated funding levels and sensor irradiation schedules. For example, delays in completing planned tests in the Advanced Test Reactor Critical (ATRC) facility during 2012 have delayed progress in providing real-time flux monitors to ATR NSUF users.

ATR NSUF-funded instrumentation development efforts began in FY 2009. Prior to that time, new ATR instrumentation was primarily developed using a limited amount of INL LDRD funding to develop "Nearer-Term" technologies. Specifically, sensors were developed that addressed needs identified by current and potential customers. Then, programmatic funding covered the costs required for qualifying the instrumentation for ATR irradiations. However, as indicated in Table ES-1, some "Developmental Technologies" research is underway prior to initiating some Nearer Term technologies. This is because of customer-specific interests. For example, the Fuel Cycle Research and Development (FCRD) program is primarily interested in instrumentation that can provide higher resolution/higher accuracies than instrumentation available at other MTRs.

Table ES-2 summarizes the status of the effort to provide enhanced in-pile instrumentation to ATR users. Similar to Table ES-1, blue text indicates current instrumentation research efforts, and red and magenta text indicates new sensors now available to users as a result of recent instrumentation research. More detailed information about on-going instrumentation activities is provided in Section 5. As indicated in Tables ES-1 and ES-2, considerable progress has been made in this program since its inception. Several new sensors are now available to users; and as indicated in Section 5, several additional sensors should soon be available. It is also encouraging to see that some level of research has been initiated on most of the sensor technologies identified in this table. Nevertheless, additional effort is needed to provide ATR users a world-class instrumentation capability.

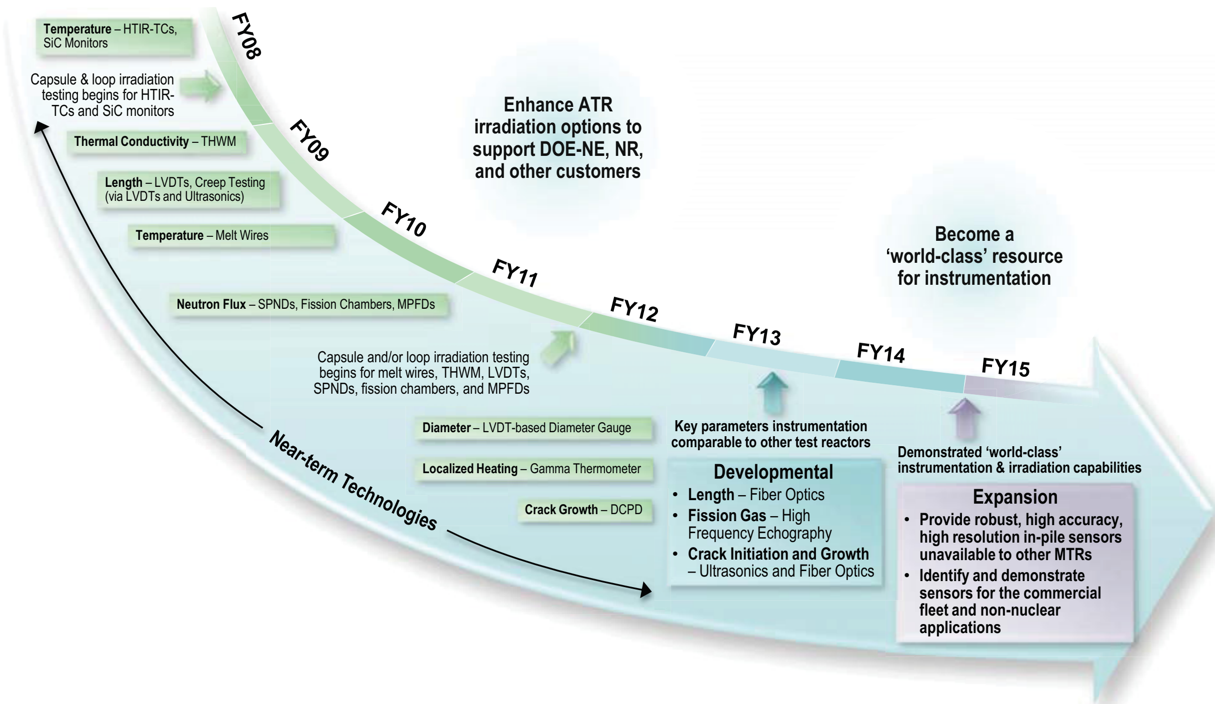

Figure ES-1. ATR NSUF advanced instrumentation research and development.

Table ES-2. Status of ATR NSUF sensor development and enhancement efforts.

Parameter	Sensor	Status
Temperature	Melt Wires	Currently used in several ATR NSUF irradiations. Both quartz and vanadium encapsulation can now be provided by INL for numerous wires with melting temperatures between 85 and 1455 °C. Documentation completed for DSC testing of melt wires and for interpreting post-irradiation results.
	SiC Temperature Monitors	Currently used in several ATR NSUF irradiations. Development of and documentation for post-irradiation measurement capability completed.
	High Temperature Irradiation Resistant ThermoCouples (HTIR-TCs)	Initial out-of-pile testing completed. In-pile testing (in the AGR-1 gas reactor fuel irradiation test) and sensor enhancement evaluations completed; HTIR-TCs provided to MIT in FY10, and HTIR-TCs for high temperature (up to 1600 °C) irradiations shipped to IFE/HRP in November 2011.
	Ultrasonic Thermometers (UTs)	Successfully developed and deployed to support high temperature fuel testing several decades ago. Efforts underway to develop and evaluate an enhanced prototype. Although prototype is focussed on the use of magnetostrictive transducers, an instrumented lead test is scheduled for FY13 that will compare the irradiation-related survivability of piezoelectric and magnetostrictive transducers.
Thermal Conductivity	Transient Hot Wire Method Needle Probe (THWM NP)	Prototype design developed and initial laboratory testing completed. Anticipated that inclusion of HTIR-TCs could allow detection at higher temperatures. Prototype THWM probes being prepared for shipment to IFE/HRP and CEA.

Table ES-2. Status of ATR NSUF sensor development and enhancement efforts.

Parameter	Sensor	Status
Elongation, Crud deposition, Corrosion	LVDTs	Out-of-pile testing completed on developmental LVDT that resists high temperature degradation and eliminates Curie temperature effects.
	Diameter gauge	Currently used in HBWR for detecting swelling, corrosion, and crud buildup. Investigations delayed due to funding limitations.
	Ultrasonic Techniques	Scoping tests completed on elongation prototype; additional prototype out-of-pile testing and results of piezoelectric transducer irradiation test needed.
	Fiber Optic Techniques	Efforts underway to develop and evaluate the accuracy of a candidate probe. Prior to deployment, an instrumented lead test needed to evaluate fiber optic survivability in radiation environments.
In-pile Creep Test Rig	LVDT-based rig with bellows	Design developed and prototype evaluated at PWR conditions in a laboratory autoclave. Enhanced design developed and fabricated and ready for insertion into an ATR PWR loop. Follow-on work underway to develop and evaluate rig with variable load capability.
Neutron Flux	Flux wires and foils	Various flux wires and foils available. Vanadium encapsulation now provided by HTTL.
	SPNDs and Fission Chambers	Specially-developed fixturing designed, fabricated, and installed at ATRC. In FY13, additional evaluations of detectors will be continued. Development of MPFDs for ATRC evaluations underway.
Gamma Heating	Gamma thermometers	Currently used at HBWR; Investigations initiated in 2012.
Crack propagation	DCPD method with CT specimens	Currently used at HBWR; Investigations initiated in 2012.
	Ultrasonic techniques	Efforts to be initiated under FCRD program. Prior to deployment, results of piezoelectric transducer irradiation test needed.
	Fiber optics techniques	Efforts to be initiated under FCRD program.Prior to deployment, an instrumented lead test needed to evaluate fiber optic survivability in radiation environments.

As discussed in Section 5, sensor development and evaluation activities rely heavily on collaborations with other research organizations, such as IFE/HRP and CEA, to maximize the benefit from research expenditures. For example, IFE/HRP and CEA will be evaluating the performance of INL-developed sensors during FY13 and FY14. In addition, collaborations were initiated with universities possessing specialized capabilities in sensor development and evaluation areas, such as the Massachusetts Institute of Technology (MIT), Idaho State University (ISU), Utah State University (USU), Kansas State University (KSU), and Pennsylvania State University (PSU). Many of these sensor development efforts are conducted in INL's High Temperature Test Laboratory (HTTL), which has specialized equipment and trained staff for sensor fabrication and evaluation.

However, funding constraints have precluded or delayed several needed sensor development research areas, such as the development and deployment of a diameter gage for measuring crud buildup or fuel swelling and the use of self-powered gamma detectors. As indicated in Section 2, several organizations provide sensors for detecting such phenomena in foreign MTRs. Nevertheless, significant accomplishments occurred in several instrumentation development and deployment areas during 2012. Specific examples include:

- Provided support for several ATR users to identify and incorporate appropriate melt wires into their tests. INL now has an established melt wire library with materials ranging from ~85 to

1455 °C, quartz and metal tube encapsulation methods, and documents describing pre-test evaluations of encapsulated melt wires to provide key insights prior to post-irradiation examinations (see Figure ES-2);

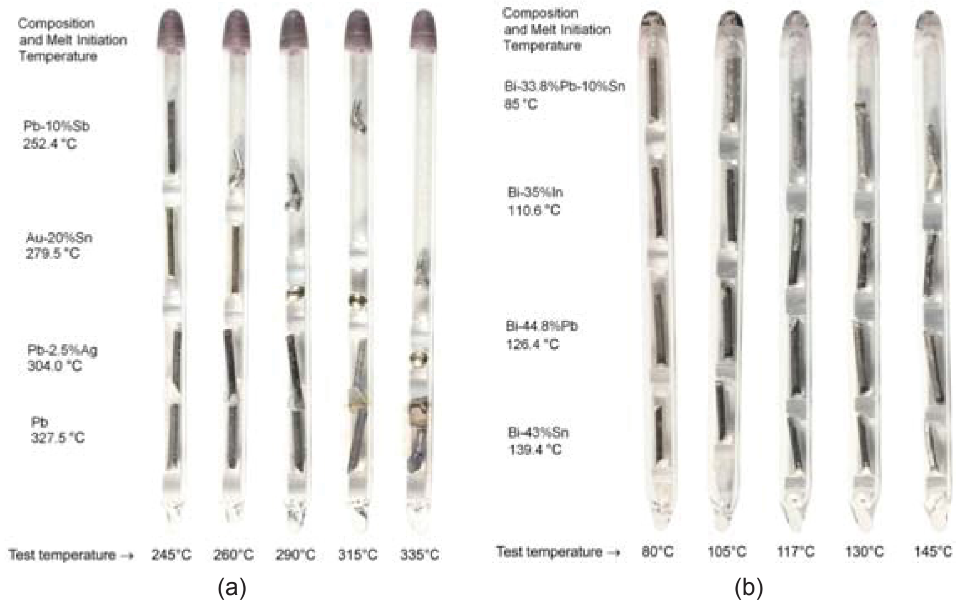

Figure ES-2. Quartz tube containing four melt wires in separated compartments: (a) Example of ideal indicator melt wires; (b) Example of non-ideal indicator melt wires.

- Provided support for several ATR users related to the use of SiC temperature monitors into their tests. Note that the first evaluations from an ATR irradiation using approved HTTL procedures were completed in December 2011 (see Figure ES-3);

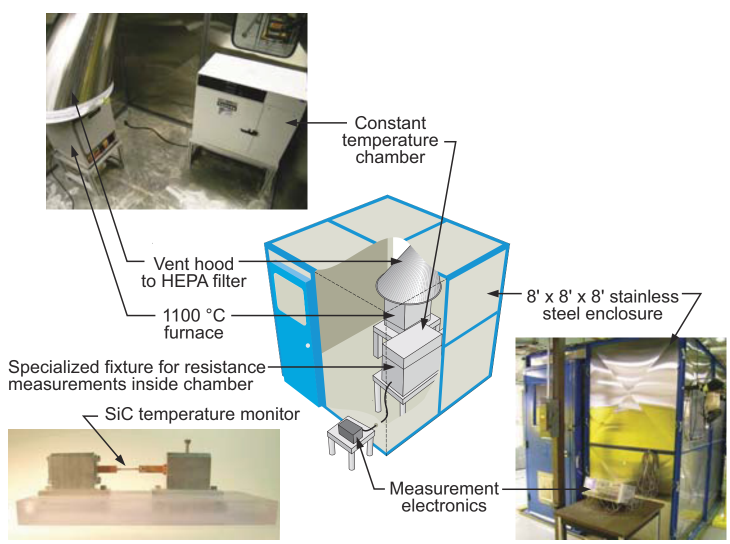

Figure ES-3. HTTL setup to anneal and measure electrical resistivity of SiC temperature monitors.

- Identified appropriate FY13 IFE/HRP HBWR irradiation for testing of four INL-developed HTIR-TCs, fabricated for operation at 1600 °C. Shipped to IFE/HRP as indicated in Figure ES-4;

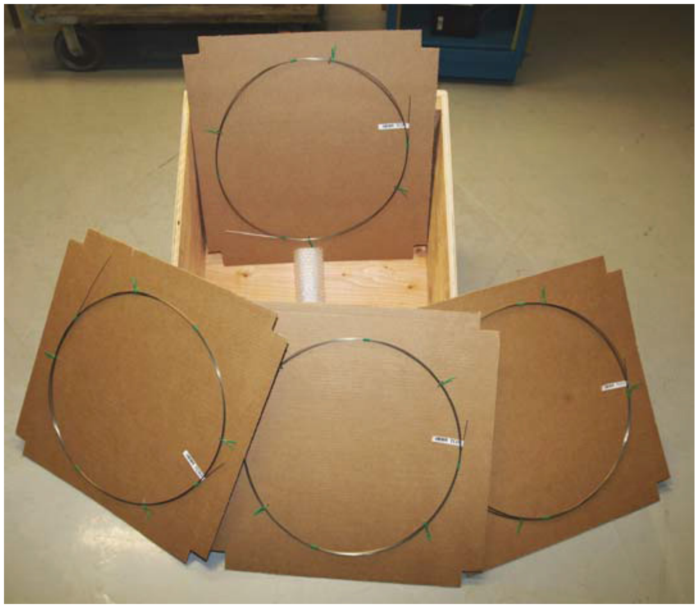

Figure ES-4. HTIR-TCs prior to shipment to IFE/HRP.

- Initiated feasibility evaluations of an ultrasonic thermometer for obtaining high resolution, high accuracy temperature profiles in FCRD irradiations (see Figure ES-5);

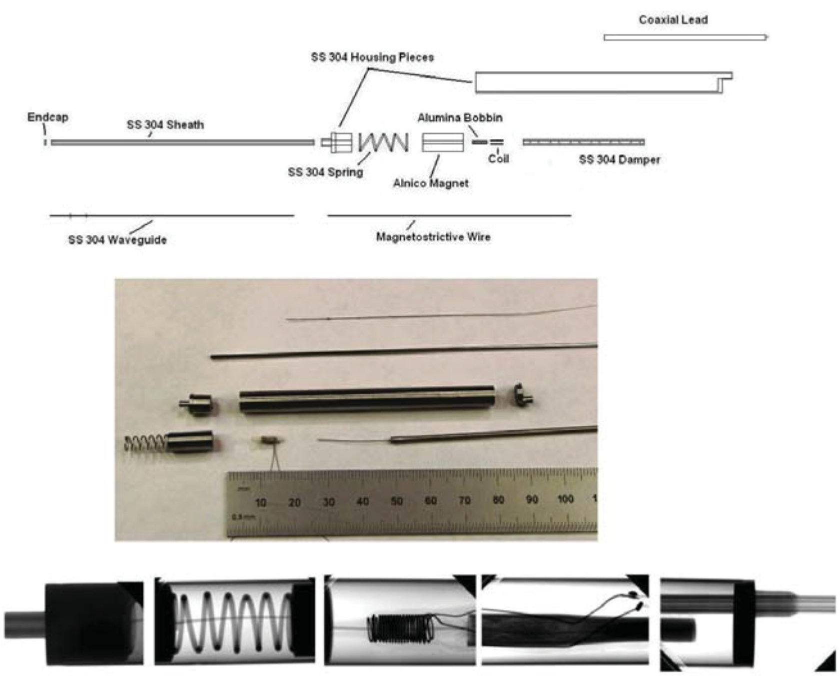

Figure ES-5. HTTL ultrasonic thermometer components.

- Initiated efforts to fabricate THWM needle probes for thermal conductivity measurements by CEA and IFE/HRP (see Figure ES-6);

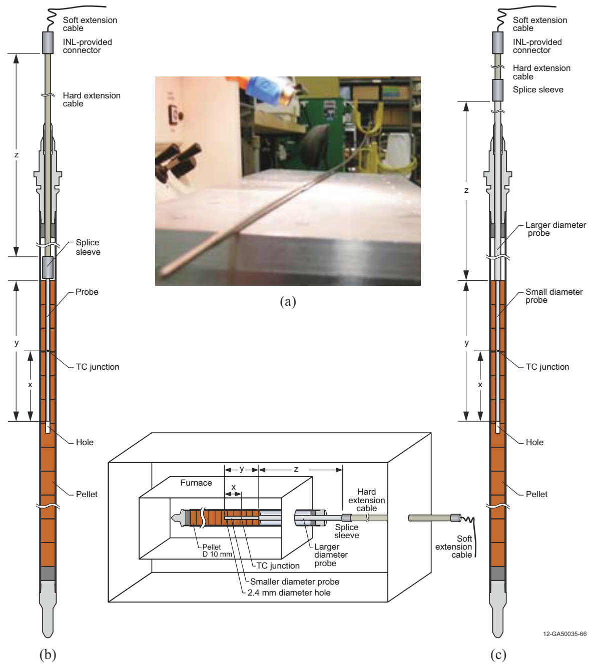

Figure ES-6. THWM NPs completed for (a) MITR and under development for (b) HBWR, and (c) CEA hot cell testing.

- Completed autoclave evaluations of an enhanced creep test rig design for use in an ATR PWR loop (see Figure ES-7);

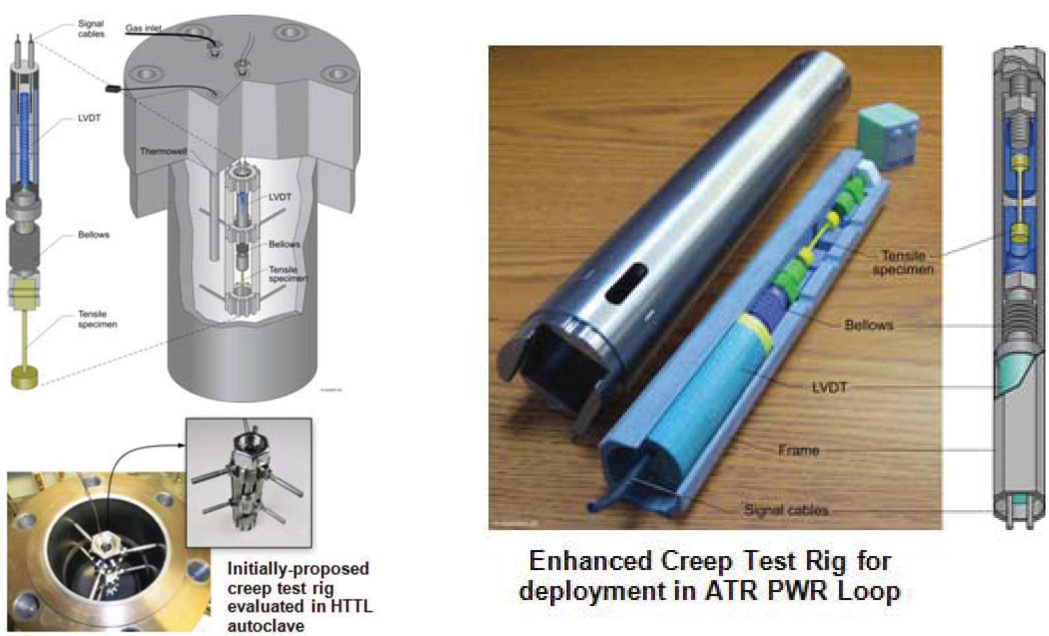

Figure ES-7. Creep test rig evaluated with autoclave testing and proposed enhanced design.

- Completed design and started fabrication of a controlled load creep test rig design for use in an ATR PWR loop (see Figure ES-8);

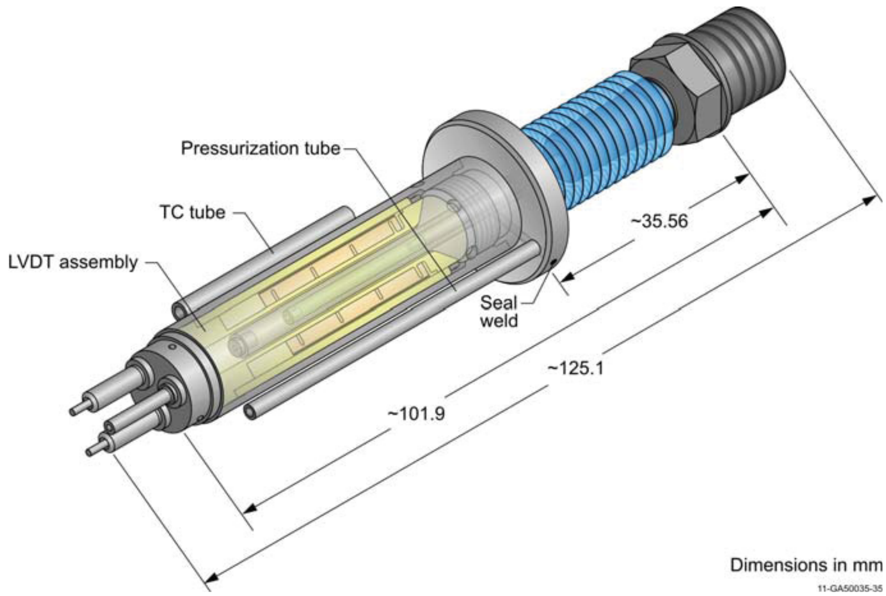

Figure ES-8. Controlled load creep test rig.

- Initiated prototype fabrication of a fiber optics-based elongation probe (see Figure ES-9);

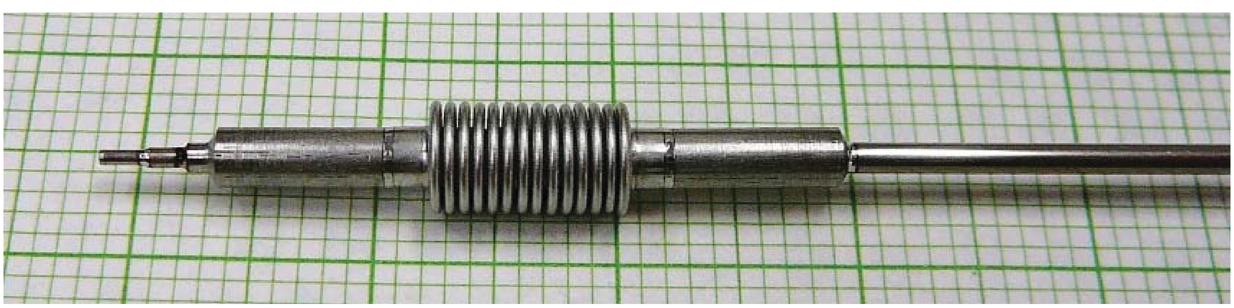

Figure ES-9. Welded fiber-optics based elongation probe.

- Initiated efforts to evaluate a gamma thermometer for use at ATR (see Figure ES-10);

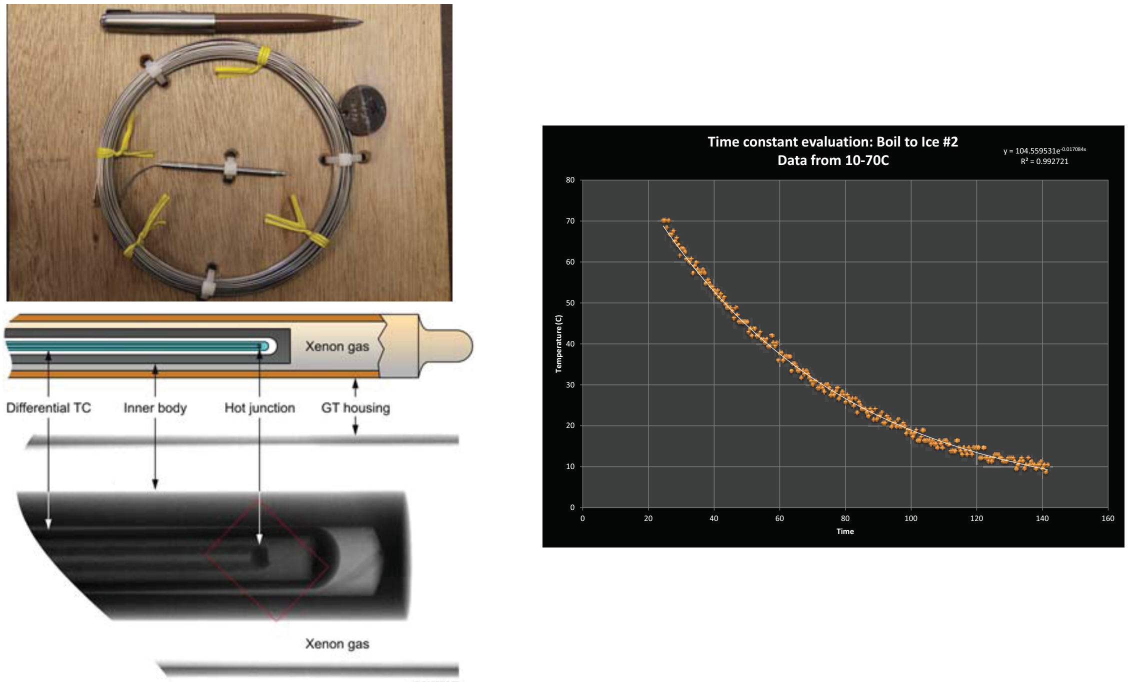

Figure ES-10. Initial evaluations of IFE/HRP gamma thermometer

- Initiated efforts to evaluate a crack growth test rig for use at ATR (see Figure ES-11);

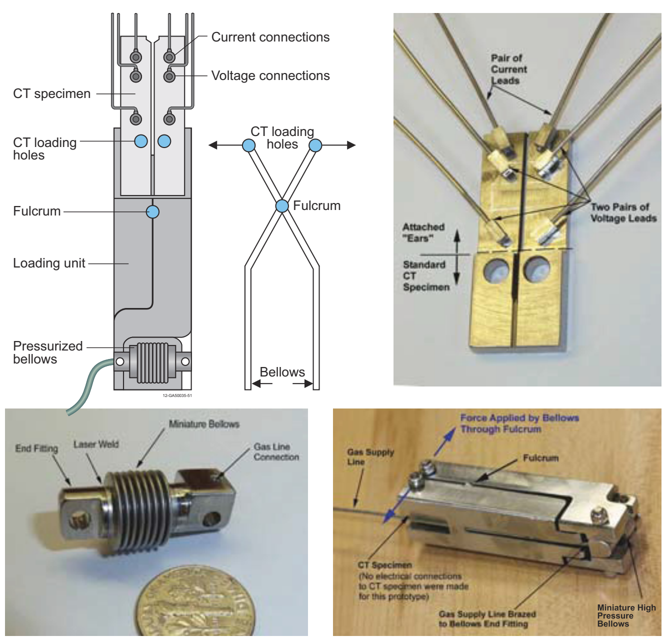

Figure ES-11. Design and fabricated components of the DCPD test rig.

- Developed flux wire encapsulated method for use at ATR (see Figure ES-12);

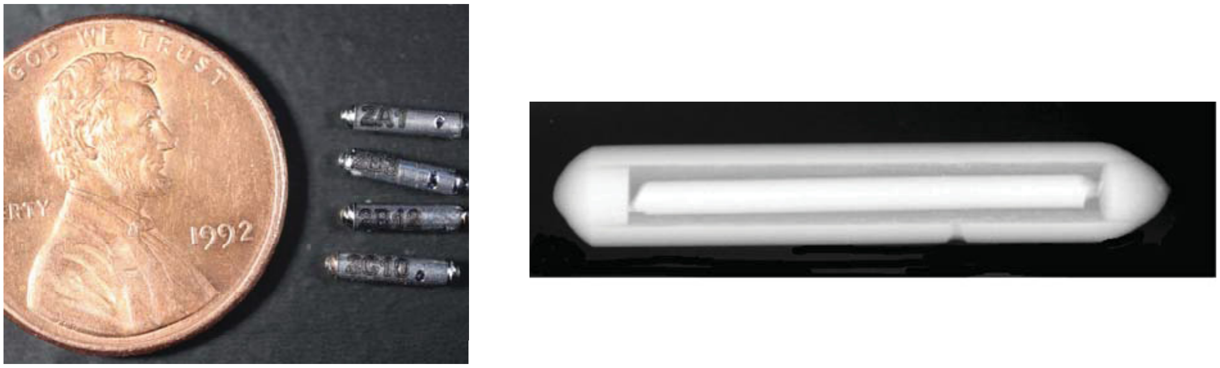

Figure ES-12. Encapsulated iron flux wires with radiograph.

- Completed fabrication of additional fixtures for evaluating flux sensors at the ATRC facility (see Figure ES-13);

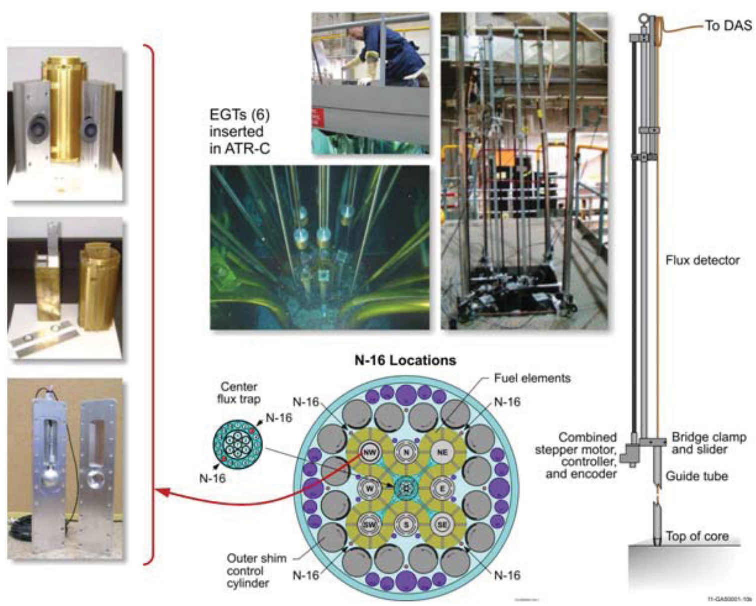

Figure ES-13. Specialized fixturing for flux detector evaluation installed at ATRC.

- Completed design and started prototype fabrication of Micro-Pocket Fission Detectors (MPFDs) (see Figure ES-14); and

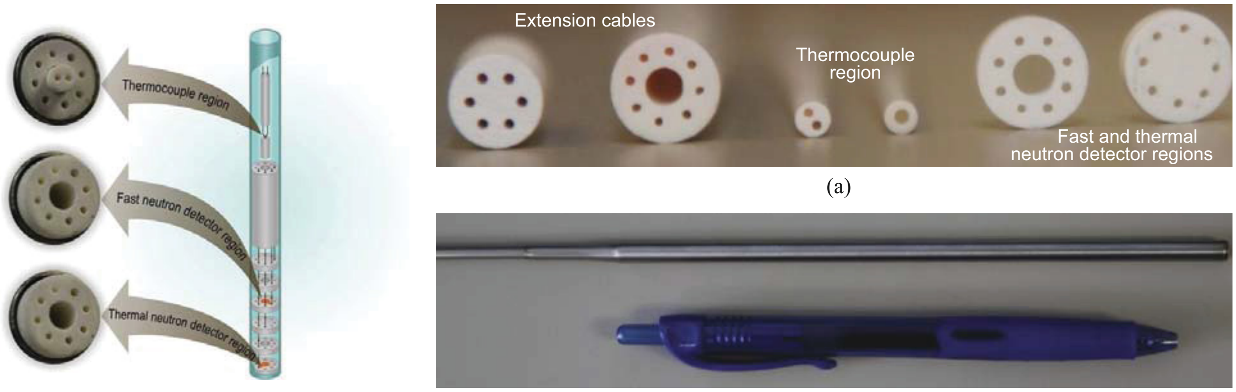

(a)

(b)

Figure ES-14. MPFDs (0.5 mm x 1.0 mm) offer unique miniature neutron detection options.

- Provided support for PSU-led ultrasonics transducer ATR NSUF irradiation to be conducted at the MITR (see Figure ES-15).

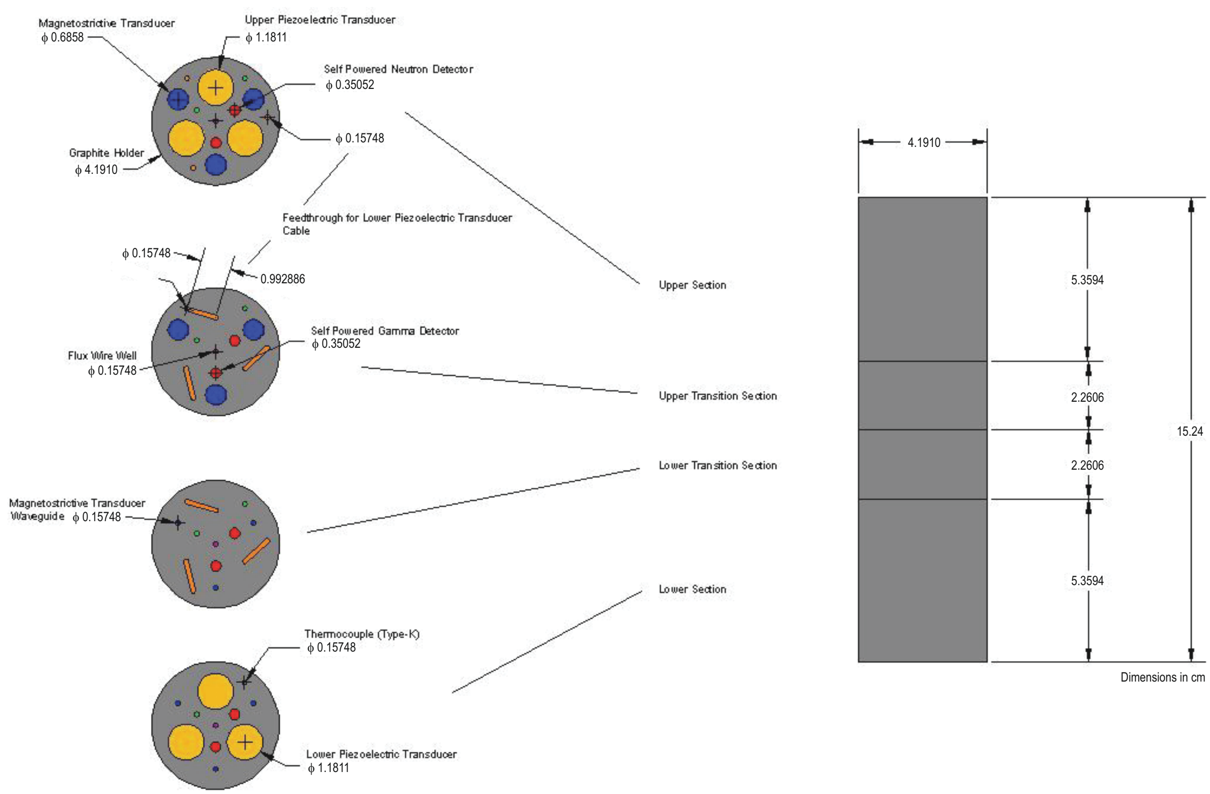

Figure ES-15. Conceptual sketch of graphite sample holder for ultrasonic transducer irradiation.

Details about each of these achievements are reported in Section 5. Note that multiple funding sources (e.g., ATR NSUF, FCRD, NEET, and LDRD) were required to achieve these accomplishments. In addition to providing ATR customers the instrumentation required for their irradiation tests, this program has clearly added to the prestige and capabilities of the ATR NSUF, INL, and to the DOE. As noted previously, international collaborations have been established with leaders in the world of in-pile testing, such as IFE/HRP and CEA. Partnerships with universities have not only helped students successfully complete their graduate level research, but have led to new INL employees. Over 26 peer-reviewed conference papers and 19 archival journal papers have been produced, and several patents have been awarded or are pending from this research. Finally, the specialized fixtures and software developed and installed at the ATRC facility for evaluating flux detectors expands its capabilities. It is anticipated that this new capability will be used in future years to develop and evaluate new, improved sensors for measuring flux and other parameters in the ATR (and other MTRs).

ACRONYMS AND ABBREVIATIONS

ACRR	Annular Core Research Reactor
ADELINE	Advanced Device for Experimenting up to Limits Irradiated Nuclear fuel Elements
ASTM	American Society for Testing and Materials
ATR	Advanced Test Reactor
ATRC	Advanced Test Reactor Critical
BR2	Belgium Reactor 2
BTB	Back-To-Back
BWR	Boiling Water Reactor
CALIPSO	In Core Advanced Loop for Irradiation in Potassium SOdium
CDC	Capsule Driver Core
CEA	Commissariat à l'Énergie Atomique et aux Energies Alternatives
CGR	Crack Growth Rate
CNEA	Argentinean National Energy Commission
COD	Crack tip Opening Displacement
CT	Compact Tension
CVD	Chemical Vapor Deposition
DCPD	Direct Current Potential Drop
DG	Diameter Gauge
DOD	Department of Defense
DOE	Department of Energy
DOE-NE	Office of Nuclear Energy in the Department of Energy
DSC	Differential Scanning Calorimeter
ECN	Netherlands Energy Research Foundation
ECP	Electrochemical Corrosion Potential
EFDA	European Fusion Development Agreement
EFPI	Extrinsic Fabry-Perot Interferometer
EGT	Experimental Guide Tube
ETR	Engineering Test Reactor
FCRD	Fuel Cycle Research and Development
FNDS	Fast Neutron Detection System
GCR	Gas Cooled Reactor
HANARO	High Advanced Neutron Application Reactor
HBWR	Halden Boiling Water Reactor
HFIR	High-Flux Isotope Reactor
HFR	High Flux Reactor
HRB	Hochtemperatur-Reaktorbau
HSIS	Hydraulic Shuttle Irradiation System
HTIR-TC	High Temperature Irradiation Resistant ThermoCouple

HTGR	High Temperature Gas Reactor
HTTR	High Temperature Test Reactor
HTTL	High Temperature Test Laboratory
IAEA	International Atomic Energy Agency
ID	Inner Diameter
IFE/HRP	Institutt for Energiteknikk (Institute for Energy Technology) at the Halden Reactor Project
INL	Idaho National Laboratory
ISU	Idaho State University
JAEA	Japan Atomic Energy
JHR	Jules Horowitz Reactor
JMTR	Japan Materials Test Reactor
JRC	Joint Research Centre
KAERI	Korea Atomic Energy Research Institute
KSU	Kansas State University
LDRD	Laboratory Directed Research and Development
LOCA	Loss of Coolant Accident
LOFT	Loss of Fluid Test
LORELEI	Light water One-Rod Equipment for LOCA Experimental Investigations
LWR	Light Water Reactor
LWRS	LWR Sustainability
LVDT	Linear Variable Differential Transformer
MADISON	Multirod Adaptable Device for Irradiations of LWR fuel Samples Operating in Normal conditions
MICA	Material Irradiation CApsule
MIT	Massachusetts Institute of Technology
MITR	Massachusetts Institute of Technology Research Reactor
MOU	Memo of Understanding
MPFD	Micro-Pocket Fission Detector
MSV	Mean Square Voltage
MTR	Materials and Test Reactor
NaK	Sodium-Potassium
NASA	National Aeronautics and Space Administration
NGNP	Next Generation Nuclear Plant
NRG	Nuclear Research & Consultancy Group
NSUF	National Scientific User Facility
NW LIPT	NorthWest Large In-Pile Tube
OD	Outer Diameter
OECD	Organization for Economic Cooperation and Development
OFS	Optical Fiber Sensors

OPD	Optical Path Difference
ORNL	Oak Ridge National Laboratory
PBF	Power Burst Facility
PCM	Power Cooling Mismatch
PHWR	Pressurized Heavy Water Reactor
PIE	Post Irradiation Examination
PSU	Pennsylvania State University
PWR	Pressurized Water Reactor
PZT	Lead Zirconate Titanate
RIA	Radiation-Induced Absorption
SCK•CEN	Studiecentrum voor Kernenergie • Centre d'Étude de l'énergie Nucléaire
SEDEIRA	SElf-powered DEtector of Ionizing RAdiation
SEM	Scanning Electronic Microscope
SE SIPT	Southeast Standard In-Pile Tube
SFR	Sodium Fast Reactor
SiC	Silicon Carbide
SPERT	Special Power Excursion Reactor Test
SPGD	Self-powered Gamma Detector
SPND	Self-Powered Neutron Detectors
THWM	Transient Hot Wire Method
THWM NPs	Transient Hot Wire Method Needle Probes
TOF	Time-Of-Flight
US NRC	U.S. Nuclear Regulatory Commission
USU	Utah State University
UT	Ultrasonic Thermometer
UV	UltraViolet
VTT	Technical Research Centre of Finland
VVER	Vodo-Vodyanoi Energetichesky Reactor
ZPPR	Zero Power Physics Reactor

1. INTRODUCTION

The Department of Energy (DOE) designated the Advanced Test Reactor (ATR) as a National Scientific User Facility (NSUF) in April 2007 to support U.S. leadership in nuclear science and technology. By attracting new research users - universities, laboratories, and industry - the ATR NSUF facilitates basic and applied nuclear research and development, further advancing the nation's energy security needs. A key component of the ATR NSUF effort is to provide new in-pile sensors and test rigs that are capable of providing real-time measurements of key parameters during irradiation. To address this need, it is important to know what instrumentation is available and under development at other test reactors. In addition, alternate sensor technologies that aren't currently deployed in test reactors, but offer enhanced sensing capabilities, must be identified. Based on an initial instrumentation review completed in 2008, recommendations were made with respect to what instrumentation is needed at the ATR, and a strategy was developed for obtaining these sensors. In 2009, a report was issued documenting this instrumentation development strategy and initial progress toward accomplishing instrumentation development program objectives.[1] Since 2009, annual reports[2,3] have been issued to provide updates on this program strategy and the progress made toward implementing the strategy. This document reports 2012 progress toward designing, developing, and deploying enhanced instrumentation.

1.1. Background

The ATR is a pressurized, light-water moderated, beryllium-reflected research reactor located at the Idaho National Laboratory (INL). Its ability to produce an extremely high neutron flux makes it possible to subject materials to the equivalent of years of radiation exposure in a commercial nuclear reactor in a matter of weeks or months. The ATR core design allows many experiments to run concurrently, with each experiment receiving a different and carefully controlled level of neutron irradiation. Originally commissioned in 1967 to evaluate fuels and materials performance for the Navy Nuclear Propulsion Program, the ATR is expected to continue operating until at least 2050.

As noted above, DOE's decision to designate the ATR as a NSUF is increasing the ATR's customer base from various nuclear science and technology programs. In addition, instrumentation development efforts to support such irradiations are now derived from several DOE-sponsored nuclear research and development programs, including the Next Generation Nuclear Plant (NGNP), the Fuel Cycle Research and Development (FCRD), and the Nuclear Energy Enabling Technology (NEET) efforts. New in-pile instrumentation will further increase the ATR's ability to attract new customers from the commercial power, defense, and manufacturing sectors.

It is recognized that new instrumentation techniques are needed to support ATR in-pile irradiations. For decades, irradiation tests at material test reactors (MTRs) have used in-pile instrumentation to measure parameters, such as temperature, dimensional changes, fission gas release, neutron fluence, and gamma heating. However, most in-pile instrumentation was developed decades ago, and INL efforts to enhance in-pile instrumentation were reduced in the 1980s. Furthermore, in several cases, ATR instrumentation for in-pile testing lags behind instrumentation available at other MTRs. Hence, a key component of the ATR NSUF is to develop, fabricate, and demonstrate the performance of new real-time sensor technologies required to measure key parameters for irradiation testing.

INL's existing High Temperature Test Laboratory (HTTL) is a unique facility for developing, fabricating, and performing laboratory demonstrations of proposed new instrumentation. This facility features specialized sensor fabrication and evaluation equipment and trained staff with an established reputation for fabricating unique sensors. In FY13, the HTTL will be relocated to INL's Research and Education Laboratory, a new facility that is being constructed in Idaho Falls. As shown in Figure 1-1, the new HTTL will include existing equipment, such as a laser welder and a real-time x-ray imaging system, specialized fabrication equipment such as a custom fabricated draw bench, several autoclaves, several tube furnaces (with temperature ranges up to 1800 °C), and a vacuum furnace capable of temperatures up to approximately 2800 °C. In addition, a special area of the new facility will house existing HTTL systems for measuring thermal properties of materials; such as a laser flash thermal property analyzer for thermal diffusivity measurements (and comparative specific heat and thermal conductivity measurements) up to 2800 °C, a push-rod dilatometer for comparison thermal elongation measurements up to 1600 °C, and a Differential Scanning Calorimeter (DSC) for obtaining specific heat capacity and melting temperature measurements up to 1600 °C. There will also be new investments. For example, the new facility will include a specially-designed clean room and locations for additional specialized equipment, such as an e-beam welder and a 3D computer tomography machine. Hence, the HTTL will continue to play a significant role in ensuring that instrumentation required at world class facilities is available.

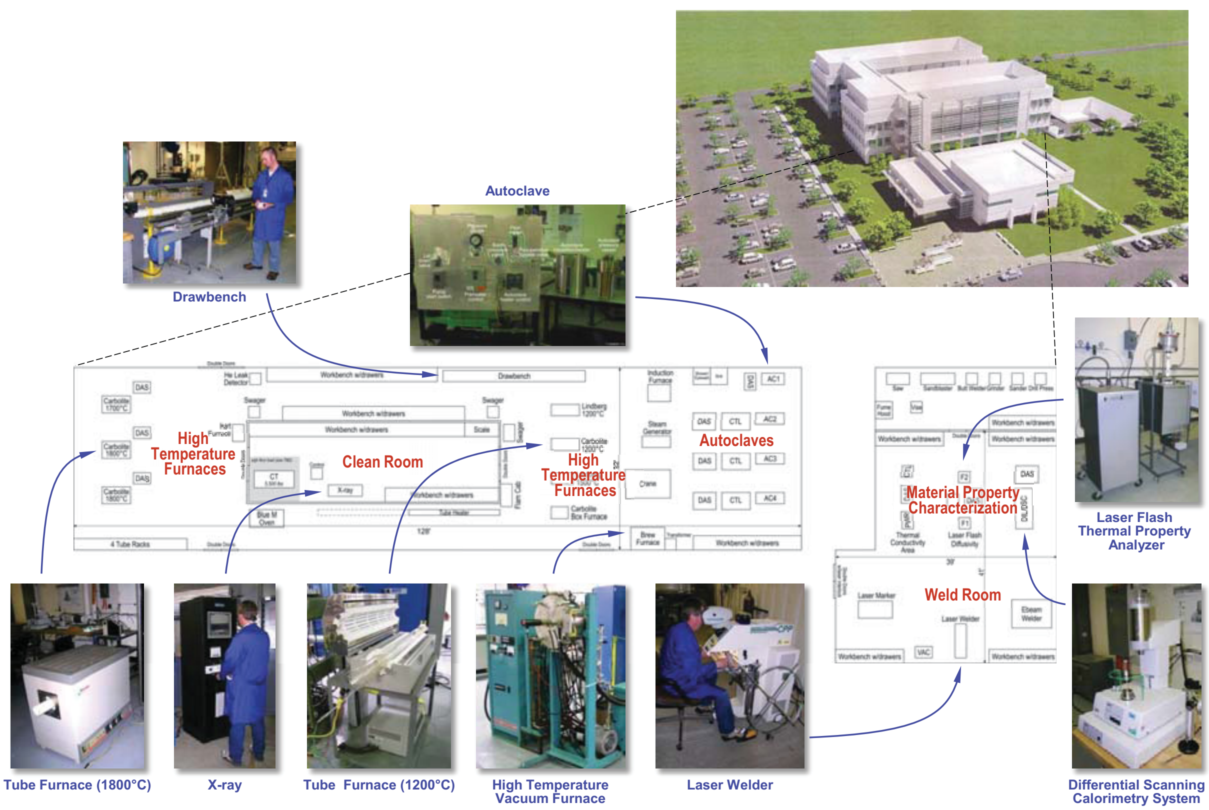

Figure 1-1. Layout for HTTL at new REL.

1.2. Report Content

As noted above, this effort began by completing a review to document what in-pile instrumentation is currently available at the ATR and other MTRs and what instrumentation could be developed or transferred from other applications to enhance in-pile irradiation testing. This report provides results from an updated review. Section 2 provides an overview of irradiation locations available in the ATR and the ATR Critical (ATRC) facility, what materials are typically irradiated in various experimental configurations, and what instrumentation is typically available for each configuration. Section 2 also highlights irradiation capabilities of other test reactors in the U.S. and abroad. Section 3 summarizes instrumentation currently used to support test reactor programs and on-going efforts to provide instrumentation to facilities outside the INL. Section 4 outlines a program for obtaining all of the higher priority instrumentation, based on customer input, required for near-term and long-term irradiations at ATR and other test reactors. Where possible, potential collaborators are identified for obtaining this instrumentation. Section 5 summarizes INL progress on accomplishing objectives in the plan presented in Section 4, identifying new in-pile instrumentation under development at INL to support ATR irradiations and reporting on the status of each research effort. References for this document are listed in Section 6.

2. BACKGROUND

As in prior status reports, this section provides an overview of irradiation locations available in the ATR and ATRC, what materials are typically irradiated in representative experimental configurations, and what instrumentation is typically available for each configuration. A brief overview of capabilities at other selected MTRs is also included.

2.1. ATR

The ATR is a unique facility for scientific investigation of the irradiation of nuclear fuels and materials.[4-8] Designed to allow simulation of high neutron radiation exposures in a short time period, the ATR has a maximum power rating of 250 MW_{th} with a maximum unperturbed thermal neutron flux of 1×10^{15} n/cm^2-s and a maximum fast neutron flux of 5×10^{14} n/cm^2-s. The ATR is cooled by pressurized (2.5 MPa) water that enters the reactor vessel bottom at an average temperature of 52 °C, flows up outside cylindrical tanks that support and contain the core, passes through concentric thermal shields into the open part of the vessel, then flows down through the core to a flow distribution tank below the core. When the reactor is operating at full power, the primary coolant exits the vessel at 71 °C.

2.1.1. Reactor Design and Characteristics

As shown in Figure 2-1, the ATR core consists of 40 curved plate fuel elements in a serpentine arrangement around a 3 x 3 array of primary testing locations, or nine large high-intensity neutron flux traps. The unique ATR control device design permits large power variations among its nine flux traps using a combination of control cylinders (drums) and neck shim rods. The beryllium control cylinders contain hafnium plates that can be rotated toward and away from the core. Hafnium shim rods, which withdraw vertically, are inserted or withdrawn for minor power adjustments. Within bounds, the power level in each corner lobe of the reactor can be controlled independently to allow for different power and flux levels in the four corner lobes during the same operating cycle. The ratio of fast to thermal flux can be varied from 0.1 to 1.0. In addition to the nine large volume (up to 48"/1.2 m long and up to 5.0"/13 cm diameter) high-intensity neutron flux traps, there are 66 irradiation positions inside the reactor core reflector tank, and there are two capsule irradiation tanks outside the core with 34 low-flux irradiation positions. A Hydraulic Shuttle Irradiation System (HSIS), more commonly referred to as the “Rabbit”, has also been installed in the ATR. The HSIS provides the ATR the capability to irradiate samples in small capsules (in the B-7 position) for materials research, rapid activations, and isotope production.[9]

2.1.2. Test Configurations and Conditions

Irradiated samples are enclosed in test capsules that are then typically placed in a basket to facilitate positioning within the reactor. This section provides summary information about the primary ATR test configurations, which are conceptually shown in Figure 2-2. More detailed information can be found in References 4 and 9.

- ***Static Capsule Experiments*** - These capsules may contain a number of small samples or engineered components. Static capsule experiments may be sealed or may contain material that can be in contact with the ATR primary coolant. Capsules may be any length, up to 122 cm and may be

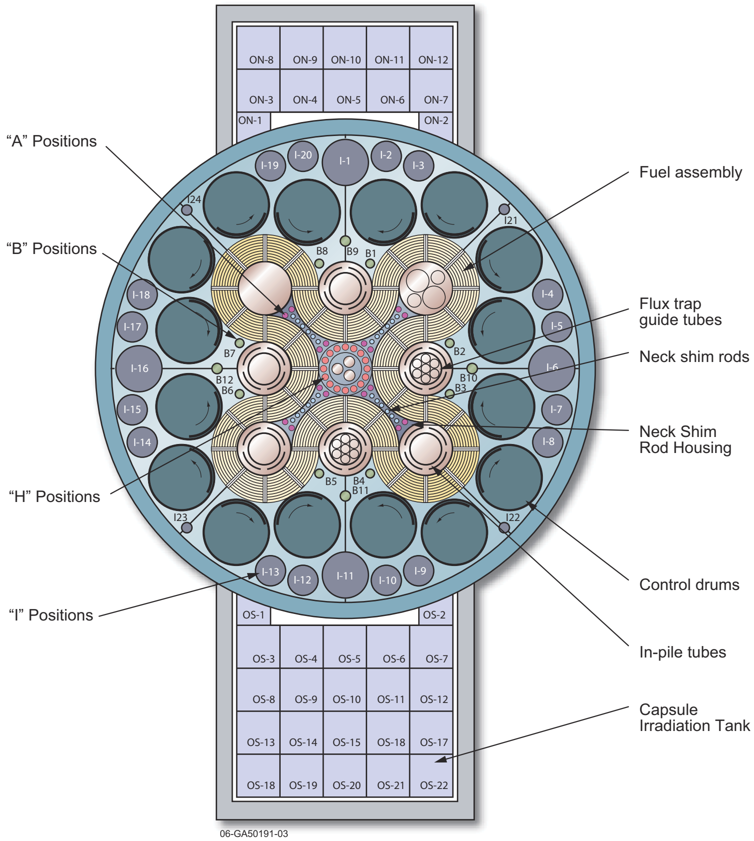

Figure 2-1. ATR core cross section showing irradiation locations.

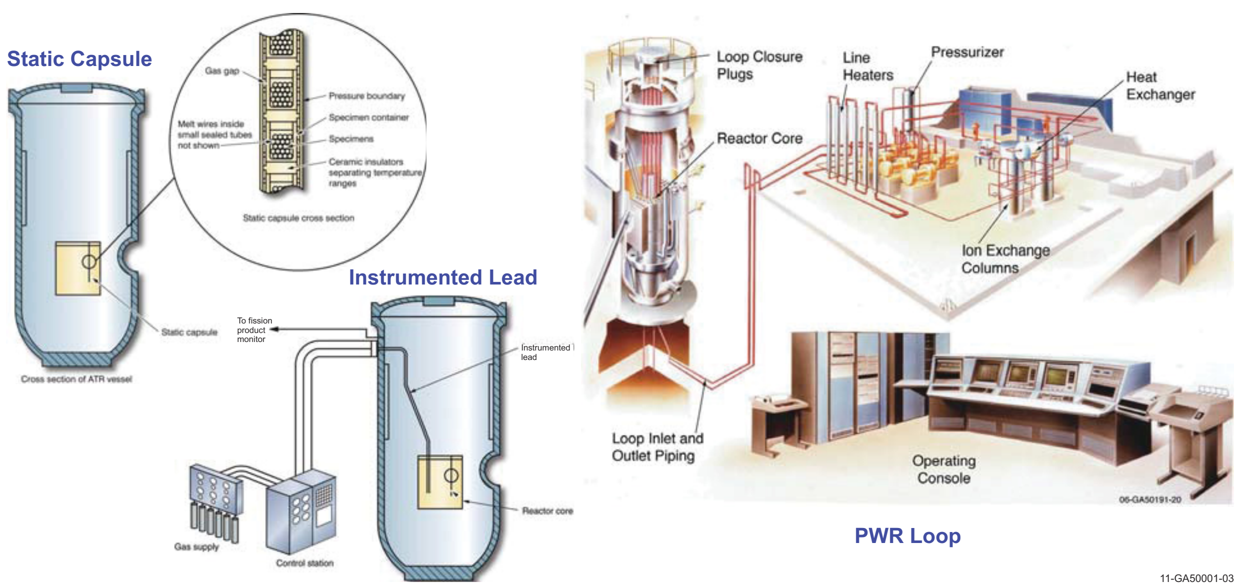

Figure 2-2. Schematic diagrams illustrating primary ATR irradiation locations.

irradiated in any core position, including the flux traps. Irradiation temperature may be selected, within limits, by including a gas gap in the capsule with a known thermal conductance. Peak temperatures may be measured using a series of melt wires or silicon carbide temperature monitors. Accumulated neutron fluences may be verified using flux wires or activation foils.

- ***Instrumented Lead Experiments*** - Active control of experiments and data from test capsules during irradiation is achieved using core positions with instrumentation cables and temperature control gases in ATR instrumented lead experiments. Such experiments can have instrumentation, such as thermocouples, connected to individual capsules or single specimens. This instrumentation can be used to control and monitor conditions within the capsule. For example, temperature control in individual zones is performed by varying the gas mixture (typically helium and neon) in the gas gap that thermally links the capsule to the water-cooled reactor structure. In addition to temperature, instrumented lead experiments can be configured to monitor the gas around the test specimen. In a fueled experiment, the presence of fission gases due to fuel failures or oxidation can be detected via gas chromatography. Instrument leads allow real time display of experimental parameters in the control room.
- ***Pressurized Water Loop Experiments*** - Five of the nine ATR flux traps used for materials and fuels testing are equipped with pressurized water loops (at the NW, N, SE, SW, and W locations). A sixth loop became operational in 2012. Each of the water loops can be operated at different temperatures, pressures, flow rates, or water chemistry requirements. These loops can operate above the standard temperatures and pressure of a commercial Pressurized Water Reactor (PWR) power plant. The great advantage of loop tests is the ease with which a variety of samples can be subjected to conditions specified for any PWR design. Each ATR pressurized loop is instrumented to measure and control coolant flows (both inert gas and water), temperatures, pressures and sample test data.
- ***Rabbit Tests -*** The HSIS, or "rabbit", enables insertion and removal of experiment specimens during ATR operational cycles. The HSIS is installed in the B-7 reflector position, which is one of the higher flux positions in the reactor with typical thermal and fast (>1 MeV) fluxes of 2.8E+14 n/cm^2/sec and 1.9E+14 n/cm^2/sec, respectively. The titanium experiment capsules, or shuttles, are approximately 16 mm in diameter x 57 mm in length with interior usable dimensions of 14 mm in diameter x 50 mm long. Up to 14 capsules can be used for irradiations simultaneously, although one does not need to fill all 14 capsules for a test.

2.2. ATRC

Located at the INL, the ATRC Facility is a full-size nuclear mock-up of the ATR core that allows researchers to characterize in advance the expected changes in ATR core reactivity due to a proposed test. This facility generally operates at a thermal power of less than 5 kW (with associated peak thermal fluxes of around 10^{10} n/cm^2-s and a maximum fast neutron flux of around 10^9 n/cm^2-s).

2.2.1. Reactor Design and Characteristics

The primary difference between the ATRC Facility and ATR is that the ATRC Facility is a pool reactor, while the ATR is a pressurized water reactor contained in a vessel. In addition, a second difference is that the highly-enriched uranium fuel in the ATRC Facility is uniformly loaded with boron while the ATR fuel is not. A third difference of note is that the ATRC Facility uses five cadmium-plated safety rods while the ATR uses six hafnium-plated safety rods. During operation, these differences are insignificant. ATRC Facility criticality is normally attained at a power greater than 0.25 mW. However, this pool-type reactor (Figure 2-3) usually operates at a power level of about 600 W and provides useful physics data for evaluating:

- worth and calibration of control elements,
- excess reactivities and charge lifetimes,
- thermal and fast neutron distributions,
- gamma heat generation rates,
- fuel loading requirements,
- effects of inserting and removing experiments and experiment void reactivities, and temperature and void reactivity coefficients.

Figure 2-3. ATRC Facility layout.

2.2.2. Test Configurations and Conditions

As part of the ATR NSUF, specialized fixtures and associated positioning software were developed and installed by INL to evaluate and calibrate real-time flux sensors and irradiate fuels and materials. Initial ATRC Facility tests (see Figure 2-4), which began in 2010, compare the response and accuracy of specially-developed real-time flux detectors to integral fluence monitors. This testing effort include experimental guide tubes (EGTs) that can position the detectors at up to six of the N-16 positions and specialized fixtures that can position detectors in the NorthWest Flux Trap and the Southeast Standard In-Pile Tube. Additional information about this effort is provided in Section 5. However, it should also be noted that the ATRC Facility's pool type design offers users enhanced flexibility for testing in lower flux conditions. Instrumented lead tests are more easily included in ATRC Facility test configurations because no pressure vessel penetrations are required.

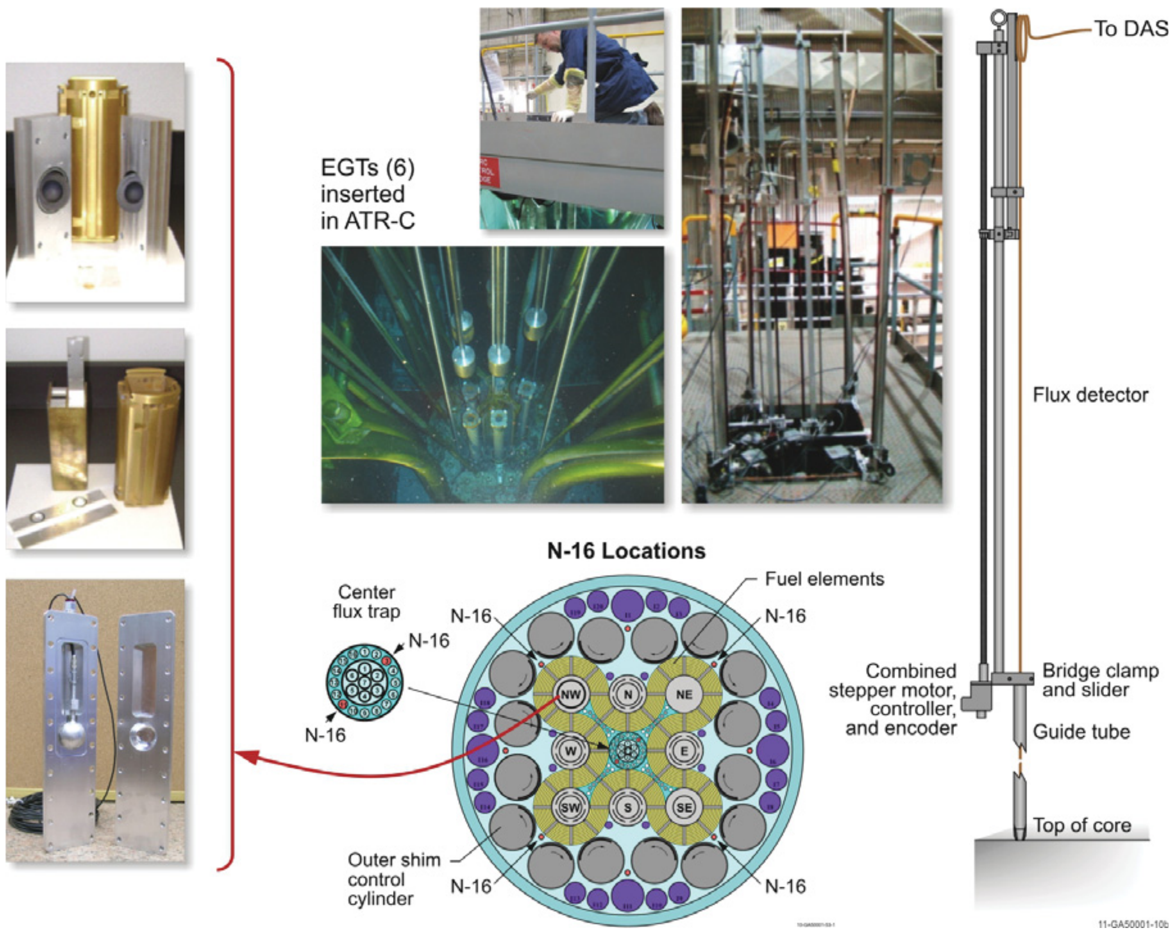

Figure 2-4. Sample /sensor positioning equipment and insertion locations at ATRC Facility.

2.2.3. Other MTRs

Table 2-1 compares operating parameters for selected test and prototype reactors used (or under construction) throughout the world. Information in this table was primarily obtained from the International Atomic Energy Agency (IAEA) Nuclear Research Reactor Database,[10] which contains information from nearly 280 research reactors (operating, shutdown, and proposed). Although these reactors range in power levels from 0 to several hundred MWt, nearly 200 of them have power levels below 5 MWt. Most of the reactors listed in Table 2-1 achieved criticality in the 1960s (or earlier). Among the operating reactors, there are two exceptions: the High Advanced Neutron Application Reactor (HANARO) reactor in South Korea, which went critical in 1995 and the prototype High Temperature Test Reactor (HTTR) in Japan, which went critical in 1998.

Table 2-1. Comparison of design parameters in selected operating test reactors.[10]

Parameter	ATR (USA)	HFIR (USA)	MITR (USA)	HBWR (Norway)	HFR (Netherlands)	OSIRIS[a] (France)	JHR (France)	BR2 (Belgium)	Hanaro (South Korea)	JMTR (Japan)
First criticality	1967	1965	1958	1959	1961	1966	2016	1961	1995	1968
Maximum thermal power, MW_{th}	250	100	5	20	60[b]	70	100	100	30	50
Max. thermal neutron flux, n/cm^2-sec	$1x\ 10^{15}$	$2x\ 10^{15}$	7×10^{13}	$1x\ 10^{14}$	3×10^{14}	3×10^{14}	6×10^{14}	1×10^{15}	5×10^{14}	4×10^{14}
Max. fast flux, n/cm^2-sec[c]	5×10^{14}	$1x\ 10^{15}$	2×10^{14}	1×10^{14}	5×10^{14}	3×10^{14}	6×10^{14}	7×10^{14}	3×10^{14}	4×10^{14}
Fuel material	UAl	UAl	UAl	UO_2	U-Al Alloy	U_3Si_2 Al	UMo[d]	UAl	U_3Si - Al	USi_2Alx
Fuel rod/plate length, m	1.22	0.61	2.0	0.800	0.625	0.950	0.600	0.914	0.700	1.27
Primary coolant	H_2O	H_2O	H_2O	D_2O	H_2O	H_2O	H_2O	H_2O	H_2O	H_2O
Test conditions[e]	PWR, HTGR	PWR, HTGR	PWR, BWR, HTGR	PWR, BWR, PHWR, VVER, HTGR	PWR, BWR, HTGR	PWR	PWR, HTGR	PWR	PWR, PHWR	BWR,

a. Scheduled for shutdown in 2015. France currently plans to build a new 100 MW_{th} materials test reactor, the Jules Horowitz Reactor (JHR).
b. Uprate possible in 1984 after new reactor vessel installed.
c. E > 0.1 MeV.
d. The reactor will be started with U_3Si_2 fuel, and transitions when it becomes available.
e. PWR- Pressurized Water Reactor; HTGR - High Temperature Gas Cooled Reactor; BWR-Boiling Water Reactor; PHWR - Pressurized Heavy Water Reactor; and VVER - Vodo-Vodyanoi Energetichesky Reactor (Pressurized Water Reactor)

The Jules Horowitz Reactor (JHR),[11 through 14] which is scheduled to go critical in 2016, is another exception with respect to its initial date for achieving criticality. The JHR is being built to replace materials irradiation capabilities of older reactors in Europe as they are retired from service. This 100 MWt reactor is designed to include static capsules, instrumented capsules, and in-pile loops. To support irradiation programs anticipated for the JHR, Commissariat à l'Énergie Atomique et aux Energies Alternatives (CEA) is developing several standard types test trains for experiments in loops at nominal and off-normal LWR conditions, for capsules at LWR accident conditions, for tests in loops containing sodium potassium with high dpa and low thermal gradients, and for tests in loops at gas reactor conditions (see Figure 2-5).[12] Recent reports[13,14] indicate that these devices will be deployed in phases. Efforts are underway to qualify prototypes for the first phase of these devices, such as:

- MADISON (Multirod Adaptable Device for Irradiations of LWR fuel Samples Operating in Normal conditions) -A test train in an in-core loop for fuel testing under normal LWR (PWR or BWR) conditions; will measure temperature, pressure, water flow and cladding elongation using Linear Variable Differential Transformers (LVDTs)
- CALIPSO (In Core Advanced Loop for Irradiation in Potassium SOdium) - A test train for in-core irradiation at controlled temperature, at low pressure, under high flux, and forced Sodium-Potassium (NaK) convection; CALIPSO is an in-core sodium potassium loop for material testing under high (~16) dpa/year, temperatures between 250 and 450 °C, and limited thermal gradients (< 8 °C); seeking to qualify for higher temperatures (up to 650 °C)
- MICA (Material Irradiation CApsule) - A test train for in-core irradiation at controlled temperature, at low pressure, under medium flux (with static NaK), similar to CALIPSO; alternate design allows testing at high temperatures (up to 1000 °C) gas reactor conditions.
- ADELINE (Advanced Device for Experimenting up to Limits Irradiated Nuclear fuel Elements) - A test train in an in-pile loop for fuel testing under LWR (BWR or PWR) off-normal conditions

(e.g. power ramps) with temperature, pressure, water chemistry, elongation, flux (using Self-Powered Neutron Detectors), and fission product measurements.

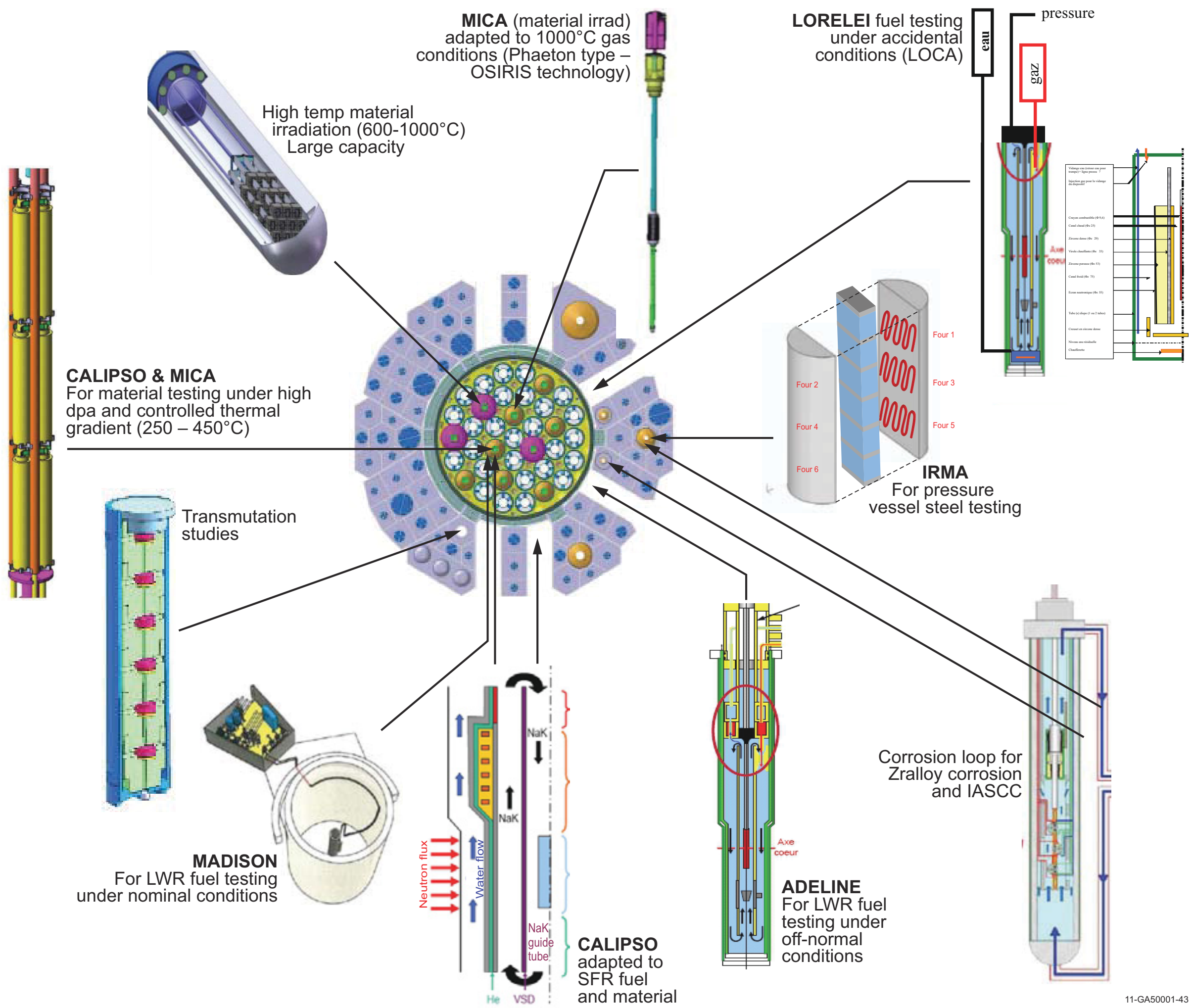

Figure 2-5. Test trains under development for JHR.

Subsequent efforts will focus upon other devices that can be deployed for various tasks, including transient fuel response testing, isotope production, and materials irradiation:

- LORELEI (Light water One-Rod Equipment for Loss of Coolant Accident (LOCA) Experimental Investigations) - A test capsule for fuel testing under LWR (PWR or BWR) LOCA conditions to observe phenomena such as clad ballooning or rupture, corrosion, and quench behavior and investigate fission product release.
- IRMA- A static capsule for testing pressure vessel steel
- MOLI - Experimental capsules for radioisotope production

CEA also plans to develop test rigs for studying Zircaloy corrosion and measuring irradiation assisted stress corrosion cracking and transmutation of fuels and materials. Finally, CEA will be developing a large capacity instrumented lead test for high temperature (600-1000 °C) material irradiations.

The Halden Boiling Water Reactor (HBWR) also merits further discussion. Although this reactor is older and its maximum power level (20 MWt) is over an order of magnitude smaller than the ATR, its testing flexibility and the expertise of its staff for instrumenting its tests make this facility unique. For decades, organizations within the international community (including the US Nuclear Regulatory Commission, vendors such as General Electric and AREVA, and the US naval reactor program) have utilized this facility for in-pile irradiation needs. Approximately 40% of HBWR testing is devoted to Organization for Economic Cooperation and Development (OECD) programs with the remainder sponsored by bilateral agreements between Norway and customers from other countries.[15] Most of these bilateral agreements allow the HBWR to perform tests for utility customers to address issues related to fuel thermal performance, fuel pellet/clad interactions, fuel fission gas release, reactor vessel embrittlement, structural materials degradation (e.g., corrosion, creep, etc.). As noted in Table 2-1, this reactor has loops for simulating BWR, PWR, Pressurized Heavy Water Reactor (CANDU), and Vodo-Vodyanoi Energetichesky Reactor (VVER) conditions. In addition, as discussed in Section 3.3, their focus on standardized test rigs and unique sensors has made them unique in their ability to investigate a wide range of phenomena of interest to the LWR industry, such as fuel thermal conductivity degradation, axial offset anomaly, etc.

2.2.4. Summary

Many materials and fuels irradiations support research programs for existing LWRs (e.g., PWRs and BWRs) and advanced reactors (e.g., gas-cooled reactors, sodium fast reactors, and fusion reactors). Successful development and deployment of advanced reactors depends to a large extent on demonstration of “enabling” technologies. For example, the high temperature irradiation performance of new fuels and structural materials must be demonstrated with instrumented tests in prototypical environments. In addition, MTRs also support a wide range of non-nuclear programs including medical isotope production research, and semiconductor industry production (neutron transmutation doping of semiconductors). Improved instrumentation for such tests offer the potential to obtain higher fidelity data, reduce irradiation costs, increase isotope production, and improve doping processes. Although other test reactors, such as the HBWR, currently have superior instrumentation capabilities and more flexible test trains, the ATR can be made competitive by adding similar, if not enhanced, capabilities.

3. INTERNATIONAL DEVELOPMENT EFFORTS

As noted in Section 1, new instrumentation is needed to support in-pile irradiation tests. In recent years, several international organizations have either initiated or enhanced their research instrumentation development programs as outlined in this section.

Table 3-1 summarizes the status of in-pile sensors that are currently-available and under development at various research organizations in Belgium, France, Japan, Korea, Norway, and the Netherlands.[16] Several test reactor programs in Europe, the United States, and Asia, such as the program conducted by the Institute for Energy Technology at the Halden Reactor Project (IFE/HRP), have maintained their instrumentation development capability and offer a selection of sensors for irradiation testing. The Japan Atomic Energy Agency (JAEA) in Japan, Studiecentrum voor Kernenergie Centre d'Étude de l'Énergie Nucléaire (SCK•CEN) in Belgium, and Korea Atomic Energy Research Institute (KAERI) in Korea also offer selected instrumentation to users performing irradiations in their test reactors. The CEA in France, which supports the existing OSIRIS and the new JHR, and INL in the United States, which supports the ATR, not only offer users a suite of instrumentation, but are rapidly trying to increase the types of sensors available to users at their facilities.

Current capabilities and recent advances by several of these foreign organizations are of interest as INL expands ATR NSUF instrumentation capabilities. For example, this section summarizes recent advances by CEA (Section 3.1) to develop calorimetry techniques for measuring localized heating and by IFE/HRP (Section 3.3) to enhance their methods for detecting crack initiation and to deploy gamma thermometers to measure localized heating. Because several ATR users have expressed interest in measuring localized heating and crack growth, new efforts (see Section 5) have been initiated at INL during 2012 to add these capabilities for ATR NSUF users. In addition, INL continues to monitor foreign efforts to deploy advanced technologies, such as the in-pile use of ultrasonics and fiber optics. Such new INL sensor development efforts are informed by considering applicable foreign experience.

3.1. CEA

The "INSNU" program was initiated by the French CEA with the aim of developing innovative in-pile instrumentation to meet the needs of emerging nuclear programs, such as GEN IV, fusion, and FCRD.[13, 14, 17- 21] The scope of this program includes:

- radiation measurements (e.g., neutron flux and gamma heating)
- measurements of physical parameters inside the irradiation rigs (e.g., temperature, pressure, sample dimensions, and fission gas release)

The orange boxes in Figure 3-1 identify instrumentation areas studied within the INSNU program.

Originally, CEA instrumentation development was focussed on the INSNU program, which was a combined CEA-Saclay and SCK•CEN effort to improve instrumentation in the OSIRIS reactor in Saclay, France, and the Belgium Reactor 2 (BR2) in Mol, Belgium. However, in preparation for the JHR that will go critical in Cadarache, France in 2016, the CEA instrumentation effort was moved to Cadarache and expanded to include a larger number of organizations and sensor development activities. In addition, as noted in Section 2, efforts include development of standardized test rigs.

Table 3-1. In-pile instrumentation status at SCK•CEN, CEA, JAEA, KAERI, IFE/HRP, and NRG.

Research Organization / Country	Technology		
	Sensor	Parameter Detection	Status
Studiecentrum voor Kernenergie • Centre d'Étude de l'Énergie Nucléaire (SCK•CEN) /Belgium	SPND[a]	Thermal flux	Operational
	Fission chambers	Thermal and fast flux	Operational (fast detectors qualified in 2009; Joint Lab with CEA)
	Fiber optics	Length	Under development (Joint Lab with CEA)
	LVDTs with unstressed bellows and stressed bellows	Length/ creep-induced elongation	Participated in qualification testing with VTT (IFE/HRP LVDTs)
	Flux wires and foils	Fluence (neutron)	Operational
	Melt wires	Peak Temperature	Operational
Commissariat à l'Energie Atomique et aux Energies Alternatives (CEA)/ France	Fission chambers (down to 1.5 mm diameter)	Thermal and fast flux	Operational (fast detectors qualified in 2009 as part of Joint Lab with SCK•CEN)
	SPND	Thermal flux	Operational
	SPGD	Gamma flux	Operational
	Flux wires and foils	Fluence (neutron)	Operational
	Gamma calorimeter	Localized heating	Operational
	Melt wires	Peak Temperature	Operational
	Thermocouples (Type K, N, and C thermocouples)	Temperature	Operational; also placed on previously irradiated fuel. Mo/Nb alloy thermocouples under development with Thermocoax
	Noise thermometry	Temperature	Under development
	Fixed point μ-cells	Temperature	Under development
	Counterpressure sensor	Fission gas release (pressure in fuel rod)	Operational (also placed on previously irradiated fuel)
	Acoustics	Fission gas composition and pressure	Operational (placed on previously irradiated fuel rod)
	LVDTs / DGs	Length (creep-induced elongation) and diameter	Operational (enhanced IFE/HRP LVDTs and DGs) under development
	Fiber optics	Length	Under development (Joint Lab with SCK•CEN)
Korea Atomic Energy Research Institute (KAERI)/ Korea	Melt wires	Peak Temperature	Operational
	Thermocouples (Type K and C)	Temperature	Operational
	Flux wires	Fast fluence	Operational
	LVDT	Pressure, UO_2 elongation / creep-induced elongation	Operational for pressure fuel elongation detection /under evaluation for creep testing (IFE/ HRP LVDTs)
	SPNDs (V-, Rh-emitter)	Thermal flux	Operational (commercially- made SPNDs)
Nuclear Research & Consultancy Group (NRG) / Netherlands	Neutron metrology sets: SS tubes containing quartz minitubes with flux wires (Nb, Ti, Fe, Ni, Co)	Fluence	Operational
	SPNDs	Thermal flux, power, fuel heatup rate	Operational (commercially-made SPNDs)
	Thermocouples (Type K and N)	Temperature	Operational[c]
	LVDT	Pressure	Operational (IFE/HRP LVDTs)
	Silicon chip transducer; tube containing silicon chip influenced by pressure.	Pressure	Operational[b]

Table 3-1. In-pile instrumentation status at SCK•CEN, CEA, JAEA, KAERI, IFE/HRP, and NRG.

Research Organization / Country	Technology		
	Sensor	**Parameter Detection**	**Status**
Japan Atomic Energy Agency (JAEA)/Japan	Fission chambers (1.8 mm diameter)	Thermal flux (with ^{235}U deposits)	Operational
	SPNDs	Thermal flux (Rh, Co, and Pt-40%Rh emitters)	Operational
	Flux wires	Fast (Fe) and thermal (Al-Co, V-Co, and Ti-Co) fluence	Operational
	Melt wires	Peak Temperature	Operational
	Thermocouples (Type K, N, and C)	Temperature	Operational[c] (also placed on previously irradiated fuel
	LVDT (stressed with bellows and unstressed)	Pressure, length/ creep-induced elongation	Operational (Japanese LVDTs and bellows)
	DCPD method with CT specimens and bellows loading	Crack growth	Operational
Institute for Energy Technology/Halden Reactor Project (IFE/HRP) / Norway	LVDT (stressed with bellows and unstressed) and DG	Pressure, length/ creep-induced elongation and diameter changes	Operational (enhancements explored with CEA and INL); DG improvements underway
	Eddy-current probe	Oxide thickness deposited on fuel rods; cladding defects; crack growth	Under development
	Melt wires	Peak Temperature	Operational
	Expansion thermometer	Temperature	Operational
	Thermocouples (Type K, N, and C)	Temperature[c] and thermal conductivity[d]	Operational (also place on previously irradiated fuel
	Flux wires	Fast (Fe, Ni) and thermal (Al-Co) fluence	Operational
	SPNDs	Thermal flux, power, fuel heatup rate and burnup; power	Operational (commercially- made and IFE/HRP-made sensors)
	Gamma thermometer	Gamma flux; gamma heating; water level	Operational (IFE/HRP- sensors)
	DCPD method with CT specimens and bellows	Crack growth	Operational
	Turbine Flowmeter	Inlet /outlet flow (single or two phase); with channel power information, outlet void fraction	Operational
	Electrical chemical potential measurements (platinum or palladium electrodes)	Oxygen concentration, hydrogen concentration (e.g., corrosion potential); Water chemistry	Operational

a. Abbreviations: LVDT, linear variable differential transformer; DG, diameter gauge; SPND, self-powered neutron detector; SPGD, self-powered gamma detector; DCPD, direct-current potential drop; CT, compact tension; HTIR-TC, high-temperature irradiation-resistant thermocouple; SiC, silicon carbide; VTT, Technical Research Center of Finland

b. Using Kulite Semiconductor Products, Inc. outside high neutron and gamma radiation location.

c. HBWR-specific corrections required to compensate for transmutation that occurs in Type C high temperature thermocouples during irradiation. However, similar temperatures and fluxes and temperature gradients and flux distributions must exist during irradiation in order to apply such correction factors, and thermocouple lifetimes are generally limited to 1 year. Informal HRP discussions indicate that batch-to-batch variations in Type C thermocouples adversely affect performance.

d. Thermal conductivity estimates require assumptions about fuel densification, and gap conductance.

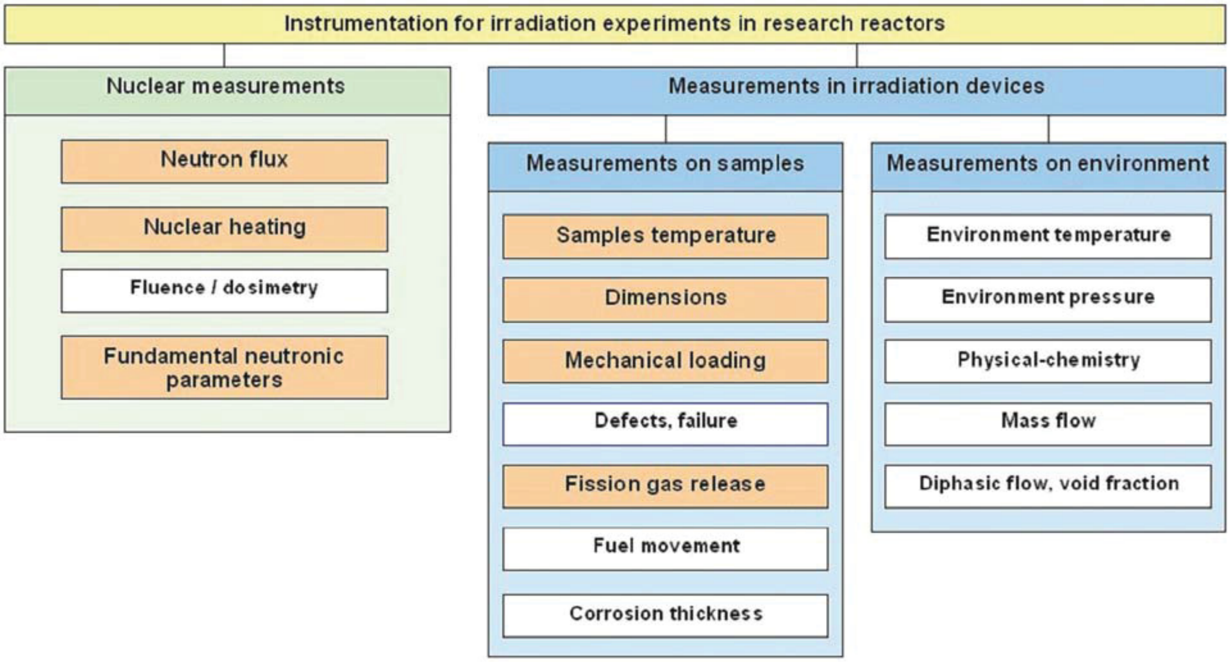

Figure 3-1. In-pile instrumentation needs pursued by INSNU for irradiation experiments.[18]

As discussed in References 13 and 14, decisions for CEA instrumentation development are based on users-needs, and development efforts include in-pile qualification. Current instrumentation development efforts are often a collaborative effort between government research laboratories [CEA, Paul Scherrer Institute (PSI), HRP, etc.] and industry (e.g., Photonis, Thermocoax, etc.). By including industry partners, developers ensure the sensor availability from a commercial supplier.

General characteristics of instrumentation developed include:

- Reliable (because it is impossible or difficult to perform maintenance on irradiated objects)
- Accurate (sensors must meet testing requirements; e.g., μm dimensional measurements)
- Miniature (irradiation volumes are limited with narrow dimensions; few mm available)
- High temperature resistant (> 300 °C, up to 1600 °C)
- Corrosion resistant (in pressurized water, high temperature gas, and liquid metals)
- Neutron / γ "resistant" (dose > 1GGy/day and > 10 dpa/year in MTRs)

As noted in References 19 and 21, in-pile instrumentation must be developed that doesn't pose a threat to the safety or economic operation of the test reactor (e.g., "simpler" is smarter). Selected examples of CEA in-pile instrumentation development are discussed below. Because some of their sensor development efforts are collaborations with SCK•CEN, additional examples may be found in Section 3.2.

3.1.1. Subminiature Fission Chambers

For decades, in-pile neutron flux measurements were obtained using Self Powered Neutron Detectors (SPNDs), and signals were generally correlated with post-irradiation analysis of activation foil dosimeters.

The development of CEA's sub-miniature fission chambers for in-pile measurements of high thermal neutron fluxes (up to 4×10^{14} n/cm²-s) represents a significant improvement. These sensors, which have external diameters of only 1.5 mm and contain a U^{235} fissile deposit, were qualified in the BR2 in the CALLISTO loop between 2001 and 2004, However, additional studies continue to verify sensor robustness. These sensors are now manufactured by the PHOTONIS Company under the name "CFUZ53" (see Reference 22).

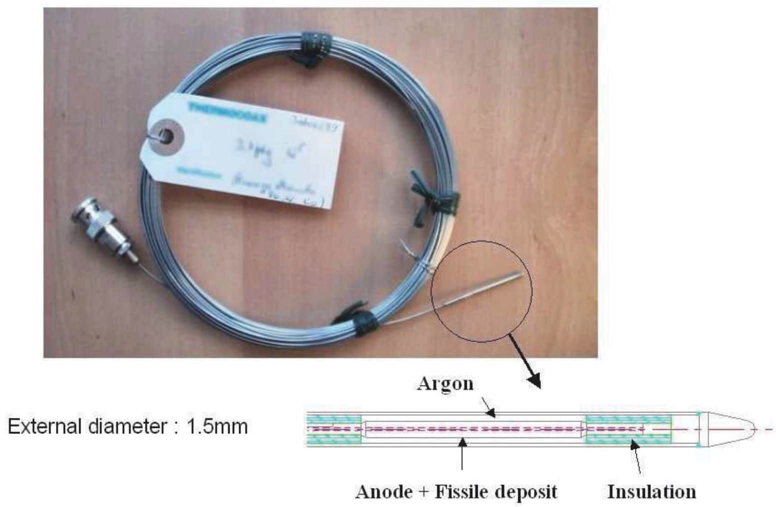

Figure 3-2. CEA-developed sub-miniature fission chamber.

In addition, as part of the Joint Instrumentation Laboratory, CEA-SCK•CEN developed fission chambers for online in-core measurement of the fast component of a high neutron flux (~ 10^{14} n/cm^2-s) with an uncertainty of 10% or less in locations with thermal fluences up to 10^{21} n/cm^2. The fast neutron detection system (FNDS; see Figure 3-3) is based on a patented miniature fission chamber with a special fissile deposit sensitive to fast flux with a low thermal contribution and is operated in Campbelling mode for a high gamma rejection. The choice of the fissile deposit is key in these fission chambers for two main reasons:[23].

- The fission cross-section is usually much larger for thermal neutrons than for fast neutrons. Moreover, even for the few isotopes presenting an energy threshold near 1 MeV, such as ^{238}U or ^{242}Pu, it remains small (e.g., a few barns) for fast neutrons.
- The potential to form other isotopes via radiative capture of (primarily thermal) neutrons. This process, either directly or after some radioactive decay, leads to new isotopes in the deposit that may fission preferentially with thermal neutrons. The sensitivity to thermal neutrons in a chamber based on these isotopes therefore increases gradually. Because of their large size and of the local perturbation induced on the thermal flux, it was decided to not use screen-absorbers that could prevent thermal neutrons from reaching the chamber.

For MTRs, analytical simulations identified ^{242}Pu as the best choice to measure the fast component of a high neutron flux. Its sensitivity to fast neutrons is excellent at the beginning of irradiation and slowly decreases with fluence.

Generally, the signal given by a fission chamber at high counting rates is the sum of a mean constant current, I_o, and a fluctuation around this value. Classically, fission chambers are used in "current mode"

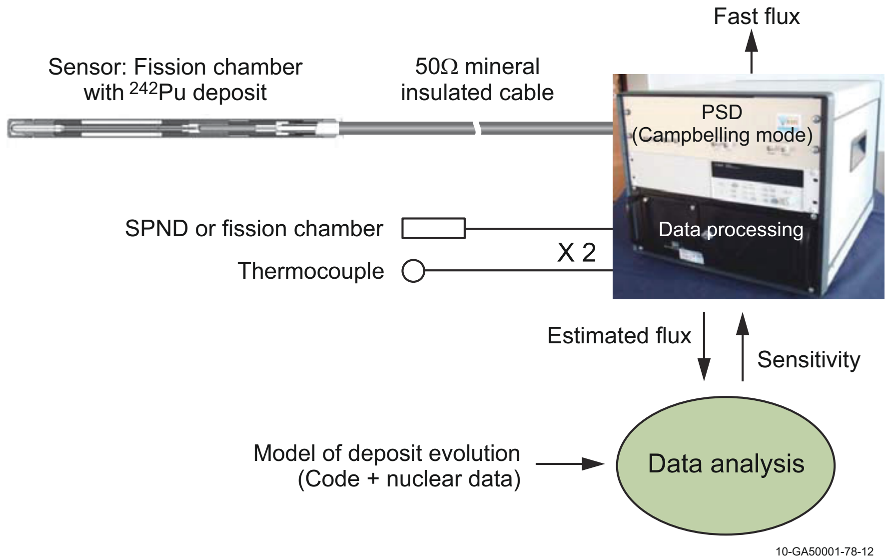

Figure 3-3. Schematic view of the FNDS prototype.

under high neutron flux where it is not possible to count individually each event in the detector. However, the FNDS system uses the variance of the signal. This parameter characterizes the random variations of the signal around its mean value and is proportional to the incident neutron flux. This method is called Campbelling mode or MSV (Mean Square Voltage). The advantage of the Campbelling mode is that the gamma contribution to the signal is significantly less than in current mode because it plays a part as the square of the charges, which are notably lower for events generated by gammas than for those induced by fission reactions. Thus, this mode is very useful for a high rejection of the gamma component. Tests performed in the BR2 in 2005 and 2006 demonstrated the viability of the Campbelling mode for measuring the fast neutron flux; the gamma contribution to the signal of a ^{242}Pu fission chamber was reduced from 50% in current mode to 0.6% in Campbelling mode.[24] The developed FNDS system has been qualified in-pile in the BR2 in 2009, and it is now operational at CEA and SCK•CEN.

Prototypes of fission chambers with ^{242}Pu deposit have been manufactured by CEA in Cadarache and tested in 2005 and 2006 in the BR2 of SCK•CEN. As part of an on-going ATR NSUF effort, the use of these fission chambers for ATR applications is being investigated. Initial evaluations began in the ATRC in October 2010 (see Section 5).

Recently,[14] CEA has initiated the CARMEN-1 experiments which contain two cell probes for characterizing conditions in OSIRIS. As shown in Figure 3-4, one cell contains multiple neutron detectors (fast and thermal fission chambers with SPNDs, and the other cell contains multiple self-powered gamma detector (see Section 3.1.2), a gamma thermometer, and a calorimeter. Initial comparisons of data to analysis results indicate that these cells can be successfully used to characterize OSIRIS conditions. Final evaluations are expected to be completed by the end of 2012.

3.1.2. Self-Powered Gamma Detectors

Nuclear heating measurements in material testing reactors are commonly based on calorimeter or gamma thermometer technologies. However, such options cannot differentiate between the heating from neutrons and gamma rays. SCK•CEN and CEA have jointly-developed a Self-Powered Gamma Detector

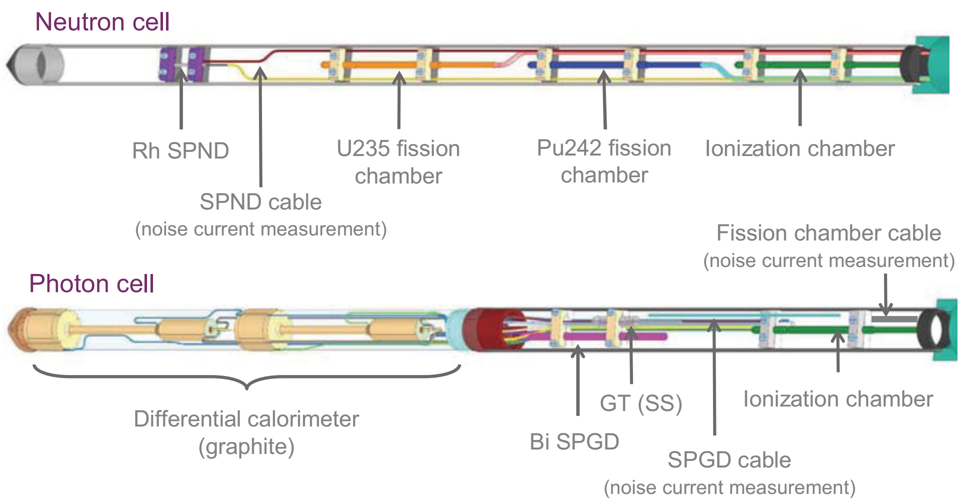

Figure 3-4. Neutron and photon measurement cells in CARMEN-1experiment.

(SPGD) for monitoring the gamma field.[25] In order to minimize the neutron response while maximizing the gamma response, bismuth was selected as emitter material. Based on detailed MCNP modeling to calculate the gamma/neutron sensitivities and irradiation experiments in pure and mixed gamma spectra (OSIRIS and BR2), a tubular geometry design was selected as the most appropriate for in-core gamma detection because this design allows a larger sensitivity with better response characteristics. These SPGDs, which are produced by THERMOCOAX (see Figure 3-5), are able to measure small power changes (until less than 1%) with a relative accuracy of about 0.2%, which is much better than possible with gamma thermometers. In summary, the bismuth SPGD is a promising small size in-core gamma-selective detector that does not suffer from burn-up effects.[13] Furthermore, this SPGD is easily implemented inside lower temperature experiments (that are well below the bismuth melting temperature of 271.5 °C).

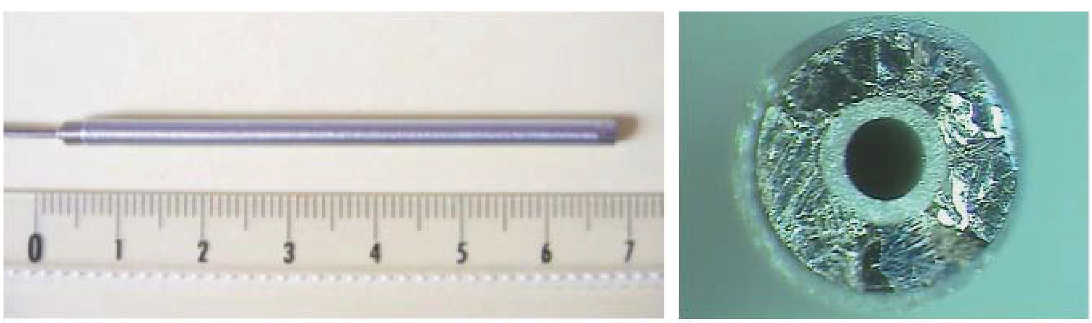

Figure 3-5. Tubular bismuth SPGD developed by SCK•CEN and CEA.

3.1.3. Mo/Nb Thermocouples

In 2003, CEA initiated a research program in collaboration with the THERMOCOAX Company, to develop high-temperature in-pile thermocouples.[26] This CEA/THERMOCOAX effort initially investigated thermoelements containing molybdenum and niobium because the low neutron absorption cross sections of these elements make them less susceptible to transmutation-induced drift during irradiation. Materials interactions tests conducted by CEA/THERMOCOAX in high temperature furnaces, in the range from 1000 to 1600 °C, indicated that materials less susceptible to interactions with Mo and Nb thermoelement wires were HfO_2 insulation and Nb or Ta sheaths. Investigations to quantify the thermoelectric response of a loose-assembly Mo-Nb thermocouple found that its emf in its intended temperature range (1000 to 1600 °C) is of the same order as commercially-available high-temperature Type C or S thermocouples.

Thermal stabilization of these thermocouples was also investigated. Candidate heat treatments to stabilize grain growth to minimize drift during high temperature use were evaluated using long-duration high-temperature out-of-pile tests. Reference 17 reports that these thermocouples were drifting at a rate somewhat lower than 0.02 °C/h at 1100 °C. After 5000 hours, this would result in 100 °C or 10% drift, which is higher than observed in the INL long duration evaluations at 1200 °C of their doped Mo/Nb alloy High Temperature Irradiation Resistant ThermoCouple (HTIR-TCs) discussed in Section 5.

References 26 and 27 reported plans for an in-pile high-temperature qualification irradiation of these thermocouples in the OSIRIS reactor. More recent information[29] suggested that there were plans to irradiate these thermocouples in the High Flux Reactor (HFR) as part of CEA's gas reactor research program and that more recent efforts are exploring the use of doped Mo/Nb-alloy thermoelement materials.[29] However, recent references[13-14] indicate that no in-pile qualification of these thermocouples has been performed.

3.1.4. In-Pile Noise Thermometry

Noise thermometers provide a signal proportional to the thermodynamic temperature that is independent of the probe material properties and hence of the environmental conditions that may affect them. In particular, the signal of a noise thermometer should not be affected by nuclear irradiations.[30,31] Moreover, this instrumentation does not require calibration when exposed to high temperatures (up to 1800 °C). Thus, CEA is exploring noise thermometry as a method for calibrating and recalibrating thermocouples in-pile.

Figure 3-6 shows a "hardened" mixed thermocouple noise thermometry (TC-NT) probe developed by CEA.[14] Out-of-pile tests and characterization of the probe (at temperatures up to ~400 °C) and its data acquisition and processing system provided by the Forschungszentrum Jülich (Germany) have been completed. Irradiation qualification testing in OSIRIS is planned for January 2013.

3.1.5. In-Situ Calibration of Thermocouples

CEA is also participating in a Joint Research Center (JRC) project effort to use fixed point μ-cells for in-situ calibration of thermocouples. As reported in Reference 14, copper and three high temperature metal carbon eutectics with melting temperatures ranging from 1084 to 1492 °C are proposed for use. These μ-cells, which are approximately 1 cm diameter by 1.5 cm long (see Figure 3-7), would be incorporated into irradiation test rigs. High temperature tests have demonstrated the viability of this technique, but references did not indicate when in-pile demonstrations were planned.

As proposed in Reference 33, this on-line calibration technique requires some assumptions. The theoretical value of the melting temperature can be affected by the irradiation process. Pure metals and alloys must be carefully enclosed to avoid contact with the corrosive atmosphere and preferentially have low activation characteristics to make them useful for long term irradiation. The mini-cells will need to be located in areas with a homogeneous temperature, neutron flux and gamma radiation field.

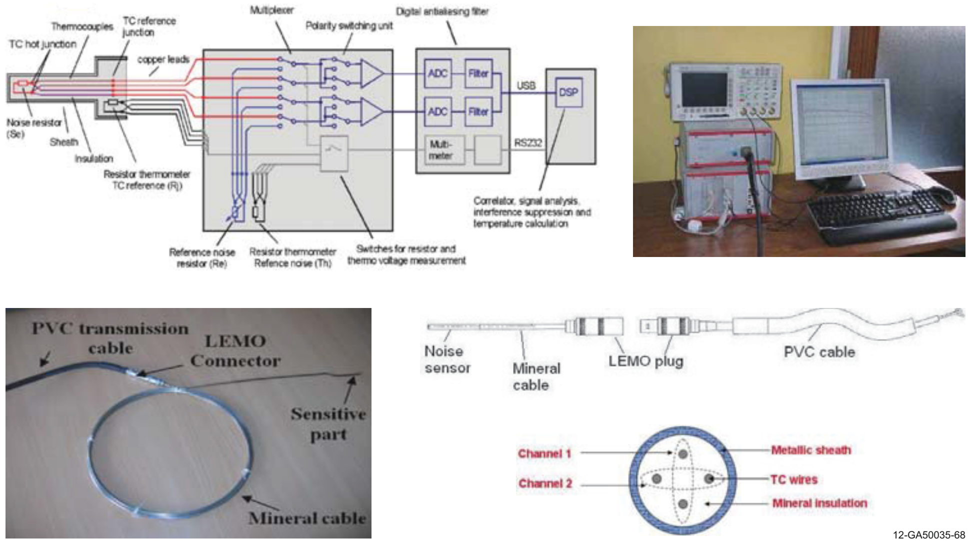

Figure 3-6. Photo and schematic of TC-NT probe developed by CEA.[14]

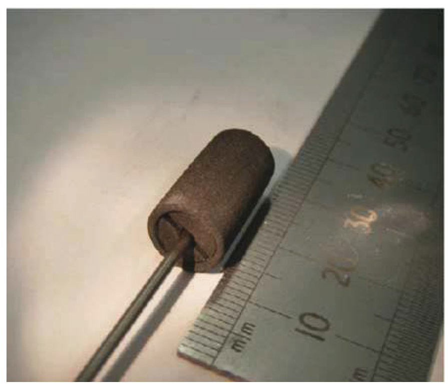

Figure 3-7. Proposed self- calibrating thermocouple design containing a Type C thermocouple with Mo sheath and HfO_2 insulation immersed in a Co-C fixed-point μ-cell.

3.1.6. Improved LVDTs and DGs

CEA and the IFE/HRP have collaborated on an effort to improve the performance of Linear Variable Differential Transducers (LVDTs). Since 2005, LVDTs fabricated by IFE-HRP have been used in the OSIRIS reactor with accuracies of ±4 μm and displacements up to ±15 mm (total range) and ± 6 mm (linear range). During 2007, CEA performed a series of out-of-pile tests to characterize and try to improve the performance of these LVDTs and diameter gauges (DGs) based on LVDT sensors. CEA investigations were focussed upon:

- Quantifying usable LVDT temperature range
- Quantifying maximum LVDT measurement range
- Developing the most appropriate LVDT signal correlation versus measurement ranges
- Developing post-test appropriate LVDT adjustments (Gain – Phase)

Tests were conducted at room temperature and at higher temperatures (up to 380 °C) in inert gas, water, and sodium potassium conditions

As part of this effort, CEA proposed several improvements to LVDT designs currently manufactured by IFE/HRP. First, to extend their measurement range, CEA requested that a polynomial equation be used to characterize the signal of LVDTs procured from IFE/HRP. Second, CEA requested that IFE/HRP develop a 'fifth wire' or "self compensating electronics setup." Figure 3-8 illustrates the wiring used for such a setup (compared to the standard 4-wire setup that only uses the wires labeled 1, 2, 3, and 4). In this configuration, wire 3 and 4 are Type K "B" thermocouple wires and Wire 5 is a Type K "A" thermocouple wire. In a 4-wire configuration, only the voltage difference between the two secondary coils is measured. Hence, the voltage output is proportional to the core displacement, or

$$Displacement = G \cdot (V_{C1} - V_{C2}) \tag{9-1}$$

where G is the gain, and V_{C1} and V_{C2}, represent the voltage of coils 1 and 2, respectively. In the 5-wire setup, the additional wire is connected as a zero reference between the two secondary coils. Hence, the ratio between the two secondary coils is used to estimate the displacement, using

$$Displacement = G \cdot \frac{(V_{C1} - V_{C2})}{(V_{C1} + V_{C2})} \tag{9-2}$$

Theoretically, the influence of global changes in the system will have negligible effect on the system because the resulting signal is a ratio. For example, this setup offers several potential improvements:

- improved linearity
- suppression of temperature sensitivity
- suppression of signal aberrations in its central area
- suppression of nickel Curie temperature effects (although experimental confirmation required)
- suppression of signal shift due to irradiation (although experimental confirmation required)

In particular, the ratio of signals from the secondary are used to quantify elongation rather than the combined secondary signal. As long as the LVDT is at a uniform temperature, the signal should be more accurate (because it is no longer susceptible to Curie temperature effects). However, experience indicates that the LVDT is not often at a uniform temperature.

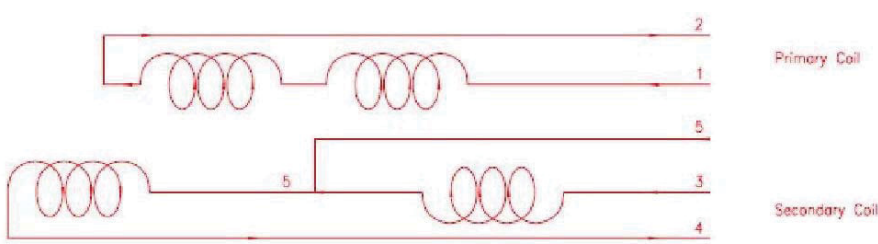

Figure 3-8. Wiring schematic for LVDTs using the five-wire method.

Reference 14 reports that the performance of the improved LVDT design and the associated DG design (which relies on LVDT-based technology as discussed in Section 3.3.5) will be evaluated in the OSIRIS reactor in the MELODIE test. As shown in Figure 3-9, the MELODIE test is designed to provide real-time elongation and diameter change data from an in-core irradiation of a PWR fuel cladding tube (90 mm) at 350 °C. The test rig, which is jointly designed by CEA and IFE/HRP and manufactured by IFE/

HRP, includes controlled mechanical loading ranging from 60 to 180 MPa (with stress steps) and variable biaxial stress ratio: ranging from 0 (hoop stress) to infinity (axial stress).

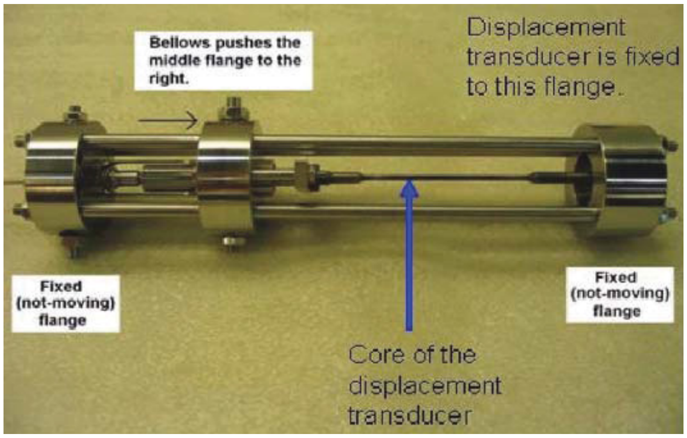

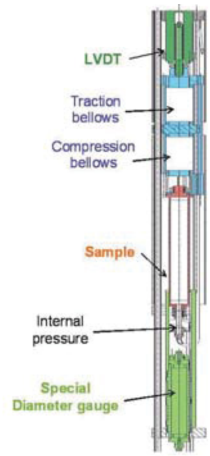

Figure 3-9. Proposed test rig for detecting elongation and diameter changes of PWR cladding during OSIRIS irradiation.

3.1.7. Fission Gas Release

In-situ measurement of the composition and amount of fission gas release is particularly important in fuel rod irradiations because fission gas release kinetics is an important indicator of nuclear reactions and its measurement is key in fuel performance studies. To address this need, CEA is investigating counter-pressure and acoustical measurement techniques.[18]

Figure 3-10 shows the counter-pressure sensor used by CEA to detect the pressure associated with fission gas release from a fuel rod during irradiation. It consists of two gas cavities separated by metallic bellows, as shown in Figure 3-10.[17,34,35] The first cavity communicates with the internal fuel rod pressure. The second cavity is connected to an external helium circuit, which is called the “counterpressure” circuit. The imbalance between the internal rod pressure and the counter-pressure is detected by two electric contacts, activated by the motion of the bellows. This sensor has been qualified in OSIRIS irradiations. Results indicate that this sensor, which is now operational in OSIRIS, has an accuracy of ±0.32 bar over its pressure range (up to 120 bars). Design and manufacturing of an enhanced counter-pressure sensor for high-pressure measurements (up to 250 bar) is underway.

A dedicated acoustic sensor (containing a piezoelectric transducer) has been developed by CEA to measure online fission gas release in a fuel rod during irradiation experiments. Figure 3-11(a) illustrates some of the details related to the design of this acoustic fission gas release sensor.[18,36-42] This assembly is composed of a small cylindrical cavity containing the gas to be analyzed. The upper part of the cavity is closed by a thin stainless steel plate. The piezoelectric transducer is fixed on this plate, in order to generate and measure acoustic waves, through the plate, in the gas cavity. Wires are directly welded on the piezo-ceramics electrodes. Acoustic waves propagate in the gas inside the cavity which is connected to the fuel rod plenum. The measurement of the reflected waves allows assessment of the acoustic impedance of this system [see Figure 3-11(b)]. The signal and its echoes are recorded, and the time of flight of the signal and its attenuation are measured. From these measurements, it is possible to deduce simultaneously the

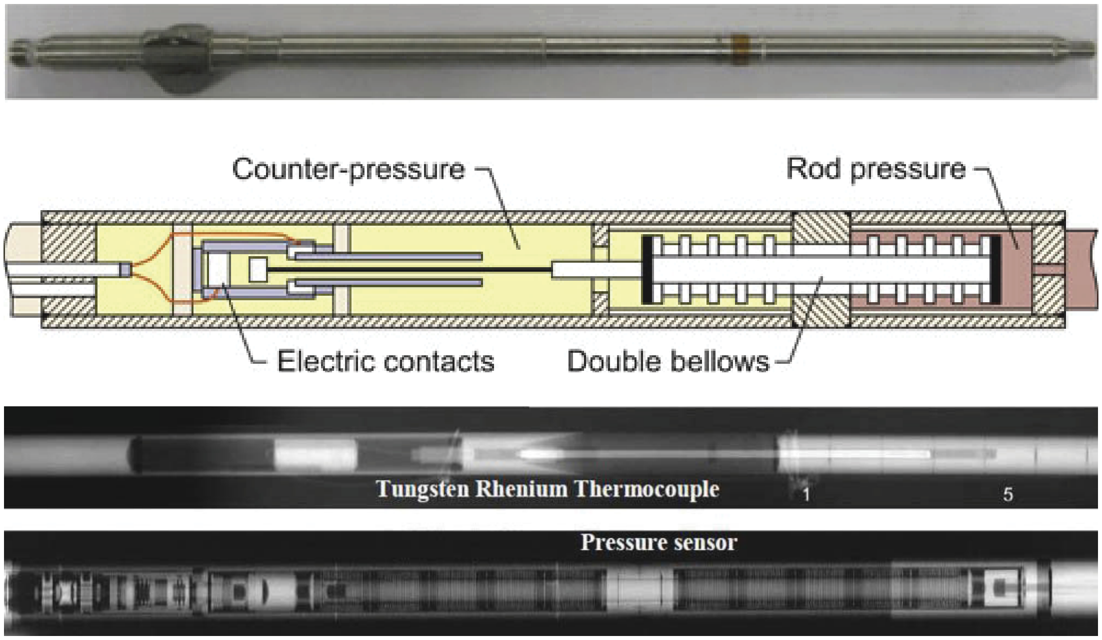

Figure 3-10. CEA counter-pressure sensor for detecting fission gas release amount.

molar mass of the gas (from the acoustic waves velocity) and the pressure of the gas (from the echoes attenuation). The online assessment of these two parameters is then used to obtain information regarding the fraction of fission gases released in the fuel rod.

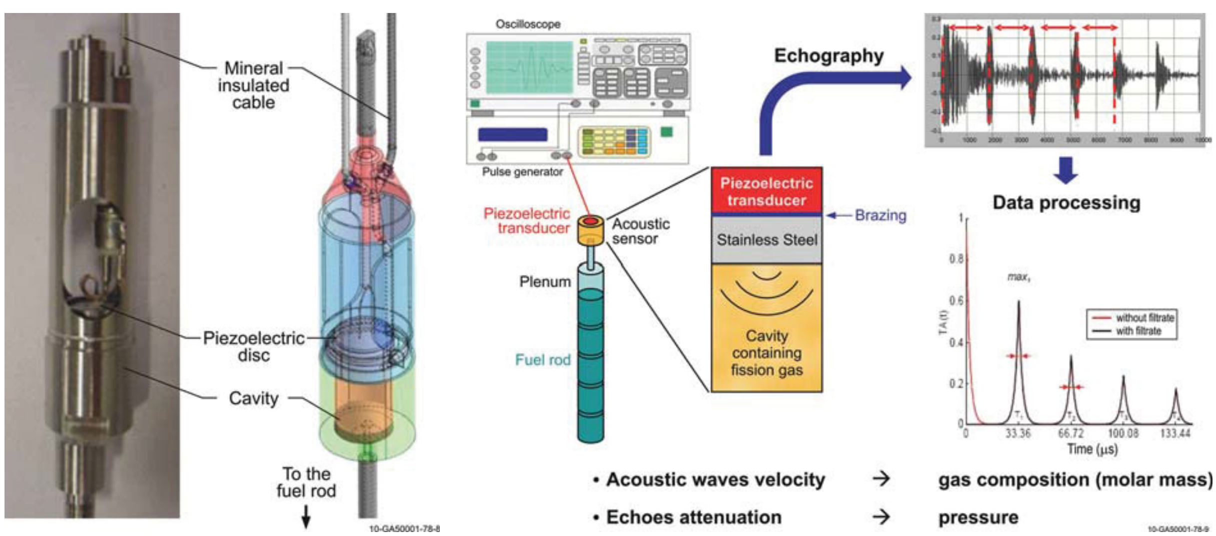

(a) (b)

Figure 3-11. CEA fission gas pressure and composition detection (a) sensor and (b) system operation.

Initial laboratory testing of acoustic sensor prototypes was completed by CEA. In 2008, final sensors for use on a pre-irradiated fuel rod were designed and manufactured. This sensor, now operational in CEA, was successfully demonstrated at OSIRIS on a pre-irradiated PWR fuel rod in the 2010 REMORA-3 irradiation experiment. Reference 14 reports that data obtained from this sensor (see Figure 3-12) is in excellent agreement with post-irradiation measurements. However, detailed information related to accumulated fluence were not provided.

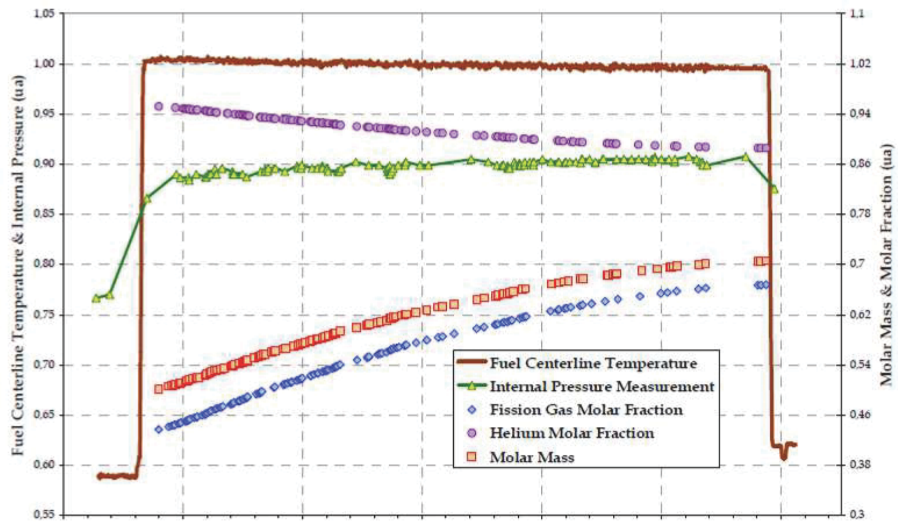

Figure 3-12. REMORA-3 data from CEA acoustic sensor.

3.1.8. Localized Heating

CEA has also pursued calorimetric techniques for local power measurements.[38] Currently-used calorimeters to measure local power in OSIRIS consist of two pairs of aluminum cells, fixed onto the same aluminum base. The cells of each pair are similar except that one contains a graphite sample and the other a corresponding volume filled with nitrogen (See Figure 3-13). The two pairs of cells are diametrically opposed on the same aluminum base in order to avoid any gradient effect. The entire structure is enclosed inside a tube in contact with external water flow for heat removal. The pedestal between the upper part of the cell and the base in contact with the external sleeve is a thermal resistance through which the deposited energy inside the cell is transferred. The energy deposit is calculated using a calibration curve obtained from experiments with different electric energy inputs and measured temperature differences between empty and full cells located at the same axial position along the core height. Note that the heating rate unit (W/g) is written as W/g (C) to emphasize the fact that the sample is graphite. Current devices for OSIRIS in-core measurements consist of five different calorimeters (each one made of four cells), positioned along the core height leading to five measurement points, from which the heating profile curve is fitted. Even though these calorimeters are reliable, they have inherent drawbacks, associated with their static nature.

To overcome drawbacks associated with the differential method, a new system, CALMOS, is being developed and tested in OSIRIS. The key point of this new device is to put only two cells (one empty and one equipped with the graphite sample) coaxially inside a same external sleeve and then to move the probe using a displacement system. Hence, this new system is able to measure the heating rate data at any level in the core and determine more accurately the heating profile inside and above the core.

This new CALMOS design includes several new features. Specifically, it:

- allows continuous axial heating rate distribution measurements instead of selected point values,

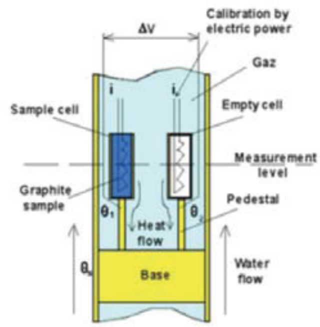

Figure 3-13. Calorimeter design currently used in OSIRIS.

- extends measurements to locations above the core, where heating levels are sufficiently high that they must be taken into account to design any new experimental device,
- reduces the irradiation aging of the cells. The probe is exposed to the irradiation field only during measurement periods. As a consequence, the aging of heater wires is limited, and calibrations can be performed during the whole calorimeter life for periodic verifications,
- facilitates point measurements because of the small size of the calorimeter (18mm),
- minimizes radial gradient effect in the probe vicinity (e.g., coaxial configuration and smaller size).

Two identical cells are included in the CALMOS conceptual design shown in Figure 3-14. The upper cell (the sample cell) contains a graphite specimen, whereas the lower cell (the reference cell) is empty. Each cell is surrounded by a gas gap (nitrogen) and set on a base surrounded by a stainless steel external tube in contact with the reactor coolant flow. A thermocouple (Type K) is embedded on the top of each pedestal (hot temperature), whereas a second one is located on the external surface of the aluminum base (cold temperature). Two heating elements, made of constantan wire embedded in alumina, are inserted inside the cells, thus allowing the calorimeter's calibration. The calorimeter works in a continuous mode, i.e., the energy deposit in each cell is flowing through the pedestal and then through the external sleeve. The temperature difference "ΔT_{sample}" is proportional to the energy deposit in the graphite and cell structure; whereas "$\Delta T_{reference}$" is proportional to the deposit in the empty cell structure. Therefore, in a first approximation, the "$\Delta T_{sample} - \Delta T_{reference}$" quantity ($\Delta\Delta T$) is proportional to the energy deposit inside the only graphite sample. This new nuclear heating measurement method has been patented by CEA.[39]

The following functional criteria were defined for CALMOS:

- a large sensitivity range is needed to be able to perform measurements above the core down to 0.1 W/g (C) and inside the core up to 13 W/g (C) [As noted previously, the heating rate unit (W/g) is written as W/g (C) to emphasize the fact that the sample is graphite].
- the cell external diameter is limited to 18 mm in order to be able to insert and move the calorimetric probe inside an external sleeve representative of OSIRIS standard experimental devices.
- the overall probe length should not exceed 220 mm compared to the core fissile height (630 mm).
- good linearity of $\Delta\Delta T$ [$\Delta T_{sample} - \Delta T_{reference}$] versus heating rate in the range of 0.1 to 13 W/g (C) is required. A maximum of 20% from linearity for 13 W/g (C) was set for the design.
- the highest temperature inside the cell structure should not exceed 500 °C in order to have a significant margin with respect to the aluminum melting point.

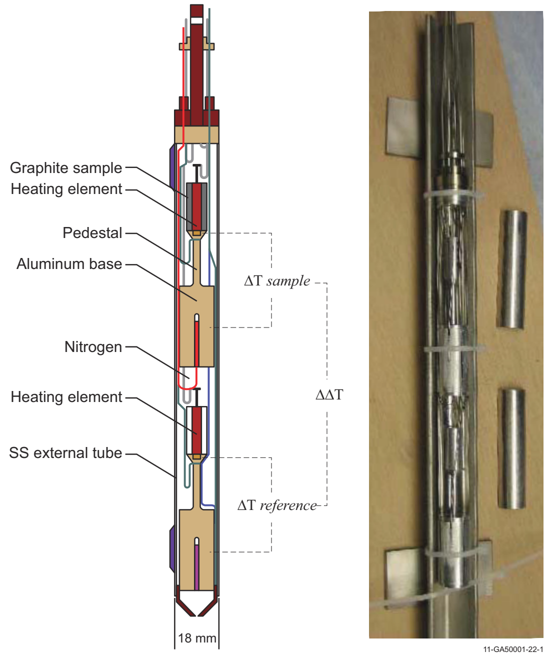

Figure 3-14. CALMOS schematic (a) and prototype (b).

Key geometric parameters of both cells are the height and diameter of the aluminum base, height, and diameter of the pedestal, height and diameter of the upper part of the cell determining the sample volume. During the design effort, a trade-off had to be found between thermal optimization and technological constraints. Main structural evolutions during the design phase led to the addition of polished stainless steel screens to limit radiative losses. Furthermore, a highly conductive aluminum alloy (230 W/m-°C) was selected to decrease the peak temperatures of the sensor.

A CALMOS prototype with the system required to move it within the OSIRIS reactor is also shown in Figure 3-15.[14] CALMOS is now operational in OSIRIS and will be adapted for commissioning tests and operation (the CARMEN device discussed in Section 3.1.1) in the JHR.

3.2. SCK·CEN

In support of their BR1 and BR2 reactors in Belgium and to facilitate irradiations at other nuclear reactors, Studiecentrum voor Kernenergie • Centre d'Étude de l'énergie Nucléaire (SCK•CEN) continues to perform research in the areas of in-pile instrumentation development, evaluation, and fabrication.[20] Selected projects currently investigated by SCK•CEN are summarized in this section. As noted in Section 3.1, many SCK•CEN instrumentation development efforts are collaborations with CEA and some SCK•CEN efforts may be found in Section 3.1. In addition, the high neutron fluxes in the BR2 also encourages other international collaborations. For example, Section 3.2.4 describes an interesting collaboration with Technical Research Center of Finland (VTT) that allows in-pile tensile testing with sensors to detect the load applied to the specimen and the elongation of the specimen.[43]

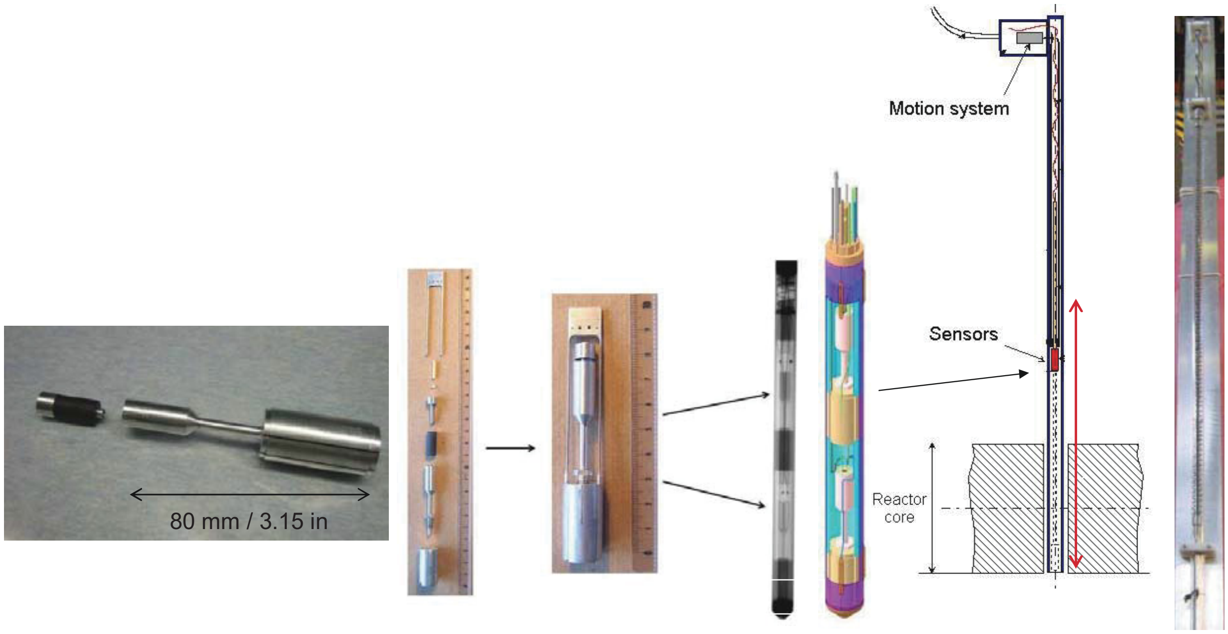

Figure 3-15. CALMOS device deployed in OSIRIS.

3.2.1. Real-time measurement of gamma and neutron fluxes

In 1999, SCK•CEN manufactured the experimental device, DOLMEN (Device for On-Line MEasurement of the Neutron flux). This instrument contains SPNDs, activation dosimeters, and gamma thermometers that can be moved vertically in any BR2 channel. Prior to manufacturing this device, SCK•CEN optimized the DOLMEN design using data from an irradiated Rhodium-SPND and two specifically designed gamma-thermometers in various BR2 channels. In addition, SCK•CEN theoretically studied the sensitivities of each type of SPND versus neutron and gamma spectra. The SCK•CEN-developed computer model SEDEIRA (SElf-powered DEtector of Ionizing RAdiation) showed the importance of the insulator in the SPND and the role played by the neutron spectrum on the detector performance. SCK•CEN is developing a new Monte-Carlo model, which will allow analysts to evaluate the signals from in-pile monitoring devices in the BR2 and parasitic effects of neutron and gamma fluxes in the instrumentation chain. The DOLMEN device has been inserted into the BR2. Objectives of this irradiation include developing an algorithm for estimating the actual neutron flux using the measured electric signal, identifying the sensitivity to each parameter (neutron spectrum, gamma spectrum), qualifying a calibration method, and assessing the best suitable SPND for specific applications.

3.2.2. Radiation-hardened Micro-electronics for Nuclear Instrumentation

SCK•CEN has also initiated an effort to develop new electronics and communication equipment capable of withstanding in-pile irradiations with radiation levels in excess of several MGy. Goals of this task are to identify commercially available equipment and to ultimately design improved radiation tolerant (> several MGy) integrated electronic circuits. Using a stepwise approach, SCK•CEN design efforts first focussed on developing circuits with discrete components that can withstand radiation. This enables SCK•CEN to develop innovative instrumentation and communication tools for the next generation of nuclear reactors, where both radiation hardening and miniaturization play a dominant role.

3.2.3. Fiber Optic Testing

MTRs could benefit from advantages offered by fiber-optic communication and sensing systems. However, the deployment of such systems in nuclear environments has been limited up to now, mainly due to reliability constraints. Prior investigations[44,46] have shown that the lifetime of fiber-optic components depends on the fiber composition, the temperature, the total dose, and the operating wavelength. Radiation (gamma and neutron exposure) affects the optical transmission of silica by creating various point defects of different nature that absorb light at specific wavelengths.[47,48] This Radiation-Induced Absorption (RIA) is particularly strong in the ultraviolet (UV) spectrum, which limits the fiber applicability to a very low dose (typically less than 10 -100 Gy) over short fiber lengths. Compared to the UV spectrum, fiber-optic transmission in the visible spectrum is less critical, but transmission can still remain a concern (especially for long fiber paths) due to the formation of an absorption band at 600 nm.

Optical absorption (< 0.5 dB/m at 630 nm) has been demonstrated in aluminum-coated fibers irradiated with γ-rays up to 6 MGy[48] and <5 dB/m under fission reactor irradiation up to ~20 MGy and neutron fluence (E_n > 0.1 MeV) of 5 x 10^{17} n/cm^2.[49,50] At the higher dose regimes encountered in MTRs, optical fiber use is possible for wavelengths above 800 nm. Previous in-core reactor experiments carried out in MTRs in Europe and Japan demonstrated that RIA can remain limited to a few dB/m in the 800- to 1100-nm range even after intense irradiation up to the GGy level and 10^{19} n/cm^2.[51,52,53] Such RIA in the near infrared spectral region opens perspectives for the development of new types of in-core reactor instrumentation based on optical fiber sensor (OFS) technology.[54,55] OFSs offer attractive and unique sensing capabilities that are of particular benefit for MTR measurements. The major advantages are the capability for passive remote sensing with the potential for high accuracy and operation at high-temperature (500–1000 °C). In addition, OFSs feature capabilities for distributed sensing with extremely limited intrusiveness. Low intrusivity is especially important, not only because of limited space availability but also because small sensors will not disturb the temperature and radiation profile of the material under study.

As part of a collaboration between CEA and SCK•CEN, a program is underway to develop a new OFS prototype with the aim of measuring dimensional changes on nuclear materials irradiated in MTRs. As part of this effort, the COSI experiment was completed in which the single mode (SM) and multimode (MM) optical fibers listed in Table 3-2 were irradiated during 2006 in the OSIRIS reactor for 92 days (corresponding to a thermal fluence of 10^{21} n_{th}/cm^2 and a fast fluence of 10^{20} n_{fast}/cm^2, and a calculated gamma dose rate of 7.2 x 10^6 Gy/hr, with an integrated ionizing dose of 16 GGy). This duration, which corresponds to representative conditions during a typical materials irradiation program, is over an order of magnitude increase than other tests reported in the literature.

Table 3-2. Single mode and multimode optical fibers tested in OSIRIS COSI test.

Fibers	Manufacturer	Manufacturer Designator (SM or MM)	Core/Cladding Diameter	Coating
FORC1 FORC2 FORC3	Fiber Optic Research Center (Moscow)	-/SM	~10 µm/150 µm	acrylate
B11 B13	Blaze Photonics (Cristal Fiber)	HC 1060-02/SM	9.7 µm (hole)/125 µm	acrylate
STU1 STU1	Polymicro	FIP100.110.125 STU//MM	~100 µm /110µm	polyimide
FIL1 FIL2	Polymicro	FIP100.110.150 /MM	~100 µm /150µm	aluminum
FVL1 FVL2	Polymicro	FIP100.110.150 /MM	~100 µm /150µm	aluminum

As shown in Figure 3-16, the fibers were mounted onto an aluminum plate and placed in a 2 mm internal diameter stainless steel tube. The fibers made a loop with a bend radius of either 23 or 32 mm. The fluence was measured using an SPND. Although placed in the periphery of the core, the central part of these 40 m fibers was close to the reactor core. Results from this test indicate that there are SM and MM optical fibers with acceptable losses for testing in MTRs. As shown by results in Figure 3-17, the most favorable spectral region (with reduced RIA) lies in the 800-1200 nm range. With measured radiation-induced losses below 10 dB, the COSI experiment confirmed that there are multimode and single-mode fibers of acceptable behavior to develop OFSs to work in the harsh nuclear environments found in MTRs.

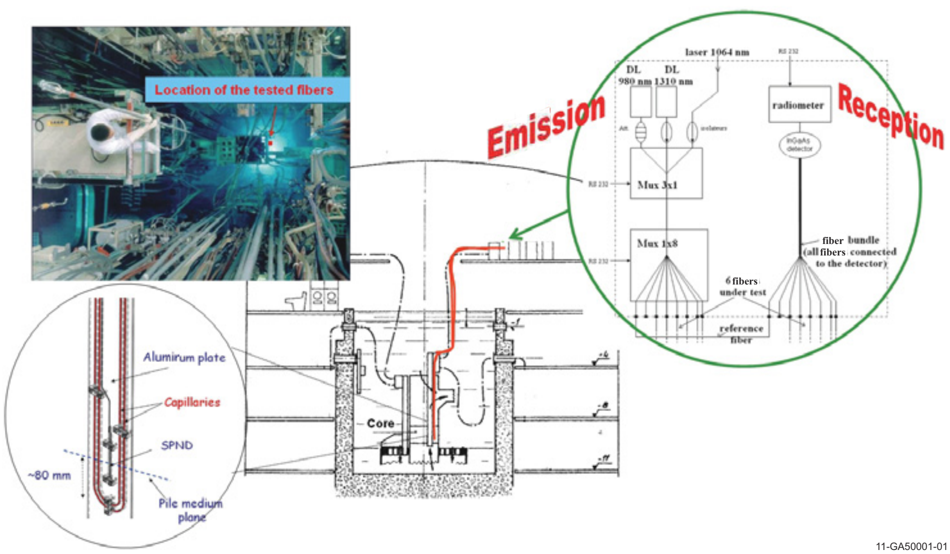

Figure 3-16. COSI test rig setup.

To address concerns about degradation of fiber optic mechanical properties, SCK•CEN also tested four standard telecom acrylate-coated Ge-doped single-mode fibers from three different manufacturers and one acrylate-coated Ge-doped multi-mode fiber. Fiber samples of 50 m were loosely coiled with a diameter of 60 mm and exposed to a dose rate of 27 kGy/h up to a total dose of 15 MGy at an ambient temperature of approximately 55 °C. Several mechanical tests were performed before and after irradiation,

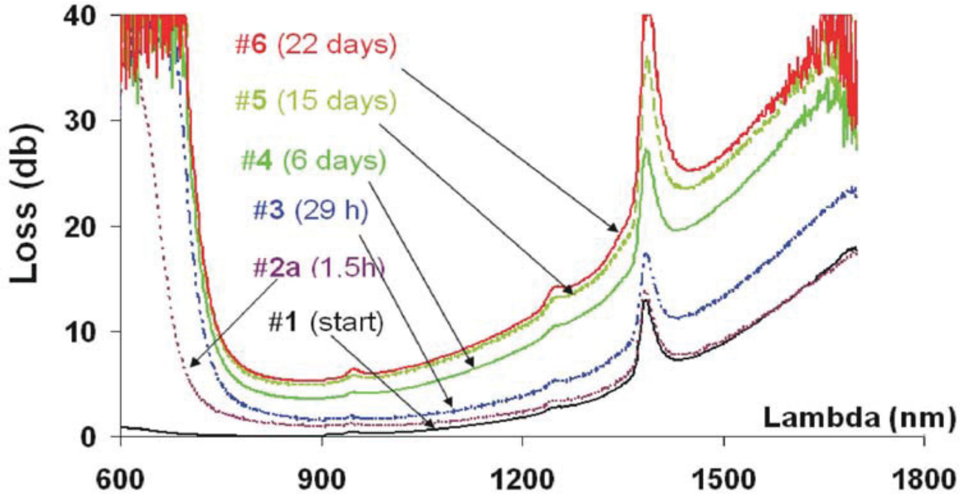

Figure 3-17. Representative results from COSI- Change in loss for the STU2 fiber (22 days corresponds to 3×10^{20} n_{th}/cm^2 and 3×10^{19} n_{fast}/cm^2).

including a two-point bend test. These destructive two-point bend tests allow quantification of the fibers' strength (50% failure stress) and the dynamic fatigue factor. Weibull analysis revealed a strength reduction of about 50% at these MGy dose levels. Scanning Electronic Microscope (SEM) images of fiber samples, which had their coatings removed after irradiation, suggest that 'roughening of the outer glass surface' may cause this degradation. These results indicate that the long-term mechanical strength of optical fibers could be seriously affected when exposed to MGy dose levels.

Figure 3-18 shows a fiber-optic based sensor jointly developed by CEA and SCK•CEN for detecting elongation of material samples during irradiation. This sensor is based on an extrinsic Fabry Perot (FP) interferometer using a radiation-resistant pure silica core fiber; a cavity is positioned at the end of the fiber and sets an optical path difference (OPD) that can be modulated by the external actions such as sensor elongation. This OPD gives rise to a characteristic optical interference pattern from which the cavity length can be retrieved by signal demodulation. The signal of this miniaturized sensor (outer diameter is about 250 µm) gives the absolute length of the cavity, which is mechanically linked to the sample elongation. This small diameter (less than 2mm) sensor takes advantage of the advantages associated with optic fiber sensors such as high resolution, easy remote sensing and multiplexing, and compact size which is of particular interest for in pile experiments. In addition, the small weight of this sensor reduces thermal effects associated with gamma heating effects. Laboratory tests have demonstrated a good accuracy, less than 1% error over a displacement of 100 µm at room temperature.

Prior to irradiation testing, improvements were made to minimize the consequence of radiation-induced silica compaction and to refine the fixing technique.[44,45] Irradiation testing of this sensor was performed in the SMIRNOF-7 experiment in the BR2 during 2012.[14] During this test, temperatures remained below 150 °C. The integrated fast neutron fluence of 2.5×10^{19} n_{fast}/cm^2. Results, as shown in Figure 3-19, indicate drifts that are a factor of 10 smaller than with commercially-available FP sensors.

Currently, CEA and SCK•CEN efforts are focussed on improving the robustness of this sensor. Specifically, an enhanced design is being developed that will allow its use at higher temperatures by employing enhanced sealing techniques with a higher temperature optical fiber with aluminum or gold coatings. The

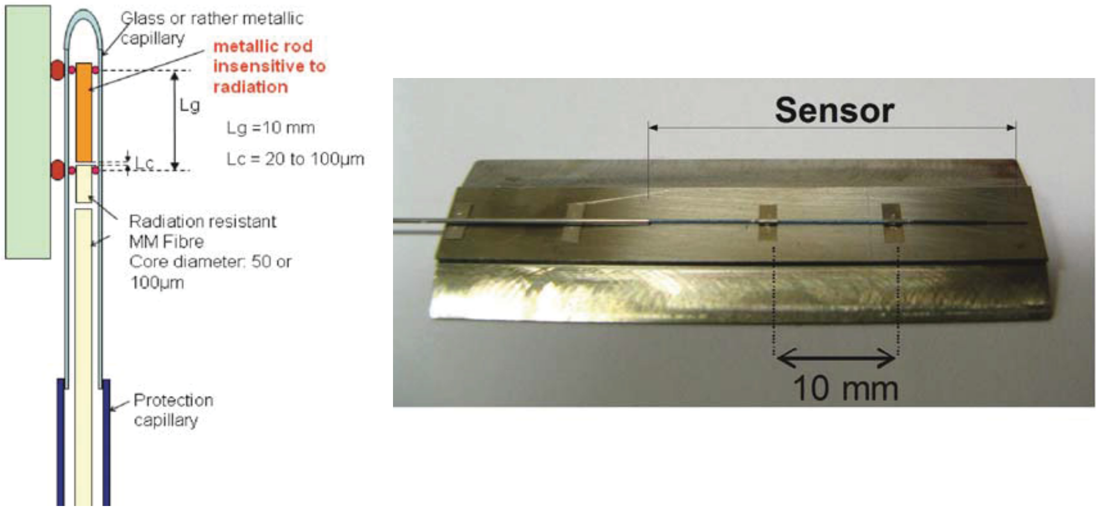

Figure 3-18. Optical fiber based elongation detection sensor developed by CEA and SCK•CEN.

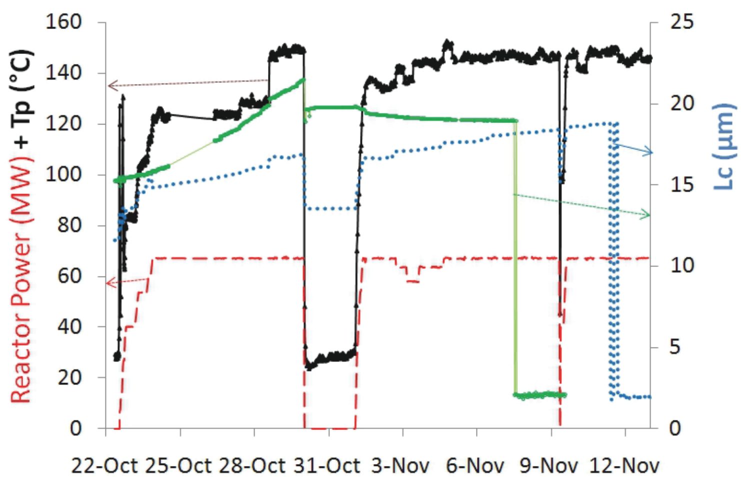

Figure 3-19. SMIRNOF-7 data obtained from fiber optics elongation probe.

test rig (see Figure 3-20) featuring this enhanced fiber optics based elongation sensor will be subjected to temperatures up to 400 °C in the SMIRNOF-8 test, which was initiated in August 2012 at the BR2.

3.2.4. In-Pile Tensile Testing

As part of a European Fusion Development Agreement (EFDA), the BR2 has been used to demonstrate the performance of an in-pile tensile test module developed by VTT. As discussed in Reference 43, it is recognized that it is unlikely that the primary damage experienced by a specimen will be affected by the applied stress during irradiation. However, it is believed that the subsequent process of dislocation formation, that is responsible for radiation hardening, yield drop, and plastic flow localization, will be substantially altered by the applied stress. It is speculated that the fatigue lifetime during in-situ cyclic loading

Figure 3-20. SMIRNOF-8 test rig incorporating fiber optics based elongation sensors.

experiments may be significantly different from the ones obtained during fatigue experiments on specimens in the post-irradiated condition. Hence, an in-situ material testing system was developed by VTT and used to perform fracture mechanic, corrosion fatigue, tensile, and electrochemical measurements in the BR2.

As shown in Figure 3-21, this test system is based on the use of a pneumatic loading unit, which loads a test specimen using gas to pressurize metallic bellows, and a LVDT from IFE/HRP (see Section 3.3.1) to measure the resulting displacement produced in the tensile specimen. The outside diameter of the module is 25 mm, and the total length of the module with the LVDT is 150 mm. Figure 3-22 shows the actual test rig with this module developed by Mol for irradiations in the BR2. During irradiation, the test assembly remained submerged in stagnant demineralized water. For approximately 300 hours, the specimens were exposed to a neutron flux of 3×10^{13} n/cm^{2}s (E > 1 MeV) corresponding to a displacement damage rate of ~6×10^{-8} dpa/s. The temperature of the test module increased rapidly (up to 90 °C within 15 minutes) due to gamma heating power of 4.4 W/g. Then, the desired strain was applied to the specimen.

The load generated by the pneumatic loading unit with the metallic bellows was calculated from the pressure difference experienced by the bellows. The stiffness and effective cross section of the bellows impacts the load produced by the specimen. However, the 'stiffness' of the pneumatic loading unit differs from the stiffness of the bellows. Hence, VTT developed a calibration unit (see Figure 3-23) to correlate the applied gas pressure in the bellows with the actual load acting on the tensile specimen. A two step calibration procedure was implemented. In the first step, the characteristic stiffness of the bellows together with friction forces of the moving parts of the module were determined. In the second step, the load induced on the tensile specimen by the applied gas was measured by a load cell.

3.3. IFE/HRP

The OECD-sponsored Halden Reactor Project (HRP), which is operated by the Norwegian Institutt for Energiteknikk (Institute for Energy Technology) [IFE], has more than thirty years of experience in performing complicated in-core measurements and experiments in the HBWR using specially-developed sensors.

As listed in Table 3-1, a wide range of in-core instrumentation has been developed, fabricated, and deployed by the IFE/HRP for measuring key fuel and material performance parameters such as fuel tem-

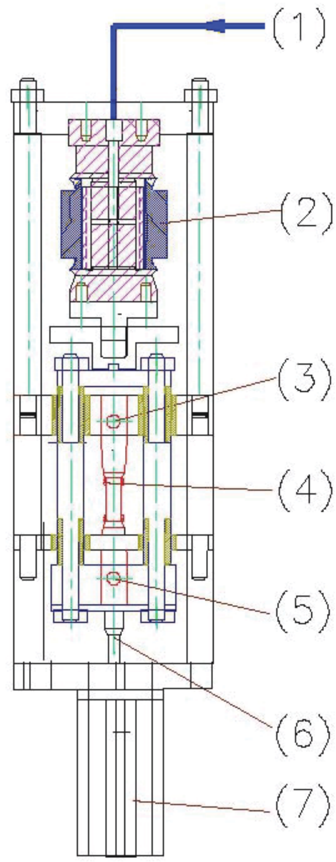

Figure 3-21. Schematic of tensile test module: (1) gas line, (2) pneumatic loading unit, (3) firm specimen fixing point, (4) specimen, (5) movable specimen fixing point, (6) LVDT plunger and (7) LVDT holder.

perature, fuel swelling/densification, fission gas release, cladding creep, corrosion/crud buildup, and crack-growth rates.[56-68] Instruments are also available for monitoring the irradiation environment (e.g., SPNDs and miniaturized gamma thermometers) and thermal-hydraulic and water chemistry conditions (e.g. flow meters, Electrochemical Corrosion Potential (ECP)-electrodes and conductivity cells). HRP-developed sensors can be attached to non-irradiated fuel rods and material samples or to pre-irradiated fuel rods and material samples by using remote operated manipulators and specially-designed re-instrumentation equipment. Ongoing IFE/HRP instrumentation development focuses on high temperature conditions and on new methods for detection of cracking, corrosion, creep, and crud buildup of materials and improved methods for studying thermo-mechanical behavior and fission gas release from LWR fuel during accident conditions and for characterizing the performance of new fuels and cladding materials proposed for LWRs.[66,67]

The HRP relies heavily on specialized in-core instrumentation and standardized test rigs in order to perform fuel and material irradiation programs in the HBWR. In recent years, IFE/HRP has become a supplier of in-pile instrumentation for other test reactors (e.g., OSIRIS, BR2, and HANARO). This section provides additional information about selected IFE/HRP instrumentation development activities. In addition, descriptions are provided for selected standardized test rigs.

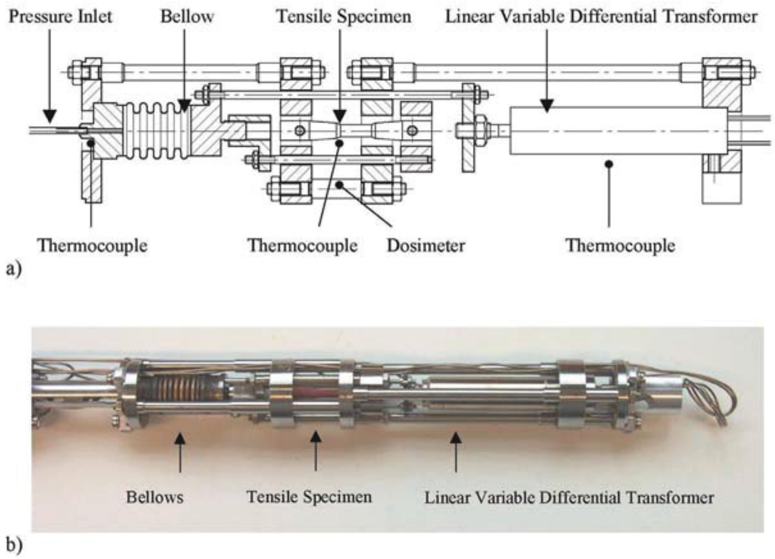

Figure 3-22. Tensile test rig for BR2 irradiations: (a) simplified layout and operational features including necessary instrumentation; and (b) final assembly of test module prior to installation in the test rig.

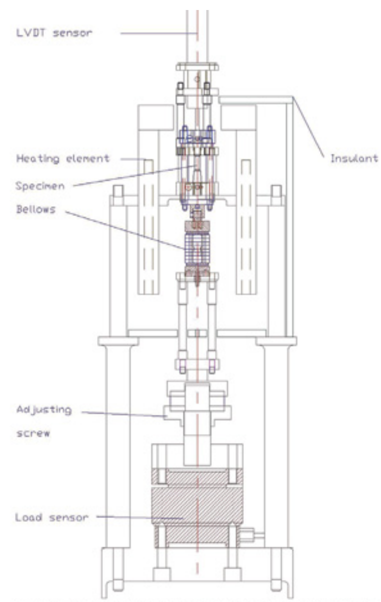

Figure 3-23. High temperature calibration device of the pneumatic loading unit.

3.3.1. LVDTs

Many IFE/HRP-developed sensors rely upon LVDTs as a base instrument. The principle design of an LVDT is shown in Figure 3-24. LVDTs are electrical transformers with three coils placed end-to-end around a tube (see Figure 3-24a). The center coil is the primary, and the two outer coils are the secondaries. A cylindrical magnetically-permeable core, attached to the object whose position is to be measured, slides along the axis of the tube. An alternating current is driven through the primary, causing a voltage to be induced in each secondary which is proportional to its mutual inductance in the primary. As the core moves, these mutual inductances change, causing the voltages induced in the secondaries to change. The coils are connected in reverse series, so that the output voltage is the difference between the two secondary voltages. When the core is in its central position, equidistant between the two secondaries, equal but opposite voltages are induced in these two coils, so the output voltage is zero (see Figure 3-24b).

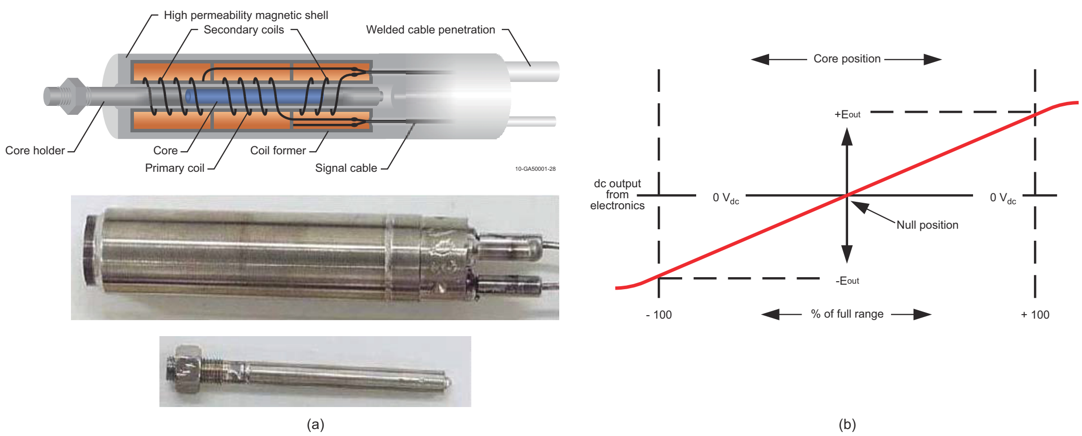

Figure 3-24. Principle design of a LVDT.

In the IFE/HRP LVDTs, the primary coil is activated by a constant current generator (at 400-2500 Hz). The position of the magnetically-permeable core can be measured with an accuracy of ± 1-10 μm (references vary on this value). IFE/HRP fabricates LVDTs in many different sizes. A frequently used size is the "type 5" LVDT, which has a linear range of 62.5 mm (e.g., the type 5 designation refers to the LVDT's linear range). This LVDT has a diameter of 11.5 mm and a length of 55 mm. The signal cables are two-wire mineral-insulated (Al_2O_3) cables with a 1.0-mm-diameter Inconel alloy 600 sheath. Since the IFE/HRP began making in-core measurements, more than 2200 different types of LVDTs have been installed in test rigs in the HBWR and other test reactors around the world. A failure rate of less than 10% after 5 years of operation is typical for IFE/HRP LVDTs operating in BWR, PWR or CANDU conditions. Hence, operating experience has shown that these frictionless sensors are robust instruments for detecting dimensional changes in lower-temperature, irradiation environments. Sections 3.3.2 though 3.3.5 describe some of the LVDT-based sensors developed and deployed by IFE/HRP.

The IFE/HRP 'type 5' LVDTs are designed to operate under PWR conditions (350 °C and 150 bars). The temperature limit is based on the Curie point of nickel. The wire used for the coils of the instruments consists of a copper conductor with nickel cladding. As the temperature passes through the Curie point of nickel (356 °C to 358 °C), there is a noticeable change in the output signal and a change in the instrument sensitivity. However, in collaboration with INL, an LVDT that can operate at temperatures up to 600 °C has been developed using alternative components and fabrication techniques (see Section 5.3). Currently, IFE/HRP is investigating additional options to extend LVDT operating temperatures to 900 °C.[67] By using alternate materials, fabrication, and component drying processes, laboratory evaluations suggest that LVDTs could operate in conditions applicable to gas, supercritical water, sodium, lead, and lead bismuth cooled reactor conditions. Higher temperature prototype LVDTs have been installed in irradiation test rigs and operated successfully at temperatures up to 700 °C for over a year in the HBWR.

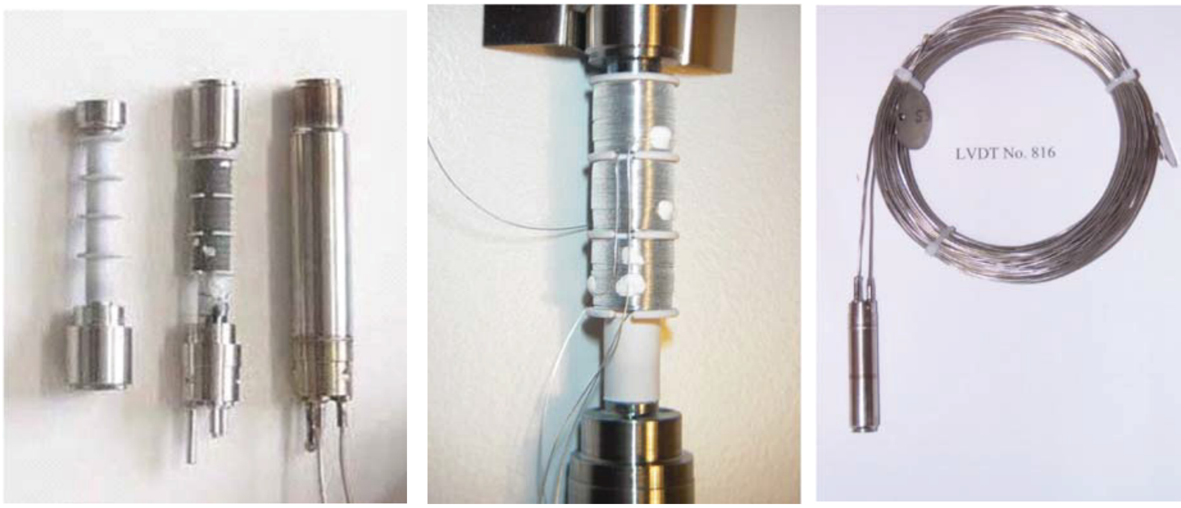

Figure 3-25. IFE/HRP LVDT components and completed sensor prior to shipping.

3.3.2. Fuel centerline temperature measurements

For monitoring fuel centerline temperatures, the IFE/HRP uses thermocouples and/or expansion thermometers. Fuel centerline temperature measurements provide important information on the thermal performance of the fuel and if desired, the fuel thermal conductivity. By monitoring the fuel thermal conductivity over a longer period of time, the fuel thermal conductivity degradation as a function of burn-up is studied. An example of UO_2 thermal conductivity data derived from fuel centerline temperature measurements is illustrated in Figure 3-26. Informal discussions[59] indicate that such tests have been done with specially-designed fuel rods with a small as-fabricated fuel-to-clad gap that minimizes the influence of gap conductance change (densification/swelling, fission gas release) on the fuel center temperature during the irradiation. Smaller diameter fuel rods are often used in such tests to increase the burnup accumulation rate. In addition, in-pile local power measurements are required for such tests.

IFE/HRP fuel centerline thermocouples normally operate for several years in-core without failure, but the lifetime of "Type C" tungsten-rhenium HBWR thermocouples has been found to decrease with increasing fuel centerline temperatures. If the fuel centerline temperature exceeds 1400 to 1500 °C, the expected lifetime of the Type C thermocouples, which must be used with an HBWR-specific correction factor to offset transmutation, is typically less than one year (although no fluence values were cited, HBWR peak thermal flux is 1×10^{14} n/cm^{2}s). Furthermore, informal discussions with HRP staff indicate that 'batch-to-batch' variations have been observed in Type C thermocouples procured from various vendors.[59]

The IFE/HRP expansion thermometer (see Figure 3-27) consists of a tungsten rod (a molybdenum rod may also be used if transmutation is of concern) that is inserted through a hole drilled in a fuel stack. The thermal expansion of the tungsten rod is measured using an LVDT. The fuel centerline temperature is then derived from the measured expansion of the tungsten rod. The expected lifetime of an expansion thermometer is longer than for a thermocouple, but the resolution of an expansion thermometer is less than a thermocouple because the expansion thermocouple only provides an estimate of the average temperature over the length of the rod. There is also the potential for mechanical interactions between the fuel and the tungsten rod that can affect expansion thermometer performance.

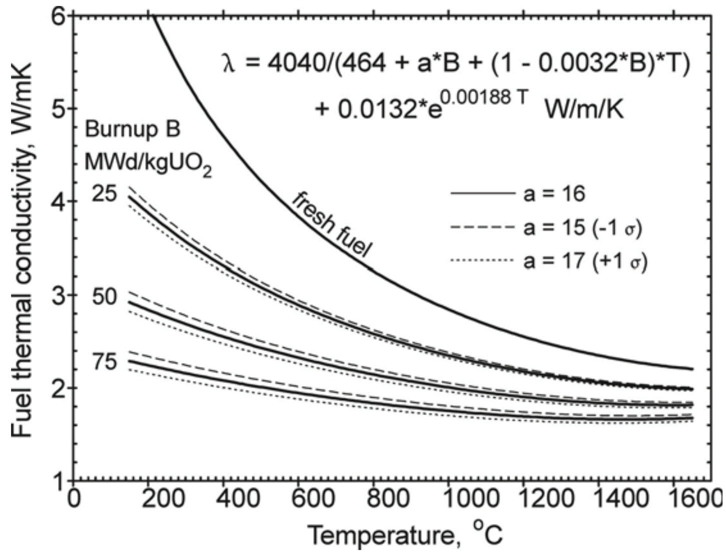

Figure 3-26. Fuel thermal conductivity derived from fuel centerline temperature measurements.

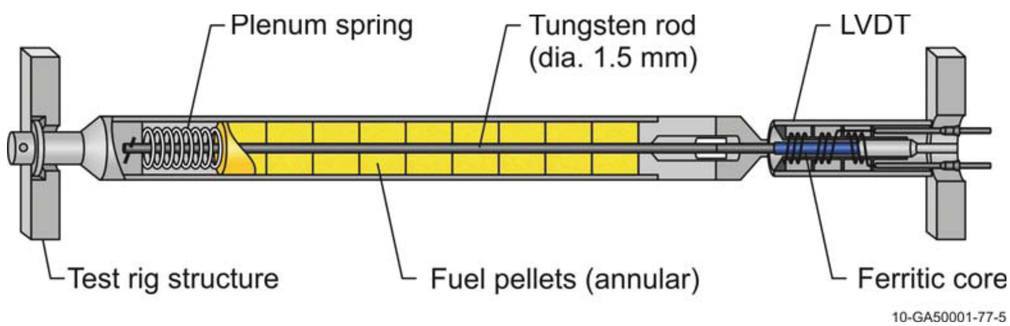

Figure 3-27. Thermal expansion thermometer.

3.3.3. Fuel densification / swelling measurements

The mechanical stability of nuclear fuels is an important performance parameter. For in-pile monitoring fuel stack-length changes, the HRP has also developed instruments based on LVDTs. In order to measure fuel densification and swelling, the magnetic core of the LVDT is attached to a spring-loaded plate in contact with a fuel pellet in one end of the fuel stack (see Figure 3-28). The magnetic core then follows the expansion and contraction of the fuel stack and provides data on the fuel's mechanical behavior.

3.3.4. Fuel rod pressure measurements

IFE/HRP monitors fuel rod internal pressure to gain insights about fission gas release during irradiation. The pressure transducer consists of a miniaturized bellows mounted in the fuel rod end plug (see Figure 3-29). A magnetic core is fixed to the free moving end of the bellows; the other end of the bellows assembly is fixed to the end plug. The bellows is typically pressurized to 2 bar less than the initial rod pressure and seal welded. Bellows/core movements are sensed by an LVDT. The bellows differential pressure will, in addition to release of fission gases, be dependent upon fuel densification/swelling characteristics, changes in gas temperature and fuel/cladding thermal expansion during operation. Densification will lower

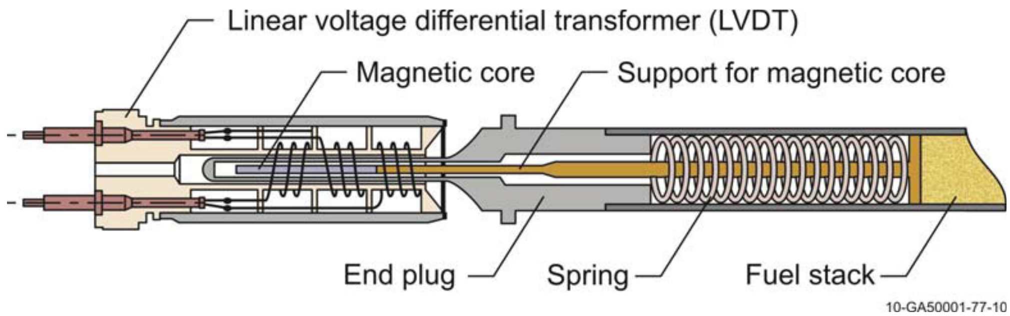

Figure 3-28. Fuel stack elongation detector.

the fuel rod internal pressure, while swelling and gas temperature effects and fuel differential expansion will increase fuel rod internal pressure.

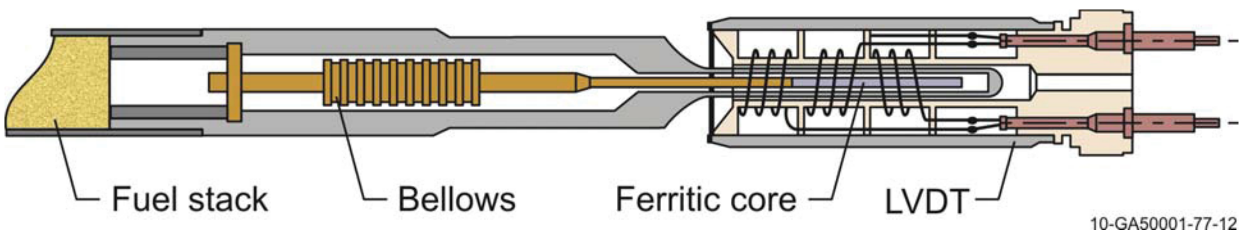

Figure 3-29. Pressure gauge

The pressure transducers are available for different pressure ranges. The most common ranges have a Δp (internal versus external pressure of the bellows) of 15 bar (type I), 30 bar (type II), or 70 bar (type III). The difference between these bellows is related to the stiffness/spring rate. During the initial stages of fission gas production, it is often necessary to use a bellows with high sensitivity (but a limited pressure range). For such conditions, the 15 bar bellows is selected. For high burnup tests in which high rod pressure is expected, the 70 bar bellows is used. The higher pressure range is achieved by sacrificing sensitivity. Under realistic conditions, the uncertainty of the pressure for the 30 bar sensor is ±0.2 bar; for the 70 bar sensor, the uncertainty is ±0.5 bar.

In order to keep the same precision as a type II transducer, while still being able to reach 70 bars, a new type of transducer has been designed. Two different bellows, having different levels of stiffness, are connected in series. In this way, the softer bellows is dominant at lower pressure. When reaching the maximum pressure for the softest bellows of the two, further compression of this bellows is restricted by an internal mechanical stop. The stiffer bellows then becomes the only contributor to the signal output. Measurement ranges up to 150 bar (15 MPa or 2180 psig) are possible. To reduce material creep at high temperature and radiation intensity, the bellows are pre-pressurized (inside) and conditioned for several days at high pressure and temperature. The pressure transducer can be systematically re-calibrated during reactor outages using procedures developed by IFE/HRP.

3.3.5. Fuel Rod Diameter Measurements

The IFE/HRP DG enables on-line measurement of cladding diameter for assessing cladding creep, pellet-cladding mechanical interaction, fuel creep / relaxation and fuel rod crud deposits. A representative standardized test rig (shown in Figure 3-30a) provides a method for real-time in-pile measurement of fuel rod diameter changes, temperature, neutron exposure and loop coolant temperature, flow, and chemistry (e.g., concentration, pH, etc.). IFE/HRP relies on LVDT-based technology in their DG. However, as shown in Figure 3-30b, the LVDT design has been modified. First, the two primary coils and the two secondary coils are wound on a ferritic bobbin, as opposed to the Inconel alloy bobbin of the LVDT. Second, the DG uses an armature instead of the magnetically permeable core used in the LVDT. As indicated in Figure 3-30b, changes in distance between each of the secondary coil loops and the armature that may occur as the diameter travels along the fuel rod changes the balance between the signals generated in the two secondary loops, leading to a change in the output signal (difference of the two secondary coil signals) from the DG.

The DG travels along the fuel rod using an in-core hydraulic drive and positioning system. In some test rigs (see Figure 3-30a), the fuel rod is moved by the hydraulic drive. The accuracy of the DG is ± 2 μm, and a calibration is performed in conjunction with each diameter trace by having calibration steps on both fuel rod end plugs. The DG can operate at up to 165 bar and 325 °C.

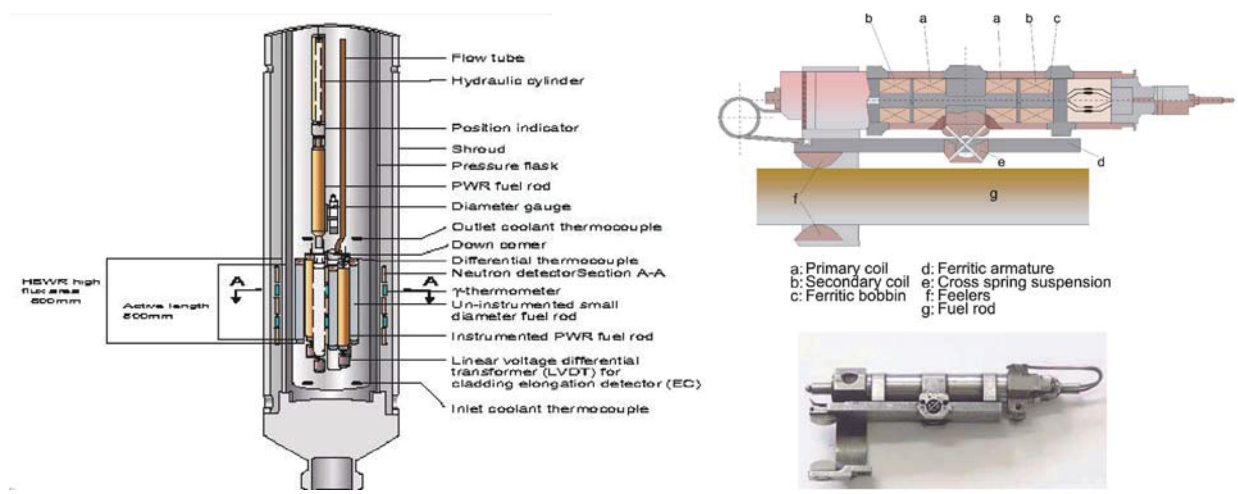

(a) (b)

Figure 3-30. HRP fuel pellet cladding interaction/crud deposition test rig (a) with DG (b).

Figure 3-31 shows results from diameter measurements on a typical PWR fuel rod irradiated in the HBWR as part of a PWR crud evaluation program. The irradiation is performed in a PWR loop system that allows variations in water chemistry parameters during irradiation. DG run no. 7275 was performed immediately after startup of the experiment to provide initial fuel rod diameter data. DG run no. 7739 was performed after approximately 230 days at full power and shows cladding creep-down typical for PWR fuel rods. Diameter run. no. 7754 was performed after an additional 25 days after changing the water chemistry in the loop system. The water chemistry change included an increase in the iron and nickel content. The diameter trace shows that crud deposits formed on the upper part of the fuel rod. The possibility of observing the formation of crud by monitoring the fuel rod diameter on-line along with changes in neutron flux and fuel temperature provides the IFE/HRP insights into developing a remedy for crud and related phenomena such as "Axial Offset Anomaly".[61]

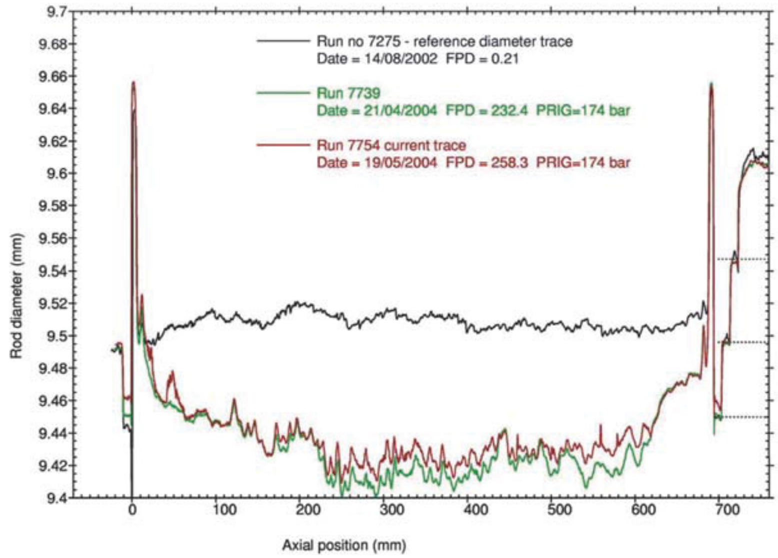

Figure 3-31. Fuel rod diameter traces showing cladding creep down and crud deposition.

As can be seen from Figure 3-30b, the design of the DG is rather complicated, and sections of nonmagnetic material have to be welded to sections of magnetic material. Therefore, a new design is under investigation by IFE/HRP in which the outer wall of the DG consists of a single tube of Inconel alloy 600. The design was optimized using finite element calculations to minimize magnetic flux leakage.

The inner body is now made from one piece, where the coil separators are integral parts of the body. In order to prevent flux linkage between the (magnetic) coil separators and the ferritic armature ("anchor"), the part of the separators facing the anchor is shaved off, making a large air gap between coil separators and the housing (see Figure 3-32). Using an outer body of Inconel increases the distance between the magnetic inner parts and the anchor, leading to a loss of sensitivity. To compensate for this, the distance between the anchor and housing has been slightly reduced. In addition, the inner body will be made out of silicon iron, which should have a significantly higher magnetic permeability than the AISI 403 currently used in the standard DG. Other possible benefits of this material are reduced eddy current losses, leading to reduced temperature sensitivity. Figure 3-32 shows an example of the coiled DG body. Tests show that the new DG, operated in self-compensating mode, has a linear response over the range ±0.9 mm, which is much longer than the 0.2-mm range typically required for in-pile applications. The accuracy of the new type of DG is ~2 µm.

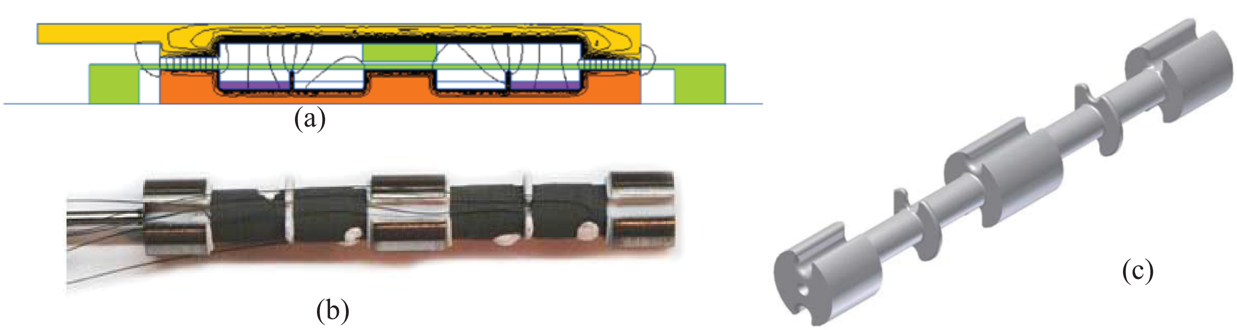

Figure 3-32. Simplified DG; (a) finite element analysis showing magnetic field patterns; (b) inner body with coils; and (c) inner body.[64]

3.3.6. Crack-growth measurements

In order to monitor crack-growth rates in core structural component materials, the IFE/HRP utilizes miniaturized Compact Tension (CT) specimens and the "direct current potential drop method" for measuring crack propagation. The direct current potential drop (DCDP) method (see Figure 3-33) is based on sending an electrical current through the specimen and measuring the potential (voltage) at several locations on the CT-specimen. The measured potentials depend on the propagation of the crack. Thus, the crack-length can be determined from the measured potential drops. Reference 64 reports results in which this approach was successfully applied to detect changes in crack growth rate due to variations in coolant pH for various metals. IFE/HRP has applied this technology to detect the impact of coolant parameters (pH, impurities, boron concentration, etc.) on fuel cladding corrosion. In addition, IFE/HRP can perform such measurements on pre-irradiated fuel removed from commercial reactors.

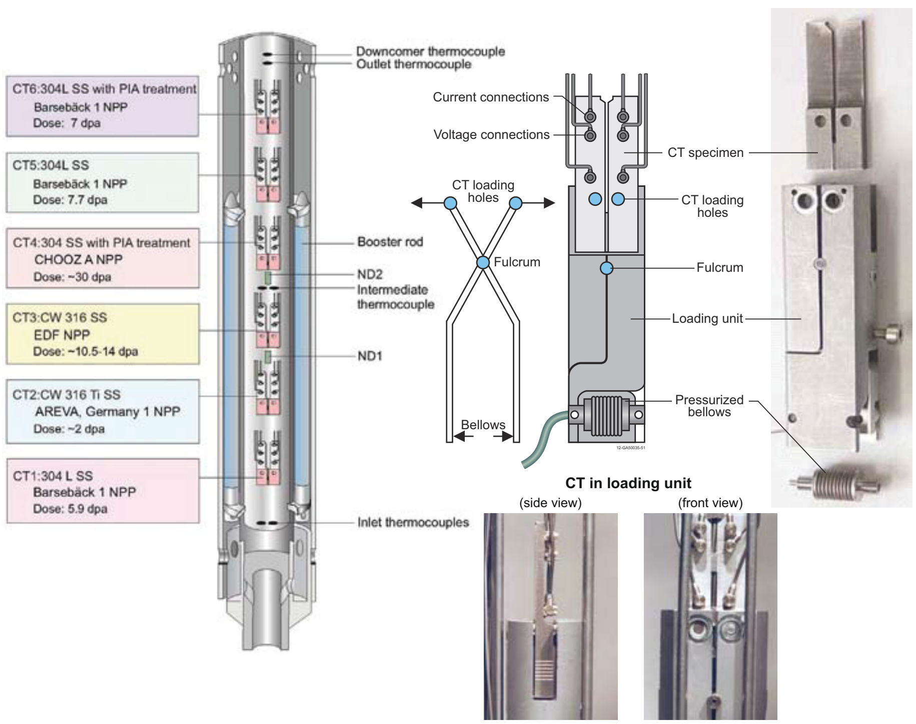

Figure 3-33. Typical crack growth test rig.

Figure 3-33 shows a CT sample for online crack growth rate measurements and a loading unit for CT specimens used in the HBWR. The figure shows a CT specimen with a square geometry. Depending on the availability of materials, the CT specimens can be made entirely from fresh materials, pre-irradiated materials, or different types of pre-irradiated inserts (square or circular). A dynamic load is applied to the CT specimens by means of individually calibrated loading units that are equipped with bellows that are pressurized with helium gas through an external system. The Direct Current Potential Drop (DCPD) method is used to measure the crack growth rate (CGR) under defined water chemistry conditions. Data for periods of stable CGR (typically 100 h) are used to calculate the actual growth rate for a CT at the given temperature, load, and water chemistry. The DCPD method can typically measure changes of ~10 µm.

3.3.7. Electrochemical Corrosion Potential

The ECP is determined by a combination of the surface conditions of the specimen and concentrations of dissolved oxidants. The ECP is a key measurement for assessing the performance of reactor structural materials. For in-core measurements, reference electrodes must be capable of withstanding in-core conditions. Although there are commercial ECP sensors on the market, the IFE/HRP has developed its own ECP reference electrodes for enhanced in-pile robustness.

Different reference electrodes are needed for different environments. A Pt electrode has been developed for use in reducing conditions. The potential sensing element consists of a Pt cylinder and end plate. The large surface area of the Pt serves to reduce the effect of any mixed potentials caused by other metal components. A schematic drawing is shown in Figure 3-34a. The Pd reference electrode is used in oxygenated water. The potential-determining reaction of the Pd hydrogen electrode is similar to that of the Pt hydrogen electrode. Palladium differs from platinum in that it can hold hydrogen within its lattice; in aqueous solutions, hydrogen can be produced by cathodic charging of the Pd. When sufficient hydrogen is produced, some will diffuse to the surface of the Pd, which can then function as a hydrogen electrode. A schematic drawing of a Pd electrode is shown in Figure 3-34b.

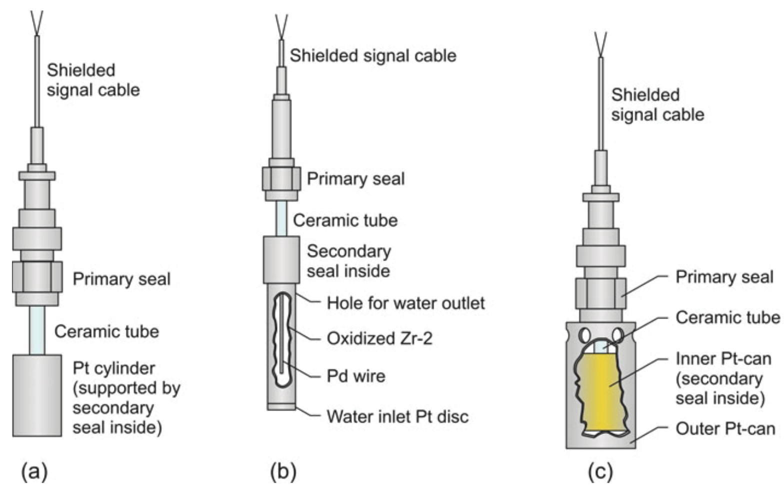

Figure 3-34. ECP sensors and conductivity cell (a) Pt ECP sensor, (b) Pd ECP sensor, and (c) conductivity cell.[63]

A novel conductivity cell, which is a modification of the Pt ECP electrode in which the Pt sensing element is surrounded by a second Pt cylinder, has been developed by IFE/HRP that can be installed in-core within pressure flasks. This design allows coolant conductivity measurements at operating temperature and pressure. An additional signal cable is included to provide current, and the conductivity of the coolant is determined from the measured voltage difference between the two Pt cylinders. A schematic drawing is shown in 3-34c. In order to characterize the chemical conditions, the IFE/HRP is also developing a miniaturized Pt electrode and a miniaturized Fe/Fe_3O_4 reference electrode (see Figure 3-35). These electrodes, which have been tested in an autoclave at 600 °C and supercritical water conditions,[67] will soon undergo in-pile testing.

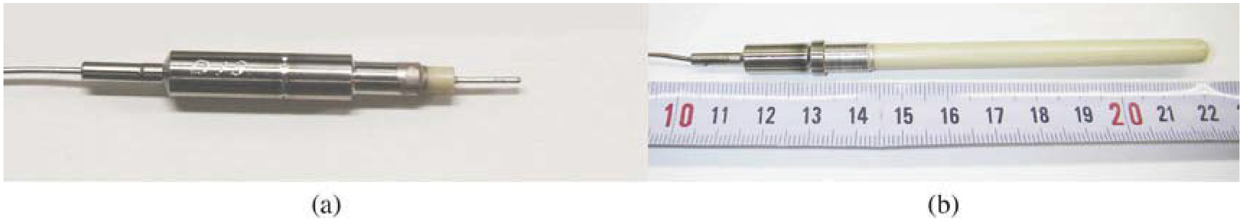

Figure 3-35. ECP-based sensors (a) Brazed Pt electrode and (b) brazed Fe/Fe_3O_4 electrode.

3.3.8. Localized Heating

Local power measurements have been made at the HBWR since 1962 using a compact (3.9 mm OD) gamma thermometer that detects heat produced by fission and fission product gamma rays.[65] Heat is transferred to the coolant sink along a closely controlled conduction path while the temperature drop is measured by a differential thermocouple. The generated signal, which is proportional to the fuel power, is strong and constant with fuel burn-up. The gamma thermometer is made of a type K differential thermocouple where the hot junction is insulated from the moderator by a gas-filled cylinder (see Figure 3-36). Heat produced by gamma absorption in an inner, thermally insulated, body results in a local rise in temperature. The temperature increase and the time constant of the gamma thermometer are used to calculate the actual gamma irradiation. The gamma thermometer can be re-calibrated in-core by applying a low direct current (DC) voltage to the differential thermocouple. The inner body of the gamma thermometer is heated by the current applied to the thermocouple for a short period of time. The decay of temperature is monitored, a relationship between temperature and decay time is used to recalibrate the gamma thermometer (see Figure 3-37).

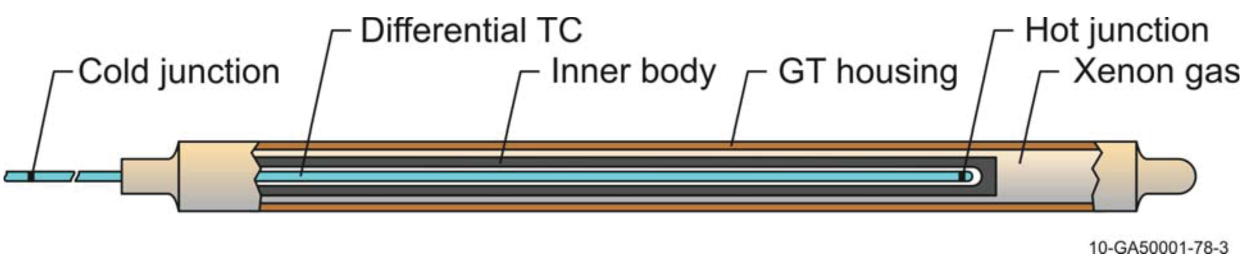

Figure 3-36. Halden miniaturized gamma thermometer.

3.3.9. Flowrate

The turbine flow meter (Figure 3-38) was the first instrument developed at the IFE/HRP. The need for accurate power calibration of individual fuel assemblies led to the development of in-core turbine flow-meters. The turbine flow meter consists of two parts: one turbine installed in a housing, and the pick up coil mounted in the test rig. If the flow meter fails, it is possible to remove the failed unit and install a new one as there are no cables associated with the turbine unit as the pick-up coil is installed in the test rig itself. Normally there are two turbines installed in an IFE/HRP test rig; one to measure the inlet flow and one to measure the outlet flow. The in-core turbine flow-meters use an electro-magnetic coil system for measuring the speed of the turbine. The rotor blades are magnetic; and each time the rotor blades pass over the pickup coil, a pulse is induced in this coil. The pulses are sensed by the electronics system giving

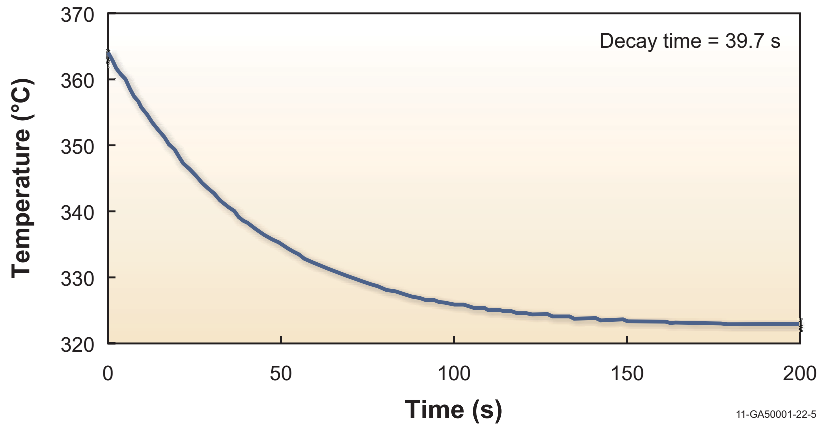

Figure 3-37. Signal decay curve used to recalibrate the Halden gamma thermometer.

online information of the flow in each test rig. Because of the high failure rates of these flowmeters, IFE/HRP is contemplating design improvements.

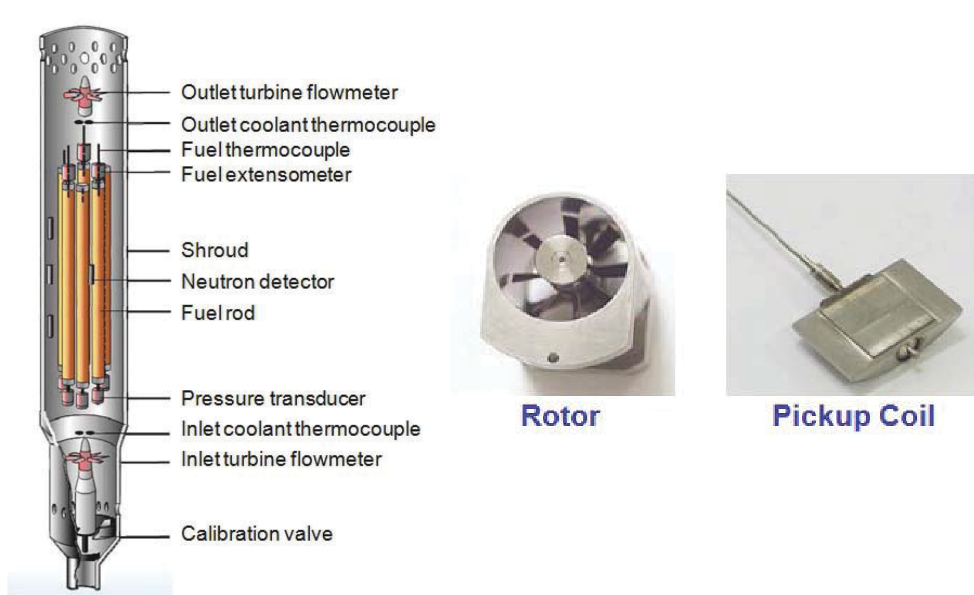

Figure 3-38. Components and position of turbine flowmeter.

3.3.10. Oxide Thickness Measurements on Fuel Cladding

Corrosion of fuel cladding under various chemical and power load conditions remains an active field of research. With the exception of the IFE/HRP DGs, such corrosion studies are nearly always performed by postirradiation examination. As an alternative to the DG, IFE/HRP is developing a probe for online in-pile measurements of oxide thickness. The probe is based on the eddy-current principle (see Figure 3-39). It consists of one sensing coil (slightly extruding) and one reference coil (situated completely inside the housing and shielded by it). The two coils are part of a resistance bridge circuit so that a small difference in coil impedance can be detected. The reason for situating the reference coil inside the probe (rather than outside the reactor) is that it allows compensation for resistance changes in the coil and the signal cables due to temperature variations. The top of the sensing coil has been designed to be sufficiently strong to withstand the external pressure while at the same time being thin enough to transmit enough of the radio frequency field to generate the eddy currents in the fuel cladding. Test results performed at room temperature show a linear response for the 0- to 100-μm region. The test setup is included in Figure 3-39. Calibrations show that the probe has a resolution as low as 1 μm. The performance of this probe has also been verified in an autoclave test (at 350 °C and 165 bar). The probe housing itself is used as the common ground connection for both coils (and in turn is connected to the cable sheath). It is planned to also verify the probe in an in-pile experiment at the HBWR.

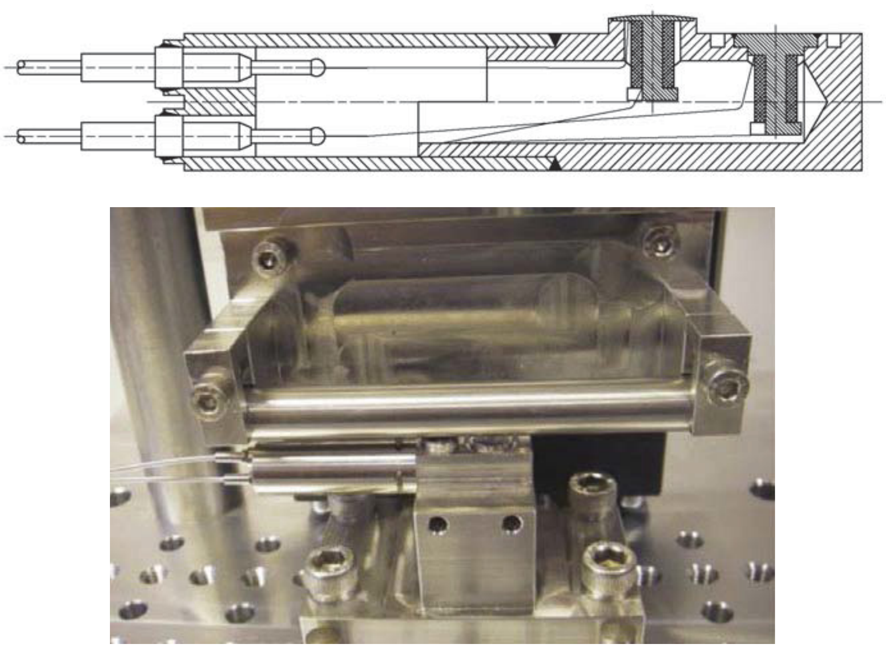

Figure 3-39. Oxide thickness probe: schematic drawing and test setup of probe with zircaloy test tube.[64]

3.3.11. Summary

Although the HBWR has a much lower power rating and is considerably older than the ATR, the instrumentation capabilities developed by IFE/HRP staff have significantly extended its irradiation capabilities. In addition, the IFE/HRP has leveraged this expertise to supply instrumentation for commercial reactors, naval reactors, and other MTRs.

The IFE/HRP use specialized in-core instrumentation in order to perform fuel and material irradiation programs in the HBWR. As discussed in this section, the IFE/HRP also has the ability to attach in-core instrumentation to pre-irradiated fuel rods and material samples from power reactors. Typically, IFE/HRP applies instrumentation to detect fission gas release and thermal conductivity degradation to pre-irradiated fuel rods. Irradiated structural material samples have also been instrumented to detect crack growth. The IFE/HRP continues to refine its existing in-pile instrumentation and develop new instruments. As discussed in this section, ongoing IFE/HRP instrumentation development focuses on high temperature conditions and on new methods for detection of cracking, corrosion, and crud buildup of materials.

3.4. JAEA

The Japan Atomic Energy Agency (JAEA) [formerly the Japan Atomic Energy Research Institute (JAERI)] provides several types of instrumentation to support tests in the JMTR.[69] Commercially-available sensors procured from Japanese vendors allow JMTR customers to detect temperatures using thermocouples and melt wires, length and diameters (using LVDT-based sensors made by Japanese vendors), fission gas release, and neutron flux (using fission chambers, SPNDs, or flux wires), and crack growth (using bellows to load a pre-cracked sample with direct current potential drop techniques). JAEA can re-instrument previously irradiated fuel rods. JAEA continues to conduct research to enhance specialized instrumentation to support high temperature irradiations. As discussed in References 69 through 74, research is focussing on new technologies for in-pile measurements of temperature, creep, neutron flux, and gamma-ray intensity distributions.

Prior to unplanned difficulties during refueling of the JOYO reactor in 2007, JAEA also conducted instrumented irradiations in this fast reactor using in-core test rigs, such as a Material Testing Rig with Temperature Control (MARICO) test rig and an Instrumented Test Assembly (INTA), and ex-vessel test rigs. In fact, the difficulties that have prevented operation of this MTR since 2007 were associated with movement of the MARICO-2 instrumented test rig. Nevertheless, some of the instrumentation typically used in JOYO tests is of interest in this review.[75]

3.4.1. Temperature

JAEA customers may select from a range of melt wire materials, including In, Sn, Pb, Ag, and Zn, and a range of alloys. Figure 3-40 illustrates a typical melt wire holder containing seven melt wires with melting temperatures ranging from 1050 to 1150 °C. In addition, Reference 75 reports the use of sodium-filled stainless steel capsules, known as Thermal Expansion Devices (TEDs) in JOYO. As shown in Figure 3-41, calibration curves have been developed for inferring the peak irradiation temperature to the observed volumetric expansion of the stainless steel capsules. JAEA reports accuracies of ± 25 °C, but earlier applications by EBR-I of these TEDs report accuracies of ± 5 °C.[76]

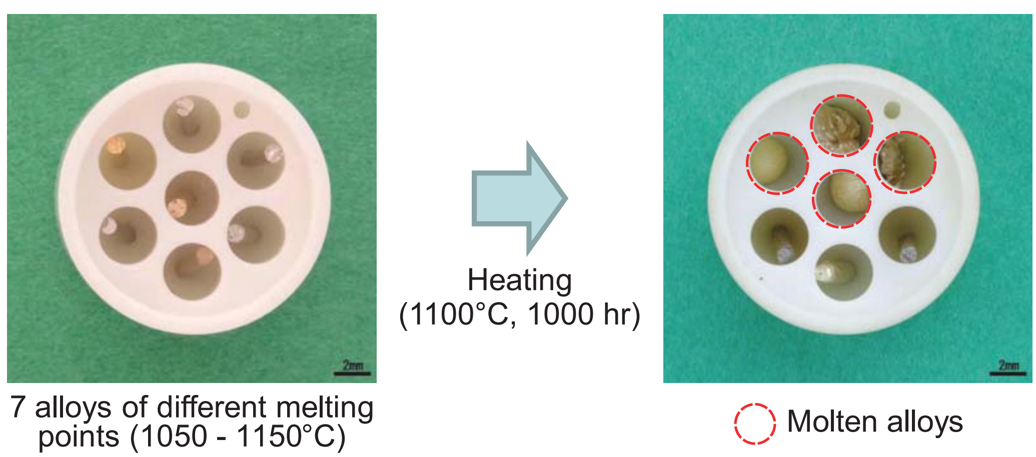

Figure 3-40. JAEA melt wire holder prior and after irradiation.

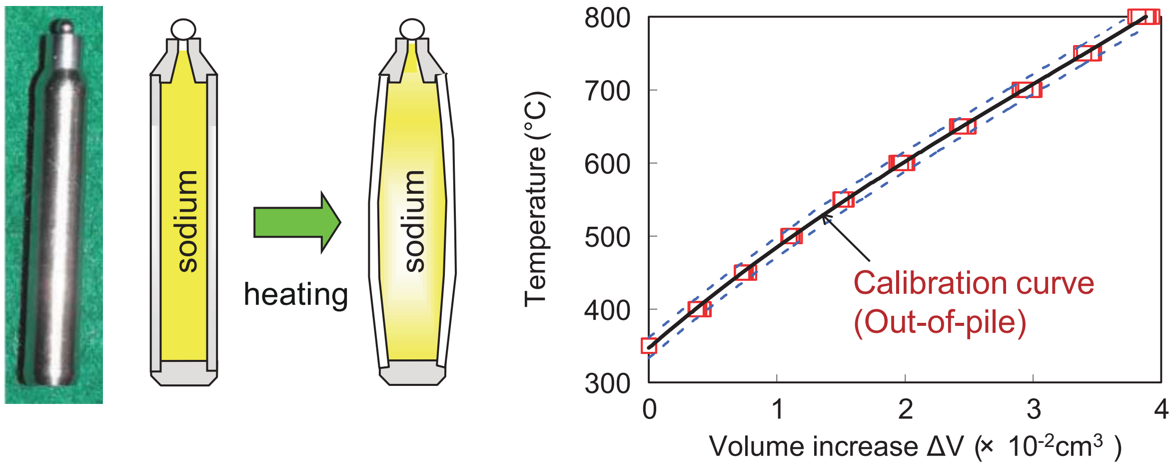

Figure 3-41. TED capsule and calibration curve relating volumetric expansion to temperature.

JAEA relies on commercially-available thermocouples (e.g., Type N, K, and C thermocouples) to measure temperatures during JMTR irradiations. Reference 74 reports JAEA efforts to develop and deploy multi-point or "multi-paired" Type K and N thermocouples (see Figure 3-42). The design of these multi-paired thermocouples is similar in that they are fabricated with MgO insulation and contained within a 1.8 mm diameter sheath (either stainless steel or Inconel). There are typically three to seven hot junction points spaced between 20 and 30 mm apart. As shown in Figure 3-42, 'dummy' MgO insulators and wires are included to fix the position of thermocouple hot junctions. Type K multi-pair thermocouples have been deployed in a 17,000 hour irradiation with peak temperatures of 700 °C. Furnace tests have demonstrated that type N multi-paired thermocouple response will remain stable after heating at 1000 °C for 3000 hours.

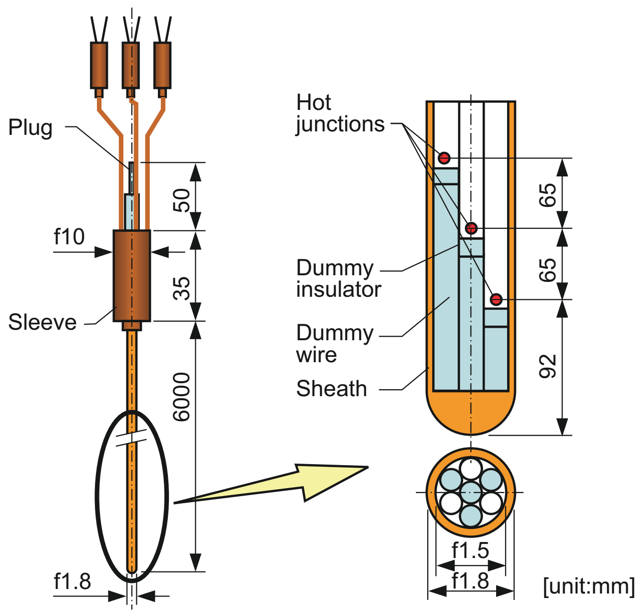

Figure 3-42. Multi-paired thermocouple design.

3.4.2. Length and Diameter

In-pile changes in length and diameter are measured by LVDTs that are made by Japanese vendors. Reference 74 reports recent JAEA efforts to increase the peak operating temperatures of two LVDT designs: one design using ceramic coated coil wire that can operate up to 550 °C and a higher temperature design mineral insulated cable for the coils that can operate up to 650 °C. The performance of these higher temperature LVDTs were recently demonstrated in a lower temperature (300 °C) irradiation test conducted at the WWR-K reactor at the Institute of Nuclear Physics at the National Nuclear Center (INP NNC) in the Republic of Kazakhstan (total fluence of ~1.5x 10^{24} n/m^2, E >1 MeV).

3.4.3. Creep and Deformation

Reference 71 describes JAEA efforts to develop irradiation equipment for in-pile creep and deformation of specimens subjected to loads of up to 10 kN at temperatures up to 600 °C. The in-vessel parts of this unit (see Figure 3-43) are installed in the reactor pressure vessel through a standpipe. This in-vessel part is 8.9 m long with the lower portion consisting of three tubular parts, two irradiation units and a guide tube, that are each 2.6 m long and 0.113 m in diameter. Although the specimens are primarily heated from reactor core heat, a smaller 300 W electric heater is included for supplementary temperature control. The neutron flux that specimens experience is monitored using SPNDs containing rhodium as the emitter. Small fluence wires are also included for post-irradiation fast and thermal fluence measurements. Temperature is monitored using Type K thermocouples, and specimen elongation is monitored by JAEA-developed LVDTs containing mineral-insulated coil material.

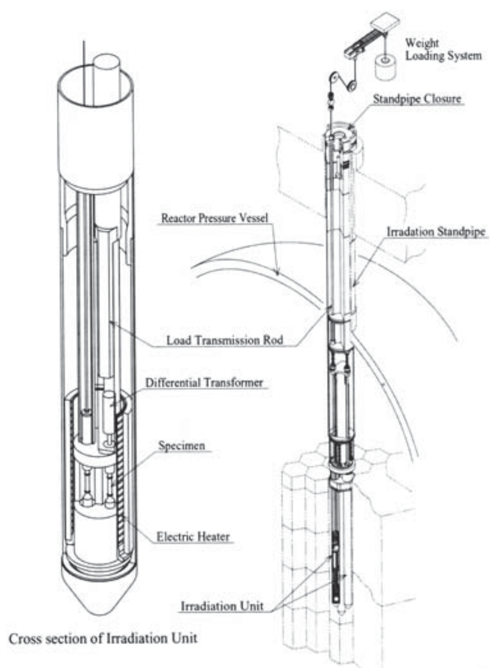

Figure 3-43. I-I type irradiation unit with weight loading equipment.

3.4.4. Fission Gas Pressure

Reference 74 also reports JAEA efforts to design and demonstrate the performance of fission gas pressure gauges that can operate at temperatures up to 650 °C and pressures up to 10 MPa. As shown in Figure 3-44, this gauge includes two springs, a bellows, and a high temperature LVDT (see Section 3.4.2). Laboratory tests indicate measurement accuracies of 1.8%. The irradiation performance of this test rig was recently demonstrated in a lower temperature (300 °C) irradiation tests conducted at the WWR-K reactor at the INP NNC in the Republic of Kazakhstan (total fluence of ~1.5x 10^{24} n/m^2, E >1 MeV).

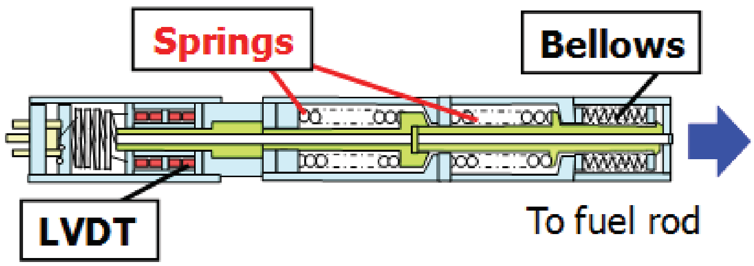

Figure 3-44. JEA fission gas pressure gauge.

3.4.5. Neutron Flux

For flux and fluence measurements, JMTR irradiations can include 1.8 mm diameter fission chambers, SPNDs, or flux wires--Fe for fast flux and Al-Co, V-Co, or Ti-Co for thermal flux. For real-time measurement of thermal neutron flux, Reference 74 reports that JAEA uses Rh, Co, and Pt SPNDs. In addition, JAEA is in the process of developing fast response/high output SPNDs containing Co emitters surrounded by Rh and Pt emitters surrounded by Rh. The irradiation performance of this new Pt-Rh type SPNDs was successfully demonstrated at the JMTR in a 17,000 hour test with a peak temperature was 700 °C.

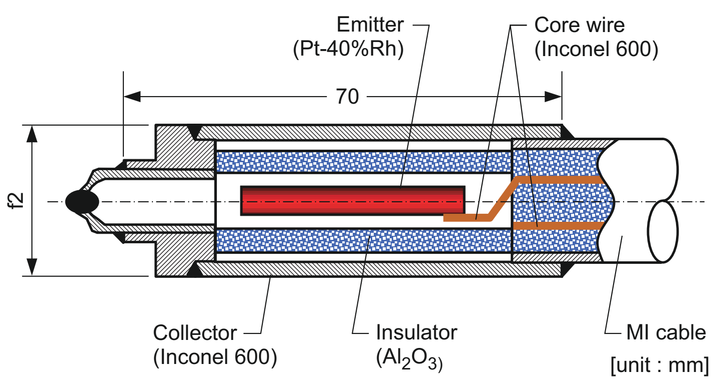

Figure 3-45. JAEA-developed Pt-40% Rh SPND.

JAEA is also exploring the use of two flux characterization methods: a scintillator optical fiber with a scanning driver and a self-powered detector with a driver. Tests were completed using the driver system to insert each type of detector into irradiation holes of the TRIGA II reactor at the Institute for Atomic Energy at Rikkyo University. Results indicate that scanning a one meter long core using an optical fiber with a scintillator (ruby) attached to the tip yields neutron flux distributions similar to that obtained with foil activation methods (see Figure 3-46). However, the foil activation method requires 4 to 5 hours whereas the fiber method only requires 10 minutes.

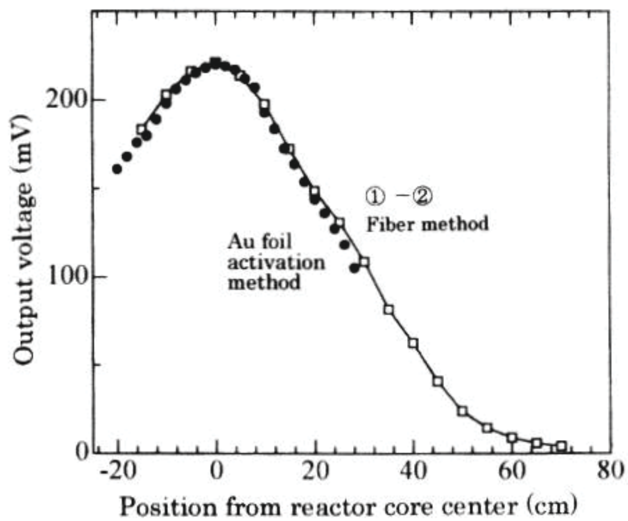

Figure 3-46. Signals obtained with optical fiber detector and Au foil activation methods.

Because light emission of the ruby scintillator decreases at high temperatures, this method is limited to temperatures of around 100 °C. Although JAEA is continuing to explore the potential of other scintillators, Reference 73 also reports results from tests using the driver system with self-powered detectors containing quartz insulators were found to function for temperatures up to 500 °C. Detectors with alumina tubes were only found to function up to 400 °C.

3.4.6. Gamma Flux

Reference 74 reports that JAEA has recently started developing of SPGDs using a lead emitter, alumina insulators, and an Inconel 600 collector (see Figure 3-47). Calibration evaluations of these SPGDs were performed using a alanine dosimeter in a Co-60 gamma-ray irradiation facility at the Takasaki Advanced Radiation Research Institute.

3.4.7. Optical Diagnostic Techniques

JAEA has been active in research to use optical diagnostic techniques to measure temperatures, reactor power, and other operating parameters. Reference 72 reports research results indicating that newly-developed fluorine doped (F-doped) optical fibers can withstand radiation damage better than silicon core fibers. Results for an F-doped optical fiber indicate that the radiation-induced optical absorption at about 600 nm was less than 0.2 dB/m for an electronic excitation exposure dose of 1.9E6 Gy (1.9e13 rads).

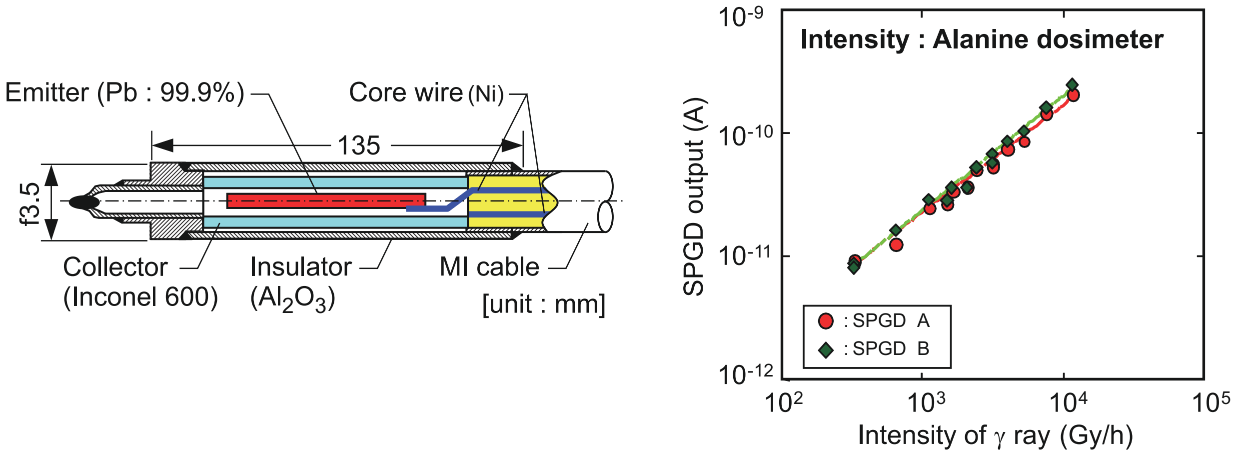

Figure 3-47. JAEA SPGD design and calibration results.

3.5. NRG

The HFR at Petten, which is owned by the European Communities and operated by the Netherlands Energy Research Foundation (ECN), has been conducting fuel irradiations using instrumented test rigs for over 40 years. The Nuclear Research and consultancy Group (NRG) was established as a Partnership Firm in 1998 through the merger of ECN's (70% share) and KEMA's (30% share) business activities in the nuclear fields. HFR test capsules have been successfully used to investigate power cycles and ramping behavior on PWR and BWR fuel rods.[77] Although the HFR originally focussed on LWR fuel irradiations, significant testing of HTGR and Sodium Fast Reactor (SFR) fuels have also been conducted in this facility. Typical instrumentation in such capsules allows measurement of fuel stack displacement, fuel rod length, fuel rod internal pressure, neutron flux, gamma flux, and fuel rod central temperatures (up to 1350 °C).

Discussions with Petten staff indicates that instruments are primarily obtained from commercial vendors or IFE/HRP.[78,79] Typical instruments employed in specialized ECN test rigs are listed in Table 3-1. Reference 80 describes a testing facility installed in Petten for continuous in-pile crack testing of samples up to 730 °C. In recent years, NRG has been involved in several internationally-sponsored tests for advanced reactor fuels.[81] In particular, this reference discusses recently completed and ongoing campaigns to evaluate gas reactor fuel elements (the HFR-EU1bis and HFR-EU1 tests), gas reactor fuel coating materials (the PYCAASSO I and II tests), liquid metal fast reactor and accelerator driven system fuel tests (CONFIRM, FUJI), transmutation fuel tests (HELIOS irradiations), and advanced fuel cycle (e.g., U-Pu and Th-U cycle tests).

3.6. KAERI

The Korea Atomic Energy Research Institute (KAERI) utilizes specialized instrumentation in test capsules supporting materials and fuel irradiations in their HANARO multipurpose, pool-type research reactor. HANARO was designed to provide a peak thermal and fast flux of $5x10^{14}$ n/cm^2·sec (E < 0.625eV) and $2.1x10^{14}$ n/cm^2·sec (E>1.0MeV) at a 30 MW thermal power, respectively. Since HANARO began operation in 1995, numerous experimental facilities have been developed and installed in its 32 vertical holes and 7 horizontal beam ports to support fuels and material irradiations.[82 through 85]

Test equipment for irradiating nuclear fuels and materials in HANARO are classified into two categories: capsules (non-instrumented and instrumented), and FTL (Fuel Test Loop). Instrumented capsules or test rigs for materials irradiations may include thermocouples, fluence monitors, and heaters. Fuel tests may include thermocouples (Types K and C), pressure transducers and elongation thermometers to measure fuel temperature, internal pressure of the fuel rod, and fuel deformation, respectively, and SPNDs to detect neutron flux. KAERI has also developed specialized capsules for creep and fatigue testing. These capsules include thermocouples, fluence monitors, and heaters. KAERI typically procures commercially-available sensors from Thermocoax (thermocouples and SPNDs), Studsvik (SPNDs) and IFE/HRP (LVDTs). Recently, KAERI has initiated efforts to obtain enhanced instrumentation for testing of LWR and advanced reactor fuels and materials, including the use of instrumentation from other countries.[83]

3.7. ORNL

The High-Flux Isotope Reactor (HFIR), which is located at and operated by Oak Ridge National Laboratory (ORNL), is an 100-MW_{th} isotope production and test reactor that is beryllium-reflected, light-water-cooled and -moderated, with highly enriched uranium-235 as the fuel. HFIR provides one of the highest steady-state neutron fluxes available in any of the world's reactors, and neutron currents from its four horizontal beam tubes are among the highest available.

Originally, HFIR was primarily designed for producing transuranium isotopes. However, many experiment-irradiation facilities were included in its original design; and several others have been added. Experiment-irradiation facilities available include (1) four horizontal beam tubes, which originate in the beryllium reflector; (2) the hydraulic tube facility, located in the very high flux region of the flux trap, which allows for insertion and removal of irradiation samples while the reactor is operating; (3) thirty target positions in the flux trap, which normally contain transuranium production rods but which can be used for the irradiation of other experiments (two are instrumented target positions provided by a recent modification); (4) six peripheral target positions located at the outer edge of the flux trap; (5) numerous vertical irradiation facilities of various sizes located throughout the beryllium reflector; (6) two pneumatic tube facilities in the beryllium reflector, which allow for insertion and removal of irradiation samples while the reactor is operating for activation analysis; and (7) four slant access facilities, called “engineering facilities,” located adjacent to the outer edge of the beryllium reflector. In addition, spent fuel assemblies are used for gamma irradiation in the gamma irradiation facility in the reactor pool.

Today, HFIR is principally used to provide a stable neutron source for fundamental scientific experiments associated with neutron scattering. A 5 inch deep flux trap located at the center of the HFIR fuel element provides a thermal neutron flux of 2 $x10^{15}$ n/cm^2-sec for instrumented lead capsules and loop tests; reflector positions are available for exposing samples in static capsules, loop, and isotope production tests to fluxes of 1 x 10^{15} n/cm^2-sec. Access to some experimental positions is via a pneumatic tube to allow rapid insertion and removal during reactor operation. HFIR irradiations are typically “static capsule” and “rabbit” tests and rely on sensors that can provide integral values, such as fluence wires, or peak values, such as flux wires. However, ORNL has significantly advanced the use of one unique sensor, Silicon Carbide (SiC) temperature monitors for detecting peak temperature in static capsule tests. The capability to deploy and evaluated these sensors, which are discussed in Section 3.7.1, has been replicated at INL to support ATR NSUF irradiations.

3.7.1. Silicon Carbide Temperature Monitors for Peak Temperature Detection

Since the early 1960s, the observation that irradiation-induced swelling of SiC begins to anneal out at temperatures exceeding its irradiation temperature has been used as a post-irradiation temperature monitor.[87 through 89]Various approaches (e.g., changes in length, density, thermal conductivity, and electrical resistivity) have been used to infer irradiation temperature from this observed phenomena. Snead et al.[88] recommends using changes in resistivity because of improved accuracy, ease of measurement, and reduced costs. Work presented by Snead in Reference 87 was conducted on SiC produced by chemical vapor deposition (CVD). This material is fully dense (3.203 g/cc) and stoichiometric. Comparisons between SiC measurements and thermocouples indicate that accuracies of approximately 20 °C are possible for dose ranges of 1 to 8 dpa and temperatures from 200 to at least 800 °C. Absolute limits for this approach are 150 °C (an amorphorous threshold) and 875 °C (due to recrystallization). Note that Reference 88 cites that measurements should be taken in a controlled environment (within 0.4 °C) with annealing periods of approximately 30 minutes to obtain these accuracies.

Figure 3-48 (from Reference 88) shows data obtained from this technique. The curves shown in this figure represent data obtained from a series of samples, all irradiated in the ORNL HFIR core at similar dose rates of ~ 8 x 10^{14} n/cm^2-s (E > 0.1 MeV). The total dose for the curves is not identical. The curve for an irradiation temperature of ~350 °C is at the lowest dose (~0.1 dpa, assuming 1 dpa = 1 x 10^{21} n/cm^2; E>0.1 MeV) while the remainder are from ~1-8 dpa. It is speculated that the apparent saturation in normalized resistivity for the 0.1 dpa sample represents the point at which the simplest of the defects in the irradiated SiC have annealed away and represents conductivity at the new dopant level for the irradiated SiC.

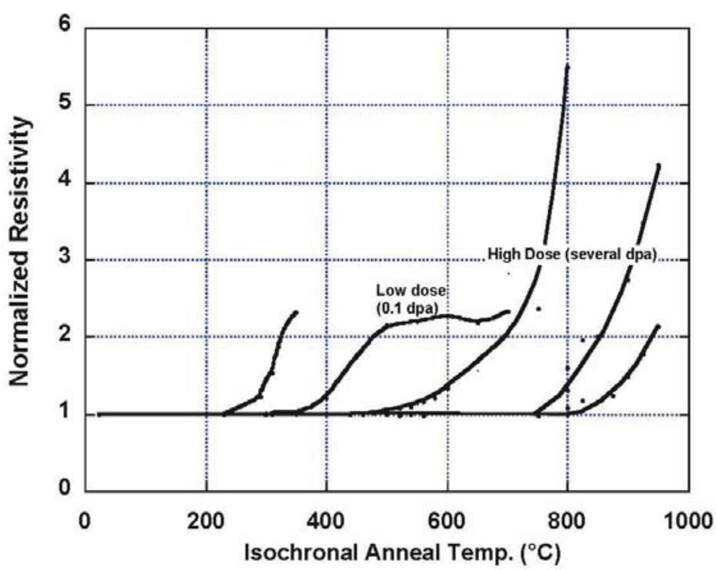

Figure 3-48. Electrical resistivity technique applied over a range of irradiation temperatures.

It should be noted that there are several limitations associated with the use of SiC temperature detectors. As discussed in Reference 88, temperatures are inferred by post-irradiation detection of changes in the stable defect population within SiC monitors that were incurred during irradiation. Some examples where errors could be inferred from SiC monitors cited in Reference 88 include:

- *Irradiation temperatures rising during the latter part of irradiation.* For damages greater than 0.1 dpa, the increasing temperature will anneal out defects that occur at the lower irradiation temperature, while creating stable defects at the higher temperature. When isochronal annealing is performed, lower temperature defects (to some or great extent) will have already been removed, and the recovery curve will be smeared to somewhat higher temperatures. If the temperature increase during irradiation is small, or the time at higher temperature is short, then the original departure from linearity will give the earlier irradiation temperature.
- *Irradiation temperatures decreasing during irradiation.* This decrease will lead to defects being created and frozen-in at the higher-temperature, while continuing to create lower temperature defects. The isochronal anneal will then give an indication of the lowest irradiation temperature (in this case at the end of the irradiation period), and the recovery curve will be smeared due to annealing of higher temperature defects.
- *Upward or downward temperature spikes during irradiation.* This case has the potential to lead to partially created or annealed defects, depending on the change and duration of the temperature increase and the damage to the SiC monitor during irradiation.

However, if irradiation tests are conducted at or near the same temperature when the reactor is at power, none of these situations are of concern.

4. ENHANCED ATR INSTRUMENTATION STRATEGY

INL has a long history of developing highly specialized instrumentation to meet demands of customers conducting unique tests in INL facilities. Such instrumentation was used in INL test reactors and in facilities from the Power Burst Facility (PBF) and Loss of Fluid Test (LOFT) research programs. Unfortunately, INL instrumentation development and research funding declined significantly in the 1980s, when large test facility programs ended. Until this in-pile instrumentation enhancement effort was initiated, ATR irradiation testing relied primarily on commercial vendors for instrumentation.

As documented in Section 3, several test reactor programs in Europe and Asia, such as the HFR (Petten), HBWR (Halden), and JAEA (JMTR and JOYO) have maintained their instrumentation development and evaluation research capability. Others, such as CEA, are rapidly trying to regain this expertise. As part of the ATR NSUF, it was recognized that a focussed effort was also needed at INL if the ATR is to become competitive as a world class irradiation facility. Hence, a research and development plan was developed in 2008 so that ATR users would have access to enhanced real-time in-pile instrumentation, comparable to (and, in some cases, superior to) that available at other MTRs, by 2015. As documented in this section, the plan identifies and prioritizes instrumentation research considering ATR NSUF customer and reactor staff needs along with technology readiness. INL progress in accomplishing the objectives outlined in the research plan is presented in this section.

When the ATR NSUF instrumentation strategic plan was originally developed, estimates for the funding required to obtain a world-class instrumentation capability for ATR were identified. During the subsequent years, the allocated ATR NSUF funding level has often been less than the estimates to implement this strategy. However, as anticipated in the original version of this report, the instrumentation capability developed with ATR NSUF funds has been sufficient for this effort to continue and to attract funding from other sources. For example, during FY12, the Office of Nuclear Energy in the Department of Energy (DOE-NE) FCRD program, the ATR Life Extension Project (LEP), and the Nuclear Energy Enabling Technology (NEET) programs funded selected instrumentation development activities. In addition, selected programs are supported by INL's Laboratory Research and Development (LDRD) program. Hence, the originally proposed schedule for this effort has been extended in the case of selected sensors and enlarged in the case of other sensors that are requested to meet user needs for these other programs. For example, activities to explore the use of fiber optics and ultrasonics-based sensors were initiated in response to FCRD programmatic needs.

4.1. Motivation/Justification for Investment

This research and development program is sorely needed and necessary if the ATR NSUF wishes to attract additional researchers from universities, laboratories, and industry. Key points for the business case to support this effort include:

- ***Vital Component for ATR NSUF Success.*** If the ATR NSUF is to become a world-class irradiation facility, adequate instrumentation must be available to its users. As noted in Section 2, the ATR has advantages over many other MTRs with smaller irradiation test locations and lower flux levels. Yet, the instrumentation capabilities developed by research staff at other test reactors allow their customers to obtain real-time data from tests that cannot be obtained from tests conducted in the ATR.

- ***Focussed Instrumentation Development to Attract Near-term Customers.*** INL's position as the lead DOE-NE lab uniquely positions this research program so that it can easily focus instrumentation research and development efforts to help meet near-term DOE-NE customer needs and help the ATR attract other customers, such as the US Nuclear Regulatory Commission (US NRC) and DOE-NE's Advanced Reactor Concepts (ARC), Advanced Small Modular Reactor (SMR), and LWR Sustainability (LWRS) programs.
- ***Expertise and Facilities for Deploying Unique Instrumentation.*** Much of the investment has already been made to obtain the right equipment and trained staff. INL's HTTL already possesses unique equipment for evaluating and fabricating required instrumentation. However, the enhanced capabilities, such as a clean room, that will be included in the HTTL when it relocates to the REL will make it a world-class facility. INL also has unique test reactors and gamma irradiation facilities for demonstrating and using new instrumentation for in-pile measurements.
- ***Market for research program task collaboration and products.*** Clearly, the primary market for products from this research program are ATR users. However, INL-developed instrumentation is also attracting customers that operate other MTRs (e.g., HBWR and MITR as noted in Section 5). In addition, there is the potential for instrumentation developed and deployed from this research to be used in commercial nuclear power plants and in applications funded by the National Aeronautics and Space Administration (NASA) or the Department of Defense (DOD).

Potential funding sources for an ATR NSUF instrumentation program and its products are summarized in Table 4-1. This table also lists potential collaborators for various instrumentation program elements.

Table 4-1. Funding sources and potential collaborators for INL instrumentation elements.

Program Elements	Funding Sources	Collaborators
Sensor Development	DOE-NE LWRS; DOE-NE FCRD DOE-NE NEET (ATR NSUF, Advanced Sensors Initiative). Others, such as the US NRC; DOD; Naval Reactors, NASA); INL LDRD	IFE/HRP; CEA; SCK•CEN KAERI; JAEA International Funding Agencies [OECD, IAEA, Joint Research Centre (JRC)]
Developed Sensors-Nuclear Customers	Other MTRs (CEA-OSIRIS and JHR, NRG/JRC - HFR, KAERI-HANARO, ORNL-HFIR, IFE/HRP- HBWR, JAEA- JMTR, SNL-Annular Core Research Reactor (ACRR), MIT-MITR) Commercial Nuclear Reactors DOE-NE (NGNP, FCRD, LWRS, ARC, Advanced SMRs) Others, such as the US NRC, Department of Defense (DOD); Naval Reactors, NASA).	Commercial Industry (fiber optic and thermocouple vendors via government sponsored grants or venture capital) to transfer technology.
Developed Sensors-Non-Nuclear Customers	DOD, NASA, Aircraft Industry, Petroleum Industry, Coal Industry	Commercial Industry (fiber optic and thermocouple vendors via government sponsored grants or venture capital) to transfer technology.

4.2. Currently Available ATR Instrumentation

Table 4-2 identifies instrumentation currently available for ATR experiments. As discussed in Section 2, ATR irradiation capabilities in static capsule, shuttle, instrumented lead, and PWR loop tests, are unparalleled. However, as indicated in column 5 of Table 4-2, available instrumentation for measuring parameters of interest during an irradiation test is limited at each irradiation location. As indicated by column 6, sensors available at other MTRs could increase measurement capabilities during ATR irradiations. Note that adapting instrumentation from other test reactors often requires laboratory demonstrations because of ATR-specific irradiation conditions and test capsule geometries. For example, devices may be required that can withstand higher temperatures and fluences. Column 7, which is labeled “Developmental” under “Proposed Instrumentation Advancement” lists developmental or non-nuclear technologies that could offer enhanced in-pile measurement capabilities. Typically, technologies listed in this column are considered to be less “ready” for implementation.

Table 4-2. Instrumentation available at ATR and proposed advanced technologies.

Parameter	Location			Available Technology at ATR	Proposed Advanced Technology	
	Static Capsule/ Shuttle	Instr. Lead	PWR Loop		Available at Other MTRs	Developmental
Temperature	✔	✔	✔	-Melt wires (peak)[a] -Silicon Carbide (SiC) temperature monitors (range)	-Paint spots (peak) -Thermal Expansion Devices (TEDs)	
		✔	✔	-Thermocouples (Type N, K, C[b], and HTIR-TCs[c])	-Expansion thermometer	- Fiber optics -Noise thermometry -Ultrasonic thermometers (UTs)
Thermal Conductivity		✔	✔	- Transient Hot Wire Method Needle Probe (THWM NP)	-Degradation using signal changes in thermocouples	
Flux/Fluence (neutron)	✔	✔	✔	-Flux wires and foils		
		✔	✔		-Self-Powered Neutron Detectors (SPNDs) -Subminiature / miniature fission chambers	- Moveable SPNDs - Micro-Pocket Fission Detectors (MPFDs)
Gamma Heating / Gamma Flux		✔	✔		-Calorimeters -Gamma thermometers -Self-Powered Gamma Detectors (SPGDs)	
Dimensional		✔	✔	-LVDT-based elongation	-Diameter gauge	-Ultrasonic techniques -Fiber optics
Fission Gas (Amount, Composition)		✔	✔	-On-line Fission Product Sampling -Gas Chromatography -Pressure sensor	-LVDT-based pressure monitors	-Acoustic measurements with high-frequency echography
Loop Pressure			✔	-Differential pressure transmitters -Pressure gauges with impulse lines		
Loop Flowrate			✔	-Flow venturis -Orifice plates	-Turbine flow meters (for individual fuel assemblies	
Loop Water Chemistry			✔	-Off-line sampling / analysis	-Electrical chemical potential probes	
Crud Deposition			✔		- Diameter gauge with neutron detectors, and thermocouples	
Crack Growth Rate			✔		-Direct current potential drop (DCPD) technique	

a. Although melt wires have been used at ATR, recent efforts have expanded the types offered to our users, allowing more accurate estimates of peak temperature with enhanced encapsulation methods.
b. Type C thermocouple use requires a “correction factor” to correct for decalibration during irradiation.
c. High Temperature Irradiation Resistant ThermoCouple (HTIR-TC)

As part of the ATR NSUF program (and now, as part of the FCRD program), several activities have been initiated to develop and implement new in-pile instrumentation capabilities. Blue text in Table 4-2 indicates current instrumentation research efforts, red text indicates demonstrated new or enhanced sensors now available to users as a result of recent instrumentation research, and magenta text indicates new sensors and capabilities that are now ready for deployment as a result of recent instrumentation research. Instrumentation development tasks were selected based on anticipated user needs by the ATR NSUF or other DOE-NE programs and 'technology readiness' (providing users needed instrumentation in the near-term). Many of these instrumentation development efforts are in collaboration with other organizations. As indicated in Table 4-2, several new or enhanced sensors are now available to ATR users as a result of this instrumentation development effort. The ultimate goal of this effort is to provide ATR users with sensors for detecting all of the parameters listed in Table 4-2.

4.3. Current Prioritization for Instrumentation Development

Figure 4-1 graphically illustrates the process for developing and demonstrating instrumentation needed to advance ATR NSUF testing capabilities. There are several major activities identified, “Nearer-Term Instrumentation Development”, and “Developmental”, and “Expansion”. Representative tasks identified in each area are also shown with qualitative judgments with respect to ATR capabilities compared to other test reactors in this figure. As indicated, it is expected to have comparable instrumentation for most parameters during FY13, and “world class” (e.g., comparable, and in some cases, superior) irradiation capabilities by FY15. Nevertheless, the ability to meet such goals is dependent upon allocated funding levels and sensor irradiation schedules. For example, delays in completing planned tests in the ATRC facility during 2012 have delayed progress in providing real-time flux monitors to ATR NSUF users.

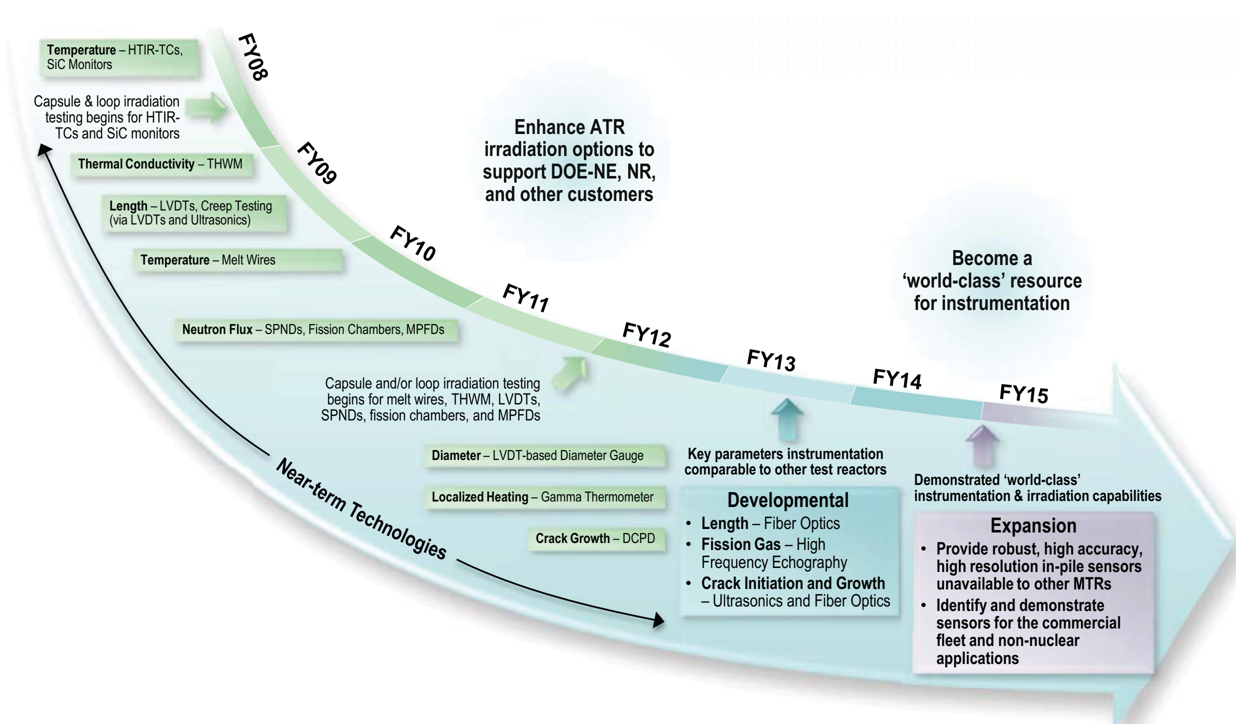

Figure 4-1. ATR NSUF advanced instrumentation research and development.

ATR NSUF-funded instrumentation development effort began in FY 2009. Prior to that time, new ATR instrumentation was primarily developed using a limited amount of INL LDRD funding to develop "Nearer-Term" technologies. Specifically, sensors were developed that addressed needs identified by current and potential customers. Then, programmatic funding covered the costs required for qualifying the instrumentation for ATR irradiations. However, as indicated in Table 4-2, some "Developmental Technologies" research is underway prior to initiating some Nearer Term technologies. This is because of customer-specific interests. For example, the FCRD program is primarily interested in instrumentation that can provide higher resolution/higher accuracies than instrumentation available at other MTRs.

Table 4-3 summarizes the status of the effort to provide enhanced in-pile instrumentation to ATR users. Similar to Table 4-2, blue text indicates current instrumentation research efforts, and red and magenta text indicates new sensors now available to users as a result of recent instrumentation research. More detailed information about on-going instrumentation activities is provided in Section 5. As indicated in Tables 4-2 and 4-3, considerable progress has been made in this program since its inception. Several new sensors are now available to users; and as indicated in Section 5, several additional sensors should soon be available. It is also encouraging to see that some level of research has been initiated on most of the sensor technologies identified in this table. Nevertheless, additional effort is needed to provide ATR users a world-class instrumentation capability.

Table 4-3. Status of ATR NSUF sensor development and enhancement efforts.

Parameter	Sensor	Status
Temperature	Melt Wires	Currently used in several ATR NSUF irradiations. Both quartz and vanadium encapsulation can now be provided by INL for numerous wires with melting temperatures between 85 and 1455 °C. Documentation completed for DSC testing of melt wires and for interpreting post-irradiation results.
	SiC Temperature Monitors	Currently used in several ATR NSUF irradiations. Development of and documentation for post-irradiation measurement capability completed.
	High Temperature Irradiation Resistant ThermoCouples (HTIR-TCs)	Initial out-of-pile testing completed. In-pile testing (in the AGR-1 gas reactor fuel irradiation test) and sensor enhancement evaluations completed; HTIR-TCs provided to MIT in FY10, and HTIR-TCs for high temperature (up to 1600 °C) irradiations shipped to IFE/HRP in November 2011.
	Ultrasonic Thermometers (UTs)	Successfully developed and deployed to support high temperature fuel testing several decades ago. Efforts underway to develop and evaluate an enhanced prototype. Although prototype is focussed on the use of magnetostrictive transducers, an instrumented lead test is scheduled for FY13 that will compare the irradiation-related survivability of piezoelectric and magnetostrictive transducers.
Thermal Conductivity	Transient Hot Wire Method Needle Probe (THWM NP)	Prototype design developed and initial laboratory testing completed. Anticipated that inclusion of HTIR-TCs could allow detection at higher temperatures. Prototype THWM probes being prepared for shipment to IFE/HRP and CEA.

Table 4-3. Status of ATR NSUF sensor development and enhancement efforts.

Parameter	Sensor	Status
Elongation, Crud deposition, Corrosion	LVDTs	Out-of-pile testing completed on developmental LVDT that resists high temperature degradation and eliminates Curie temperature effects.
	Diameter gauge	Currently used in HBWR for detecting swelling, corrosion, and crud buildup. Investigations delayed due to funding limitations.
	Ultrasonic Techniques	Scoping tests completed on elongation prototype; additional prototype out-of-pile testing and results of piezoelectric transducer irradiation test needed.
	Fiber Optic Techniques	Efforts underway to develop and evaluate the accuracy of a candidate probe. Prior to deployment, an instrumented lead test needed to evaluate fiber optic survivability in radiation environments.
In-pile Creep Test Rig	LVDT-based rig with bellows	Design developed and prototype evaluated at PWR conditions in a laboratory autoclave. Enhanced design developed and fabricated and ready for insertion into an ATR PWR loop. Follow-on work underway to develop and evaluate rig with variable load capability.
Neutron Flux	Flux wires and foils	Various flux wires and foils available. Vanadium encapsulation now provided by HTTL.
	SPNDs and Fission Chambers	Specially-developed fixturing designed, fabricated, and installed at ATRC. In FY13, additional evaluations of detectors will be continued. Development of MPFDs for ATRC evaluations underway.
Gamma Heating	Gamma thermometers	Currently used at HBWR; Investigations initiated in 2012.
Crack propagation	DCPD method with CT specimens	Currently used at HBWR; Investigations initiated in 2012.
	Ultrasonic techniques	Efforts to be initiated under FCRD program. Prior to deployment, results of piezoelectric transducer irradiation test needed.
	Fiber optics techniques	Efforts to be initiated under FCRD program.Prior to deployment, an instrumented lead test needed to evaluate fiber optic survivability in radiation environments.

In addition to providing ATR customers the instrumentation required for their irradiation tests, this program has clearly added to the prestige and capabilities of the ATR NSUF, INL, and to the DOE. International collaborations have been established with leaders in the world of in-pile testing, such as IFE/HRP and CEA. Partnerships with universities have not only helped students successfully complete their graduate level research, but have led to new INL employees. HTTL staff have authored/co-authored 26 peer-reviewed conference papers and 17 archival journal papers. In addition, HTTL staff are inventors/co-inventors for 3 patents/patents pending. During 2012, two new Invention Disclosure Records (IDRs) were filed on sensors developed from in-pile instrumentation research activities. Finally, the specialized fixtures and software developed and installed at the ATRC Facility for evaluating flux detectors expands the capability of this facility. It is anticipated that this new capability will be used in future years to develop and evaluate new, improved sensors for measuring flux and other parameters.

5. DEVELOPMENT - IDAHO NATIONAL LABORATORY

Several INL efforts are underway to enhance in-pile instrumentation for ATR users. As indicated in Section 4, these efforts continue to focus on obtaining instrumentation for measuring a wide range of parameters and conditions to support irradiation needs for the ATR NSUF and other DOE programs. In addition, as some sensors developed by HTTL become available, INL efforts are focussed on supporting various domestic and international irradiation tests. This section summarizes the status of on-going and planned sensor development and evaluation efforts at INL.

5.1. Temperature Sensors

Temperature is a key parameter of interest during fuel and material irradiations. As indicated in Table 4-2, available temperature detection sensors to ATR NSUF users are comparable, if not superior, to those used at other MTRs. Melt wires and commercially-available thermocouples (e.g., Types K, N, and C) have been available for decades, but were procured from external vendors. To meet recent customer requests for peak temperature indicators in static capsule and hydraulic shuttle locations, an increased selection of melt wires with enhanced encapsulation is now available from in-house sources. In addition, SiC temperature monitors can now be evaluated by HTTL staff. These ‘peak temperature’ indicators, commercially-produced thermocouples, and doped molybdenum/niobium alloy HTIR-TCs are available for instrumented lead and PWR loop applications. Development of enhanced ultrasonic thermometers for temperature measurement is also underway.

5.1.1. Melt wires

Melt wires are the simplest and least expensive option available for monitoring temperature in ATR tests. Metallic wires of a known composition and well characterized melting temperature are included in a test to determine if a specific peak temperature has been reached or exceeded. As described in American Society for Testing and Materials (ASTM) E 1214-06,[86] melt wire materials should consist of metals with 99.9% purity or be eutectic alloys such that their measured melting temperatures are within ± 3 °C of the recognized melting temperatures. The standard states that transmutation-induced changes of selected wires should not be considered significant up to 1×10^{20} n/cm^2 (E > 1 MeV). As noted in Reference 86, melt wires should be selected to measure temperature at 5 to 12 °C intervals, with at least one melt wire that possesses a melting temperature greater than the highest anticipated temperature.

INL has established a library of melt wires and developed in-house capabilities to verify the melting temperature of candidate wire materials (ranging from ~85 to 1455 °C) using a DSC installed at INL's HTTL.[90] When possible, INL selects high purity materials with low thermal neutron capture cross-sections. Table 5-1 lists the melt wire materials currently available for irradiation testing that have undergone verification testing. Note that the current library has been developed according to user requests. It is anticipated that the number of materials in this library will increase as additional user requests are received.

INL has developed several options for encasing melt wires, including encasing multiple melt wires into a single 1.6 mm diameter quartz tube or a single wire in a 1.7 mm diameter metallic capsule. Figure 5-1 shows a quartz tube containing multiple melt wires after progressive heating steps during verification testing in high temperature furnaces installed at INL's HTTL. The wires selected are chosen based

Table 5-1. Melt wire materials and melting temperatures currently available in INL library.

Material (component weight%)	Melt Onset Temperature, °C
56.2Bi 33.8Pb 10Sn	85.0
65Bi35In	110.6
55.2Bi 44.8Pb	126.4
57Bi43Sn	139.4
100Sn	231.8
95Sn5Sb	238.6
90Pb10Sb	252.4
80Au 20Sn	279.5
100 Bi	271.4
97.5Pb5Ag5Sn	302.9
97.5Pb1.75Sn 1.75Ag	309.3
100 Pb	327.5
100 Zn	419.6
100 Al	660.5
49Ag16Cu23Zn7.5Mn4.5Ni	681.3
40Ti20Zr20Cu20Ni	850.7
98.2Cu1.8Be	865.1
100Ge	938.3
82Au 18Ni	955.0
100 Ag	961.9
65Cu35Au	995.6
100Au	1064.0
100Cu	1084.6
70Cu30Ni	1191.0
28Mo69Ni2Fe1Co1Cr	1370.0
Ni	1455.0

on expected irradiation test temperatures and required resolution. The melt wires depicted in Figure 5-1a are considered good materials for this purpose because melting may be determined by visual inspection. This is important because this determination must be made during Post Irradiation Examination (PIE) in a hot cell. Figure 5-1b shows melt wires that were determined to be less-ideal choices for use. For these wires, melting (confirmed through DSC testing) could not easily be determined by visual inspection; and microscopic examination was required. Melting in these cases had to be determined by changes to the surface condition of the wires rather than bulk deformation of the wires. As noted above, metallic tubes are also available for encapsulation in ATR tests. However, post-test examination is more complicated, requiring radiography, computer tomography, or destructive examination of the tube to allow inspection of the wire after irradiation.

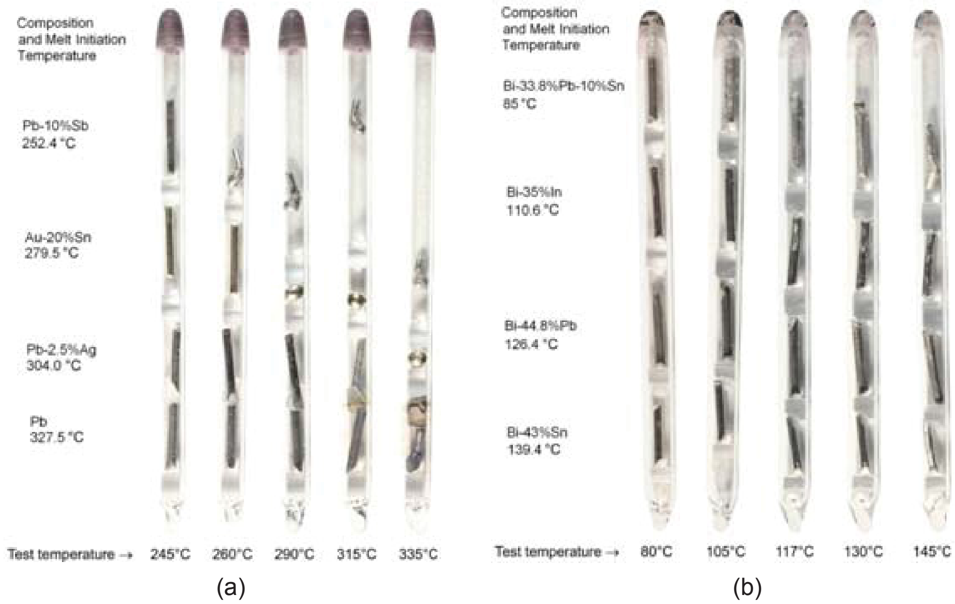

Figure 5-1. Quartz tube containing four melt wires in separated compartments: (a) Example of ideal indicator melt wires; (b) Example of non-ideal indicator melt wires.

5.1.2. Silicon Carbide Temperature Monitors

Another option available to ATR users for peak temperature detection is the use of SiC temperature monitors. The benefit of this option is that a single small monitor (typically 1 mm x 1 mm x 10 mm or 1 mm diameter x 10 mm length) can be used to detect peak irradiation temperatures between 200 and 800 °C (and possibly up to temperatures near 1000 °C). SiC incurs damage in its crystalline structure during irradiation. This causes several measurable physical changes to the monitor (i.e. changes in dimensions, thermal conductivity, electrical resistivity, etc.). When the monitor is annealed at a temperature greater than the peak irradiation temperature, the altered properties rapidly change.[87-89]

As discussed in Section 3.7.1, Snead et al. at ORNL successfully used changes in electrical resistivity to detect peak irradiation temperatures with accuracies of approximately 20 °C for dose ranges of 1 to 8 dpa and temperatures between 200 and 800 °C.[88] Experimental data[89] suggest that upper and lower bounds for this range may be extended.

Specialized equipment at INL's HTTL now allows peak temperature detection with irradiated SiC monitors. With this equipment, the SiC sensor electrical resistivity is measured after annealing in a furnace located within a stainless steel enclosure at the HTTL (shown in Figure 5-2). After annealing, cooled samples are placed into a constant temperature environmental test chamber to ensure electrical resistivity measurements are taken within 0.2 °C of a predetermined temperature (typically near 30 °C). A high accuracy (9 digit) multimeter, located outside the stainless steel enclosure, is used to obtain resistance measurements. Specialized fixturing (Figure 5-2) was developed to ensure that measurements are taken with the SiC sensors placed consistently in the same orientation. A four point probe technique is used with the points connected to the sample through spring-loaded, angled electrodes that hold the SiC temperature monitor in place. Current and voltage are provided to the sample via wires that are threaded through the holes in the electrodes. The accuracy of this new INL capability was verified by completing comparison measurements with ORNL on identical sensors that had been subjected to identical irradiation conditions.[90] Results, as shown in Figure 5-3, indicate that similar peak irradiation temperatures are inferred from ORNL and INL measurements in these evaluations (e.g., significant increases in normalized electrical resistivity at 300 °C and at 670 °C were observed).

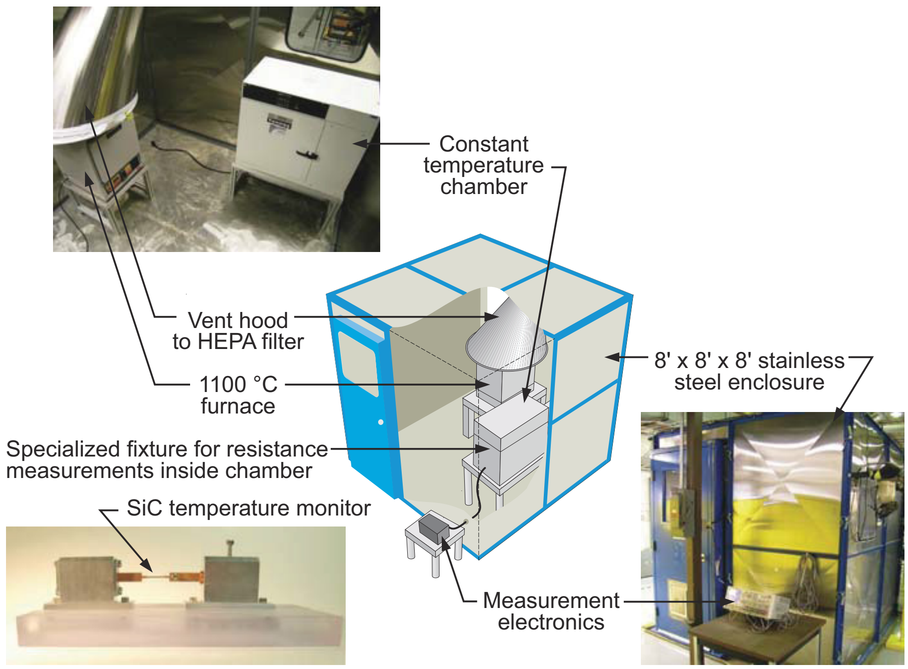

Figure 5-2. Setup to anneal and measure electrical resistivity of SiC temperature monitors.

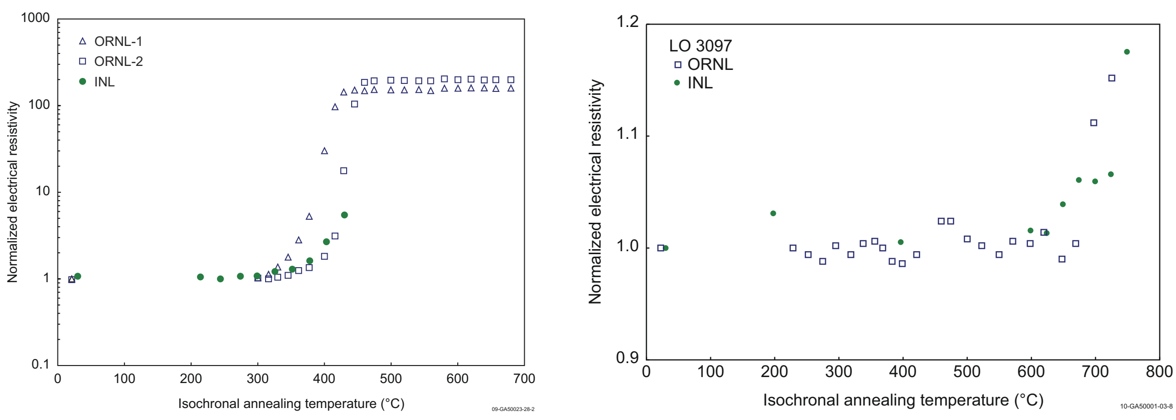

Figure 5-3. Electrical resistivity measurement comparison on SiC monitors irradiated at peak temperatures of (a) 300 °C and (b) 670 °C.

Several irradiation capsules in the ATR now contain SiC temperature monitors. During 2011, two of the SiC monitors included in the ATR NSUF University of Wisconsin test[92] were evaluated using the HTTL procedure[93] developed for such evaluations; and results are documented in Reference 94. It is anticipated that the use of SiC monitors will continue to increase as additional ATR users include SiC temperature monitors in their tests.

5.1.3. High Temperature Irradiation Resistant Thermocouples (HTIR-TCs)

Real-time temperature measurements during irradiation tests are typically made with commercially-available, mineral insulated, metallic sheathed thermocouples. These thermocouples are used to monitor and/or control the temperature achieved during irradiation. For temperatures below 1000 °C, experimental needs are typically met using Type K or Type N thermocouples, which have demonstrated excellent reliability and signal stability under irradiation, even for very high neutron fluences exceeding 10^{22} n/cm^2 (thermal neutrons). However, these thermocouples decalibrate when exposed to temperatures above 1100 °C. Although other types of commercially-available thermocouples exist for higher temperature applications (up to 1800 °C), the thermoelements used in these thermocouples contain materials such as tungsten and rhenium (in the case of Type C and D thermocouples) or platinum and rhodium (Type R, S, and B) that decalibrate due to transmutation from absorption of neutrons. Hence, thermocouples were needed that could withstand both high temperature and high radiation environments.

To address this need, INL developed a HTIR-TC that contains commercially-available doped molybdenum paired with a niobium alloy. HTIR-TC component materials were selected based on data obtained from materials interaction tests, ductility investigations, and resolution evaluations (see References 95 through 104). HTIR-TC long duration performance has been demonstrated through testing, in which thermocouples were held at elevated temperatures (from 1200 °C to 1800 °C) for up to 6 months. The 1200 °C test included nineteen commercially-available Type N thermocouples, three commercially-available Type K thermocouples, and nine INL-developed swaged HTIR-TCs. As indicated in Figure 5-4, some Type K and N thermocouples drifted by over 100 °C or 8%. Much smaller drifts (typically less than 20 °C or 2%) were observed in the INL-developed HTIR-TCs. As documented in Reference 102, similar drifts (2%) were observed in HTIR-TCs in a long duration (4000 hour) test completed at 1400 °C and smaller drifts (less than 1%) have been observed in HTIR-TCs with enhanced fabrication techniques for higher temperatures (up to 1800 °C).

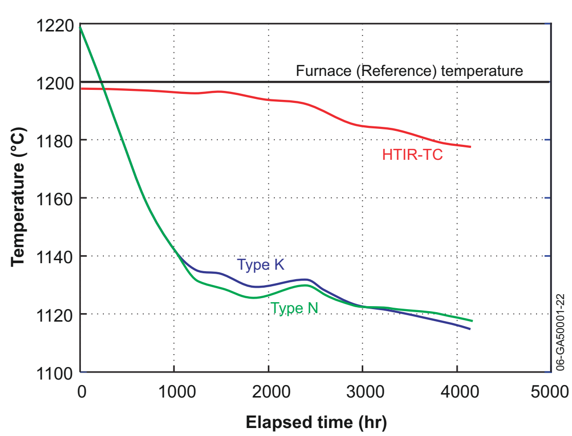

Figure 5-4. Representative thermocouple response in INL 1200 °C tests.

HTIR-TCs were also installed in a multi-capsule experiment where gas reactor fuel samples were irradiated at temperatures up to 1200 °C in INL's ATR. The test started in February 2007 and ended in October 2009. Figure 5-5 shows signals from two INL-developed HTIR-TCs and one Type N thermocouple located within one of the capsules (Capsule 4). Signal variations are due to ATR power fluctuations and outages (e.g., gray regions correspond to when the ATR was shutdown). As shown in this figure, the HTIR-TC (TC-4-1) located near the Type N thermocouple (TC-4-3) yielded a signal consistent with the signal from this Type N thermocouple at the beginning of this irradiation. In addition, the HTIR-TC located at a higher temperature region within the capsule (TC-4-2) yielded a consistent, but higher temperature, signal. However, in October 2008, the Type N thermocouple failed; and its signal ceased. The successful operation of HTIR-TCs in this test has led to INL supplying them to other test reactors.

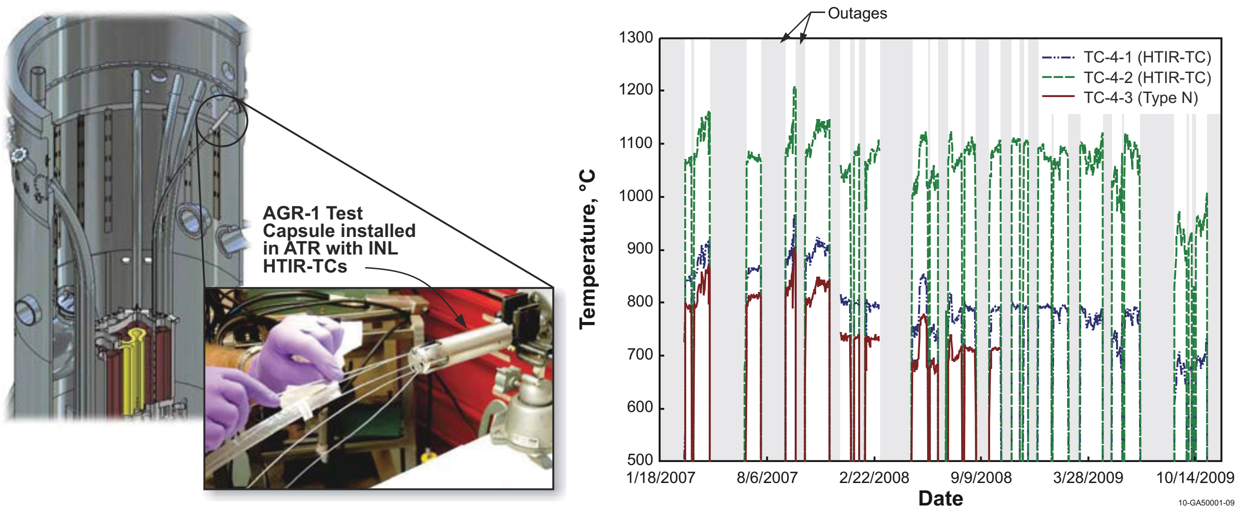

Figure 5-5. HTIR-TCs installed in AGR-1 test capsule and representative HTIR-TC and Type N data during AGR-1 irradiation.

In 2010, three HTIR-TCs were supplied to the Massachusetts Institute of Technology (MIT) for an irradiation test in their research reactor. As discussed in Reference 105, two HTIR-TCs were included in a MIT research reactor (MITR) In-core Sample Assembly (ICSA) test of materials with four capsules (see Figure 5-6). These two HITR-TCs were positioned in the lower two capsules of this test, where peak temperatures were less than 800 °C. The test was conducted in three phases. At the end of the first phase, the upper two capsules were removed (with the lower two capsules and the HTIR-TCs remaining in position). At the start of the third phase, two new upper capsules were inserted. One of the two HTIR-TCs failed during the middle of the second phase of this test, while the second HITR-TCs remained stable throughout the duration of the test. It is suspected that the removal of the upper two capsules after the first phase of the test could have led to mechanical damage to the HTIR-TC that failed. However, final PIE has not yet been completed.

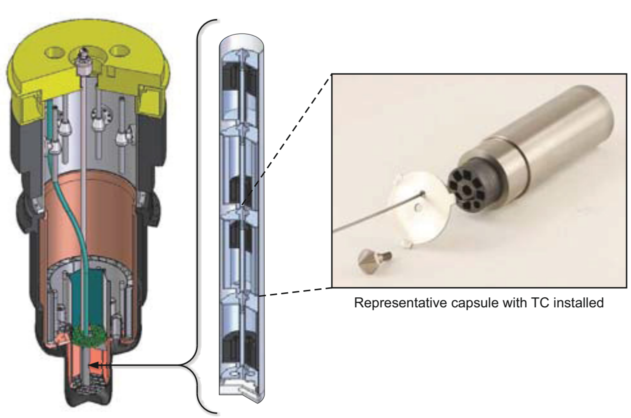

Figure 5-6. Cutaway of MITR core showing position of ICSA assembly with four sample capsules) installed in an in-core position (reactor fuel elements not shown for clarity).

As part of a Memo of Understanding (MOU) between the IFE/HRP and the INL, the HTTL shipped four enhanced HTIR-TCs to IFE/HRP in 2011 for use as fuel centerline thermocouples in upcoming HBWR irradiations. Deployment of HTIR-TCs at the HBWR represents a unique opportunity to observe the performance of enhanced HTIR-TCs in a higher temperature (1600 °C) irradiation (although HTIR-TC performance at 1800 °C has been demonstrated in laboratory furnaces, prior irradiations have been limited to peak temperatures of 1200 °C and did not include sensors fabricated with improved processes to enhance HTIR-TC ductility). As indicated in Figure 5-7, prototypes of the enhanced HTIR-TCs exhibited good ductility after stabilization heat treatments.

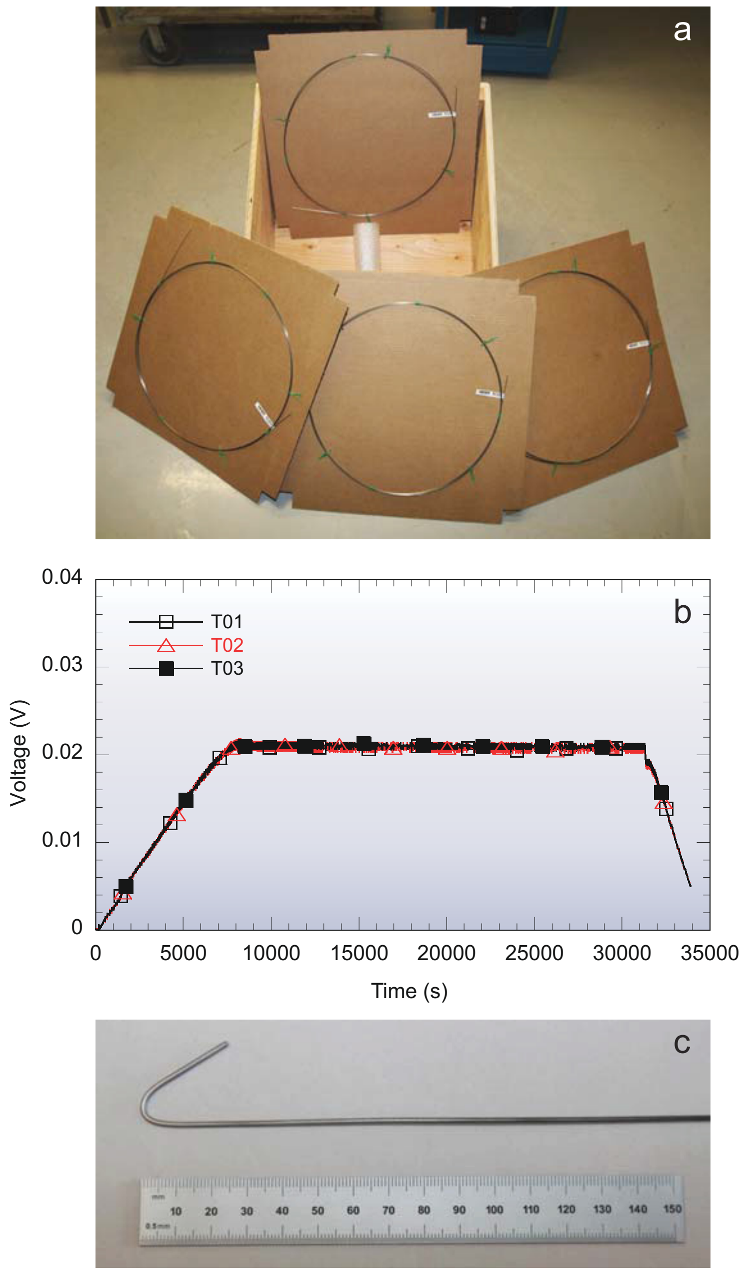

Figure 5-7. HTIR-TCs for IFE/HRP: (a) final HTIR-TCs prior to shipment; Enhanced fabrication techniques demonstrated (b) enhanced stability and (c) ductility after 1700 °C stabilization heat treatment.

As noted in Section 3.3, the HBWR has relied on Type C thermocouples to support high temperature irradiations. To overcome the decalibration that occurs in Type C thermocouples due to transmutation, the IFE/HRP applies correction factors (based on the fact that the irradiations are always performed at the same flux and temperature distributions in the HBWR). However, in recent years, IFE/HRP staff has expressed interested in deploying HTTL-developed HTIR-TCs. The four HTIR-TCs were shipped to the IFE/HRP in November 2011. IFE/HRP currently plans to include these HTIR-TCs in a fuel irradiation test rig that will be inserted into the HBWR in February 2013. This HTIR-TC shipment represents the first time that HTTL-developed sensors have been deployed in a foreign MTR. Transmittal of these sensors facilitates on-going HTTL efforts to obtain IFE/HRP assistance in deploying their LVDT-based and crack growth rate sensors at the ATR.

5.1.4. Ultrasonic Thermometers

Ultrasonic thermometry has the potential to improve upon temperature sensors currently used for in-core temperature measurements.[106] Ultrasonic Thermometers (UTs) can be made with very small diameters while maintaining a high level of durability because the sensor consists of a small diameter rod (typical diameters range from 0.25 mm to 1 mm, although a sheath may be required for some environments).[107] In fact, a small diameter rod is desirable; as wave dispersion is avoided when the rod diameter is sufficiently smaller than the acoustic wavelength.[108] Even though the HTIR-TCs developed by INL have overcome most of the difficulties associated with nuclear-based applications of thermocouples, the resistivity of electrical insulators can degrade if subjected to high temperatures (> 1800 °C), causing shunting errors. However, UT temperature measurements may be made near the melting point of the sensor material, allowing monitoring of temperatures potentially in excess of 3000 °C. A clear line of sight is not required with UTs, as is the case for most optical pyrometry applications. With proper selection of materials, UTs may be used in very harsh environments, such as high temperature steam or liquid metals. Furthermore, thermocouples typically only allow measurement at a single location, and examination of melt wires or silicon carbide monitors only allow estimation of the maximum test temperatures at the point of installation. However, UTs offer the potential for real time in-pile measurement of a temperature profile using a single multi-segment sensor. By introducing multiple acoustic discontinuities into the sensor, UTs are able to perform temperature measurements at several points along the sensor length.

UTs work on the principle that the speed at which sound travels through a material (acoustic velocity) is dependant on the temperature of the material. Temperatures may be derived by introducing an acoustic pulse to the sensor and measuring the time delay of echoes. A conceptual design of a ‘notched-probe’ UT, with key components identified, is shown in Figure 5-8. If the magnetostrictive transducer shown in this figure is considered, a narrow ultrasonic pulse is generated in the probe by a short duration magnetic field pulse produced by an excitation coil (though previous in-pile research utilized magnetostrictive transducers, piezoelectric transducers may potentially be used in this effort). The ultrasonic pulse propagates to the sensor wire, where a fraction of the pulse energy is reflected at each discontinuity (notches or diameter change). Each reflected pulse is received by the excitation coil, transformed into an electrical signal, amplified and evaluated in a start/stop counter system. The time interval between two adjacent echoes is evaluated and compared to a calibration curve to give the average temperature in the corresponding sensor segment. When a number of notches are available on the wire sensor, the various measurements give access to a temperature profile along the probe.

Prior US UT applications demonstrated the viability of this technology for LWR, HTGR, and SFR test conditions (see Figure 5-9).[109] However, prior in-pile applications were primarily limited to fuel damage

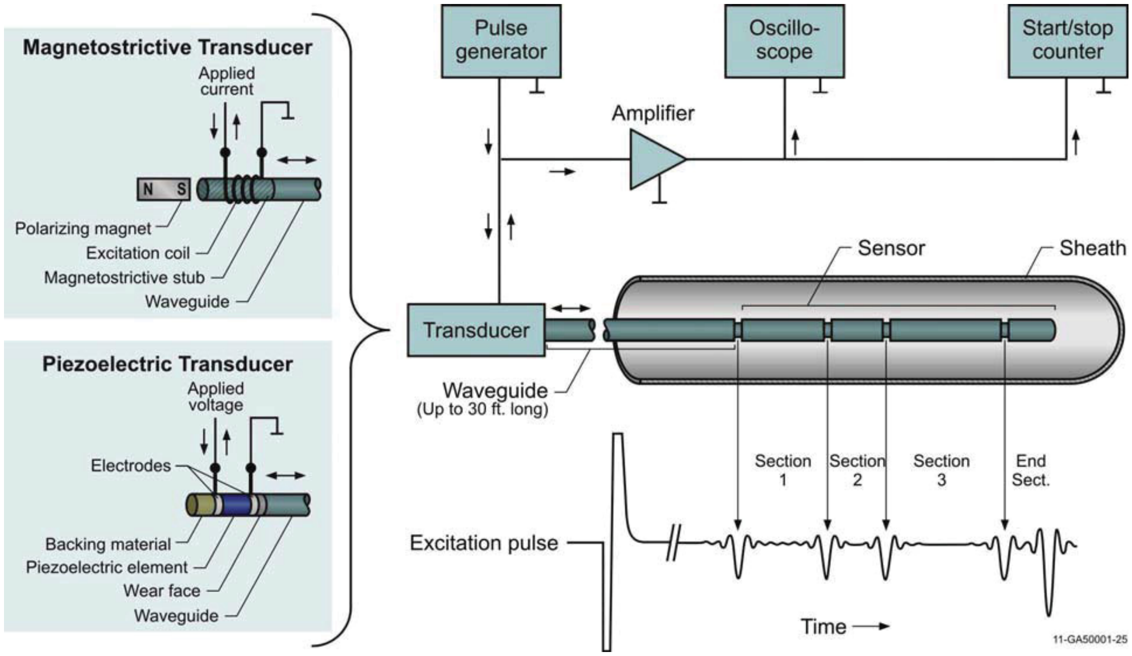

Figure 5-8. Schematic showing typical components of a UT and signal processing equipment.

tests that ceased several decades ago.[109] Although these tests clearly demonstrated the ability of UTs to withstand high temperatures (up to nearly 2900 °C), test durations were typically limited to less than 100 hours; and data acquisition was cumbersome due to the limitations of signal processing systems available at the time. The availability of new materials and signal processing techniques suggests that this technology could be ideally suited for irradiations that require robust, high accuracy, compact sensors.

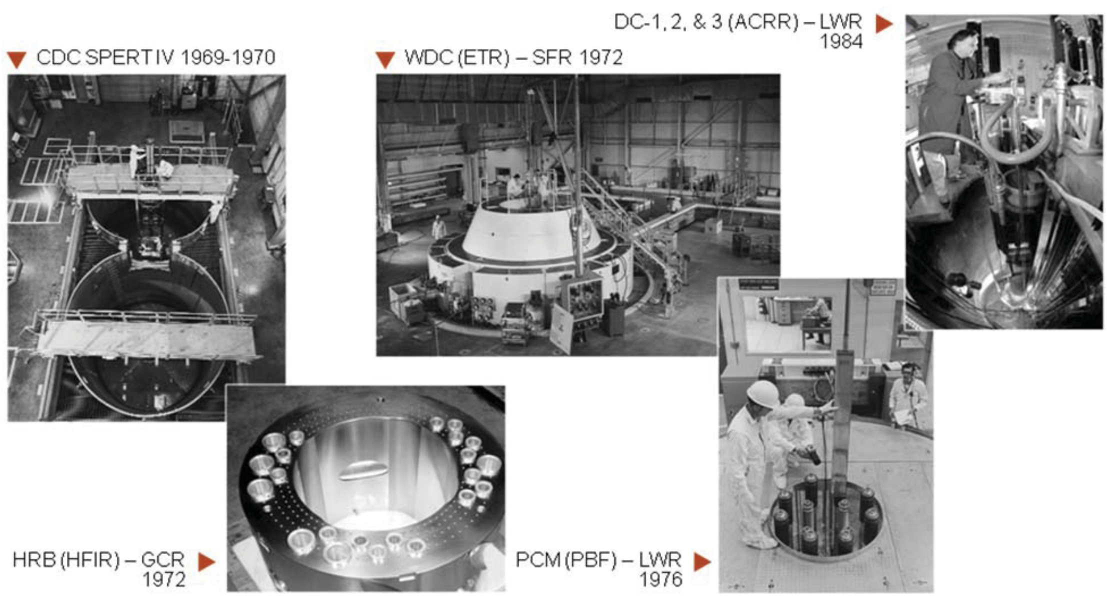

Figure 5-9. Prior UT in-pile applications in the US.

INL is currently developing an optimized UT design that, depending on funding availability and results from laboratory evaluations, could be deployed in a fuel irradiation in FY14. As discussed in this section, optimization activities[110, 111] are focussed on component construction, material selection, stabilization and calibration, and enhanced signal processing development.

As an initial step in the UT system development effort, acoustic velocity characterization tests were completed in order to reduce the number of candidate materials by comparing temperature response, ease of fabrication, transmitted signal quality, etc. The tests were also used to evaluate and make appropriate adjustments to a signal processing technique for UT applications. The steps required to perform these tests (candidate material selection, test sample fabrication, test setup, and signal processing adaptation) are summarized in this section.

The materials selected for initial evaluations are listed in Table 5-2 with relevant material properties and envisioned irradiation environments. Candidate sensor materials were selected based on melting temperature, thermal neutron capture cross section, and compatibility with likely in-pile test conditions. For higher temperature applications, such as inert gas-filled tests of oxide fuels, refractory metals are an obvious choice due to their high melting temperatures. Tungsten and rhenium were not considered (despite high melting points and previous use in UTs for very short term measurements) due to their high thermal neutron capture cross sections, as both are known to be prone to decalibration due to transmutation. Molybdenum and niobium have high melting points and low thermal neutron capture cross sections. Variations of these materials, KW-molybdenum (e.g., molybdenum doped with small amounts of potassium, silicon, and tungsten) and niobium-1% zirconium were selected for initial testing. Prior experience with these materials indicates that they retain ductility better than pure metals after heating. For lower temperature tests (less than 1000 °C) in liquid metal or liquid sodium bonded metallic fuels, stainless steel and Inconel were selected for cost, corrosion resistance, and ease of fabrication.

Table 5-2. Candidate sensor materials.

Material	Melting Temperature, °C	Thermal Neutron Capture Cross Section, Barns	Identified Irradiation Test Application
302 Stainless Steel	1510	3.02	Liquid Metal Bonded Metallic Fuel (T<1000 °C)
304 Stainless Steel	1510	3.03	
Inconel 606	1400	4.35	
Molybdenum	2620	2.51	Inert Gas Filled Ceramic Fuel (T>1000 °C)
KW-Molybdenum	2620	2.51	
Niobium-1%Zirconium	2470	1.14	

Test specimens were isolated from each other in alumina tubes, which were installed in a tube furnace equipped with an argon purge gas system (note that Figure 5-10 shows a single installed sample, but a total of six were included in the test). Signals were generated using a commercial pulser/receiver system, and coils were fabricated in-house. Data were monitored and recorded using a high speed digital oscilloscope.

Temperatures were monitored using a National Institute of Standards and Technology traceable Type-S thermocouple. Data were collected in 100 °C increments from room temperature to 1300 °C.

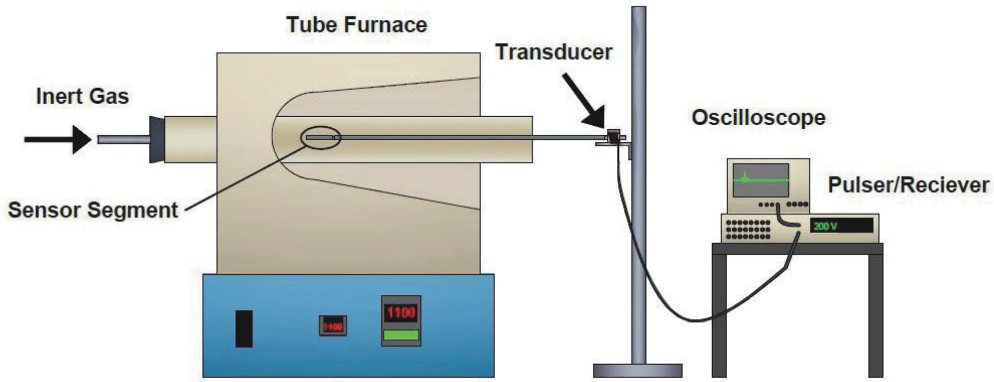

Figure 5-10. Acoustic velocity characterization test setup.

Acoustic velocity was calculated from the delay time between the maxima in the filtered data and the known length of the sensor segment (after correcting for thermal expansion) using the following equation:

$$c = \frac{2(l + \Delta l)}{\Delta t} \tag{5-1}$$

where:

c is the acoustic velocity,

l is the initial sensor length at room temperature,

Δl is the change in length due to thermal expansion, and

Δt is the delay time between maxima.

A signal processing method described by Roberts, et al.,[112] was implemented in the acoustic velocity characterization test. This method consists of cross-correlating the time series data to a known signal (typically either the input signal or the expected reflection), then squaring and low pass filtering the correlated data. This method greatly increases the signal-to-noise ratio and simplifies identification of reflections, even in the presence of significant noise. This makes the technique especially useful when reflected wavelets are noisy and when reflection shape varies between test specimens. The input signal used in this test was a simple square pulse, and could not be used in the cross-correlation. The reflection signals were observed to vary from sample to sample, due to differences in material, reflector geometry, quality of welds between samples and the magnetostrictive wire used to generate signals, etc. Therefore, a computer program (using commercially available mathematics software) was developed that allows the graphical selection of a feature, ideally a relatively clear reflection, of the recorded data to use for cross-correlation. Conditioning of the data is then done automatically. Maxima of the filtered data can then be graphically selected, and the velocity is calculated from the delay time between these maxima. The correlation and filtering process cause a time shift in the signal. However, the acoustic velocity is calculated from the time difference from successive reflections, which does not change. This technique, and the code developed for it, may be easily adapted for temperature measurements, as the delay times used for calculating acoustic velocity are also used in calculation of temperature. A graphical example of the process is shown in Figure 5-11.

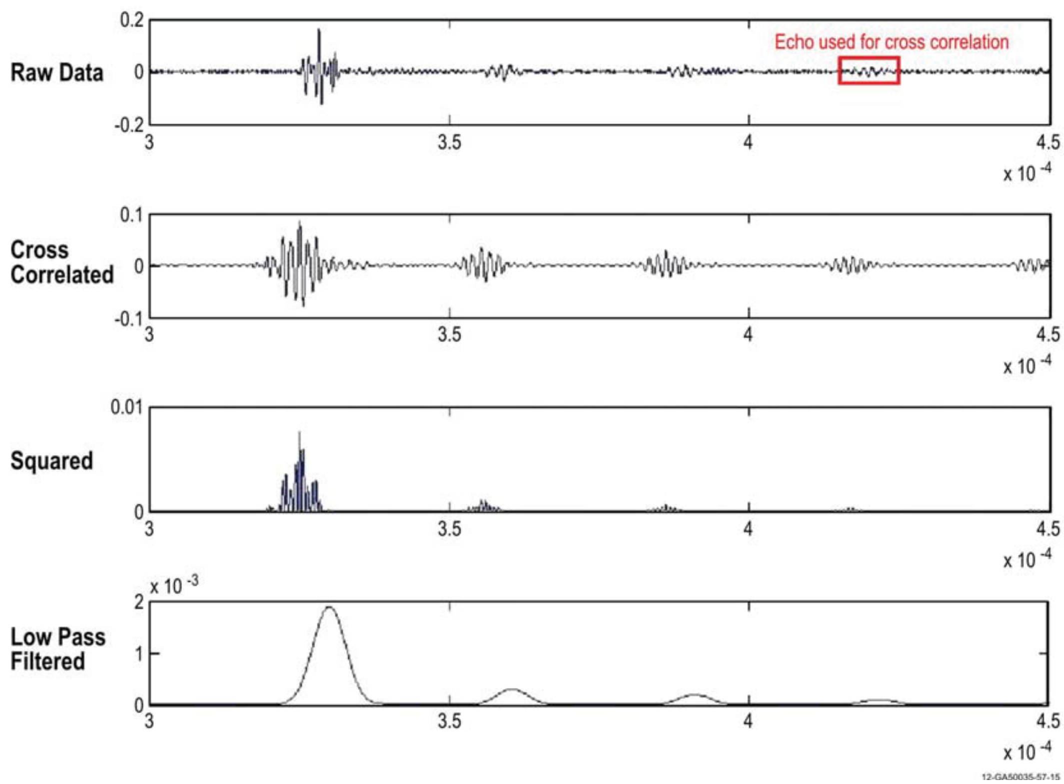

Figure 5-11. Graphical representation of data analysis process.

Results from the acoustic velocity characterization tests, which are documented in Reference 113, indicate that stainless steel and molybdenum are ideal candidates for the two temperature ranges considered in the current evaluations.

Figure 5-12 compares measured acoustic velocities of 302 and 304 series stainless steel samples to values calculated from reference data.[114,115] As shown in this figure, calculated velocities based on test data are somewhat higher than reference values found in the literature (about 5% for temperatures below 800 °C). This difference can be attributed to differences in the manufacturing process used in production of the wires. However, the trend is appropriate for UT applications. High temperature attenuation increased signal noise and eventual loss of signal for temperatures above 1100 °C for the 0.254 mm diameter sample and above 1200 °C for the 1.58 mm diameter sample. It was also observed that the increased signal noise remained after cooling the sample.

Figure 5-13 compares measured acoustic velocities for pure molybdenum and KW-molybdenum samples to values calculated from reference data.[114,116] The temperature response of the molybdenum samples is close to values inferred from the literature, except at the highest and lowest test temperatures. Signals for molybdenum samples did not attenuate significantly over the evaluated temperature range.

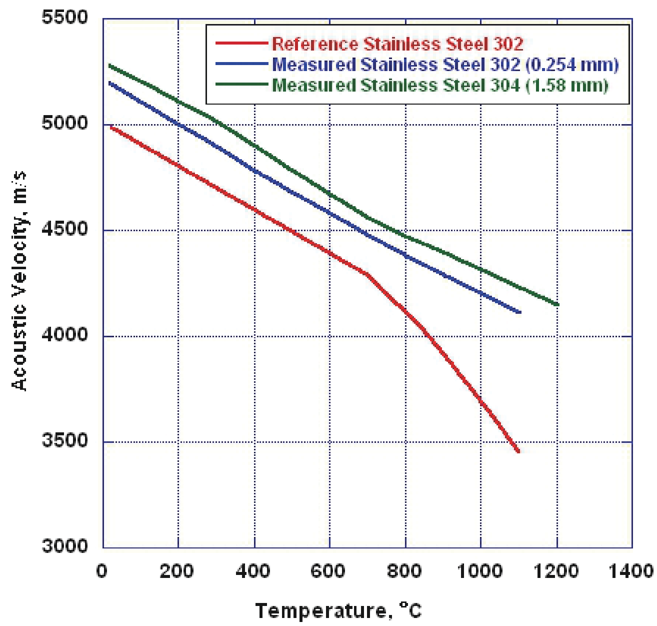

Figure 5-12. Comparison of measured acoustic velocity of stainless steel to calculated reference values.

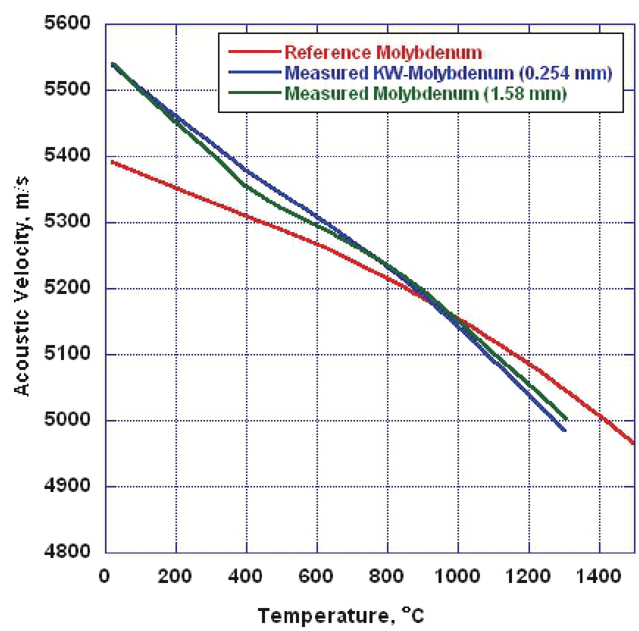

Figure 5-13. Comparison of measured acoustic velocity of molybdenum to calculated reference values.

Inconel 606 is also a good candidate, but test results indicate that it does not offer any significant advantages over stainless steel. Due to difficulty in manufacturing the samples as well as poor temperature response, testing indicates that niobium-1% zirconium is not a good candidate. Additional details about tests with these materials are documented in References 113 and 117.

The accuracy of an ultrasonic system is partially dependent on the operating frequency of the transducer. Higher frequencies allow resolution of smaller physical features (such as reflectors) as well as signal features (such as zero crossings). The frequency of a magnetostrictive transducer is primarily a function of the transducer (i.e. coil or rod) length, with the transducer length equating to one half of its acoustic wavelength. Increasing frequency necessarily requires decreasing length. However, decreasing transducer length also decreases signal strength. To overcome this, a new coil type was developed which utilizes a multi-segment design. As documented in Reference 117, this new coil design consists of several short coils wound from a single wire on a common bobbin. The coils are wound such that the spacing between coils is equal to the length of each coil segment. When the coil is energized, constructive interference of waves generated by each segment causes significant increase in signal strength compared to a single, short coil.

Magnetostrictive transducers require a biasing magnetic field to pre-align the magnetic moments within the magnetostrictive material. Without a biasing field, the signal does not have sufficient amplitude for detection. Typically, biasing is accomplished by placing a permanent magnet parallel to the driving coil and magnetostrictive rod. Asymmetric magnet placement can cause unwanted wave modes, primarily flexural waves. These wave modes travel at different velocities and may interfere with the waves being used for measurements, obscuring the desired information. To eliminate this effect, ring magnets were used, placed on each end of the coil. This results in a more uniform magnetic field, as well as reducing the overall transducer diameter.

Ultrasonic transducers used to generate acoustic waves in a wire waveguide generate these waves in both directions along the wire (both toward and away from the sensor section of the waveguide). The waves propagating away from the sensor strike the free end of the waveguide and are reflected back toward the transducer, where they may interfere with the signals being used for measurement. In order to eliminate this problem, the free end of an ultrasonic transducer is damped. This is typically accomplished (in the case of piezoelectric transducers) by compressing a highly attenuating material against the free side of the transducer crystal. This is not an option with a small wire waveguide, as the area of the wire end is too small. A different damping method was developed that allows complete damping of the back end echo when used with a small waveguide (i.e., 0.010 inch diameter). This method becomes significantly less effective as waveguide diameter increases. For use with a thin wire waveguide, a short section of metallic tubing is filled with an attenuating material and swaged onto the free end of the waveguide, compressing the damping material, as shown in Figure 5-14.

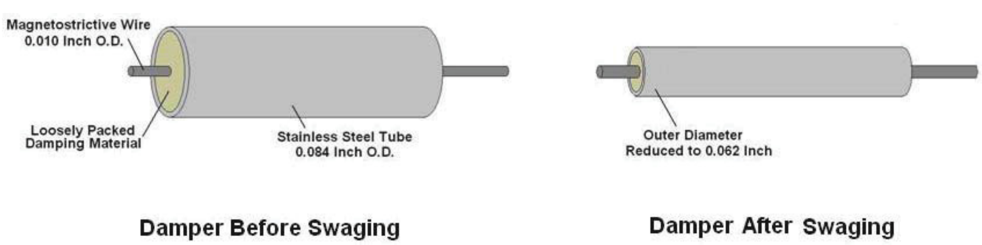

Figure 5-14. Description of swaged damper.

For in-pile testing with a stainless steel or Remendur waveguide, most damping materials (i.e. polymers and greases/gels) are not usable. Therefore, crushable oxides and stainless steel wool were selected as potential damping materials. It was determined that the signal improvement yielded by a swaged damper is primarily dependent on two properties; the acoustic impedance mismatch between the damping material and the waveguide, and the compression of the damper. For a 26% reduction in damper diameter (3 inch damper length), complete back-end echo attenuation was observed for dampers constructed with stainless steel wool or magnesium oxide powder.

A complete magnetostrictive transducer incorporating all current design enhancements is shown in Figure 5-15. Candidate materials for various components are also shown in this figure. During FY13, evaluations will be conducted to finalize the selection of component materials.

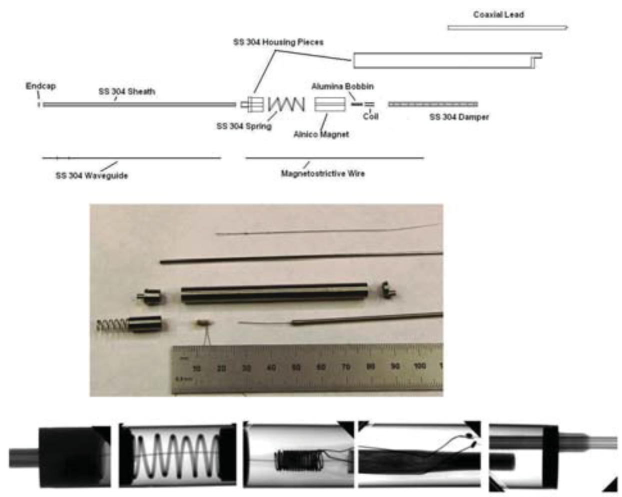

Figure 5-15. Current driving coil design with ring magnets and swaged damper.

5.2. Thermal Conductivity Sensors

Thermal conductivity is a key property needed to characterize fuel or material performance during irradiation testing. Thermal conductivity is highly dependent on the physical structure, chemical composition, and the state of the material. Currently, changes in fuel or material thermal conductivity during ATR irradiations are evaluated out-of-pile. However, as discussed in this section, a new real-time method for detecting changes in thermal conductivity during irradiation in instrumented lead and loop tests is now available.

Historically, in-pile thermal conductivity measurements were made using an approach with one (or more) thermocouples embedded near the center of the fuel rod and one exterior to the fuel (in the coolant or a structure outside the fuel element). As part of a collaborative effort with Utah State University (USU) and the Institute for Energy Technology at the Halden Reactor Project (IFE/HRP), INL compared the multiple thermocouple steady-state thermal conductivity approach and the transient hot wire thermal conductivity method (with a single probe containing a line heat source and thermocouple embedded in the fuel as shown in Figure 5-16b) as candidate in-pile effective thermal conductivity measurement techniques.[118 through 122] Evaluations compared the accuracy of each approach for various fuel types and test conditions. Results indicate that the Transient Hot Wire Method Needle Probe (THWM NP) offers an enhanced method for in-pile detection for thermal conductivity.[124]

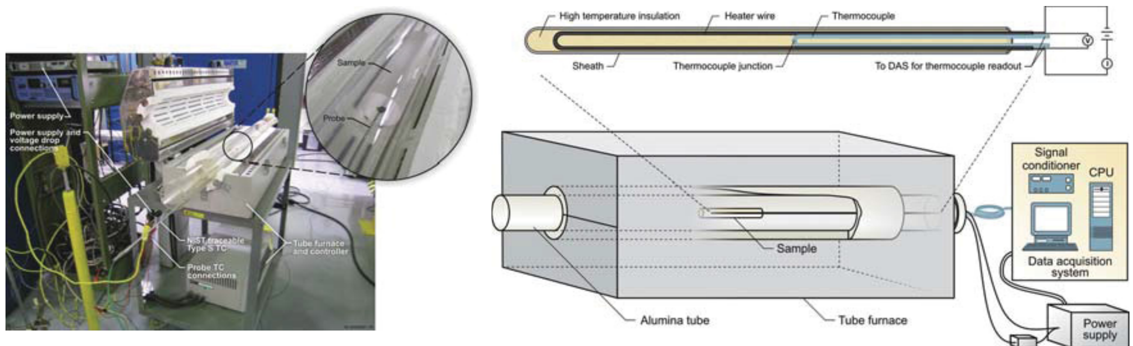

(a) (b)

Figure 5-16. Setup for evaluating transient hot wire needle probe.

The THWM or line heat source method was first suggested by Schleirmacher.[125] Numerous references may be found in the literature describing applications of this method to measure the thermal conductivity of solids, fluids, and gases (e.g., see References 128 through 133). In the THWM approach, thermal conductivity is determined from the temperature rise in the sample when the heat source is energized.[128] In a solid, this method may be applied by embedding the probe in the material whose thermal conductivity is to be measured. From a condition of thermal equilibrium, the probe is energized and heats the sample with constant power. The temperature response of the sample is a function of its thermal properties, and the thermal conductivity is calculated from the temperature rise detected in the sample. Following a brief transient period, a plot of temperature versus the natural logarithm of time becomes linear, as shown in Figure 5-16 (linear region of the time period between times, t_2 and t_1, and temperatures, T_2 and T_1). The slope of the linear region is used to calculate the test material thermal conductivity.

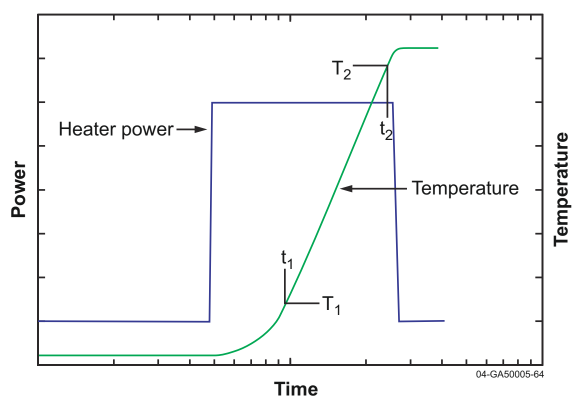

Figure 5-17. Semi-log temperature rise plot for transient hot wire methods.

THWM NPs were designed and fabricated by INL for room temperature proof-of-concept evaluations and high temperature testing. Using the setup shown in Fig. 5-16a, the needle probe was demonstrated to work very well for materials with thermal conductivity ranging from 0.2 to 16 W/m-K with measurement errors of less than 5%, delivering thermal conductivity measurements with a high degree of accuracy and consistency (see Figure 5-18). Test results indicate that special considerations are needed for high thermal conductivity sample materials and for smaller diameter samples. Methods were explored to reduce the challenges associated with such samples, primarily techniques that could reduce signal noise and allow better characterization of the probe response time. In addition, results from long term evaluations indicate that the INL-developed THWM NP for in-pile detection of thermal conductivity is a robust sensor that could survive in the harsh environments associated with in-pile fuel testing. The DOE has filed a patent on the THWM NP.[124]

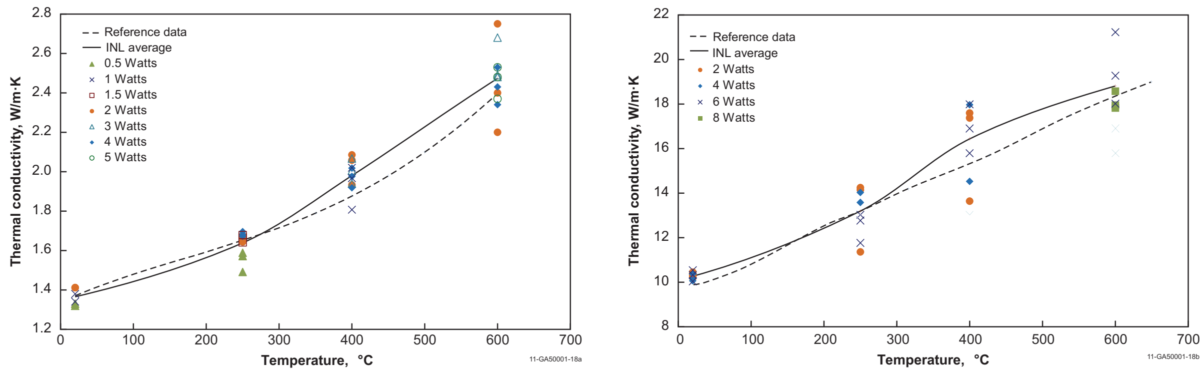

(a) (b)

Figure 5-18. Comparison of THWM NP results for various power levels for (a) fused silica and (b) Inconel Alloy 625.

Insights gained from these evaluations have been used to develop probes for several organizations. During FY11, a prototype needle probe (see Figure 5-19a) was fabricated and shipped to MIT for a MITR irradiation with high thermal conductivity, hydride fuel, with peak temperatures less than 700 °C. During FY13, INL will fabricate and ship a THWM NPs to IFE/HRP for a low thermal conductivity ceramic fuel HBWR irradiation with peak temperatures less than 1300 °C (see Figure 5-19b) and to CEA for hot cell low thermal conductivity fuel measurements in a hot cell containing a furnace with peak temperatures less than 400 °C (see Figure 5-19a). Materials and geometries of each of these THWM NPs are optimized for the fuel materials and test conditions. Experience gained from these applications provide additional insights related to optimizing the design and performance of the THWM NP.

5.3. Elongation/Deformation/Creep/Swelling

New materials are being considered for fuel, cladding, and structures in next-generation and existing nuclear reactors. Such materials can experience significant dimensional and physical changes during irradiation. Currently, such changes are measured at the ATR by repeatedly irradiating a specimen for a specified period of time and then removing it from the reactor for evaluation. The labor and time to remove, examine, and return irradiated samples for each measurement makes this approach very expensive. In addition, such techniques provide limited data and handling may disturb the phenomena of interest. Commercially-available LVDTs are being evaluated as a near-term option for detecting geometry changes in-pile during ATR irradiations; thereby eliminating the problems associated with the current “cook and look” approach. In addition, ultrasonics and fiber optic technologies are being explored as options that can measure geometry changes with higher precision in multiple dimensions at higher temperatures.

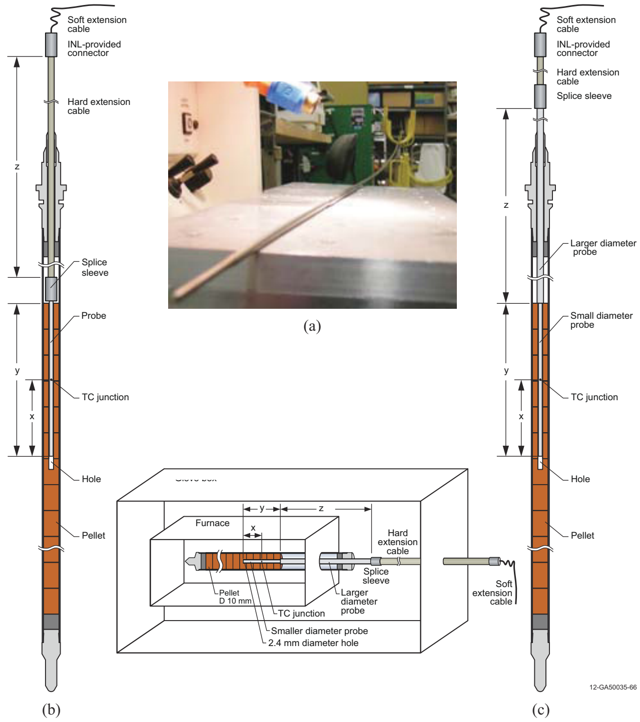

Figure 5-19. THWM NPs completed for (a) MITR and under development for (b) HBWR, and (c) CEA hot cell testing.

5.3.1. LVDT-based Elongation

Earlier references[134,135] report using miniature strain gauges encased in zircaloy sheaths welded on the cladding in the circumferential and axial directions to detect dimensional changes. These references indicate that strain gauge measurements were unstable due to high sensitivities of the gauges to temperature and neutron fluence. Today, most MTRs rely on LVDTs (see Section 3.3) to detect dimensional changes during irradiation; and many of the LVDTs in use today are made by the IFE/HRP. As discussed in Section 3.3, operating experience has shown that these sensors are a robust, frictionless, high resolution instrument for detecting dimensional changes in lower-temperature, irradiation environments. However, some IFE/HRP LVDTS suffer from Curie temperature effects near 360 °C, the temperature that corresponds to the Curie point for the nickel used in the LVDT windings. More recent evaluations of LVDTs using alternate coil materials, completed in collaboration with IFE/HRP, have led to an LVDT without Curie temperature limitations for detecting dimensional changes during irradiation testing at the ATR and other MTRs.

Initially, nuclear-grade LVDTs from US and foreign sources were evaluated as candidates for in-pile deployment. INL efforts, which included calibration evaluations and long duration, high temperature testing, clearly indicated the superiority of LVDTs supplied by the IFE/HRP (see Figure 5-20a). However, evaluations indicated that Curie temperature effects, due to the nickel contained in the LVDT coil material, have the potential to affect accuracy near 360 °C. Consequently, use of these LVDTs could be an issue depending on the in-core position of the sensor and the corresponding gamma heating levels. For that reason, INL worked with IFE/HRP to develop and evaluate enhanced LVDTs with an alternate coil material that is not susceptible to the Curie effect. Calibration and long term high temperature testing of these enhanced LVDTs, which was performed by INL, demonstrate that the enhanced LVDTs can operate in a very stable manner for long periods (1000 h) at high temperatures (500 °C). As shown in Figure 5-20b, the degradation of the original LVDTs was not observed in the enhanced LVDTs provided by IFE/HRP. Hence, these enhanced LVDTs are recommended for use in ATR high temperature irradiation tests.

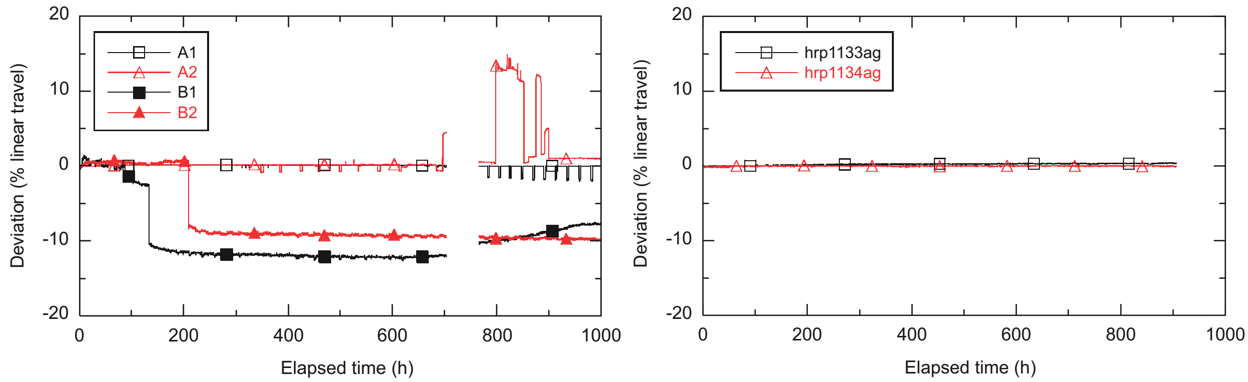

(a) (b)

Figure 5-20. Long duration (1000 hour) test at 500 °C results: (a) LVDTs originally provided by nuclear grade vendors (IFE/HRP LVDTs designated with "A"); and (b) enhanced IFE/HRP LVDTs.

5.3.2. Initial LVDT/bellows-based Creep and Tensile Test Rigs

As discussed in Section 3, several organizations (e.g., VTT, INL, KAERI, and CEA) have been involved in developing and deploying in-pile tensile test rigs to detect growth of tensile and creep specimens using a bellows to apply a load to a specimen and LVDTs to detect growth of the specimen. During 2012, INL completed efforts to develop an initial in-pile creep test rig for deployment in an ATR PWR loop. As discussed in References 136 through 141, the enhanced creep test rig design shown in Figure 5-21 represents a refinement of the original creep test rig shown in Figure 5-22. As indicated in both figures, major components include a tensile specimen, a bellows, an LVDT, and the fixturing needed to connect these components within a supporting frame. (In a pressurized water environment [i.e., an autoclave or a PWR test loop], external water pressures tend to collapse the bellows producing a tensile load on the specimen.) IFE/HRP provided the LVDT and welded the LVDT, bellows, and the associated connecting fixturing in both test rigs using e-beam welding techniques.

The primary refinements embodied in the enhanced creep test rig (relative to the original creep test rig), and the factors motivating those modifications, include changes in the:

- LVDT - Coil wires are made from a silver alloy rather than a copper-nickel alloy to eliminate Curie-point temperature instabilities associated with earlier versions of the IFE/HRP LVDT (see Reference 139).
- Connecting Fixturing - Specimen to fixture interfaces were designed to minimize potential mating mismatch while promoting easier assembly/disassembly. In addition, the lower adaptor was fitted with a hex nut to allow pre-loading sufficient to minimize the effects of compliance issues.
- Frame - The mass of stainless steel was reduced to minimize gamma heating. The frame was also re-designed for to ensure compatibility with the ATR test holder for PWR Loop 2A (see Figure 5-23).

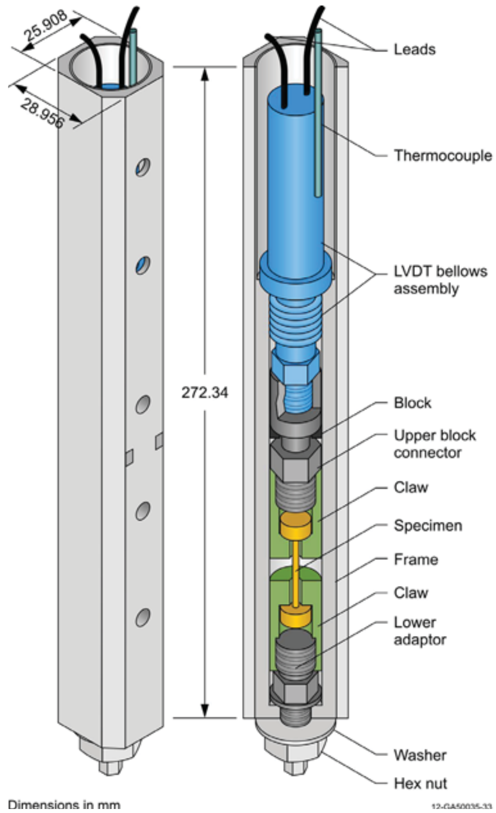

Figure 5-21. Enhanced creep test rig.

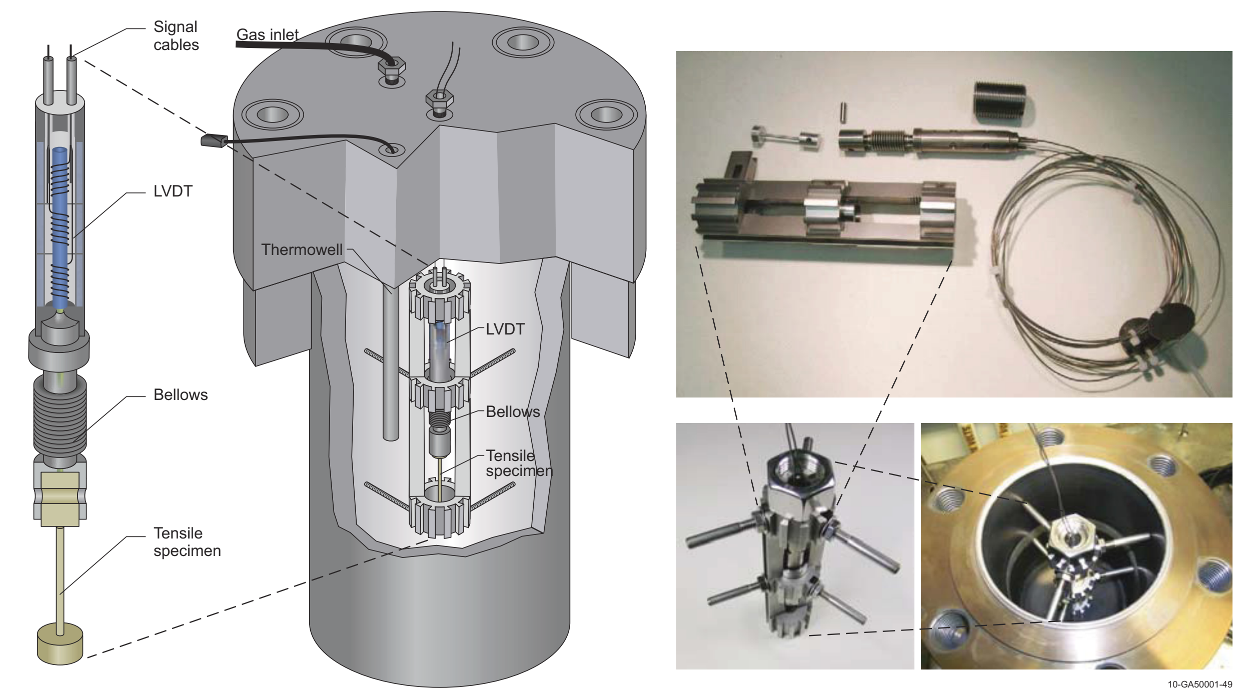

Figure 5-22. Original creep test rig positioned in autoclave for testing.

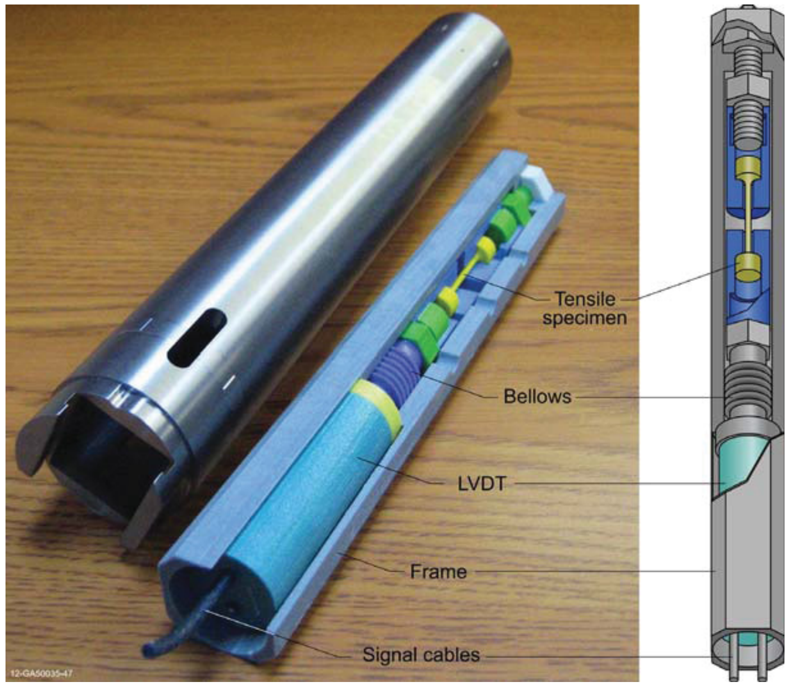

Figure 5-23. Enhanced creep test rig (holder, three-dimensional model and schematic).

Key components in the enhanced test rig design are listed in Table 5-3. Note that an aged Inconel 718 bellows was selected because of its higher strength, although the bellows may be fabricated from other materials (e.g., Inconel 625, Inconel X-750, or stainless steel). Additional information regarding the enhanced creep test rig can be found in Reference 141.

Table 5-3. Summary description of components used in enhanced creep test rig.

Component	Manufacturer	Model Number	Material
Bellows	Mini-Flex	I718-320-110-790, Rev: -- C	Inconel 718, aged
LVDT	IFE/HRP	Type 5	Inconel 600; Core - AISI 403; Coils - Silver Alloy (Alloy 406; Alcal Type E Insulation)
Connecting Fixturing	IFE/HRP	NA	Inconel 600
Tensile Specimen	INL	NA	304 stainless steel and copper

To qualify this enhanced test rig for use in the ATR, tests were completed to characterize the bellows spring rate and effective area. Although the bellows manufacturer provides a range of nominal values for these parameters, detailed evaluations are required to precisely quantify the specimen load as a function of pressure and displacement measurements. Bellows spring rate and effective area characterization required development of specialized fixtures and processes as shown in Figure 5-24.

As described in Reference 141, the specimen load (F_S) is given by

$$F_s = PA_B - k_B \Delta L \tag{5-2}$$

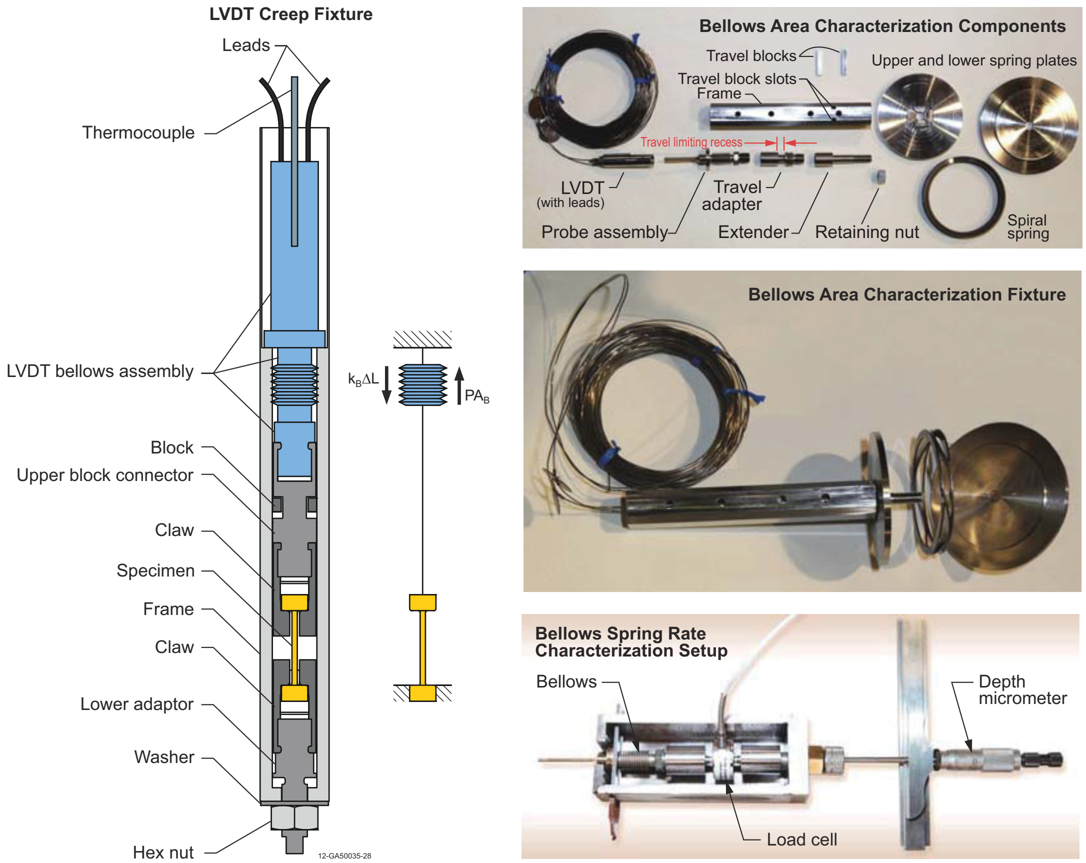

Figure 5-24. Bellows characterization configuration with an equivalent specimen load diagram.

where

P = pressure acting on the exterior surface of the bellows,

A_B = bellows effective area,

k_B = bellows spring rate, and

ΔL = displacement of the bellows (and the specimen) as detected by the LVDT.

The bellows spring rate was determined through a series of bench top measurements where the probe assembly was constrained by one end of a fixture so that the bellows could be collapsed by incrementally tightening a hex bolt into threads in the opposite end of the fixture. As the bolt was tightened, an ever increasing force was registered by the (calibrated) load cell consistent with the bellows spring rate and displacement. Displacement of the bellows was periodically measured during incremental bolt tightening, using a depth micrometer and/or by converting the revolutions of the bolt into an equivalent linear movement based on the bolt pitch. The depth micrometer was clamped in line with the fixture, and the micrometer was simply advanced to touch the head of the hex bolt each time the bolt was tightened as indicated in Figure 5-24. Relative to Equation (5-2), P was effectively zero and (F_S) was registered through the load cell while ΔL was measured. That allowed direct calculation of the bellows spring rate (k_B) based on the measured values. Note that all bench top measurements were completed at room temperature with the assumption that the spring rate is temperature independent.

The bellows effective area was determined through a series of measurements in an argon atmosphere in an autoclave using components shown in Figure 5-24. As autoclave pressures were increased, the (constrained) bellows imparted an ever increasing force in the (calibrated) load cell. The effective area characterization process consisted of incrementally increasing the autoclave pressure and recording that pressure along with the associated load cell output. Relative to Equation (5-2), it should be clear that ΔL was held at zero while (F_S) was registered through the load cell and P was measured. That allowed direct calculation of the bellows effective area (A_B) based on the measured values.

As discussed in Reference 141, the enhanced LVDT bellows assembly was then calibrated at room temperature and at 150, 250, and 350 °C, which covers the range of temperatures expected during deployment in the ATR Loop 2A. This calibration provides the means to relate any measured LVDT output voltage to a corresponding displacement. Although IFE/HRP provided calibration as part of their LVDT delivery agreement with INL, their calibration could differ from INL data based primarily on potential differences in signal conditioning electronics. INL calibration was therefore required.

Bench top and autoclave calibrations at room temperature were completed. Bench top measurements (at room temperature) provided a way to check results that were subsequently obtained through (room temperature) autoclave testing. That way, a degree of confidence was achieved relative to the validity of all autoclave testing, which was deemed the best method to obtain higher temperature calibration results.

The bench top setup was essentially identical to the spring rate characterization configuration shown in Figure 5-24. The addition of the LVDT to the end of the probe assembly was the only difference relative to the figure. With the LVDT in place, each advancement of the bolt (which was measured with the depth micrometer) was accompanied by a change in the LVDT output voltage. The bench top calibration process consisted of incrementally tightening the bolt, recording the LVDT output voltage, and measuring the associated displacement.

Autoclave testing was considerably more complex than bench top testing because of difficulties measuring displacement inside the autoclave. Those difficulties were addressed through the design and fabrication of a specialized fixture with positive mechanical stops to accurately define a displacement. Components in that fixture, and the (semi-)assembled fixture, is shown in Figure 5-24 (see Bellows Area Characterization).

The autoclave fixture was assembled with the retaining nut tightened just enough to (slightly) stretch the bellows and pull the top of the travel limiting recess (in the travel adapter) into contact with the travel blocks. That provides the initial position of the LVDT for all autoclave testing. As the pressure is increased during each test, the bellows contracts, which collapses the spiral spring and allows movement of the travel adapter. At some autoclave pressure, bellows contraction is sufficient for the bottom of the traveling limit recess to contact the travel blocks, which defines the final LVDT position for all autoclave testing. All autoclave calibration testing was conducted in a pressurized argon environment, where autoclave heaters were used to achieve the desired temperature for each test.

Calibration measurements are compared to IFE/HRP calibration data in Figure 5-25. Although the general trends in the data sets are very similar, there is clearly a shift (or an offset bias) between the data sets. All reason(s) behind this shift are unknown; however, differences between INL and IFE/HRP LVDT signal conditioning electronics have been identified as the major contributor.

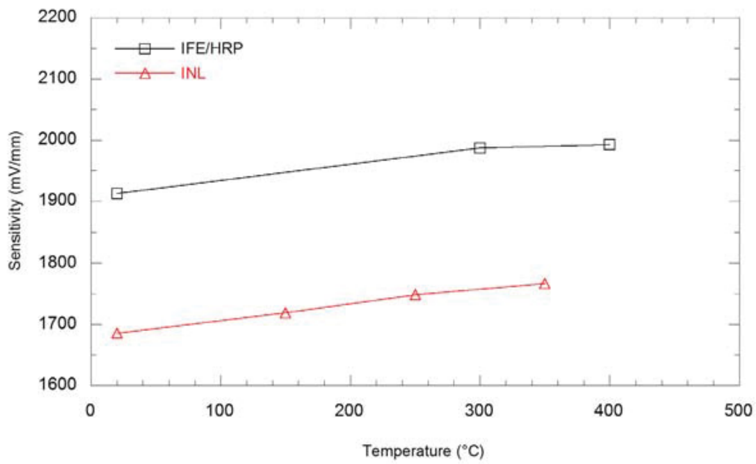

Figure 5-25. Calibration results from IFE/HRP and INL.

In summary, an enhanced creep test rig has been designed, characterized, and calibrated. The rig is ready for deployment to measure specimen elongation in real time during irradiation testing in ATR Loop 2A. Once it is deployed in the ATR, data from this test rig will be evaluated to assess its performance and refine the design (if appropriate) to develop standard LVDT-based test rig designs for ATR testing.

5.3.3. Enhanced Creep Test Rig with Variable Loading

As discussed in Section 3, several MTRs (e.g., BR2 with assistance from VTT, HANARO with assistance from KAERI, JMTR with assistance from JAERI, and OSIRIS with assistance from CEA) have deployed creep test rigs with a bellows to apply a variable load to a specimen and LVDTs to detect growth of the specimen. Selected aspects of these various creep test setups are compared in Table 5-4. In most cases, test pressures external to the bellows are offset by internal bellows pressurization to produce the variable loads. As indicated, however, most of the setups are designed to test specimens in inert gas. A notable exception is specimen testing in reactor coolant conducted in BR2.

The rig developed by VTT and tested in BR2 is shown in Figures 3-21 and 3-22. The materials used in the irradiation test were thin (0.3 mm) sheets of oxygen free high conductivity copper containing trace amounts of Ag, Si, Fe, Mg, and CuCrZr alloy because these materials are expected to be exposed to thermal and mechanical loads in International Thermonuclear Experimental Reactor. The test rig includes a pneumatic loading unit, which applies a tensile load on the test specimen using inert gas to pressurize a metallic bellows and a LVDT from IFE/HRP to measure the resulting displacement produced in the specimen. The load generated by the pneumatic unit is calculated from the pressure differential applied to the bellows. The stiffness and effective cross section of the bellows also impacts the load exerted on the specimen. However, the stiffness of the pneumatic loading unit differs from the stiffness of the bellows. Hence, VTT developed a calibration unit to correlate the applied gas pressure in the bellows with the actual load acting on the specimen (see Figure 3-23). Test results demonstrated that it is technically feasible to carry out well-defined, controlled, dynamic in-pile tensile tests, making it possible to investigate the intrinsic role of applied stress and displacement damage acting concurrently in determining the global deformation behavior of the specimen under dynamic irradiation conditions.

Table 5-4. Summary of creep testing in MTRs.[136]

Country/MTR	Test Conditions	Real Time Load Control	Method	Real Time Elongation Detection	Method
Belgium/BR2 with assistance from VTT	Stagnant reactor coolant (~ 90 °C)	Yes	Internally pressurized bellows	Yes	Monitored LVDT
France/OSIRIS[a]	Inert gas, water, and NaK (from room temperature up to 380 °C)	Yes	Internally pressurized bellows	Yes (also external diameter gauges)	Monitored LVDT
Norway/HBWR	Inert gas (240-400 °C)	Yes	Internally pressurized bellows	Yes (also external diameter gauges)	Monitored LVDT (under development for 600 °C and 250 bar)
Japan/JMTR	Inert gas (550 °C)	Yes	Internally pressurized bellows	Yes	Monitored LVDT
Netherlands/HFR	Inert gas and NaK (300-600 °C)	Yes	Self-contained spring-washer system	Yes (semi-continuous)	Monitored LVDT
Korea/HANARO	Inert gas (up to 600 °C)	Yes	Internally pressurized bellows	Yes	Monitored LVDT

a. In upcoming tests. Previous tests relied on out-of-pile measurements with strain gauges.

Based on VTT concepts and the INL enhanced creep test rig (described in Section 5.3.2), efforts were initiated under the FCRD program during FY12 to develop a conceptual design for a creep test rig for deployment in US MTRs with the ability to apply a variable load to a specimen. Like the enhanced creep test rig, this design will allow testing in reactor coolant at PWR conditions. As indicated in Table 5-4, the enhanced creep test rig, and completion of this design for variable specimen loading, will position INL as the second organization in the world capable of real-time creep testing in reactor coolant.

During FY12, an LVDT was procured from IFE/HRP. An LVDT / bellows assembly was then designed with provisions for internal pressurization of the bellows via an Inconel tube (with an OD of 1.59 mm) as shown in Figure 5-26. The key to internal pressurization lies in a small diameter hole (~1 mm ID) that will be drilled through the edge of the flange separating the LVDT from the bellows. This hole will tap into an annular gap between the LVDT core and the core guide tube (inside the LVDT). The small hole provides the means for pressurization because the annular gap accessed by the hole also extends beyond the flange to regions inside the bellows. The Inconel pressurization tube, which will be seal welded to the flange, will connect the small hole to a high pressure inert gas supply with an appropriate control system. (Note that the penetration of the small hole through the edge of the flange will also be seal welded.)

Test articles were made to develop and evaluate a laser welding technique and design dimensions for the bellows' end plugs. Using the dimensions and laser weld parameters that evolved from test article development, two bellows assemblies with prototypical end plugs were successfully fabricated and found to be leak tight with a helium leak rate of less than 1 $\times 10^{-8}$ atm cc/sec. A welded bellows and bellows with prototypical end plug are shown in Figure 5-2.

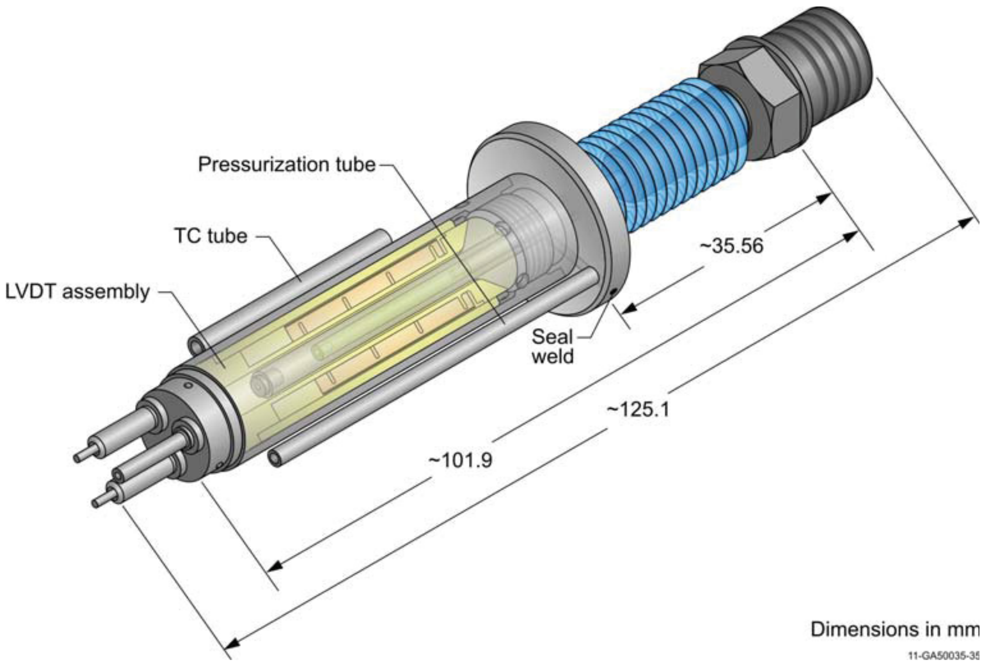

Figure 5-26. LVDT / bellows assembly with provisions for internal pressurization of the bellows.

Figure 5-27. Laser welded bellows (top) and bellows with prototypical end plug prior to welding (bottom).

The LVDT / bellows assembly was designed so that it can be used interchangeably with the enhanced creep test rig described in Section 5.3.2. As indicated in Figure 5-28, the LVDT / bellows assembly, and the hardware associated with connections to the specimen, fit in the frame for the enhanced creep test rig. As previously discussed, this frame also fits inside the test holder as shown in Figure 5-23. Ultimately, this means that enhanced creep test rigs, with or without variable specimen loading capabilities, can be deployed in established ATR test configurations for PWR Loop 2A. During FY13, the creep test rig design with variable specimen loading capabilities will be completed, fabricated, and tested from room temperature and pressure conditions up to PWR temperature and pressure conditions in an HTTL autoclave. This testing will be used to calibrate the rig as a function of temperature while verifying all test rig functions.

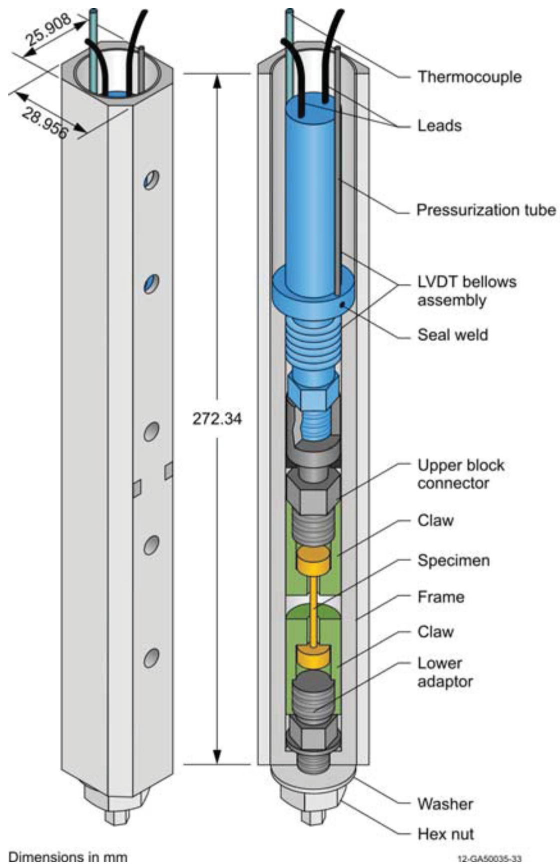

Figure 5-28. Creep test rig incorporating variable specimen loading capabilities.

5.3.4. Ultrasonics

Although LVDTs have been successfully deployed at other test reactors and are being investigated for ATR applications, ultrasonics offer the potential for a more compact, higher temperature, more accurate, and multi-dimensional real-time sensor for detecting geometry changes during irradiation. However, the use of ultrasonic techniques as an in-pile sensor is challenging because of their current reliance on piezoelectric transducer materials. First, typical in-pile operating conditions (350°C) are well above the Curie temperature of piezoelectric transducer materials that are often used for out-of-pile ultrasonic inspections,[142] and the transducer will stop functioning. Second, piezoelectric transducers are typically not suitable for radiation exposure. Radiation can damage piezoelectric transducer materials and degrade their performance.[143-144] Finally, conventional piezoelectric transducers often contain elements, such as lead, lithium, and gold, that transmute into toxic substances. Magnetostrictive transducers have been successfully deployed for short duration, lower frequency in-pile applications, such as ultrasonic thermometry (see Section 5.1.4). The use of magnetostrictive transducers in combination with guided wave options has the potential overcome the limitations of the piezoelectric transducers for in-pile measurement of geometry changes.

A three-year project was recently completed, using INL LDRD funding, to investigate the feasibility of using ultrasonic methods for in-pile measurement of geometry changes in creep specimens of candidate new reactor materials during irradiation testing. In this project, laboratory evaluations were completed at

INL and at the Pennsylvania State University (PSU) to optimize components required for using ultrasonic techniques for in-pile elongation measurement. Key components of an in-pile setup initially investigated (see Figure 5-29a) include a magnetostrictive transducer (e.g., a driver coil with magnetostrictive core), a Remendur guide, a coupling between the Remendur guide and a long stainless steel wave guide that allowed the transducer to be located outside of the reactor, and a creep specimen with an acoustic horn to optimize the signal. Laboratory evaluations identified several options that would eliminate unwanted reflections in this initial setup, such as (1) significant reductions in the length of the stainless steel wave-guide, (2) elimination of brass coupling between Remendur and stainless steel waveguides, (3) replacement of the acoustic horn on the creep specimen with an acoustically-clean “button,” (4) optimization of the magnetostrictive transducers, and (5) elimination of acoustic reflections from the end of the Remendur waveguide. The “buttons” that were found to be superior to acoustic horns were similar to conventional butt-end shoulders used in tensile testing, except the buttons were designed to slide onto the specimen. Attachment methods were developed to ensure that the buttons could impart the desired tensile load and be easily attached without concerns about perfect specimen-to-button alignment. As illustrated in Figure 5-29(b), these buttons were found to be very effective at eliminating unwanted reflections, especially when implemented in conjunction with other enhancements identified in this effort.

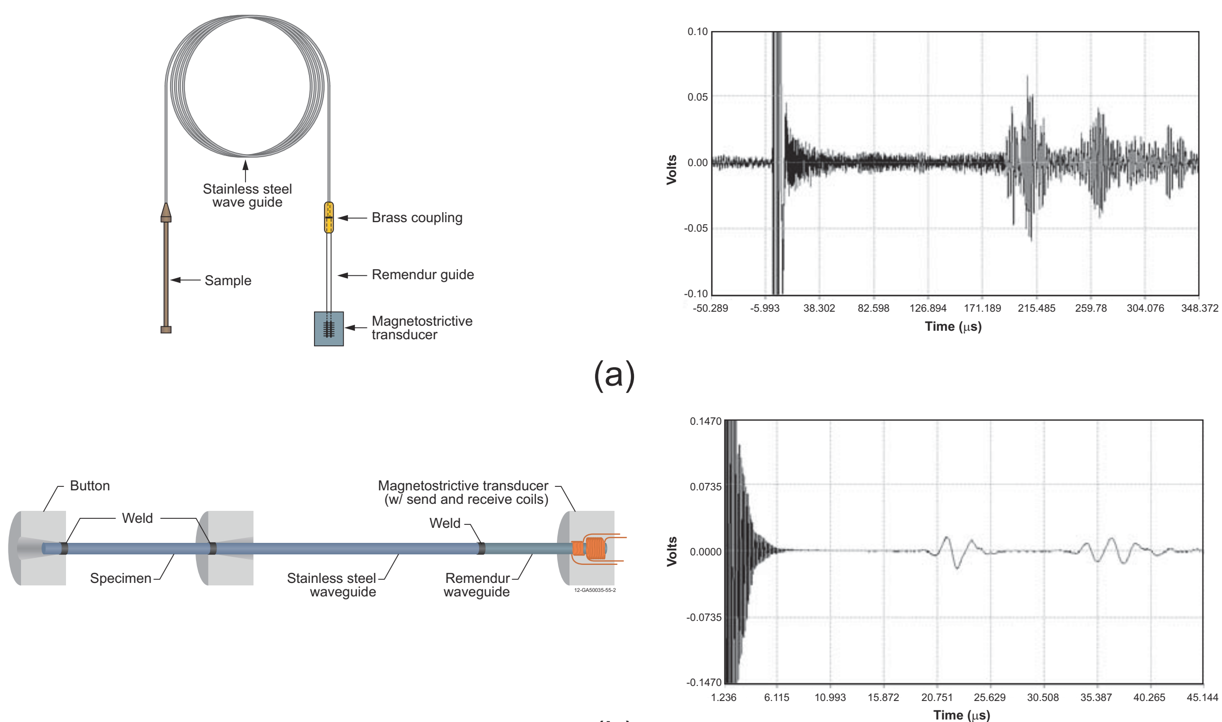

Figure 5-29. Representative system components and typical pulse/echo results using (a) initial concept with an acoustic horn and (b) enhanced concept with buttons.

Although it was demonstrated that acoustic signals can be transmitted through the very long (~9 m) stainless steel waveguide under carefully controlled laboratory conditions, a number of potential issues were identified that raised concerns about use of this waveguide in any MTR irradiation test. Specifically, unwanted acoustic reflections can occur due to inadvertent contact with surrounding structures along the waveguide length, attenuation of the signal as a function of waveguide length is unavoidable, and the task of routing the waveguide from the core to a point outside the vessel without interference with other reactor components and test train structures would be difficult. Laboratory testing confirmed that unwanted acoustic reflections can completely mask the reflections that are needed to determine specimen elongation. In addition to acoustic reflections associated with inadvertent contact, generation of unwanted reflections by small bends, nicks, and other minor imperfections in the waveguide was also observed. For those reasons, efforts focussed on developing a design that could minimize the stainless steel waveguide length used for irradiation testing in MTRs.

Hence, laboratory testing was conducted with stainless steel waveguides ~1 m long, or less. This length was deemed sufficient to allow positioning of the creep specimen inside the ATR core and positioning of the magnetostrictive transducer above the core. In addition, an ex-core position of the transducer (where the radiation dose is substantially lower than in-core positions) may be needed given the current uncertainty with respect to the irradiation resistance of magnetostrictive transducers. Further reductions in the stainless steel waveguide length may be possible depending on results from an upcoming ATR NSUF irradiation test of magnetostrictive and piezoelectric transducers (see Section 5.7.1). However, bench top laboratory testing was completed using stainless steel waveguides limited to 1 m in length in the fixture shown in Figure 5-30. (Note that a 0.062 in OD stainless steel rod was used as both the specimen and the waveguide in this figure.)

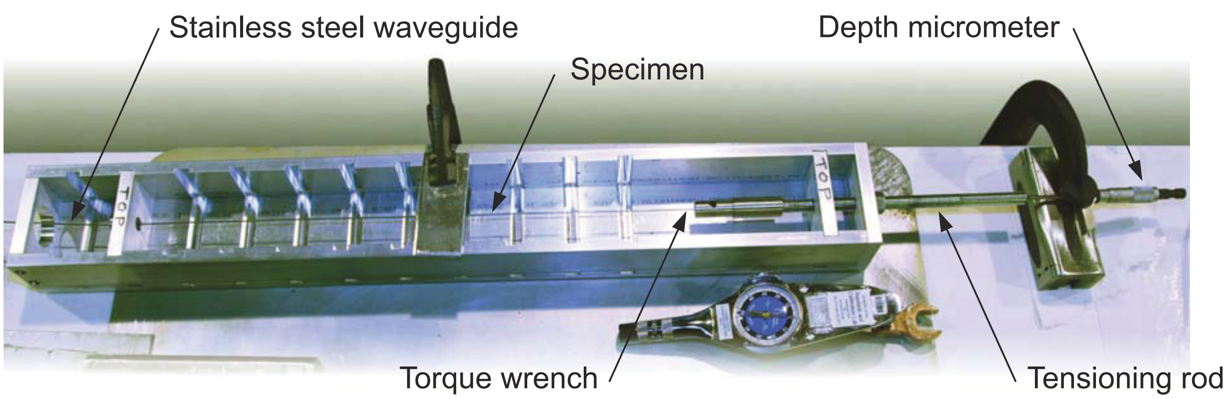

Figure 5-30. Benchtop fixture for laboratory testing of elongation detection using ultrasonic techniques.

As previously indicated, this effort focussed on optimizing the test rig design by eliminating unwanted acoustic reflections that adversely affect the accuracy of this method, such as reflections from the brass coupling proposed in the design shown in Figure 5-29a. A number of direct stainless steel to Remendur joining techniques were therefore investigated in an effort to eliminate the coupling. Success was achieved using a tungsten inert gas butt welding process. The resulting joint was found to be durable and very close to ultrasonically transparent, which eliminated the need for the brass coupling.

Laboratory evaluations also indicated that multiple reflections were generated in the acoustic horn. As shown in Figure 5-29a, those reflections make it difficult to accurately determine Time-Of-Flight (TOF) in the gauge length and any elongation. This difficulty arises from the fact that there is no accurate way to identify any characteristic point within reflected waves (i.e., characteristic points such as peak values, zero crossings, or even the onset of refections cannot be identified without considerable uncertainty).

Buttons were found to be an improvement over the acoustic horn. The buttons were similar to conventional butt-end shoulders used in tensile testing, except the buttons were designed to slide onto the specimen instead of being a machined part of the specimen. Laboratory testing revealed that a button design with conical recess machined into the button was a superior replacement for the horn because it did not promote unwanted acoustic reflections (see Figure 5-29b). In addition, this button design proved to have sufficient strength to impart the desired tensile load and be attached without rigorous measures to ensure perfect specimen-to-button alignment.

Efforts also were made to improve and optimize the design of the magnetostrictive transducer. Although the initial concept relied on a single transducer for sending and receiving ultrasonic pulses, the use of separate transducers for sending and receiving was evaluated. The motivation for these efforts stem from the fact that sending and receiving ultrasonic pulses tends to have conflicting requirements. Specifically, a low impedance transducer is desirable when sending an ultrasonic pulse while a high impedance transducer is desirable when receiving an ultrasonic pulse. A low impedance transducer, typically constructed using a relatively large diameter wire to form a coil with a relatively small number of turns, allows relatively high current flow (for a given voltage). High current flow is needed to generate a large magnetic field, which, in turn, produces a large magnetostrictive effect in the Remendur resulting in transmission of a strong acoustic pulse into the waveguide. On the other hand, a high impedance transducer, typically constructed using a relatively small diameter wire to form a coil with a relatively large number of turns, is best for transforming a magnetic field (associated with reflection of an acoustic pulse) into a relatively high voltage output signal.

Laboratory testing also indicated that significant reductions in unwanted reflections (i.e., noise) may be achieved using a pitch/catch mode (which requires separate send/receive transducers) as opposed to a pulse/echo mode (which relies on a single transducer for sending/receiving ultrasonic pulses). However, in a conventional pitch/catch configuration, the sending transducer and the receiving transducer are normally separated by the specimen being evaluated. In the case of ATR irradiation testing, that would mean that one of the transducers would normally be positioned in-core near the end of the specimen gauge length. However, as previously discussed, the irradiation resistance of magnetostrictive transducers remains unknown until completion of the ATR NSUF test program described in Section 5.7. This prompted a further refinement of the test concept, which places send and receive transducers next to each other in an ex-core position. The receiving transducer thereby detects acoustic reflections (from the buttons used to impart the specimen tensile load) instead of detecting acoustic transmission (through those buttons). The fact that reflections are detected improves resolution and accuracy (compared to conventional pitch/catch arrangements) because TOF is effectively doubled.

Laboratory evaluations also indicated that coil length can negatively extend the pulse width. Wider pulses (and corresponding increases in the reflected pulses) tends to reduce the accuracy of TOF measurements from point to point. For that reason, efforts were made to produce transducers with the shortest length physically possible. Send and receive coils consistent with that objective are shown in Figure 5-31.

Finally, efforts were made to minimize acoustic reflections from the end of the Remendur. This was necessary because these reflections interfere with the waveforms needed to correctly interpret specimen response (like all other unwanted reflections). Although a wide variety of different damping mechanisms may conceivably work, a very simple approach was adopted for use during laboratory evaluations. Specifically, a long length of Remendur wire was welded to the stainless steel waveguide. The Remendur length was sufficient to ensure that acoustic reflections from the end of the Remendur will not arrive at the transducers until a time well past arrival of specimen acoustic reflections. In other words, TOF associated with the long Remendur wire eliminates interference by separating the Remendur reflections from the specimen reflections of interest. While this approach was perfectly acceptable for laboratory evaluations, a more compact solution may be preferable for irradiation testing in MTRs.

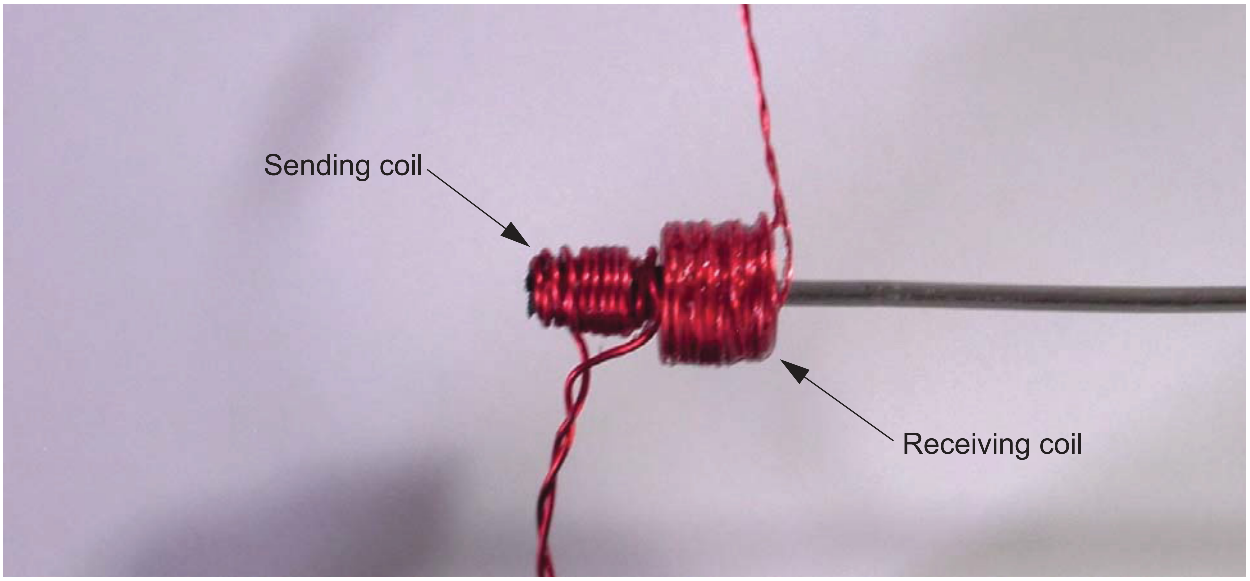

Figure 5-31. Coils developed and evaluated for use in sending and receiving transducers.

Significant progress was made with LDRD funding to examine the viability of using ultrasonic techniques for the in-pile measurement of elongation due to creep. Laboratory evaluations resulted in enhanced designs for components that could be used for these in-pile measurements. However, several activities are still required to enable in-pile deployment of ultrasonic techniques for elongation measurement. Those activities include development of a pressure and water resistant case for magnetostrictive transducers, laboratory temperature/pressure testing of magnetostrictive transducers, monitoring results from the ATR NSUF irradiation testing of magnetostrictive and piezoelectric transducers, further elimination of acoustic reflections (including development of a more compact solution for handling Remendur reflections), and finalization of a creep test rig design. It is currently planned to defer further exploration of this method until irradiation tests described in Section 5.7.1 are completed.

5.3.5. Fiber Optic Elongation Measurements

The FCRD program is funding an effort to develop and deploy an optical fiber sensor for the measurement of fuel rod elongation. The sensing method for this sensor is based on the Extrinsic Fabry-Perot Interferometer (EFPI) using a low coherence white light source. In order for any fiber optic technique to be deployed in-pile, the following parameters of the sensing technique and probe must be determined or developed:

- The accuracy of the proposed approach must meet objectives (e.g., selecting appropriate system components to obtain measurement with desired accuracy),
- A probe design that can be deployed in a MTR instrumented lead capsule must be developed, and
- The life expectancy requirements under irradiations at proposed test conditions.

During FY11, efforts were initiated to gain insights about the first two parameters. The technique was demonstrated in the lab, and the accuracy and limitations of the sensing methodology were evaluated. FY12 efforts focused on the development and testing of a sensing probe.

Initial laboratory investigations extended the concept presented by the CEA/SCK•CEN Joint Laboratory (see Section 3.2.3).[46] In this technique, the distance between the end of an optical fiber and a reflecting surface is determined using the interference of the light reflected from the end of the fiber, "R1," and that reflected from surface on the opposite side of the cavity space, "R2," as shown in Figure 5-32.

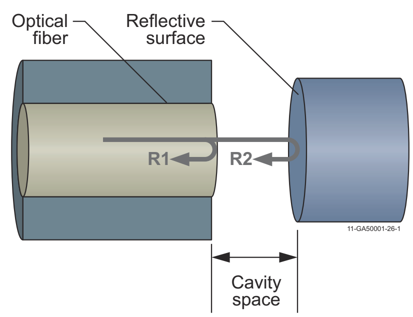

Figure 5-32. Cavity space measurement using EFPI.

The interference of these two beams produces a fringe pattern when viewed using a spectrometer, which displays the returning light intensity versus wavelength. The length of the cavity space can then be determined from the wavelength of two adjacent fringe peaks by using the following equation[146]

$$d = \frac{\lambda_1 \lambda_2}{2(\lambda_1 - \lambda_2)} \tag{5-3}$$

where:

d is the cavity length, and

λ_1 and λ_2 are the wavelengths of adjacent fringe peaks.

During FY11, a laboratory experiment was completed to gain experience using this technique. The technique is implemented by introducing broadband light into an optical fiber. The light in the fiber passes through a 50/50 fiber splitter in which 50% of the light continues to the probe at the end of the fiber. The probe contains a variable cavity space as previously outlined. Reflected probe light returns through the fiber to the beam splitter which delivers 50% of this returning light to the spectrometer as shown in Figure 5-33. A grating in the spectrometer separates the returning light into a spectrum of the wavelengths of light present. The interference creates a modulation of the spectrum intensity as described above.

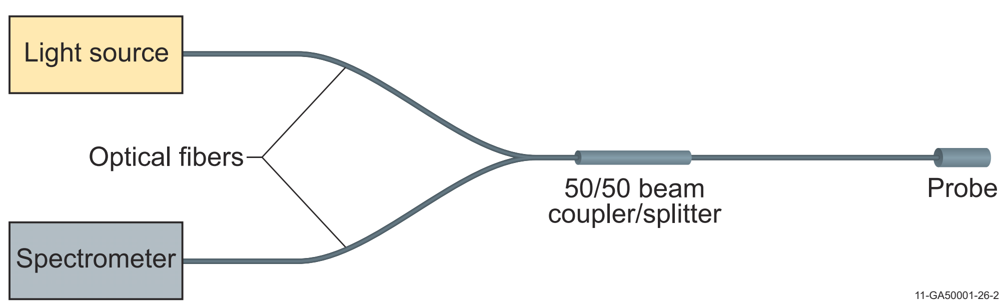

Figure 5-33. Experiment configuration for EFPI technique evaluation.

The FY11 evaluations included testing multiple light sources and fiber core sizes. It was determined that a broadband halogen light source was both cost effective and provided a wide usable light spectrum. Multimode fibers with small core sizes (50 µm) produced better results than larger core (200 µm) fibers. It was also determined that for maximum fringe modulation, the light intensity reflected from the fiber tip should be equal to the light intensity from the reflector (R1 and R2 in Figure 5-32). This can be accomplished by using a polished fiber for the reflector or by applying a partial reflective coating to the fiber tip and using polished metal for the reflector. The equipment used for the final FY11 technique evaluations and subsequent FY12 testing included: an Ocean Optics halogen light source (HL-2000-FHSA), an Ocean Optics model QE65000 spectrometer, and a Thor Labs model FCMM50-50A-FC 50/50 fiber optic splitter. The ability to measure elongation was evaluated using a Newport VP-25X stage with a Newport ESP301 driver for control and position readout. This setup is shown in Figure 5-34.

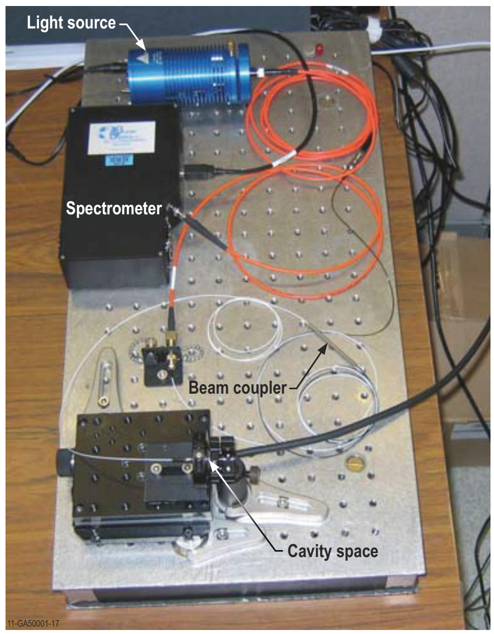

Figure 5-34. Laboratory setup for initial evaluation of fiber optic in-pile elongation detection.

Initial technique evaluations used an optical fiber for delivery and a quartz window for the reflector. The resulting fringe modulation using the halogen light source is shown in Figure 5-35, and the cavity spacing versus the stage readout is shown in Table 5-5.

Minor differences in the absolute cavity length calculated from the fringes versus the readout from the stage controller were attributed to the inability to zero the stage exactly where the cavity length was zero. However, the change in cavity space versus the change in stage position from point to point were in very good agreement (typically less than 0.3 µm). It should be noted that a simple routine of graphically picking fringe peak wavelengths and calculating an average cavity space using Equation (5-3) was used. In future evaluations, a more sophisticated analysis for determining the fringe spacing will be employed to enhance accuracies.

In FY11, an initial probe was fabricated using stainless steel hypodermic tubing. In this design, the optical fiber was bonded inside of a short length of stainless steel tube, and the reflecting side of the cavity was fabricated by bonding a short length of larger core optical fiber into a small piece of the same stainless

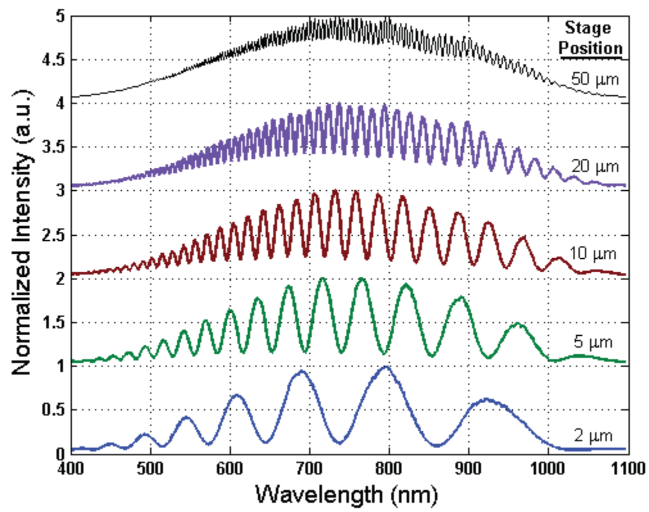

Figure 5-35. Spectra showing EFPI fringe modulation at several cavity lengths.

Table 5-5. Comparison of measured cavity length versus length inferred from fringe spacing.

VP-25X Stage Position (µm)	Cavity Based on Measured Fringe Spacing	Change in Measured Cavity (µm)	Difference Between Change in Stage Position and Measured Cavity (µm)
0	0.73	-	-
1	1.63	0.901	0.10
2	2.64	1.010	-0.01
3	3.55	0.911	0.09
4	4.55	0.995	0.00
5	5.54	0.991	0.01
7	7.45	1.917	0.08
10	10.46	3.009	-0.01
15	15.45	4.988	0.01
20	20.59	5.141	-0.14
25	25.61	5.023	-0.02
30	30.55	4.934	0.07
35	35.48	4.933	0.07
40	40.70	5.219	-0.22
45	45.57	4.871	0.13
50	50.77	5.196	-0.20
60	60.82	10.057	-0.06
70	70.73	9.904	0.10
80	80.75	10.017	-0.02
90	90.78	10.035	-0.03
100	101.06	10.277	-0.28
125	126.06	25.002	0.00

steel tubing. The fiber ends were polished and inserted into a larger diameter sleeve such that the space between the tips created the measurement cavity. The sleeve served to maintain axial alignment between the fibers as the cavity space was changed. A schematic of the probe design is shown in Figure 5-36.

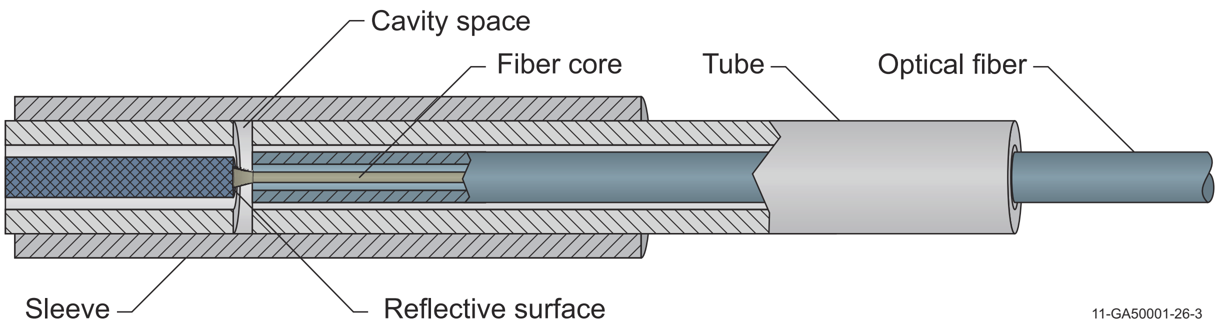

Figure 5-36. Elongation probe concept using hypodermic tubing.

In FY12, efforts were focused on developing a sealed probe that could be deployed in an irradiation test. A probe design was developed that was functionally similar to the concept probe, but incorporated a bellows, which would provide isolation from the environment and allow expansion of the probe. A cross-section of the probe design is shown in Figure 5-37.

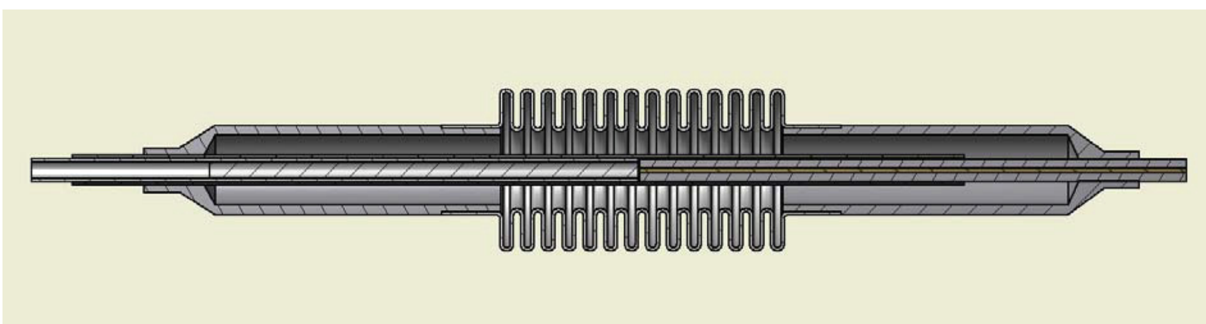

Figure 5-37. Elongation probe cross section.

A number of obstacles were resolved in fabricating this probe. Bonding of the optical fiber in the stainless steel hypodermic tubing presented problems as initial attempts at stripping the fiber coating and bonding in the tube resulted in fracture of the fiber at moderate temperatures. It was found that gold coated fiber, which can withstand temperatures of 700 °C, could be bonded inside the hypodermic tube using Cotronics Resbond 907TS Green threadlocker without fiber fracture at elevated temperatures. Issues related to assembly and welding of small probe components were also resolved. The smallest readily available stainless steel bellows was a MiniFlex Corporation Model SS-125-46-168. An adapter was developed which could be welded to the bellows on one end and the hypodermic tubing on the other end. Welding of these components was accomplished using a laser welding system. A photo of the completed sensor is shown in Figure 5-38.

Initial testing of the probe revealed an increasing discrepancy between the readings from the stage and the probe. However, it was determined the discrepancy was due to flexing of the support posts. A more substantial test fixture was fabricated, and the probe was retested. For the first test, the probe was clamped

Figure 5-38. Welded elongation probe.

in position, and the stage was first zeroed and then moved from 0 µm to 150 µm in increments from 1 to 10 µm. This test yielded very good results with the discrepancy between the stage position reading and the probe being generally less than 0.3 µm up to a 90 µm displacement. The increased error observed with displacements greater than 100 µm was primarily due to difficulty reading the fringe pattern. Repeatability was then evaluated by randomly moving the stage between 3 and 92 µm. Position readings from both the stage and probe were plotted, and a linear fit performed. The data and linear fit are shown in Figure 5-39. The linear fit slope was 1.0037, which is essentially 1.00; and the intercept was 0.50 µm. The intercept is simply a measure of how close the stage zero was to the probe zero. The average difference between probe measurements and the stage readings (adjusted for the zero offset) was less than 0.2 µm.

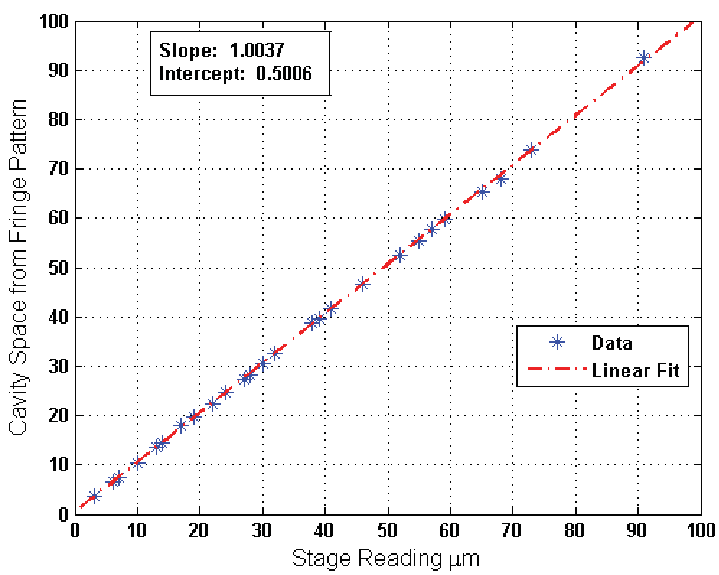

Figure 5-39. Elongation probe data.

Additional probes for testing were fabricated in early FY13. Two of these probes incorporated partial reflective coatings on the fiber tips and polished metal reflectors. The 25% reflective coating was applied by Cascade Optical Corporation and allowed significantly more light to be returned to the spectrometer. During testing of these probes, the source light output was reduced by 80% to prevent saturation of the spectrometer, and the signal intensity was still higher than the uncoated sensors. The stronger signal allowed fringe modulation to be resolved to a displacement of 130 µm.

Initial high temperature testing of the sensors has yielded promising results. A sensor incorporating a partial reflective coating on the fiber tip was mounted to an aluminum rod and inserted into a tube furnace to measure thermal expansion of the rod. The clamp fixture slipped as the temperature rose above 150°C, but the thermal expansion determined from the data collected was in general agreement with expected values. Further testing using improved fixturing will be completed in FY13.

Evaluation of the EFPI technique and testing of an elongation probe based on this method have led to a better understanding of the sensitivity and cavity length range of this technique. Upon closer inspection of Equation (5-3) and observation of the recorded spectrum, it can be seen that the fringe spacing is long for a small cavity length and short for a longer cavity length. Consequently, as the cavity length increases, the sensitivity decreases. It has been shown that the radiation induced attenuation of optical fibers is the lowest in the near-infrared wavelength, particularly in the range from about 800 to 1300 nm.[46] If the probe were designed to operate in this window and two fringe peaks were required within this range to determine fringe spacing, the minimum detectable cavity space would be approximately 1.5 µm. The maximum detectable cavity space is based on the resolution of the spectrometer. As the cavity space increases and the fringe peaks get closer together, the ability to resolve individual peaks becomes the limiting factor. The Ocean Optics QE65000 used in these tests had a resolution of about 0.8 nm which resulted in a maximum measurable cavity space of about 125 µm. Testing of the probe revealed high precision for measurements between approximately 3 and 100 µm using a probe with a glass reflector and up to 130 µm when a partial reflective coating is applied to the fiber tip and a metallic reflector is used. Measurement errors increased above this range. Some improvements for longer displacements may be possible by using a spectrometer which is sensitive to longer wavelengths than the QE65000.

Work on the elongation probe has lead to a number of observations about the technique which are summarized below:

- The technique is viable and has demonstrated an accuracy on the order of 0.3 µm.
- Small core, low numerical aperture fibers tend to work better.
- Return light from the reflections at the end of the fiber and the mirrored surface should be approximately the same intensity for good fringe modulation depth. A partial reflective coating of 25% applied to the fiber tip used in conjunction with a highly reflective surface opposite the fiber end face can significantly increase the light returned from the probe and the signal to noise ratio.
- The fiber face should be polished flat and alignment of the fiber axis perpendicular to the reflective surface must be maintained.
- The sensitivity of the probe is a function of the spectrometer resolution and the fringe modulation depth.
- The minimum detectable cavity space is based on the bandwidth of the light source and “transmission window” of the irradiated optical fiber. The best transmission range for irradiated optical fibers extends from approximately 800 nm to 1300 nm.
- The approximate measurement range of a probe based on this technique is 1.5 to 125 µm (based on the fiber transmission window and a spectrometer resolution of 0.8 nm).

FY11 and FY12 efforts demonstrated the viability of a fiber optic elongation sensor based on the EFPI technique. A probe has been fabricated and tested, and an IDR was filed related to its design.[147] However, continued development will be required to produce an in-pile service ready sensor. The following list outlines the status of activities required to bring the desired sensor to fruition:

- Optimization of probe design parameters - During FY12, an elongation probe was fabricated and tested. Many improvements were made over the initial concept probe. Optimization will continue throughout the development process. Probes using fibers with lower numerical apertures and smaller core diameters will be investigated. The use of smaller diameter bellows will also be evaluated. Coating the end of the fiber with a partially reflective coating and using a highly reflective surface on the opposite side of the cavity has been shown to be advantageous.
- Develop a seal - The probe developed during FY12 is a sealed design.
- Fabrication Capabilities - Capabilities at the INL were sufficient to fabricate the initial elongation probe. Improved commercial processes may be used for the final sensors.
- Radiation Resistance - Work to date has been conducted using standard commercially available fibers and components. Radiation resistant fibers and fiber to tube bonding materials/methods need to be incorporated into the design. A broadband light source operating in the 800 to 1300 nm range also needs to be identified or developed. As discussed in Section 4.4, results from an irradiation test are required before this probe can be deployed.
- Signal Analysis Software - During the current evaluation phase of the sensor development the signal from the probe is displayed as a modulated wavelength spectrum on the screen of a PC. This is not convenient for an operator. Automated signal analysis software will be developed so that cavity length or elongation can be provided directly to the user.
- Final Design & Testing - Once the probe has been optimized it will still need to be attached to the sample and incorporated into a test capsule. This final design configuration will then be tested in a simulated reactor environment prior to deployment.

Although development efforts were planned to enable deployment of this probe by FY14, the development schedule has been extended due to funding limitations. In addition, deployment will be delayed until completion of the irradiation test discussed in Section 5.7.

5.4. Direct Current Potential Drop (DCPD)

Crack initiation and growth of samples irradiated in instrumented lead and PWR loop tests in the ATR are evaluated out-of-pile. However, crack-growth rates in core structural component materials irradiated in the HBWR are monitored in-pile using miniaturized CT specimens and the DCPD method. The DCPD method (see Section 3.3.6) is based on sending a precisely controlled electrical current through the specimen and measuring the drop in voltage at several locations on the CT-specimen. The measured voltage changes as a function of crack growth. Thus, the crack-length can be determined from the measured voltages. IFE/HRP has applied this technology to detect the impact of coolant parameters (pH, impurities, boron concentration, etc.) on fuel cladding corrosion. In addition, IFE/HRP can perform such measurements on pre-irradiated fuel removed from commercial reactors.

The major aspects of choosing a crack growth measurement technique are: specimen geometry, loading mode (active or passive) and crack length measurement technique. Crack length measurement by the DCPD technique is very well established and has become a de facto standard for in-core measurements. It is applicable to most specimen geometries, although specimen extensions are often used to provide adequate space to connect current leads and voltage probes. As discussed in Section 3, this method has been applied in several research and test reactors. In addition, this technique has been applied in-core and in recirculation piping autoclaves of commercial BWRs. Some out-of-core measurements have used AC potential drop, but there do not appear to be significant advantages for this technique. Another method frequently applied in out-of-core tests is to measure “crack tip opening displacement” (COD) using a strain gauge. However, this is a very delicate procedure requiring elements that are not readily adaptable to in-core environments.

During 2012, an effort was initiated to adapt the DCDP method to high flux MTRs in the US, such as INL's ATR. Currently, the HBWR performs irradiations with on-line crack propagation monitoring. Figure 5-40 shows the essential features of the in-pile hardware used at HBWR. A loading mechanism is used to stress the crack in a CT specimen. The mechanism utilizes a miniature high pressure bellows, which expands to apply the force required to propagate the crack. The CT specimens are fabricated with “ears” above the loading holes to provide locations for current and voltage connections.

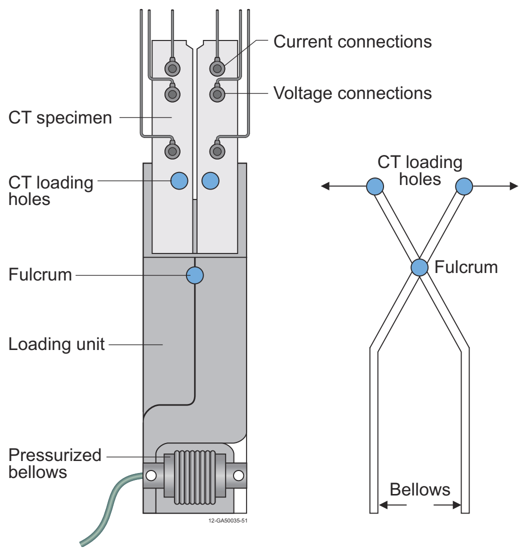

Figure 5-40. Essential hardware elements for implementing the DCPD method in-pile.

As a first step to implementing this technology, a prototype loading mechanism was constructed at INL based primarily on the HBWR design. Techniques were developed for making laser welds between the miniature bellows and the end fittings used to transfer the loads as shown in Figure 5-41.

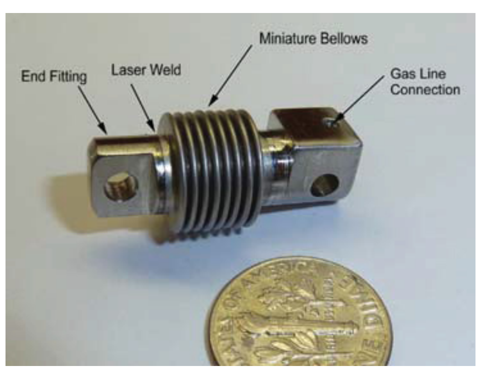

Figure 5-41. Example of end fittings laser welded to bellows.

The balance of the loading mechanism was fabricated and assembled (see Figure 5-42). This work included developing techniques for brazing the small gas supply line to an end fitting.

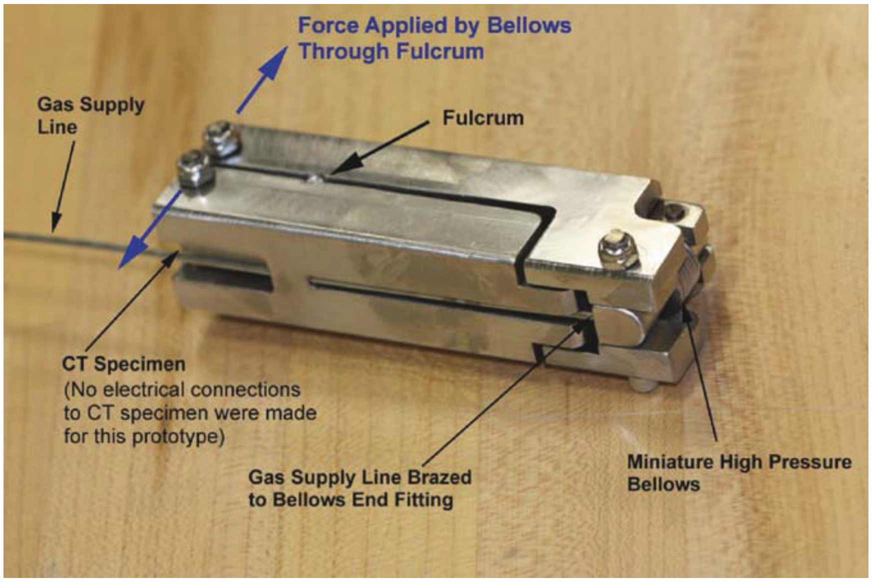

Figure 5-42. Prototype loading mechanism for in-pile DCPD testing - fabricated at INL.

The loader shown in Figure 5-42 was tested using an Instron machine in an effort to characterize the pressure versus force applied to the specimen relationship. Figure 5-43 shows the setup in the Instron tester. Figure 5-44 shows the results of two runs where the loader opening was held fixed and the pressure was ramped from 0 psig to 2000 psig and back down again. The two runs show very consistent results as evidenced by the best fit curves being nearly identical and extremely linear. For these runs the slope of the line (0.316) represents the effective area of the bellows multiplied by the mechanical advantage of the loader.

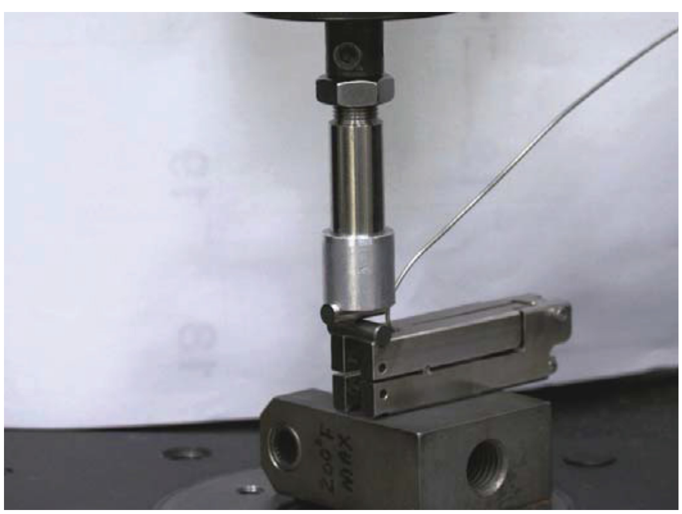

Figure 5-43. Crack growth loading mechanism during testing.

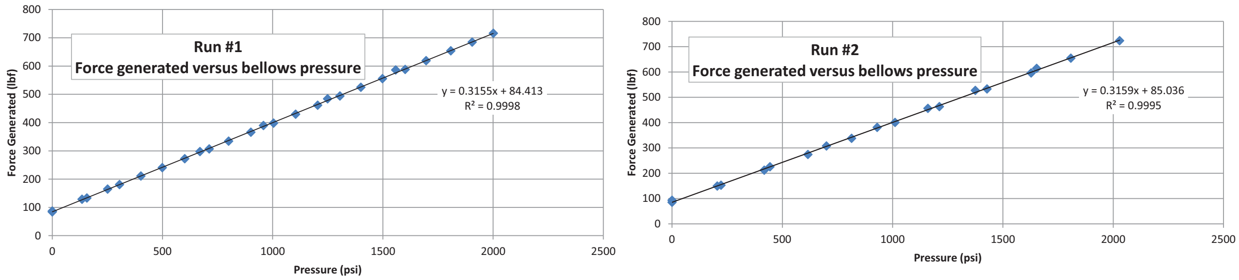

Figure 5-44. Force generated versus bellows pressure with fixed loader opening - two runs.

However, in actual operation with a specimen connected, the loader opening will not be fixed, but will gradually increase as a crack is propagated. Figure 5-45 shows the results of two runs where the bellows pressure was held constant at 1500 psig and the opening was allowed to gradually increase by 0.015 inch (or 15 “mils” as denoted on the horizontal axis). In this case, the slope of the best fit lines (approximately 6.64 lb/mil) is the effective spring constant of the bellows. For a mechanism like this, the effective spring constant is the actual spring constant of the bellows multiplied by the square of the mechanical advantage built into the device. The mechanical advantage for this arrangement is approximately 2.9.

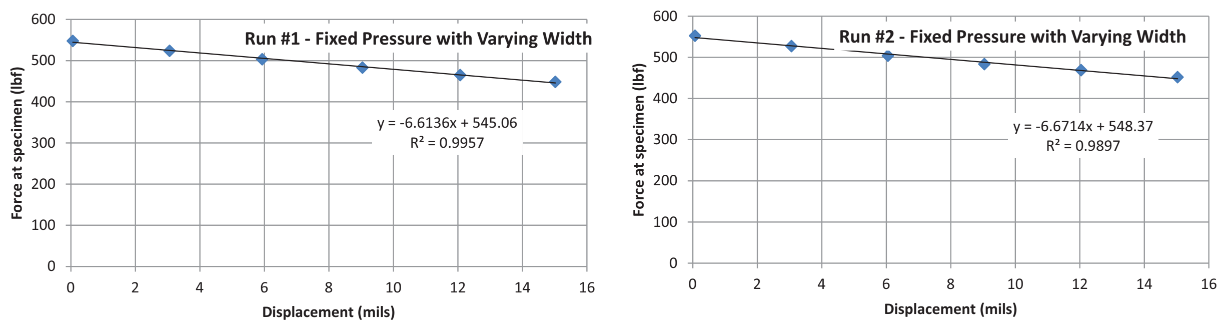

Figure 5-45. Force at specimen as jaws open - two runs.

Ideally, the force applied to the specimen would not be dependent on the loader opening. The loader opening represents an uncertainty in the system since it cannot be directly measured when the mechanism is being used to crack specimens in-core. Approximate relationships are available which can be used to estimate the loader opening given a crack length. Because the relationships are approximate, the smaller the effective spring constant of the bellows, the less uncertainty in the applied load. This suggests that the mechanical advantage of the mechanism should be reduced to the degree possible to minimize this uncertainty, while still retaining enough force capability to propagate a crack. It is a simple matter to reduce the mechanical advantage by cutting a new groove for the fulcrum pin shown in Figure 5-42 closer toward the bellows.

A few specially modified miniature (0.2 scale) CT specimens have been fabricated and an example is shown in Figure 5-46. The assembly shown in Figure 5-46 consists of the modified CT specimens with the current and voltage leads fit up dry, i.e., the leads have not been welded or brazed in place. Efforts are on-going to determine the best way to connect the leads to the CT specimens.

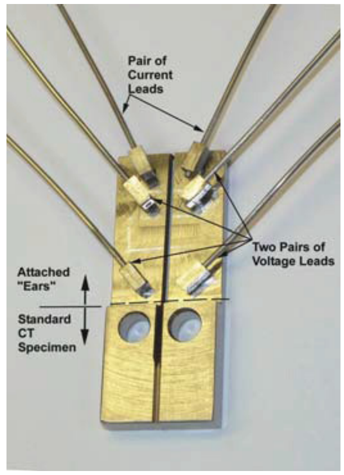

Figure 5-46. Specimen with leads fit-up “Dry”.

Because the CT specimens do not match the traditional CT geometry, but rather incorporate “ears” attached to the top of the specimens. This geometry has been deemed beneficial for the robustness and reduced space available for in-pile testing. However, typical software packages developed for the DCPD method cannot be used, and new mathematical relationships must be developed for the specimens.

Future work includes modifying the profile (end view) of the loading mechanism so that it will fit in the pressurized loop at the MITR. Engineers at MIT will modify the box-shaped loader profile to a more circular version as shown in Figure 5-47.

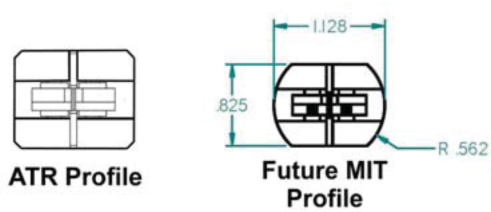

Figure 5-47. Loader mechanism profile must be modified to fit MIT pressurized loop.

5.5. Flux and Fluence

Typically, ATR tests use flux wires and post-irradiation evaluations to detect the total fluence to which the fuel or sample was exposed. However, as noted in Section 3, MTRs in Norway, France, the Netherlands, Japan, Belgian, and the Republic of Korea routinely incorporate self-powered neutron detectors (SPNDs) during irradiation tests to gain real-time knowledge of the fission reaction rate. In recent years, French and Belgium test reactors have also incorporated specialized fission chambers to provide users real-time data related to neutron flux (see Section 3).

Several efforts are underway to enhance ATR flux and fluence measurements. As discussed in this section, new in-house capabilities have been developed for encapsulating wires for post-irradiation fluence measurements. In addition, a joint Idaho State University (ISU)/ INL ATR NSUF project is underway to evaluate new real-time state-of-the-art in-pile flux detection sensors at the ATRC. Finally, efforts are underway to design and deploy a new small compact sensor that can simultaneously measure fast and thermal flux and temperature.

5.5.1. Activation Foils

Because the sensitivity of different foil materials to neutron energies varies, a selection of foil materials are included in ATRC evaluations. A list of the neutron interactions of interest for ATRC validation experiments is given in Table 5-6 below.

Table 5-6. Activation interactions of interest for ATRC validation experiments.[148]

Neutron Interaction	Nominal Mass and Composition of Standard Foil	Half-life of Product of Interest	Energy Range of Primary Response	Activation Gamma Energy of Interest (keV)
$^{115}In\ (n,\gamma)\ ^{116}In$	25 mg, 100% In	54 Minutes	1 eV Resonance	1293,1097, 416
$^{197}Au\ (n,\gamma)\ ^{198}Au$	60 mg, 100% Au	2.694 Days	Thermal & 5 eV Resonance	412
$^{186}W(n,\gamma)\ ^{187}W$	60 mg, 100% W	23.9 Hours	18 eV Resonance	686
$^{55}Mn(n,\gamma)\ ^{56}Mn$	50 mg, 80% Mn, 20% Cu	2.578 Hours	Thermal & 340 eV Resonance	847
$^{63}Cu\ (n,\gamma)\ ^{64}Cu$	140 mg, 100%Cu	12.7 Hours	Thermal & 1 keV Resonance	511 (Positron)
$^{115}In\ (n,n')\ ^{115m}In$	25 mg, 100% In	4.49 Hours	0.5 MeV Threshold	336.3
$^{47}Ti\ (n,p)\ ^{47}Sc$ $^{46}Ti\ (n,p)\ ^{46}Sc$ $^{48}Ti\ (n,p)\ ^{48}Sc$	157 mg, 100% Ti	3.349 Days 83.81 Days 43.7 Hours	1.0 MeV Threshold 3.5 MeV Threshold 5.5 MeV Threshold	159.4 1121,889 984,1312,1038
$^{58}Ni\ (n,p)\ ^{58}Co$	286 mg, 100% Ni	70.88 Days	1.2 MeV Threshold	811
$^{64}Zn\ (n,p)\ ^{64}Cu$	117 mg, 100% Zn	12.7 Hours	1.5 MeV Threshold	511 (Positron)
$^{54}Fe\ (n,p)\ ^{54}Mn$ $^{56}Fe\ (n,p)\ ^{56}Mn$	132 mg, 100% Fe	312.2 Days 2.578 Hours	1.5 MeV Threshold 5.0 MeV Threshold	834.8 847
$^{93}Nb\ (n,2n)\ ^{92m}Nb$	270 mg, 100%Nb	10.13 Days	6.0 MeV Threshold	935

As part of the ISU-led ATR NSUF project, specialized fixturing was designed and fabricated for comparing the accuracy, response time, and long duration performance of several activation sensors in several positions throughout the ATRC core. As shown in Figure 5-48, some foils are placed inside standard 40-mil (1 mm) cadmium foil covers or boron-10 spectral modification shields to enhance their response in the epithermal and fast neutron ranges. Ongoing evaluations are performed in the ATRC NorthWest Large In-Pile Tube (NW LIPT) and the Southeast Standard In-Pile Tube (SE SIPT). As shown in Figure 5-48 (Case 1), the foils used for thermal and epithermal neutron measurements are placed in covered aluminum strips that fit into a square holder, which in turn, fits into the square cavity in the cylindrical LIPT insert. A second fitting (Case 2 of Figure 5-48) that goes directly into the square cavity of the cylindrical insert is used to hold the boron sphere, which will contain the foils used for the fast-neutron spectral range. The insert fittings shown in Figure 5-48 have O-rings around their cavities to keep the contents out of contact with the reactor water.

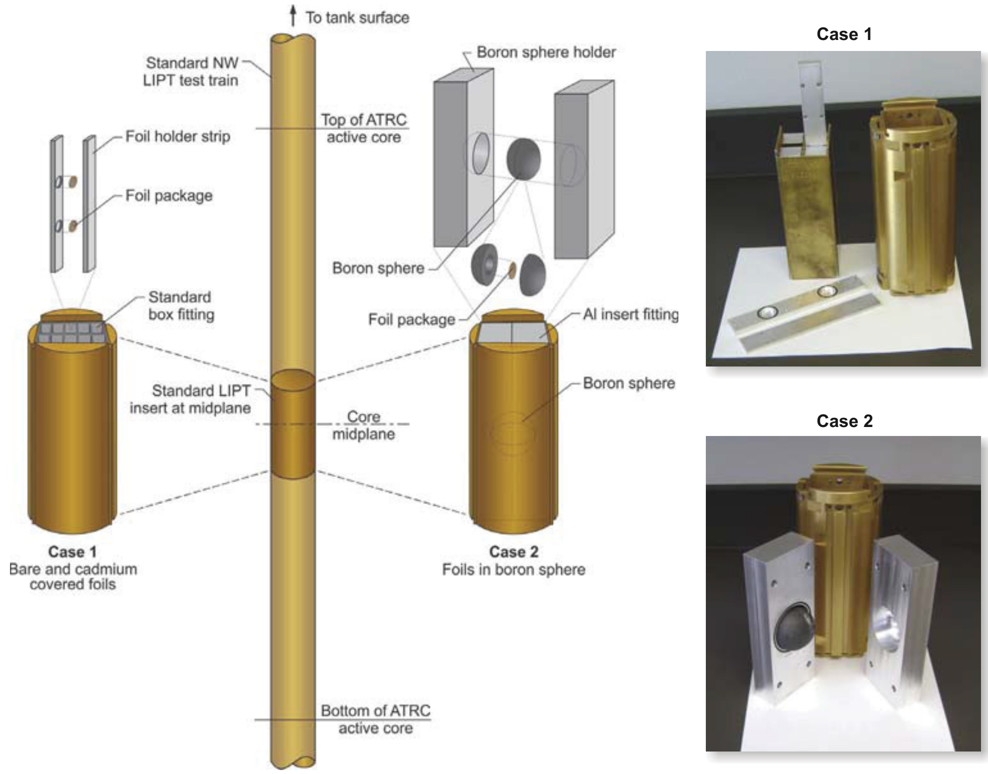

Figure 5-48. ATRC test hardware and activation foils.

A similar test rig has been fabricated that will be installed in the SE SIPT (see Figure 5-49) to observe any spectral differences across the core. However, because of the smaller size of the SIPT, it not possible to include the boron sphere.

5.5.2. Vanadium Capsules

In response to ATR NSUF experimenter needs, the HTTL has developed in-house encapsulation processes using vanadium capsules for iron flux wire monitors. Although a range of geometries are possible, the flux monitor capsules were constructed to fit within a 7.6 mm length and 1.7 mm diameter envelope for the EPRI 1, 2, and 3 Test Packages that will be deployed in the ATR NSUF In-Pile Tube Test Train. It should be noted that these vanadium encapsulation processes may also be used to encapsulate melt wires or other components as ATR experimental needs arise.

Specialized equipment available at the HTTL is used to fabricate and inspect these vanadium capsules. Capsules are constructed from vanadium tubing and rod material. Using a laser welder, the iron wires are encapsulated in the vanadium tubes in an inert atmosphere, typically helium or argon, to avoid oxidation or corrosion issues while under irradiation in ATR experiments. In addition, the capsules are appropriately identified and numbered using a laser marker (see Figure 5-50).

A radiograph of a vanadium capsule with iron wire is shown in Figure 5-51. X-ray inspection is used during development to optimize the laser welding parameters and to measure critical dimensions such as wall thickness, Fe wire placement, and laser weld penetration.

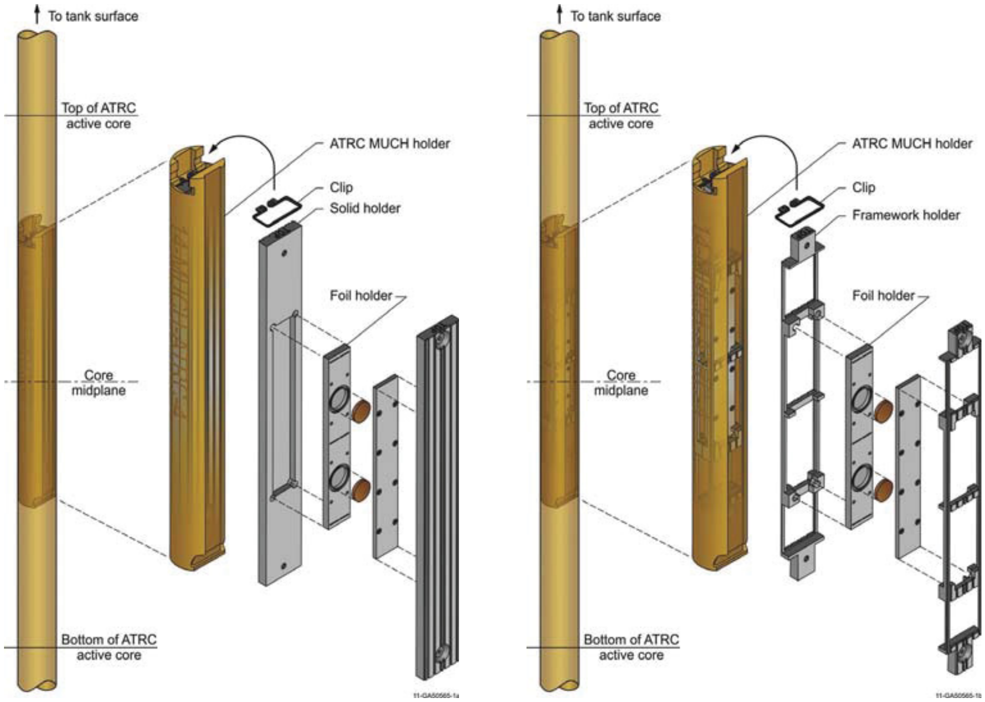

Figure 5-49. ATRC SIPT hardware representative diagrams.

Figure 5-50. EPRI capsules 2A1, 2B3, 2B12, and 2C10 shown with a Lincoln cent for perspective.

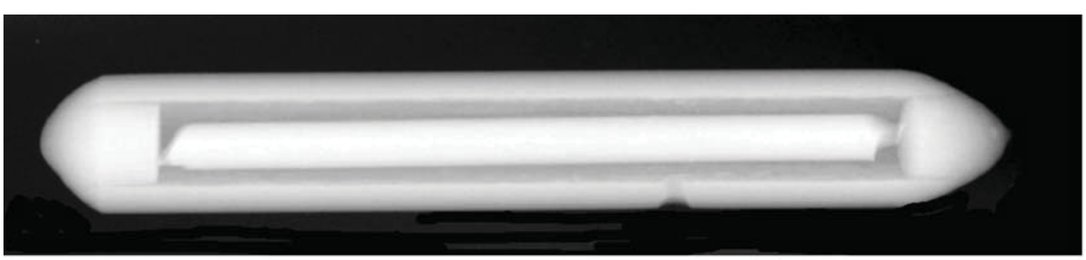

Figure 5-51. Radiograph of vanadium capsule with iron wire in the center.

5.5.3. Real-time Flux Sensors

As part of the ISU-led ATR NSUF project, real-time in-pile flux detection sensors are being evaluated in the ATRC. Initially, the project is comparing the accuracy, response time, and long duration performance of several real-time flux sensors (see Figure 5-52), including CEA-developed miniature fission chambers, specialized Self-Powered Neutron Detectors (SPNDs) developed by the Argentinean National Energy Commission (CNEA), specially developed commercial SPNDs, and Back-to-Back (BTB) fission chambers[1] developed by Argonne National Laboratory (ANL) for the Zero Power Physics Reactor (ZPPR) programs. In support of this effort, specialized fixturing (see Figure 5-53) was designed and fabricated for evaluating real-time flux detectors in six of the N-16 positions in the ATRC Facility and integral fluence detectors in the NW LIPT flux trap (the largest irradiation facility in the ATRC Facility).

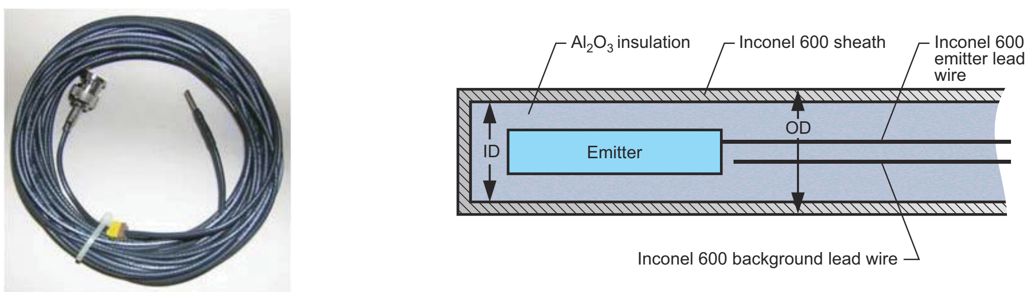

a) SPNDs

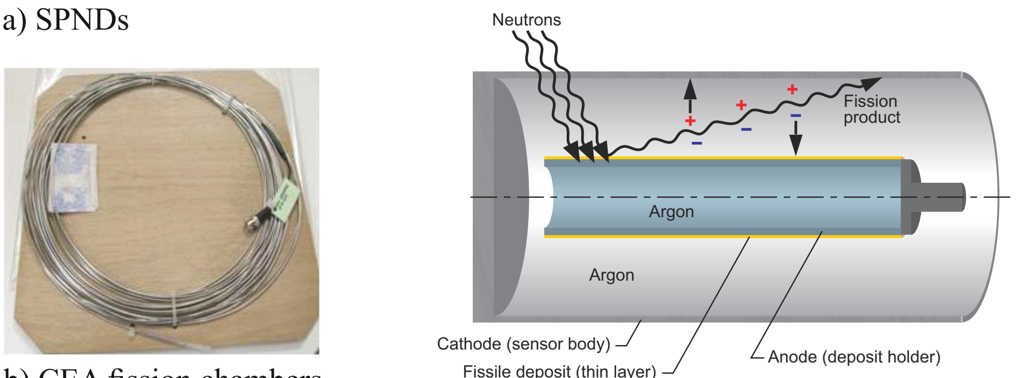

b) CEA fission chambers

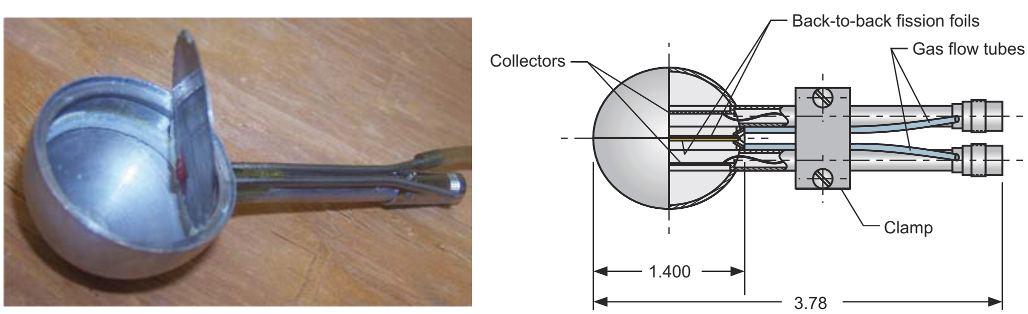

c) BTB fission chambers

Figure 5-52. Representative real-time flux sensors evaluated at ATRC facility.

1. BTB fission chambers are often called 2π fission chambers because they are designed to count almost all fission fragments emitting from a thin deposit in a 2π solid angle.

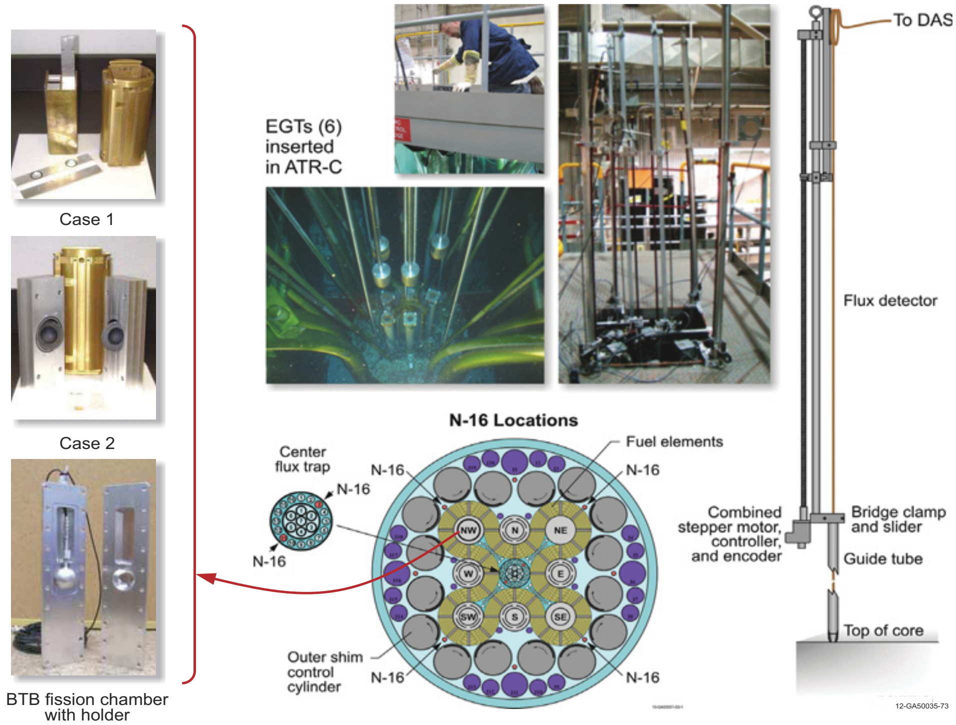

Figure 5-53. Specialized fixturing for flux detector evaluation in the NW LIPT (left) and EGTs for evaluations in six N-16 positions (right).

Reactor testing in the ATRC requires several of the flux sensors to be shielded from the reactor cooling water. The SPNDs and CEA fission chambers are housed in tinted Lucite tubes to prevent any unwanted leakage of component materials (if they are not leak-tight) and to reduce unwanted noise from having sensor cabling in contact with metal surfaces. As shown in Figure 5-53, sensors are inserted into the ATRC N-16 positions using specially-designed EGTs. The EGTs are primarily fabricated from aluminum to minimize their weight. However, selected components, such as the guide tube shown in Figure 5-53, are made from stainless steel 304. As illustrated in Figure 5-53, the six EGTs mechanically position detectors at a specified vertical location in the four N-16 exterior positions and two Center Flux Trap N-16 positions. The position control and detector response are controlled and measured via LabView to allow all detectors to either individually or simultaneously move and measure the local neutron flux and provide a 3-dimensional measurement of the overall neutron flux. The EGTs are supported above the reactor by attaching to the reactor control bridge.

As shown in Figure 5-54, specialized fixturing has been completed that allows a BTB fission chamber to be inserted into the ATRC NW LIPT alongside other real-time flux detectors, such as SPNDs or the CEA fission chambers, to compare responses in nearly identical flux conditions. The water-tight test fixture that will be used to insert these BTB fission chambers into this ATRC location is shown in Figure 5-53. An additional insert has been fabricated that positions three fission chambers across the NW LIPT for assessment of the flux gradient across the flux trap.

Evaluations of these real time flux sensors are expected to be performed in 2013. The tests will utilize three different critical configurations of the ATRC reactor with different power splits across the core. The response and accuracy of each type of flux detector will be compared. In addition, data obtained from real-time flux sensors will be compared to results from previous tests using activation analysis methods.

Figure 5-54. Equipment for positioning BTB and CEA miniature fission chambers in ATRC NW-LIPT.

Ultimately, results of this effort will be used to select the detector that can provide the best online regional ATRC power measurement. It is anticipated that this may offer the potential to improve its ability to perform low-level irradiation experiments using the specialized fixturing and software developed in this project. In addition, the data should provide insights about the viability of using these detectors in the ATR. Hence, this effort complements current activities to improve ATR software tools, computational protocols and in-core instrumentation under the ATR Modeling, Simulation and V&V Upgrade initiative, as well as the work to replace nuclear instrumentation under the ATR Life Extension Project (LEP) and provide support to the ATR NSUF.

5.5.4. Micro-Pocket Fission Detector Development

The Nuclear Energy Enabling Technology (NEET) program is funding a joint INL, Kansas State University (KSU), and CEA collaborative task to develop a Micro-Pocket Fission Detector (MPFD). Miniature fission chambers and thermocouples have been used in-pile at research and test reactors throughout the world; however, none have been deployed in a single compact package to survive the harsh conditions that exist in high performance MTRs. The MPFD is unlike typical fission chambers in that it has a very small detection area (1 mm diameter), incorporates fast and thermal neutron detectors and a thermocouple within a single sensor (Figure 5-55). In addition MPFDs are constructed from materials that are resistant to radiation damage. These qualities make the MPFD an attractive sensor for ATR users requiring real-time data from experiments.

Within the last decade, efforts were initiated by KSU to develop MPFDs that have the potential to simultaneously detect thermal and fast flux along with temperature in a single miniature sensor. Initial

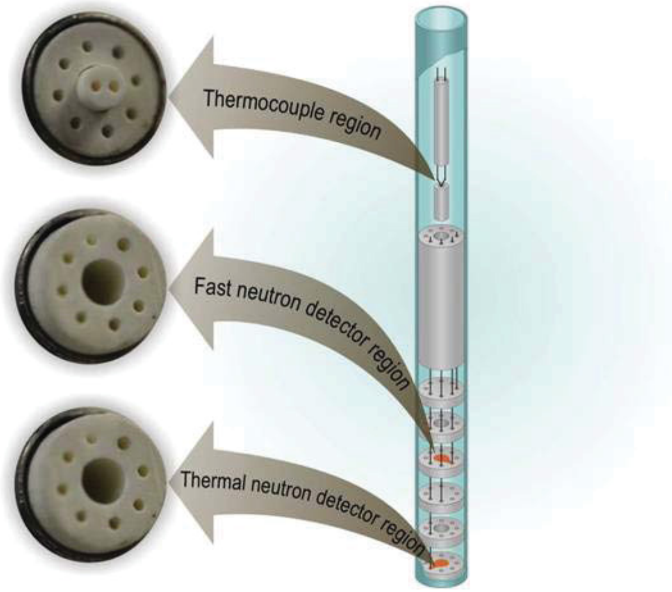

Figure 5-55. MPFD parts and exploded view.

evaluations to demonstrate the MPFD proof of concept were performed at the KSU TRIGA reactor.[150-155] However, prior to deployment of these new MPFDs in a high pressure, high temperature, and high flux environment of a test reactor, such as the ATR, it was recognized that a more robust sensor design was required. The current effort is focussing on development, evaluation and deployment of a more robust MPFD design using fabrication techniques perfected by INL's HTTL staff during development of high temperature irradiation sensors (as described in this section) and expertise in miniature fission chamber design possessed by CEA.[156,157]

MPFDs are uniquely suited to address several challenges:

- Current fission chamber technologies do not offer the ability to measure fast flux, thermal flux and temperature within a single compact probe; MPFDs offer this option. The real-time, high accuracy data from a MPFD will significantly enhance various development and qualification efforts and new multi-physics code validation efforts.
- MPFD construction is very different then current fission chamber construction; the use of high temperature materials allow MPFDs to be specifically tailored to survive harsh conditions encountered in the core of high performance MTRs.
- New high-fidelity reactor physics codes will need a small, accurate, multipurpose in-pile sensor to validate the codes without perturbing the validation experiment; MPFDs fill this requirement.
- MPFDs can be tailored with variable sensitivities, allowing them to survive the lifetime of various experiment or fuel assemblies in a range of MTRs.
- The small size of the MPFDs allows multiple sensors to be deployed to accurately visualize the flux and temperature profiles in the reactor.

The MPFD project consists of two research tasks. The objective for the first task is to develop an enhanced MPFD design and prototype and test its performance in a laboratory setting, while the objective for the second task is to construct an enhanced MPFD prototype with fissile deposits and evaluate it in reactor facilities. It is currently anticipated that MFPD development and evaluation tasks will be completed within approximately three years. The work in FY12 was devoted to enhancing the MPFD design to accommodate INL-developed HTIR-TCs and improve robustness for high temperature, high flux, long-duration ATR applications. Readout electronics have been built at KSU, and prototype fabrication is underway.

Fission chambers (see Figure 5-52b) are typically constructed with two coaxial cylindrical electrodes, one of which has a fissile material deposit that is sensitive to neutron interactions. The gap between the electrodes is filled with a gas, typically argon; and a voltage potential is applied between the electrodes. After a neutron interacts with the fissile material, a fission product is ejected into the gas, and a large number of charge pairs are created in the device. These charges are separated and collected at their respective electrode which leads to a current pulse being generated.[158]

MPFDs utilize the same concept, but with a different geometry (see Figure 5-56) that uses parallel plate electrodes instead of coaxial cylinders. This design is known as a parallel plate fission chamber. However, the MPFD design is set apart from other fission chamber designs because their signal is obtained by capturing only part of the available fission product energy deposition whereas all of the energy deposition must be captured in a classical fission chamber. This departure from conventional fission chamber design and operating characteristics allows the MPFDs to have a much smaller chamber size with a much lower fill gas pressure. The design has excellent discrimination characteristics because the energy deposited by the fission products is much greater then that of other types of background radiation interactions in the detector. As another added benefit, the small size allows them to have a faster response time, and thus have the potential to achieve higher count rates then conventional fission chamber designs. As such, MPFDs offer the potential for in-pile applications and for instrumenting the fuel itself.

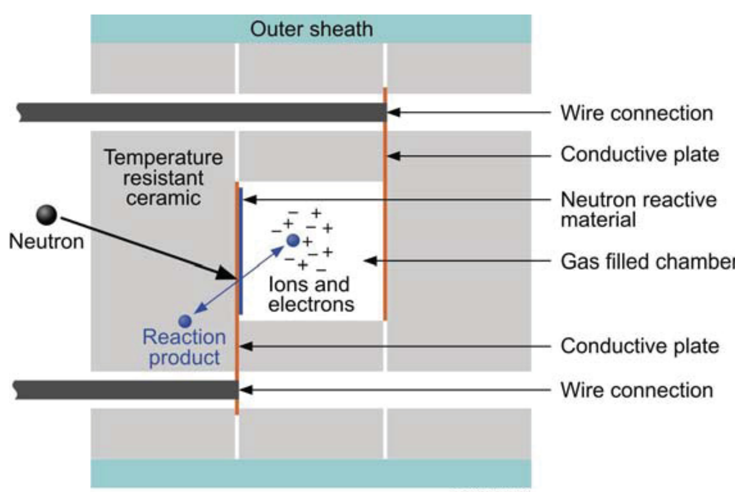

Figure 5-56. Schematic diagram of MPFD fission chamber operation.

MPFDs are unique because of their ability to measure three reactor parameters at very nearly the same location in the reactor core with a single compact detector that is the approximate size of either SPNDs or CEA-developed subminiature fission chambers that can only detect thermal or fast flux (see Section 3). MPFDs utilize two miniature parallel plate ionization chambers that contain a deposit of U-235 for thermal flux detection and a deposit of Th-232 for fast neutron detection. The design also includes a provision to install a thermocouple directly above the fission chambers. Initial MPFD testing at the KSU TRIGA reactor demonstrates that material selection minimizes local flux perturbations and that response time is sufficiently fast to provide time-dependent monitoring of the fission reaction rate or fast and thermal flux during a high power reactor transient. However, initial MFPD prototypes did not include temperature sensors, and testing was completed at the KSU TRIGA Mark-II nuclear reactor at low temperatures and low fluence.[150-155]

During FY12, KSU focused on two tasks to aid in enhanced MPFD development. The first task developed new detector electronics for the new MPFD design (Figure 5-57). The amplifiers were designed, built, and tested at the KSU Electronics Design Laboratory (EDL).[159] After initial testing at EDL was complete, the amplifiers were connected to an older fission chamber installed in the KSU TRIGA Mark II nuclear reactor[160] and demonstrated to INL staff to verify the amplifier would capture neutron induced pulses. The amplifier captures the expected pulses as shown in Figure 5-57.

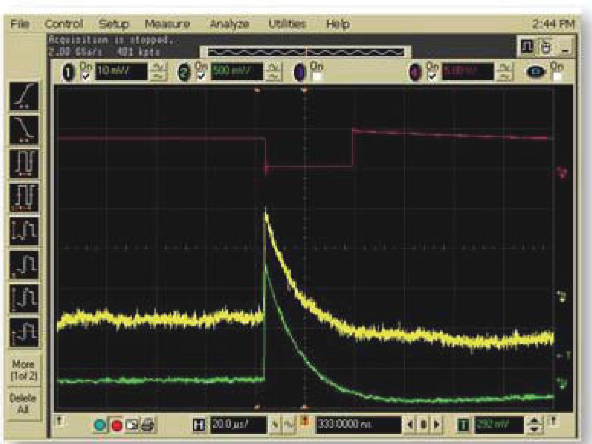

(a)

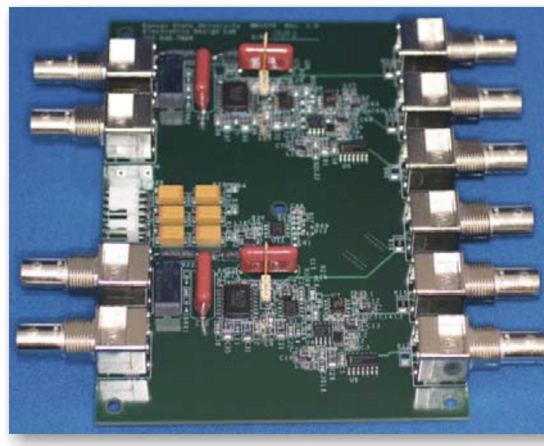

(b)

Figure 5-57. KSU-designed electronics: (a) Neutron induced pulses from MPFD electronics (b) amplifier board.

KSU's second task in FY12 focused on developing an enhanced plating system for deposition of the electrical contacts and fissile material on the MPFDs. Initial work performed at the Semiconductor Materials and Radiological Technologies (SMART) Laboratory[161] included fabricating tooling required to deposit the electrical contacts via electron beam evaporation (Figure 5-58). The fissile material deposition evaluations considered two methods; the first method used standard electroplating, while the second used electro-less plating. Initial evaluations have demonstrated that electro-less plating is not a viable method to deposit the fissile materials. Hence, electroplating has been chosen for the fissile deposition method. Current research at KSU is focusing on optimizing the plating recipes to achieve a uniform fissile deposit.

INL work in FY12 focused on redesigning the MPFD layout to be more robust and more easily deployable in high performance reactors, such as the ATR. The new design, as shown in Figure 5-59 uses a cylindrical geometry that is inserted into an outer sheath that can be sealed and tested leak-tightness. The new design places the sensors on top of each other while moving the wire connections to the edge of the detector electrodes. The signal wires will run inside the insulators for the entire length of the detector and extension cable. This design isolates each wire and has solved wire cross-talk issues with past MPFD designs. The materials selected for the MPFD are end-use dependent. For initial prototype construction,

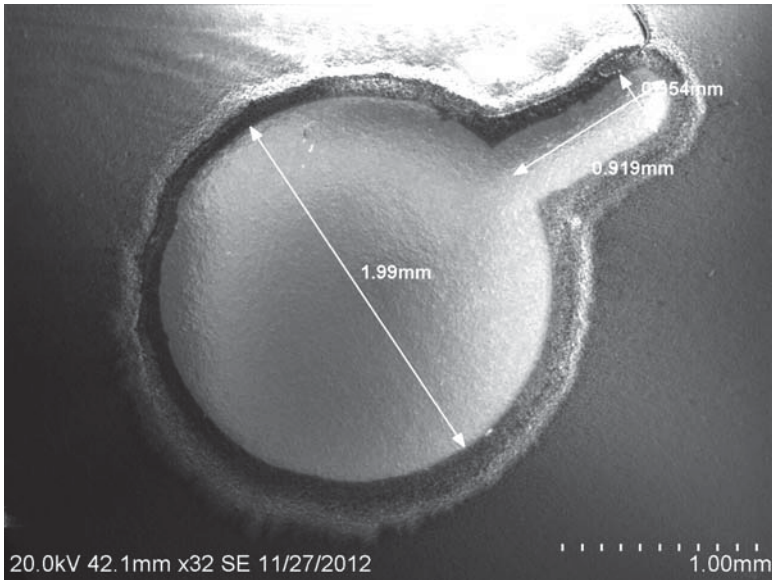

Figure 5-58. KSU SEM picture of MPFD electrode using electroplating.

less expensive, lower temperature materials were selected (e.g., alumina insulators (see Figure 5-60), stainless steel tubes, and alumel and chromel thermocouple wires.

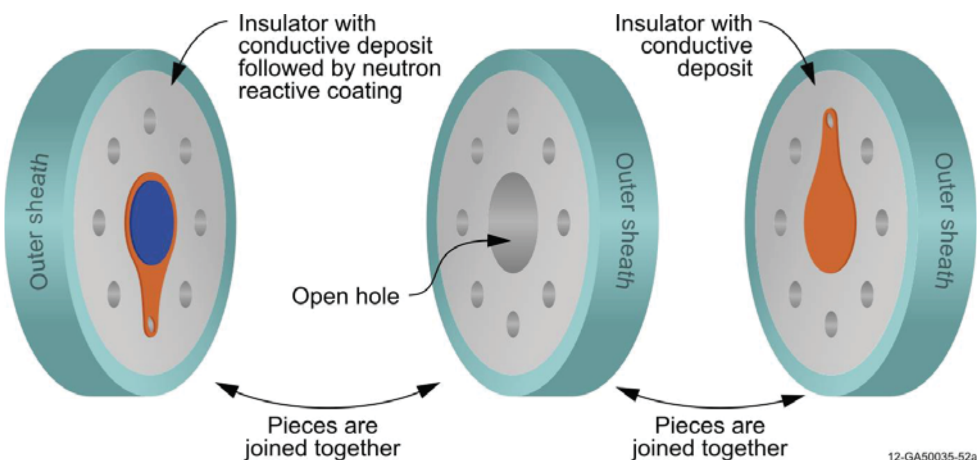

Figure 5-59. Enhanced MPFD design.

MPFD prototype construction is underway using equipment and techniques perfected by INL's HTTL staff for other high temperature in-pile sensors. The unique design of the MPFD required several construction steps to be performed opposite of conventional in-pile sensor fabrications. Several pieces of fabrication equipment required modification to support construction of the new MPFD design. Despite construction differences in the MPFD design, the final sensor will undergo laboratory evaluations (e.g., leak testing, high temperature furnace testing, and high pressure/high temperature autoclave testing, etc.) to ensure that is as robust as other HTTL-developed instrumentation.

A mock-up of the initial prototype assembly is shown in Figure 5-60 next to a typical ballpoint pen. It is expected that the final design of the MPFD, scheduled to be completed in FY14, will be smaller and more compact. Helium leak tests of the prototype using standard HTTL methods revealed that probe can be sealed with leak rates less than 8 x10^{-6} cc/s. This is considered a major achievement because previous designs of MPFDs had major issues with leak tightness.

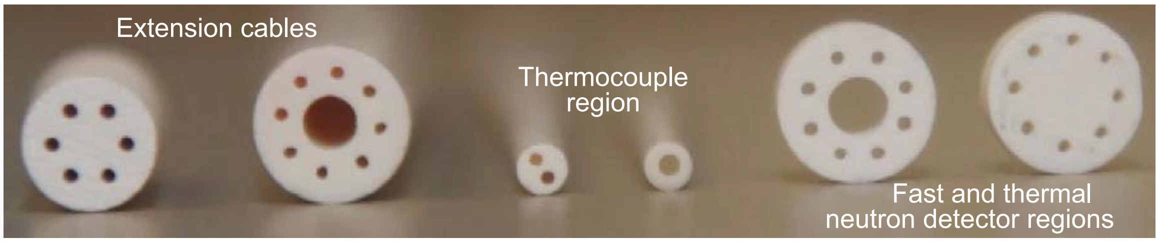

(a)

(b)

Figure 5-60. Enhanced MPFD design: (a) various alumina parts, (b) assembled MPFD mockup.

During FY13, detector prototype fabrication, high temperature evaluations and neutron flux evaluations will be performed at INL and KSU. High temperature evaluations will be performed in furnaces at the HTTL. Pending funding availability, simple response testing will be performed at the INL Health Physics Instrument Laboratory (HPIL) neutron and gamma panoramic irradiators (see Figure 5-61b) and at KSU using their 1 MW TRIGA Mark II research reactor. More complex evaluations, expected in FY14, will utilize the INL's ATRC using specialized fixturing installed at the ATRC shown in Figure 5-61a.

As previously discussed, the ATRC fixturing is used to characterize and cross-calibrate a wide range of flux detectors, including SPNDs, CEA-developed fission chambers, and specially-developed back to back fission chambers. In addition, CEA has agreed to model the detector response and compare to actual results. This data will be used to develop a smaller, improved design of MPFD that will be constructed and evaluated in FY14. Ultimately, it is anticipated that the ATR NSUF program will deploy a MPFD in a higher flux reactor irradiation test at an appropriate NSUF facility.

5.6. Localized Heating

Gamma heating sensors have several advantages over neutron detectors. The main advantage is that gamma heating signals are constant with fuel burnup. Gamma heating devices are also quite versatile. Gamma thermometers can be used to measure some thermal characteristics of coolant and core materials

(a) (b)

Figure 5-61. INL irradiation facilities for MPFD evaluation: (a) ATRC and (b) HPIL panoramic irradiator.

as well as local power. Commercial and test reactors have utilized vertical stacks of gamma thermometers to provide water level and other data related to the properties of the coolant.[162]

Evaluations of localized heating measurement methods were initiated in 2012 by the ATR NSUF. The objective of this effort is to research the methods used for local gamma heating measurements and to gain experience with the use of a gamma heating sensor. After investigating the sensors currently available, gamma thermometers, which are designed and fabricated similar to thermocouples, were selected for further evaluation as a viable local gamma heating sensor in ATR NSUF irradiations. Commercially-available gamma thermometer designs were evaluated, and vendors were contacted to determine the best gamma thermometer for evaluation at the HTTL. Due to design features, cost, irradiation testing history, and other logistical factors, the IFE/HRP gamma thermometer design was selected for evaluation. This IFE/HRP gamma thermometer is shown in Figure 5-62.

Figure 5-62. IFE/HRP gamma thermometer.

The IFE/HRP gamma thermometer was X-rayed to determine the internal composition. Figure 5-63 is one of the radiographs of the IFE/HRP gamma thermometer. The distance between the insulated junction and the cold junction is an important quantity for the experimental setup; however, the cold junction could not be located in the radiographs. IFE/HRP was contacted and provided drawings which indicate that the distance between the junctions is 75 mm.[163]

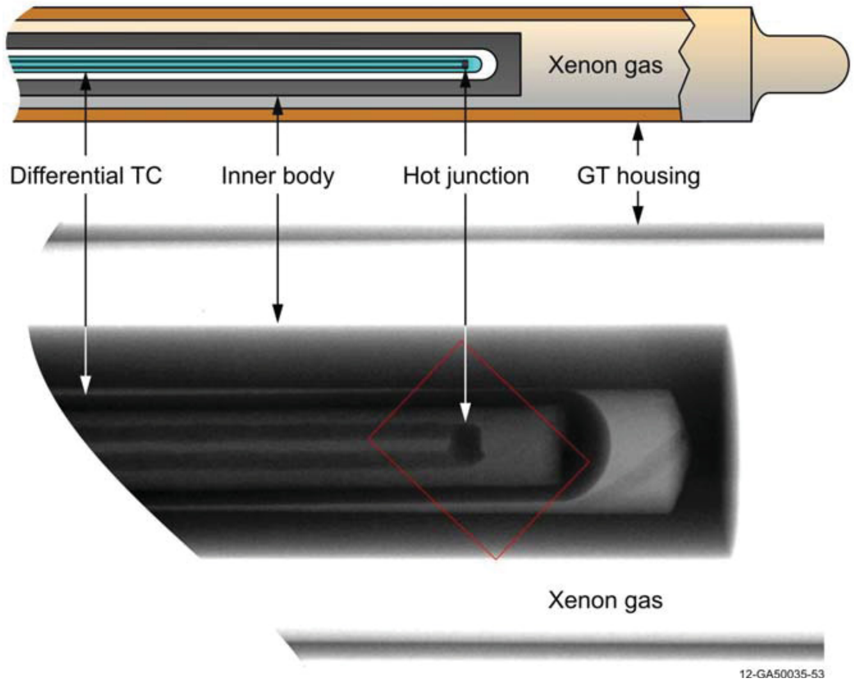

Figure 5-63. Insulated junction radiograph of IFE/HRP gamma thermometer.

Initial FY12 evaluation of the gamma thermometer focused on reproducing the time constant that was provided by IFE/HRP. The experimental setup to perform time constant measurements consists of a beaker of ice-water and a beaker of boiling water on a hot plate. The gamma thermometer is transferred between the two states of water with known temperatures. At the moment the gamma thermometer is switched from one state to the next, an electric potential is established between the junctions of the differential thermocouple. The non-insulated junction reacts to the change in temperature immediately; however, the insulated junction has a delayed reaction. Data are logged as the insulated junction heats or cools to the same temperature as the non-insulated junction at which point the potential difference between the two junctions returns to zero. Once the equilibrium temperature is attained, the data logging is terminated and the data are evaluated. In order to obtain the time constant, the data are converted from a voltage signal to a temperature. This is done by utilizing the linear relationship between temperature and voltage for a Type K thermocouple. Once the temperature is plotted, a curve fit can be applied to the data using Equation (5-4).

$$T = T_0 e^{-\frac{t}{\tau}} \tag{5-4}$$

where

T = temperature,

T_0 = initial temperature,

t = time, and

τ = time constant.

The resulting curve fit contains the information needed to extract the time constant. A graph with the curve fit is shown in Figure 5-64. The data for the case where the gamma thermometer is transferred from the boiling water to the ice water have less variation and produced a time constant similar to the value provided by IFE/HRP. The IFE/HRP evaluated time constant is 57.83 s. The time constant evaluated with the HTTL experimental setup is 58.53 s. This time constant is inferred from the data shown in Figure 5-64.

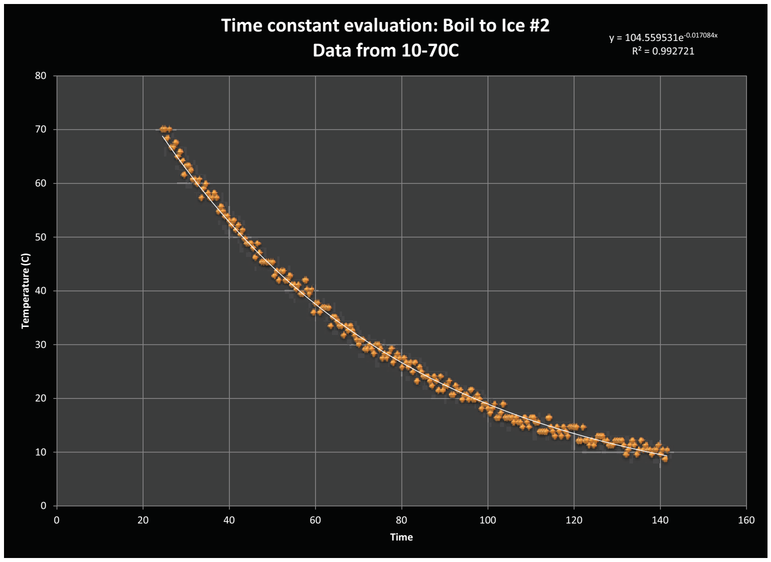

Figure 5-64. IFE/HRP gamma thermometer time constant evaluation.

In order to improve the accuracy and repeatability of the time constant measurements, an improved experimental setup was devised. Larger beakers have been acquired, and enhanced fixturing for the gamma thermometer has been developed. These improvements will allow for better control over the key parameters involved in the time constant measurements.

As evaluations continue in 2013, an improved understanding of the gamma thermometer operation will be gained. Plans for future testing include utilizing gamma fields in INL facilities to understand the sensitivity and calibration of the gamma thermometer. Further research will elicit improvements that can be implemented in the design of an improved gamma heating sensor that could be deployed for use in US MTR applications.

5.7. Cross-Cutting

Some research activities benefit multiple sensor development activities. Two such cross-cutting activities are documented in this section: a recently initiated effort to compare the irradiation performance of ultrasonic transducer materials and a proposed effort to compare the irradiation performance of fiber optics. Results from these tests have the potential to enable the use of a host of new sensors to support irradiation testing.

5.7.1. Ultrasonic Transducer Irradiation

The objective of this cross cutting task is to address implementation issues that apply to all ultrasonics-based sensors. The long and successful history of out-of-pile ultrasonic measurements suggest that ultrasonics-based sensors could be used in-pile for materials and fuels characterization, including detection and characterization of degradation and damage.[164] Limited PIEs have successfully shown that fuel microstructural parameters, such as porosity and grain size, can be correlated to ultrasonic velocity.[165] According to Villard,[166] frequency requirements for such measurements are restricted to greater than 10 MHz. However, lower frequencies can be used for some applications, such as ultrasonic thermometry, where frequency requirements may be 100 – 150 kHz or lower.[167]

The development of ultrasonic tools to perform a variety of in-pile measurements requires a fundamental understanding of the behavior of ultrasonic transducer materials in high-radiation environments. While a number of irradiation studies of ultrasonic transducers have been described in the literature, a one-to-one comparison of these studies is difficult, as the materials and irradiation test conditions often differ. In addition, the tests to date are generally at lower flux/fluences than what might be seen in US MTRs. As a result, a series of experiments to baseline the performance of ultrasonic transducer materials (in terms of change in sensitivity as a function of temperature and irradiation) are necessary to support the irradiation test.

Results of this irradiation test will enable development of ultrasonic sensors for in-pile measurements, including fuel and material morphology changes, fission gas composition and pressure measurements, fuel and material geometry changes, and temperature. Results from these tests will provide a method for selecting optimum ultrasonic transducer materials for different in-pile measurements and guide the development of signal processing tools to enhance the measurement to demonstrate the intended in-pile measurements.

During 2012, the ATR NSUF announced that funding would be provided to support an ultrasonics transducer irradiation proposed by PSU in collaboration with researchers from INL, Argonne National Laboratory, and Pacific Northwest National Laboratory. The irradiation will be performed at the MITR. Relevant MITR design information is summarized here to provide perspective about the design of the ultrasonics transducer capsule and test conditions developed by this project. The MITR is a tank-type research reactor.[168] It is currently licensed for 5 MW and is being relicensed for 6 MW operation.

The identified MITR irradiation position will have a peak thermal flux of $3x10^{13}$ n/cm^2-s and a peak fast flux (E > 0.1 MeV) of $1x10^{14}$ n/cm^2-s. Temperature control will be afforded by a helium/neon gas gap with adjustable gas composition, and a test temperature target of approximately 300 ^{o}C. It is proposed that the test exceed fast neutron fluences of prior piezoelectric transducer irradiations (e.g., > $1x10^{21}$ n/cm^2). In order to observe rapid changes at relatively low fluences, it is proposed to start the test with the reactor coming to power slowly. Capsule irradiation for at least 310 days is anticipated.

The MITR configuration restricts the test capsule to a cylinder 46 mm in diameter and 610 mm in length. The currently proposed capsule design uses structural graphite as a holder material. Graphite is an ideal material. It has a low density (for reduced gamma heating); it is thermally conductive (to produce a uniform predictable temperature); it is less susceptible to neutron activation; and it has a high melting temperature. The graphite will hold the test specimens in place while also efficiently conducting heat generated during the test to the coolant. Based on estimated space requirements for each transducer, it is proposed to include six piezoelectric samples and three magnetostrictive samples. Each sample would be encapsulated separately (this will allow samples with cobalt to be easily separated from the other samples, such that all non-cobalt bearing samples may undergo PIE). It may be advantageous to place transducers at each end of the waveguides used for monitoring signals, as this effectively doubles the number of samples included in the test. Recommended instrumentation for this test should be included to allow accurate monitoring of temperature, gamma heating, and both fast and thermal neutron flux. It is advised to include at least two sensors of each type, both to increase the accuracy of the measurements and for redundancy in the case that some instruments may be damaged during the test. A conceptual drawing of the proposed test capsule is shown in Figure 5-65.

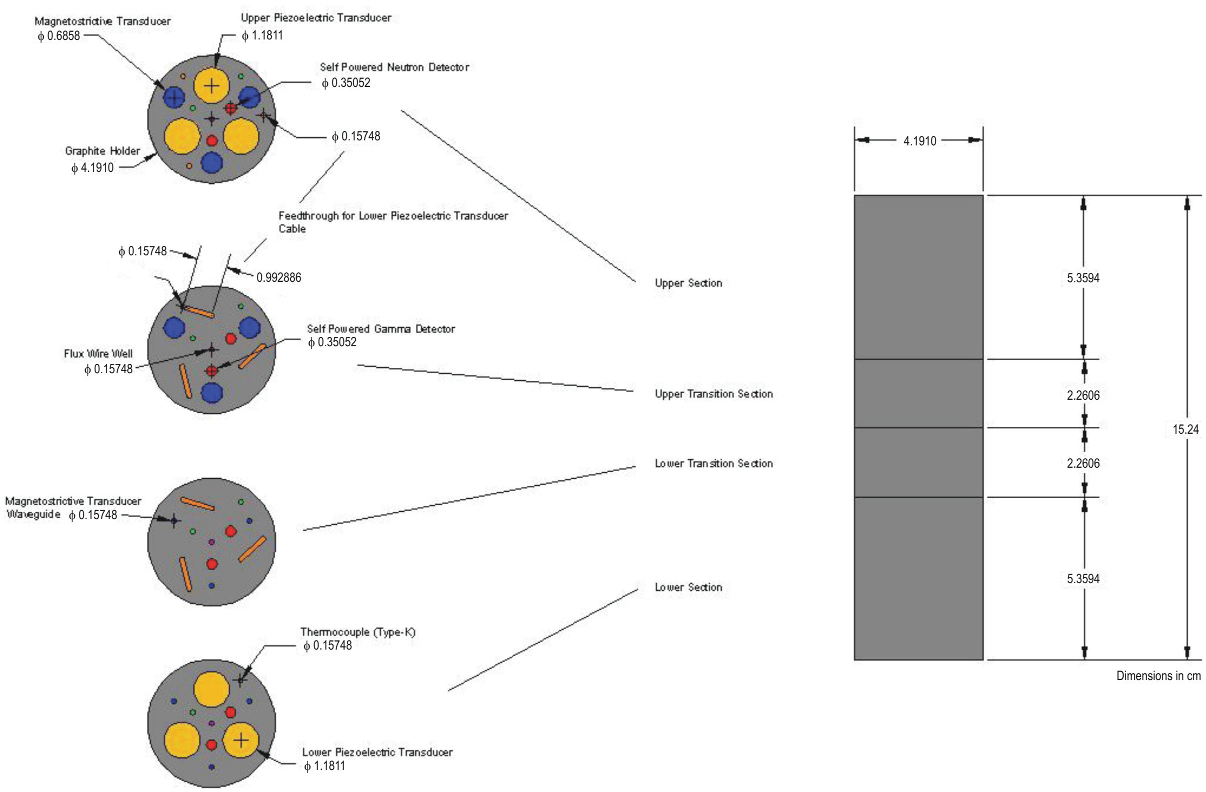

Figure 5-65. Conceptual sketch of graphite sample holder.

Prior studies have shown that typical piezoelectric and magnetostrictive materials used in transducers degrade when subjected to high temperature and radiation.[169-174] Candidate magnetostrictive and piezoelectric materials must, therefore, be carefully selected; and transducer assemblies must be carefully designed. As discussed below, only limited radiation effects data are available to guide this process. Additional studies and tests are needed to select the optimum transducer materials for various in-pile ultrasonic sensors. The MITR irradiation test and associated laboratory supported by this project will provide important information for selecting appropriate transducers for ultrasonic sensors.

5.7.1.1. Selected Piezoelectric Transducers

The piezoelectric transducers proposed for this test were selected based on research by Parks and Tittmann[175] and from early ultrasonic sensors developed at the Hanford Engineering Development Laboratory (HEDL)[176] for under-sodium viewing, which shared many similar constraints with respect to thermal and neutron radiation tolerance. Schematics of the transducers used by HEDL and Parks and Tittmann[175] are shown in Figure 5-66 a) and b) respectively, and the preliminary transducer design for ATR insertion is shown in Figure 5-66 c). Both transducers rely on spring loading pressure for coupling the piezoelectric element to the faceplate or test piece. Electrical contact with the piezoelectric element is also achieved through application of pressure. A backing layer behind the piezoelectric sensor provides damping and prevents excessive “ringing” of the transducer. In the design of Parks and Tittmann,[175] the backing layer material is carbon/carbon composite, whereas some other designs incorporate a stainless steel “sponge”.

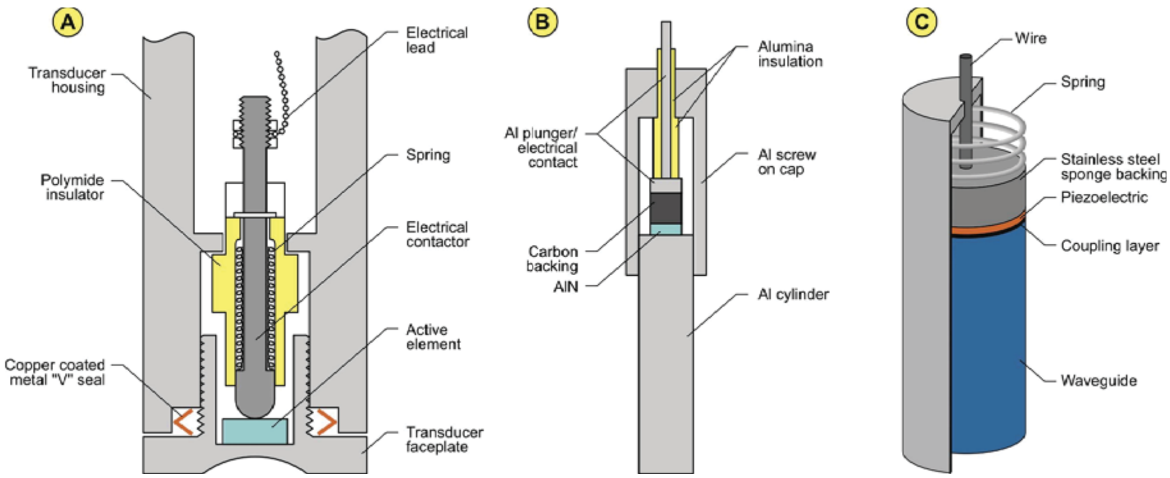

Figure 5-66. Piezoelectric transducer designs.

Due to volume limitations in the proposed tests, the number of piezoelectric transducer materials that can be included in this test is limited. The following two candidate piezoelectric transducer materials have been selected for inclusion in the MITR irradiation.

- ***Aluminum Nitride (AlN)***

Aluminum nitride is a relatively new material, as far as bulk single crystals are concerned. In fact, the work of Parks and Tittmann[175] with this material is the first of its sort. In the past, thin film AlN has been shown to be unaffected by gamma irradiation up to 18.7 MGy[177] and temperatures of 1000 ^{o}C.[178,179] Moreover, this material has been explicitly cited in numerous independent studies as a highly radiation tolerant ceramic.[180] Further, tests of bulk single crystal AlN in a TRIGA nuclear reactor core showed this material to be completely unaffected by a fast and thermal neutron fluence of 1.85 x 10^{18} n/cm^2 and 5.8 x 10^{18} n/cm^2 respectively and a gamma dose of 26.8 MGy.[175] This work along with that of Yano [181] and Ito[182] have indicated that the $^{14}N(n,p)^{14}C$ is not of concern. These factors indicate that AlN is an excellent candidate material.

- ***Bismuth Titanate Niobate (Bi3TiNbO9)***

A literature review revealed bismuth titanate niobate to be the most promising of commonly used material tested to date.[183] However, prior testing indicates that this material a significant fraction of its one way piezoelectric response at a fast neutron fluence of 10^{20} n/cm^2. Nevertheless, based on promising results from previous testing, it has been selected for inclusion and will be used as a baseline for comparison for the other selected materials.

- ***Zinc Oxide (ZnO)***

Zinc oxide is found in the Wurzite crystalline structure, as is AlN, and has been cited as a highly radiation tolerant material.[184] The evaluated nuclear data files do not show any detrimental nuclear cross sections. Furthermore, this material possesses a high transition temperature and moderate piezoelectric coupling. ZnO has been selected for inclusion in this irradiation test although there are some concerns about its s high temperature performance.

5.7.1.2. Selected Magnetostrictive Transducers and Candidate Biasing Magnets

A general schematic of a proposed magnetostrictive transducer is shown in Figure 5-67. The components of the transducer consist of the magnetostrictive wire, driving coil (with bobbin), biasing magnet (or, alternatively, biasing coil), and damper.

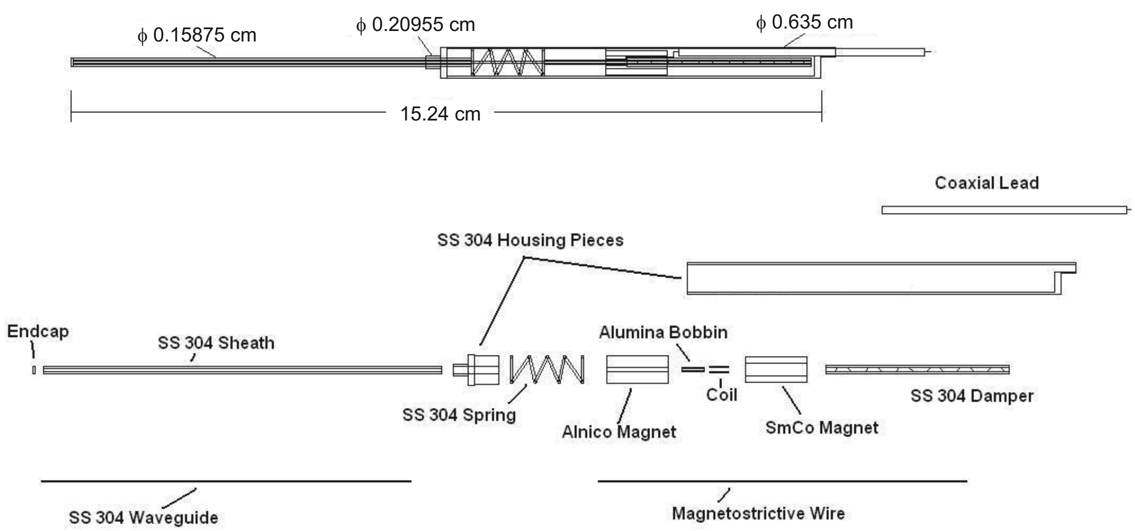

Figure 5-67. Magnetostrictive transducer exploded view.

Most materials appropriate for use as biasing magnets contain constituent elements that are not well suited for use in a reactor environment. Specifically, the presence of cobalt or components with high thermal neutron capture cross sections, such as boron, samarium, or neodymium. The primary magnetic materials considered are Alnico (an aluminum-nickel-cobalt alloy), Nd-B-Fe (a neodymium-boron-iron ceramic), and Sm-Co (a samarium-cobalt ceramic). Alnico provides the weakest magnetic field strength of these options, but it also has the highest Curie temperature. Activation of the cobalt is the primary concern with this material. Prior testing has shown that Alnico magnets can retain their field for at least half the accumulated fluence proposed for this test. Samarium cobalt magnets have high field strength and moderately high Curie temperatures. The concerns with this material are activation of the cobalt and transmutation of the samarium. Prior testing indicates that the nuclear environment does not strongly affect the performance of these magnets. The strongest magnets available are Nd-B-Fe. These magnets are not considered suitable as the Curie temperature is below the proposed test temperature. Another option for generating the biasing magnetic field is the use of a DC biasing coil. This option is not preferred as the coil may increase the volume of the transducer and would necessarily add an additional electrical lead to each magnetostrictive transducer.

Selected magnetostrictive transducer materials for the MITR irradiation include:

- ***Remendur***

Remendur has the most extensive use in nuclear applications of all the magnetostrictive alloys, having been used previously for short duration thermometry applications. Remendur has a high Curie temperature and high magnetostriction. Given this, and its previous use, Remendur is also highly recommended for testing, despite the presence of cobalt. Although Remendur is no longer commercially available, several identical alloys are available under different names.

- ***Arnokrome^{TM} (Arnold Magnetics)***[185,186,187]

Arnold Magnetics produces several magnetostrictive alloys, Arnokrome 3, Arnokrome 4, and Arnokrome 5. Arnokrome 3 contains cobalt and has much lower magnetostriction than Remendur, and is therefore not of interest in the current study. Arnokrome 4 and 5 have similar magnetostriction to Arnokrome 3, but without the presence of cobalt. Although not as promising as some candidates, it is recommended that either Arnokrome 4 or 5 be included in the irradiation test.

- ***Galfenol***[188]

Galfenol is a relatively new alloy of iron and gallium. Galfenol is a member of the “giant” magnetostrictive alloys and has a very large saturation magnetostriction. It also has an appropriately high Curie temperature. Neither constituent element reacts strongly with neutron radiation.

Final selection of biasing magnet materials may be impacted by on-going out-of-pile evaluations. Candidate biasing magnets that are being considered for this irradiation include:

- ***Alnico***

Alnico magnets are considered primarily because they have a very high Curie temperature. The magnetic field strength is not high, compared to ceramic rare-earth magnets, but is sufficiently high for use as a biasing field source. Alnico magnets do have some history of testing in-pile, being tested to approximately half the target fluence of the current study with little loss of performance.[189] The low coercive force is a concern as this indicates that the magnets lose strength over time.

- ***Sm-Co***

Samarium-cobalt magnets have magnetic properties nearly as good as Nd-B-Fe magnets and Curie temperatures nearly as high as Alnico magnets. Although samarium has a high thermal neutron absorption cross section, previous irradiation testing indicates that neutron irradiation has a negligible effect on its magnetic properties.[190]

Several tests must be conducted out-of-pile either prior to or in conjunction with the irradiation test (prior to the test being preferable, as it would allow identification of any systematic problems before the full test is installed in the reactor). These tests are needed to help separate the effects of the neutron radiation from effects of the elevated temperature the test will likely reach while in the reactor. A list of proposed out-of-pile tests is given in Table 5-7.

Table 5-7. Proposed out-of-pile tests.

Test	Materials	Description
Endurance test (ET)	All candidate materials	The ET includes operation of candidate transducers at 300 ^{O}C. This test is to be used as reference for the data collected during the irradiation test. Two types of endurance tests can be performed, one at an elevated temperature relative to the nuclear reactor environmental conditions to accelerate the degradation process. The other is to be at the anticipated irradiation temperature of 300 ^{O}C. The time necessary for each of these tests is at least several weeks, if not for a month. The samples are to be inserted in the reactor for about a year, so a several month long test is proposed. This test will allow separation of temperature induced changes from radiation induced changes, as well as identification of design flaws.
Maximum operating temperature (MOT)	All candidate materials	The MOT is determined by placing the transducer in the tube furnace and increasing the temperature linearly at a slow rate so that at each measurement could be considered isothermal. In the past rates such as 1 degree per minute have been used. As such, the time necessary for each experiment will depend on the Curie temperature; on the order of 500-1000 minutes or 8-16 hours. This test will allow identification of possible temperature induced changes at temperatures near irradiation temperature, effects of temperature transients, and maximum operating temperature.
Saturation magnetostriction	All magnetostrictive candidate materials	This test involves measurement of magnetostriction of candidate materials as a function of applied DC magnetic field using a DC current supply and a pushrod dilatometer. These data are needed to characterize the performance of candidate magnetostrictive materials.
Hysteresis measurement	All candidate materials	The HM characterizes remnant polarization and indicates changes in material structure. This test can be performed with the transducer in situ and will be completed alongside the MOT and ET.

PIE will be needed to quantify the irradiation effects on the piezoelectric candidate materials. Appropriate PIE evaluations are being identified by the project and will be finalized during 2013. assembly needs to be taken apart, and the sensor needs to be individually measured.

5.7.2. Fiber Optic Irradiation

The objective of this cross cutting task is to address optical fiber implementation issues that apply to all fiber optic sensors. For example, pressure boundary seals are necessary to pass the optical fiber into the reactor environment. An INL-developed method of addressing this issue has been reported previously,[191] and commercial off the shelf seals and feed throughs are becoming more readily available. Optical fiber temperature limitations are also an issue. Copper and gold coated fibers are available which can endure long term temperatures in the 600 to 700 °C range. Fiber optic sensing applications in temperatures over 1000 °C have been reported, but longevity may only be a few hours.[192] This temperature limitation may preclude the use of optical fibers from in-situ direct fuel measurements. The temperature capabilities of fiber optic sensors would be sufficient for measurements near the fuel cladding or in cases where the fiber could be used to direct light to or collect light from the fuel surface.

Radiation effects on optical fibers and the probe components are an important issue for the long term survivability of fiber based sensors. A summary of the fiber issues and related research has been reported previously.[46] Irradiation testing of the optical fiber and components is paramount to quantitatively determining the effects on the sensor accuracy and lifetime. Collaborations with Ohio State University and Texas A&M University have led to development of an ATR NSUF proposal for fiber optic radiation testing, which is planned for submission in FY13. The objective of the proposal would be the measurement of radiation induced attenuation in several optical fibers in an ATR instrumented lead experiment.

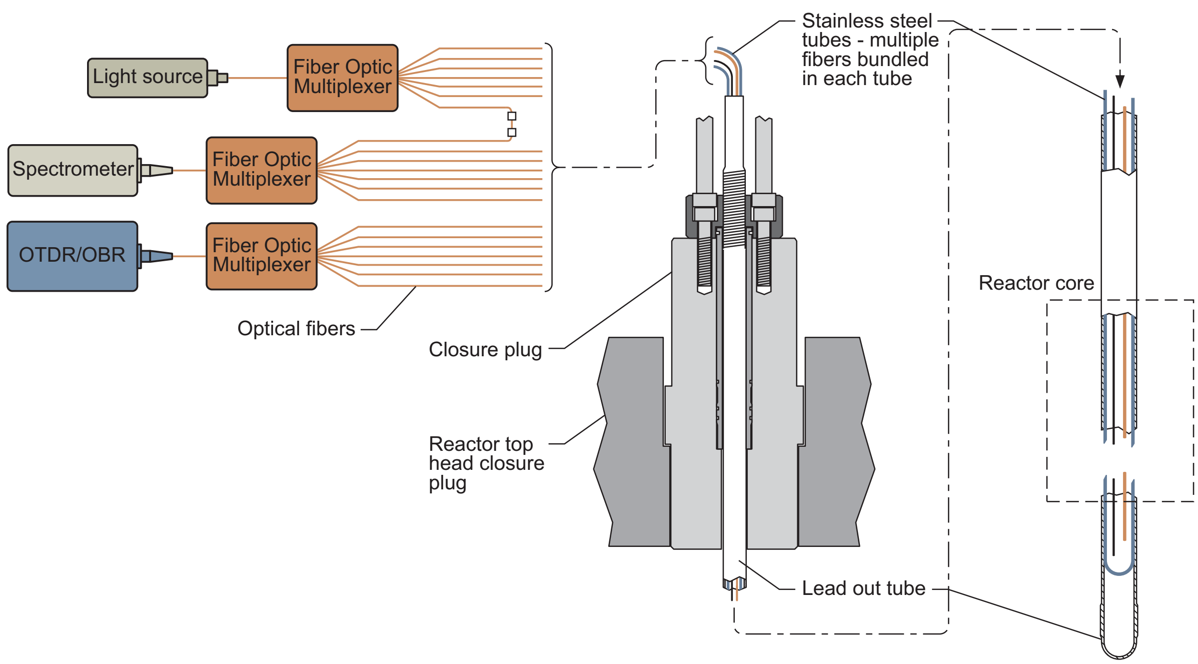

Figure 5-68. ATR fiber optic attenuation test schematic.

The test methodology would involve both through transmission testing using a spectrometer and single ended fiber testing using either OTDR or OBR. In the through transmission test, the fiber would be routed down to the reactor core and back essentially forming a long “U”. Light from a broadband source would be coupled into one end of the fiber and the opposite end would be connected to a spectrometer. This would allow attenuation across a broad wavelength range to be continuously monitored. As the tight bend radius necessitated by the small test positions could be detrimental to the fibers, OTDR or OBR instruments would also be employed. These instruments allow attenuation measurements to be made from one end of a fiber but are limited to discrete wavelengths. Fiber optic multiplexers would be implemented in both test methods to allow multiple fibers to be tested using the same instrument.

The design concept uses a lead out tube which would be inserted through the reactor top head closure plate and down into the test position. The lead out tube would serve as the primary pressure boundary. Individual optical fibers would be bundled inside separate small diameter stainless steel tubes. These smaller tubes could be hard mounted in the lead out tube to maintain proper positioning and added protection for the fibers. If funded, the proposal would help answer long standing questions on the longevity of optical fiber based sensors in the ATR.

5.8. Summary

As outlined in this section, INL has initiated efforts to develop and obtain new sensors for measuring key parameters (e.g., temperature, length, diameter, etc.) during irradiation testing at the ATR. As discussed in Section 4, initial ATR NSUF efforts are primarily focussing on sensors that can provide data needed for ATR NSUF users and on ‘lower risk" technologies that are already deployed at other MTRs. These initial efforts have led to several new or enhanced sensors becoming available to ATR users: the doped Mo/Nb HTIR-TCs (Section 5.1.3), silicon carbide temperature monitors (Section 5.1.2), enhanced melt wire selection and encapsulation options (Section 5.1.1), THWM needle probes for thermal conductivity measurements (Section 5.2) and creep elongation (Section 5.3.2). During 2013, it is anticipated that the new creep test rig developed in this program will be deployed in an ATR PWR loop. In addition, it is anticipated that the HTIR-TCs shipped to IFE/HRP will be irradiated in the HBWR and that thermal conductivity THWM needle probes will be shipped to CEA and IFE/HRP. During 2013, it is planned to continue testing of miniature fission chambers developed by CEA and other flux detection systems (e.g., SPNDs) at the ATRC. Efforts initiated in 2012 will also continue. In particular, efforts will continue to explore the use of gamma thermometers and to develop MPFDs, a controlled load creep test rig, and a crack growth test rig. In addition, FCRD efforts to develop ultrasonic thermometers and fiber optics-based length detectors and NEET efforts to deploy a ultrasonics transducer irradiation in the MITR will continue.

6. REFERENCES

1. J. L. Rempe, et al., *Instrumentation to Enhance Advanced Test Reactor Irradiations*, INL/EXT-08 -13985, September 2009.

2. J. L. Rempe, D. L. Knudson, and J. E. Daw, *Status Report on Efforts to Enhance Instrumentation to Support Advanced Test Reactor Irradiations*, INL/EXT-11-21231, Idaho National Laboratory, March 2011.

3. J. L. Rempe, D. Knudson, J. Daw, T. Unruh, B. Chase, K. Davis, R. Schley, S. Taylor, D. Nigg, and K. Condie, *2011 Status Report on Efforts to Enhance Instrumentation to Support Advanced Test Reactor Irradiations*, INL/EXT-11-24233, December 2011.

4. "FY2009 Advanced Test Reactor National Scientific User Facility User's Guide," INL/ EXT-07-13577, Idaho National Laboratory, 2008.

5. S. B. Grover, "Irradiation Facilities at the Advanced Test Reactor," *Transactions of the 11th International Topical meeting on Research Reactor Fuel Management and Meeting of the International Group on Reactor Research,* March 2007, Lyon, France.

6. R. V. Furstenau and S. Blaine Grover, "The Advanced Test Reactor Irradiation Facilities and Capabilities," *Proceedings of the Americas Nuclear Energy Symposium 2002 (ANES 2002),* October 2002.

7. F. M. Marshall, "Advanced Test Reactor Capabilities and Future Operating Plans," *presented at Test Research and Training Reactors (TRTR) Annual Meeting*, September 2005, Gaithersburg, MD.

8. C. J. Stanley and F. M. Marshall, "Advanced Test Reactor - A National Scientific User Facility," proceedings ICONE2008-48426, May 11-15, 2008, Orlando, Florida, USA.

9. A. J. Palmer, G. L. McCormick, S. J. Corrigan, "Hydraulic Shuttle Irradiation System (HSIS) Recently Installed in the Advanced Test Reactor (ATR)," *Proceedings of ICAPP '10, Paper 10354,* San Diego, CA, USA, June 13-17, 2010

10. International Atomic Energy Agency, "Nuclear Research Reactors in the World," www.iaea.or.at/ worldatom/rrdb/, accessed December 9, 2011.

11. G. Bignan, "The Jules Horowitz Reactor: a new High Performance European MTR open to International Community," *presentation at the Idaho National Laboratory*, Idaho Falls, ID, September 2010.

12. G. Bignan, J.-F. Villard, C. Destouches, P. Baeten, L. Vermeeren, and S. Michiels, "The Key Role of Instrumentation for the New Generation of Research Reactors," *Proceedings of the Second International Conference on Advancements in Nuclear Instrumentation, Measurement Methods and their Applications (ANIMMA2011),* Ghent, Belgium, June 2011.

13. C. Destouches and J.-F. Villard, "Improved In-Pile Measurements for MTR Experiments," *IAEA Technical Meeting on In-Pile Testing and Instrumentation for Development of Generation-IV Fuels and Materials, 2*1-24 August 2012, Halden, Norway.

14. J.-F. Villard, “Progress in Instrumentation Development for the Future Jules Horowitz Reactor,” *presentation at joint Idaho ANS-IEEE-ICIS Seminar,* September 12, 2012, Idaho Falls, ID.

15. H. Thoresen and S. Solstad, An overview of nuclear fuels and materials research at the OECD Halden Reactor Project, seminar presented at the Idaho National Laboratory, Idaho Falls, ID, July 15, 2008.

16. B. G. Kim, J. L. Rempe, J-F Villard, and S. Solstad, “Review of Instrumentation for Irradiation Testing of Fuels and Materials,” *invited review paper, Nuclear Technology,* **176**, November 2011, p 155-187.

17. J.F. Villard, “Innovative in-pile instrumentation developments for irradiation experiments in MTRs,” *IGORR 10,* Gaithersburg, Sept. 2005.

18. J. F. Villard, “INSNU Project - Instrumentation for Irradiation Experiments in Research Reactors,” *presentation at the Idaho National Laboratory*, Idaho Falls, ID, June 2008.

19. J. F. Villard, “INSNU Project - Instrumentation for Irradiation Experiments in Research Reactors,” *presentation at CEA-Cadarache*, Cadarche, France, October 2008.

20. J-F Villard and M. Schyns, “Advanced In-Pile Measurements of Fast Flux, Dimensions, and Fission Gas Release,” *Proceedings of the ANS NPIC HMIT 2009 Topical Meeting on Nuclear Plant Instrumentation, Controls, and Human Machine Interface Technology,* Knoxville, TN, April 2009.

21. D. Iracane, G. Bignan, Ph. Guimbal, and J-F. Villard, “Advanced Instrumentation for Irradiation Experiments in Material Testing Reactors (MTRs),” *Proceedings of the First International Conference on Advancements in Nuclear Instrumentation, Measurement Methods and their Applications (ANIMMA)*, Marseille, France, June 2009.

22. C. Blandin, S. Breaud, JM. Laurens, L. Oriol, L. Vermeeren, M. Weber “In-pile CFUZ53 sub-miniature fission chambers qualification in BR2 under PWR conditions – *10th International Group on Research Reactors (IGORR) meeting,* Gaithersburg (USA), September 2005.

23. P. Philliatre, et al., “Reasons Why Plutonium 242 is the Best Fission Chamber Deposit to Monitor the Fast Component of a High Neutron Flux,” *Nucl. Instrum. Meth. Phys. Res. A*, **593**, 510, 2008.

24. L. Vermeeren, M. Wéber, L. Oriol, S. Breaud, P. Filliatre, B. Geslot, C. Jammes, S. Normand, and B. Lescop, “Experimental Verification of the Fission Chamber Gamma Signal Suppression by the Campbelling Mode,” *Proceedings of the First International Conference on Advancements in Nuclear Instrumentation, Measurement Methods and their Applications (ANIMMA),* Marseille, France, June 2009.

25. L. Vermeeren, H. Carcreff, L. Barbot and al. “Irradiation Tests of Prototype Self-Powered Gamma and Neutron Detectors,” *Proceedings of the Second International Conference on Advancements in Nuclear Instrumentation, Measurement Methods and their Applications (ANIMMA2011)*, Ghent, Belgium, June 2011.

26. S. Fourrez, G. Bailleul, M. Kollen, JF. Villard, "Characterisation of a thermocouple for high temperature measurement under irradiation - Definition and properties of the Molybdenum Niobium thermocouple, *12th International Metrology Congress*, Lyon (France), June 2005.

27. J. F. Villard, S. Fourrez, "High temperature measurement needs for irradiation experiments in Material Testing Reactors - Development of a new type of thermocouple and interest of high temperature fixed points for its characterisation and in-pile qualification," *Physikalisch-Technische Bundesanstalt Seminar on High-temperature fixed-points for industrial and scientific applications*, Berlin (Germany), April 2005.

28. J. F. Villard, S. Fourrez, D. Fourmentel, and A. Legrand, "Improving High-Temperature Measurements in Nuclear Reactors with Mo/Nb Thermocouples," *Int. J. Thermophys.*, **29**, 1848, 2008.

29. M. Laurie, M. Futterer, J. Lapetite, S. Fourrez, and R. Morice, "New Temperature Monitoring Devices for High-temperature Irradiation Experiments in the High Flux Reactor Petten," P*roceedings of the First International Conference on Advancements in Nuclear Instrumentation, Measurement Methods and their Applications (ANIMMA)*, Marseille, France, June 2009.

30. H. Brixy, H. Hecker, K. F. Rittinghaus, and H. Howener, "Application of Noise Thermometry in Industry Under Plant Conditions," *Temperature, Its Measurement and Control in Science and Industry,* Vol. 5, pp. 1225–1237, American Institute of Physics, New York (1982).

31. M. Decreton, L. Binard, and C. Delrez, "High Temperature Measurements by Noise Thermometry," *High Temp.–High Press.,* **12**, 395, 1980.

32. S. Lopez Legrand and J. F. Villard, "Noise Thermometry for Nuclear Applications," *presented at ANIMMA Int. Conf.*, Marseille, France, June 7–10, 2009.

33. M. Laurie, M. A. Fütterer, J.M. Lapetite, S. Fourrez, R. Morice, "New temperature monitoring devices for high-temperature irradiation experiments in the High Flux Reactor Petten," *presented at ANIMMA Int. Conf.*, Marseille, France, June 7–10, 2009.

34. J. F. Villard, "State-of-the-Art and Improvement of Online Measurements in Present and Future French Research Reactors," presented at INL, Idaho Falls, Idaho, September 15, 2009.

35. J. F. Villard, G. Lemaitre, J. M. Chaussy, and F. Lefevre, "High Accuracy Sensor for Online Measurement of the Fuel Rod Internal Pressure During Irradiation Experiments," 7*th Int. Topl. Mtg. Research Reactor Fuel Management (RRFM 2003)*, Aix-en-Provence, France, March 9–12, 2003.

36. M. F. Narbey, D. Baron, G Despaux, JM Saurel, "Determination of the composition of a gas mixture in a nuclear fuel rod by an acoustic method," *Journal of the British Institute of Non-Destructive Testing (INSIGHT)*, **42**, 603-605 (2000).

37. J.Y. Ferrandis, G. Leveque, F. Augereau, E. Rosenkrantz, D. Baron, J-F. Villard, "An ultrasonic sensor for pressure and fission-gas release measurements in fuel rods for pressurised water reactors, *9th International conference on CANDU fuel*, Belleville (Canada), September 2005.

38. H. Carcreff, V. Clouté-Cazalaa, L. Salmon, "Development, calibration and experimental results obtained with an innovative calorimeter (CALMOS) for nuclear heating measurements," *Proceedings of the Second International Conference on Advancements in Nuclear Instrumentation, Measurement Methods and their Applications (ANIMMA2011)*, Ghent, Belgium, June 2011.

39. H. Carcreff, Patent N° FR 1060068, December 3, 2010.

40. F. Augereau, J.-Y. Ferrandis, J.-F. Villard, D. Fourmentel, M. Dierckx, and J. Wagemans, "Effect of intense neutron dose irradiation on piezoceramics," *Transactions from Acoustics '08,* June 29-July 4, 2008, Paris, France.

41. D. Fourmentel, J. F. Villard, J. Y. Ferrandis, F. Augereau, E. Rosenkrantz, and M. Dierckx, "Acoustic Sensor for In-Pile Fuel Rod Fission Gas Release Measurement," *presented at ANIMMA Int. Conf.,* Marseille, June 7–10, 2009.

42. F. Algaber, JY. Ferrandis, F. Augereau, J-F. Villard, "PZT Materials under Gamma irradiation," *4th European Workshop on Piezoelectric Materials,* Montpellier (France), July 2004.

43. P. Moilanen, S. Tahtinen, B.N. Singh, and P. Jacquet, "In-Situ Investigation of the Mechanical Performance and Life Time of Copper - Final report on design, construction, and calibration of test module for in-reactor tensile tests in BR-2 reactor," VTT Report BTUO 76-031127, October 27, 2004.

44. G. Cheymol, B. Brichard, J.F. Villard, "Fiber optics for metrology in nuclear research reactors applications to dimensional measurements," *ANIMMA International Conference,* Marseille, 7-10 June 2009.

45. G. Cheymol, J.F. Villard, A. Gusarov, B. Brichard, "Fibre optic extensometer for high radiation and high temperature nuclear applications," *Proceedings of the Second International Conference on Advancements in Nuclear Instrumentation, Measurement Methods and their Applications (ANIMMA2011)*, Ghent, Belgium, June 2011.

46. G. Cheymol, H. Long, J-F. Villard, and B. Brichard, "High Level Gamma and Neutron Irradiation of Silica Optical Fibers in CEA OSIRIS Nuclear Reactor," *IEEE Transactions on Nuclear Science,* Vol. 55, No. 4, August 2008, pp 2252-2258.

47. L. Skuja, M. Hirano, H. Hosono, and K. Kajihara, "Defects in Oxide Glasses," *Physica Status Solidi C*, Conf., **2**, 15, 2005.

48. D. Griscom, "The Nature of Point Defects in Silicon Dioxide," *Defects in SiO_2 and Related Dielectrics: Science and Technology*, pp. 117–161, Kluwer Academic Publishers, 2000.

49. B. Brichard, A. L. Tomashuk, H. Ooms, V. A. Bogatyrjov, S. N. Klyamkin, A. F. Fernandez, F. Berghmans, and M. Decréton, "Radiation Assessment of Hydrogen-Loaded Aluminium-Coated Pure Silica Core Fibres for ITER Plasma Diagnostic Applications," *Fusion Eng. Des.*, **82**, 2451, 2007.

50. B. Brichard, A. F. Fernandez, H. Ooms, F. Berghmans, M. Decréton, A. Tomashuk, S. Klyamkin, M. Zabezhailov, I. V. Nikolin, V. Bogatyrjov, E. Hodgson, T. Kakuta, T. Shikama, T. Nishitani, A. Costley, and G. Vayakis, "Radiation-Hardening Techniques of Dedicated Optical Fibers Used in Plasma Diagnostics Systems in ITER," *J. Nucl. Mater.*, **329–333**, 1456, 2004.

51. T. Shikama, T. Kakuta, M. Narui, T. Sagawa, and H. Kayano, "Optical Properties in Fibers During Irradiation in a Fission Reactor," *J. Nucl. Mater.*, **225**, 324, 1995.

52. B. Brichard, A. F. Fernandez, F. Berghmans, and M. Decréton, "Origin of the Radiation-Induced OH Vibration Band in Polymer-Coated Optical Fibers Irradiated in a Nuclear Fission Reactor," *IEEE Trans. Nucl. Sci.*, **49**, 2852, Dec. 2002.

53. T. Kakuta, T. Shikama, T. Nishitani, B. Brichard, A. Krassilinikov, A. Tomashuk, S. Yamamoto, and S. Kasai, "Round-Robin Irradiation Test of Radiation Resistant Optical Fibers for ITER Diagnostic Application," *J. Nucl. Mater.*, **307–311**, 1277, 2002.

54. S. Shikama, K. Toh, S.Nagata, and B. Tsuchiya, "Optical Dosimetry for Ionizing Radiation Fields by Infrared Radioluminescence," *Measure. Sci. Technol.*, **17**, 1103, 2006.

55. B. Brichard, A. F. Fernandez, H. Ooms, and F. Berghmans, "Fibreoptic Gamma-Flux Monitoring in a Fission Reactor by Means of Cerenkov Radiation," *Measure. Sci. Technol.*, **18**, 3257, 2007.

56. B. Aarset, "In-reactor Instrumentation for Fuel Behavior Studies at the OECD Halden Reactor Project," *Proceedings from the Conference on Fast, Thermal, and Fusion Reactor Experiments*, p 1-85 through 1-96, April 12-15, 1982, Salt Lake City, Utah.

57. O. Aarrestad and H. Thoresen, "Fuel Rod Performance Measurements and Re-Instrumentation Capabilities at the Halden Project," *In-core instrumentation and core assessment: proceedings of a Specialists' Meeting,* Mito-shi, Japan, 14-17 October, 1996.

58. C. Vitanza, "On-line fuel rod performance measurements and fuel inspection applications," *Kerntechnik,* **56**, 1991, pp 124-130.

59. S. Solstad, HRP, email to J. Rempe, INL, February 6, 2008.

60. R. Van Nieuwenhove and S. Solstad, "In-Core Fuel Performance and Material Characterization in the Halden Reactor," *presented at ANIMMA,* Int. Conf., Marseille, France, June 7–10, 2009.

61. W. Wiesenack, "Experimental Techniques and Results Related to High Burn-up Investigations at the OECD Halden Reactor Project, *Proceedings of a Technical Committee Meeting held in Pembroke,* Ontario, Canada, April 28 - May 1, 1992, IAEA-TECDOC-697, p. 118.

62. P. Bennett, "In-core Measurements of Fuel-Clad Interactions at the Halden Reactor," *IAEA Technical Meeting on Fuel Rod Instrumentation and In-Pile Measurement Techniques,* Halden, Norway, 3-5 September 2007.

63. P. Bennett and T. Karlsen, "In-core Corrosion Monitoring in the Halden Test Reactor," *Energy Materials: Materials Science and Engineering for Energy Systems,* **3,** 2, June 2008, pp. 81-90.

64. S. Solstad and R. Van Nieuwenhove, "Instrument Capabilities and Developments at the Halden Reactor Project," *Nucl. Technol.,* **173**, 78 (2011).

65. O. Aarrestad, "Instrumentation Capabilities at Halden," I*FE/HRP Report HWR-351*, February 1993.

66. W. Wisenack, “Overview of the Halden Reactor Project,” *presented at IAEA Technical Meeting - In-pile Testing and Instrumentation for Development of Generation IV Fuels and Materials, Halden*, Norway, 21-24 August 2012.

67. R. Van Nieuwenhove, “Development and Testing of Instruments for Generation IV Fuel and Materials Research at the Halden Reactor Project,” *presented at IAEA Technical Meeting - In-pile Testing and Instrumentation for Development of Generation IV Fuels and Materials, Halden*, Norway, 21-24 August 2012.

68. T.M. Karlsen, “Halden Reactor Materials Testing Techniques and Selected Results,” *presented at IAEA Technical Meeting - In-pile Testing and Instrumentation for Development of Generation IV Fuels and Materials, Halden*, Norway, 21-24 August 2012.

69. K. Tsuchiya, “Irradiation Technology Development in JMTR” and “New JMTR,” presentation and handouts provided to J. Rempe at JAEA meeting, September 29, 2009, Oarai, Japan.

70. M. Narui, T. Shikama, M. Yamasaki, and H. Matsui, “Development of High-Temperature Irradiation Techniques Utilizing the Japan Materials Testing Reactor,” *Basic Studies in the Field of High Temperature Engineering, Second Information Exchange Meeting,* Paris, France, 10-12 October, 2001, pp. 145-152.

71. T. Shibata, T. Kikuchi, S. Miyamoto, K. Ogura, and Y. Ishigaki, “Development of the I-I TYpe Irradiation Equipment for the HTTR,” *Basic Studies in the Field of High Temperature Engineering, Second Information Exchange Meeting,* Paris, France, 10-12 October, 2001, pp. 191-199.

72. T. Shikama, M. Narui, T. Kakuta, M. Ishitsuka, K. Hayashi, T. Sagawa, and T. Hoshiya, “Application of Optical Diagnostics in High-Temperature Gas-Cooled Systems,” *Basic Studies in the Field of High Temperature Engineering, Second Information Exchange Meeting,* Paris, France, 10-12 October, 2001, pp. 153-160.

73. C. Mori, A. Uritanit, T. Kakuta, M. Katagiri, T. Shikama, M. Naikazawa, T. Iguchi, J. Kawarabayashi, I. Kimura, H. Kobayashi, and S. Hayashi, “Measurement Method of In-core Neutron and Gamma-Ray Distributions with Scintillator Optical Fibre Detector and Self -Powered Detector,” *Basic Studies in the Field of High Temperature Engineering, Second Information Exchange Meeting,* Paris, France, 10-12 October, 2001, pp. 161-196.

74. H.Hanakawa, A. Shibata, H. Nagata, N. Kimura, N. Ohtsuka, M. Tanimoto, T. Saito, J. Nakamura and K. Tsuchiya, “Development of Instrumentation for Fuel and Material Irradiation Tests in JMTR,” *presented at IAEA Technical Meeting - In-pile Testing and Instrumentation for Development of Generation IV Fuels and Materials, Halden*, Norway, 21-24 August 2012.

75. T. Soga, W.Itagaki, Y.Kihara, Y.Maeda, “Endeavor to Improve In-pile Testing Techniques in the Experimental Fast Reactor JOYO,” *presented at IAEA Technical Meeting - In-pile Testing and Instrumentation for Development of Generation IV Fuels and Materials, Halden*, Norway, 21-24 August 2012.

76. J. Sackett, “Measurements of Thermal-hydraulic Parameters in Liquid-me1al-cooled Fast-breeder Reactors,” *presented at the International Center for Heat and Mass Transfer Symposium: Measurement Techniques in Power Engineering,* August 29 - September 3, 1983, Beograd, Yugoslavia.

77. J. Markgraf, D. Perry, and J. Oudaert, "LWR Fuel Rod Testing Facilities in High Flux Reactor (HFR) Petten for Investigation of Power Cycling and Ramping Behavior," *Res Mechanica*, **13**, 1985, 187-210.

78. Email from K. Bakker, NRG, to J. Rempe, INL, dated December 11, 2007.

79. K. Bakker, NRG, discussions with J. Rempe, INL, at Petten, Netherlands, October 2008.

80. P. Blanchard, P. May, and H. Scheurer, "A Machine for the Fatigue Testing of CT type samples in the HFR," *Fusion Technology 1982, Proceedings of the 12th Symposium*, **2**, pp 749-752, 1983.

81. M. A. Fütterer, et al., "Next generation fuel irradiation capability in the High Flux Reactor Petten," Journal of Nuclear Materials," **392**, 2009, pp 184-191.

82. B. G. Kim, et al., "Status and Perspective of Material Irradiation Tests in the HANARO, *paper and presentation from the 1st International Symposium on Materials Testing Reactors*, JAEA-Oarai, Japan, July 2008.

83. B. G. Kim, K-N Choo, J. M. Sohn, S. J. Park, K.Kim and Y. J. Kim, "Instrumentations for Materials Irradiation Tests in HANARO," *Proceedings of the ANS NPIC HMIT 2009 Topical Meeting on Nuclear Plant Instrumentation, Controls, and Human Machine Interface Technology,* Knoxville, TN, April 2009.

84. B.G. Kim, J. M. Sohn, and K-N Choo, "Development Status of Irradiation Devices and Instrumentation for Material and Nuclear Fuel Irradiation Tests in HANARO," *Nuclear Engineering and Technology*, **42**, 2, pp 203-210, April 2010.

85. S.H. Ahn, J.T. Hong, C.Y. Joung, and S.J. Park, "An Instrumentation and Control for Loop Test," *presented at IAEA Technical Meeting - In-pile Testing and Instrumentation for Development of Generation IV Fuels and Materials, Halden*, Norway, 21-24 August 2012.

86. Standard Guide for Use of Melt Wire Temperature Monitors for Reactor Vessel Surveillance, E706 (IIE), ASTM E 1214-06, dated February 13, 2006.

87. N. F. Pravdyuk, V. A. Nikolaenko, V. I. Kapuchin, V.N. Kusnetsov, in: Ed. D. J. Littler, *Proceedings of the Properties of Reactor Materials and the Effects of Radiation Damage,* Butterworths, 1962, p. 57.

88. L L. Snead, A. M. Williams, and A. L. Qualls, "Revisiting the use of SiC as a Post Irradiation Temperature Monitor," *Effects of Radiation on Materials,* ASTM STP 1447, M L. Grossbeck, Ed, ASTM International, West Conshohocken, PA, 2003.

89. L. L. Snead, "Revisiting the use of SiC as a Post Irradiation Temperature Monitor," *presented at the Int. Symp. Materials Test Reactors*, Idaho Falls, ID, September 28, 2009.

90. K. L. Davis, D.L. Knudson, J.E. Daw, J.L. Rempe and A.J. Palmer, "Melt Wire Sensors Available to Determine Peak Temperatures in ATR Irradiation Testing," *Proceedings of the ANS NPIC HMIT 2012 Topical Meeting on Nuclear Plant Instrumentation, Controls, and Human Machine Interface Technology,* San Diego, CA, July 2012.

91. J. L. Rempe, K. G. Condie, D. L. Knudson, and L. L. Snead, “Comparison Measurements of Silicon Carbide Temperature Monitors,” *IEEE Transactions on Nuclear Science,* **57**, No. 3, June 2010.

92. MacLean, H.J, and K. Sridharan, T. A. Hyde, “Irradiation Test Plan for the ATR National Scientific User Facility - University of Wisconsin Pilot Project,” PNL-2784, Revision 1, Idaho National Laboratory, July 21, 2008.

93. J. L. Rempe, K. G. Condie, and D. L. Knudson, “Silicon Carbide Temperature Monitor Evaluation,” PLN-3473, April 2010.

94. K. L. Davis, B. M. Chase, T. C.Unruh, D. L. Knudson, and J. L. Rempe, “Evaluations of University of Wisconsin Silicon Carbide Temperature Monitors 300 LO and 400 LO B,” INL/EXT-11-24226, December 2011.

95. J. Rempe, D. Knudson, K. Condie, J. Daw, H. Ban, B. Fox, G. E. Kohse, S. C. Wilkins, “New Sensors for In-Pile Testing at the ATR NSUF,” *Proceedings of the First International Conference on Advancements in Nuclear Instrumentation, Measurement Methods and their Applications (ANIMMA)*, Marseille, France, June 2009.

96. J. Rempe and M. Meyer, “ATR NSUF Instrumentation Enhancement Efforts,” *Proceedings of the ANS NPIC HMIT 2009 Topical Meeting on Nuclear Plant Instrumentation, Controls, and Human Machine Interface Technology,* Knoxville, TN, April 2009.

97. J. L. Rempe, D. L. Knudson, K. G. Condie, and S. C. Wilkins, “Thermocouples for High-Temperature In-Pile Testing,” *Nuclear Technology*, **156**, No. 3, December 2006, pp 320-331.

98. J. L. Rempe, D. L. Knudson, K. G. Condie, and S. C. Wilkins, “High Temperature Thermocouple Design and Fabrication,” *US patent filed by Battelle Energy Alliance (IDR #BA-142) on behalf of DOE (Serial Number 11/678,901)*, published by US PTO as No. 2008/0205483 and issued January 18, 2011, Patent 7871198.

99. J. L. Rempe, D. L. Knudson, K. G. Condie, and S. C. Wilkins, “Long Duration Performance of High Temperature Irradiation Resistant Thermocouples,” *Proceedings of the 2007 International Congress on Advances in Nuclear Power Plants (ICAPP'07)*, Nice, France, May 13-18, 2007.

100. J. Rempe, D. Knudson, K. Condie, J. Daw, and S. C. Wilkins, “New Sensors for In-Pile Temperature Detection at the ATR NSUF,” *Proceedings of the 13th International Topical Meeting on Nuclear Reactor Thermal-Hydraulics (NURETH13),* Kanazawa, Japan, October 2009.

101. D. L. Knudson, J. L. Rempe, K. G. Condie, S. C. Wilkins, J. E. Daw, and J. C. Crepeau, “High Temperature Irradiation Resistant Thermocouples - A Low Cost Sensor for In-Pile Testing at High Temperatures,” Paper 8222, *Proceeding of the 2008 International Congress on Advances in Nuclear Power Plants (ICAPP '08)*, Anaheim, CA, June 8-12, 2008.

102. J. L. Rempe, D. L. Knudson, K. G. Condie, and S. C. Wilkins, “Thermocouples for High-Temperature In-Pile Testing,” *Nuclear Technology*, **156**, No. 3, December 2006, pp 320-331.

103. J. L. Rempe, D. L. Knudson, K. G. Condie, S. C. Wilkins, J. C. Crepeau, and J. E. Daw, "Options Extending the Applicability of High Temperature Irradiation Resistant Thermocouples," *invited paper for NURETH12 Special Edition, Nuclear Technology*, **167**, July 2009, pp 169-177.

104. J. E. Daw, J. L. Rempe, D. L. Knudson, S. C. Wilkins, and J. C. Crepeau, "High Temperature Irradiation-Resistant Thermocouple Performance Improvements," *ANS NPIC HMIT 2009 Topical Meeting on Nuclear Plant Instrumentation, Controls, and Human Machine Interface Technology,* Knoxville, TN, April 2009.

105. G. Kohse, "Summary Report of Irradiation of INL HTIR-TCs in the MITR," Draft report, December 2012.

106. H.A. Tasman, M. Campana, D. Pel, J. Richter, "Ultrasonic Thin-Wire Thermometry for Nuclear Applications," *Temperature: Its Measurement and Control in Science and Industry,* Vol. 5, Part 2, pp. 1191-1196, 1982.

107. R.J. Grossman, "Ultrasonic-Thermometry Development for In-Situ Measurement of Nuclear-Fuel Temperatures (AWBA Development Program)," KAPL-4160, General Electric Company Knolls Atomic Power Laboratory, 1982.

108. E.P. Papdakis, L.C. Lynnworth, D.R. Patch, E.H. Carnevale, "Ultrasonic Thermometry in LMFBR Systems," Final Report NYO-3906-13, Panametrics Inc. 1972.

109. M. Laurie, D. Magallon, J. Rempe, S. Wilkins, J. Pierre, C. Marquié, S. Eymery, and R. Morice, "Ultrasonic High Temperature Sensors: Past Experiments and Prospective for Future Use," *Joint International Symposium on Temperature, Humidity, and Moisture and Thermal Measurements in Industry and Science*, Portorož, Slovenia, May 31 - June 4, 2010.

110. J. Daw, J. Rempe, and S. C. Wilkins, "Ultrasonic Thermometry for In-Pile Temperature Detection," *7th International Topical Meeting on Nuclear Plant Instrumentation, Control, and Human Machine Interface Technologies (NPIC&HMIT 2010),* Las Vegas, NV, November 7-11, 2010.

111. J. Rempe, J. Daw, D. Knudson, R. Schley, L. Bond, J. Coble, M. Good, and R. Meyer, *In-pile Instrumentation to Support Fuel Cycle Research and Development - FY11 Status Report, F*CRD-FUEL-2011-000307 (also issued as INL/EXT-11-23119), September 2011.

112. M.J. Roberts, D.E. Holcomb, and R.A. Kisner, "Signal Processing Algorithm Implementation for In Vessel Level Measurement," https://inlportal.inl.gov/portal/server.pt/gateway/PTARGS-0-2-3310-277-2604-43/http%3B/inlpublisher%3B7087/publishedcontent/publish/communities/inl-gov/ about-inl/gen-iv-technical-documents/signal-processing-algorighm.pdf, September 2006.

113. J. Rempe, J. Daw, D. Knudson, R. Schley, T. Unruh, and B. Chase, In-pile Instrumentation to Support Fuel Cycle Research and Development -FY12 Status Report, FCRD-FUEL-2012-000282, September 2012.

114. Y. S. Touloukian, et al., *Thermophysical Properties of Matter*, IFI/Plenum Publishing, New York, New York, 1973.

115. S.A. Chavez, G.E. Korth, D.M. Harper, and T.J. Walker, "High-temperature tensile and creep data for Inconel 600, 304 stainless steel and SA106B carbon steel," *Nuclear Engineering and Design,* **148**, pp. 351-363, 1994.

116. R. Syre, "Niobium, Molybdenum, Tantalum and Tungsten: a Summary of Their Properties with Recommendations for Research and Development," *AGARDograph,* **50**, 1961.

117. J. Daw, J. Rempe, and S. C. Wilkins, "Ultrasonic Thermometry for In-Pile Temperature Detection," *7th International Topical Meeting on Nuclear Plant Instrumentation, Control, and Human Machine Interface Technologies (NPIC&HMIT 2010),* Las Vegas, NV, November 7-11, 2010.

118. B. Fox, H. Ban, J. Rempe, D. Knudson, and J. Daw, "Development of an In-pile Technique for Fuel Thermal Conductivity Measurement," *Proceedings of the ANS NPIC HMIT 2009 Topical Meeting on Nuclear Plant Instrumentation, Controls, and Human Machine Interface Technology*, Knoxville, TN, April 2009.

119. B. Fox, H. Ban, J. Rempe, J. Daw, K. Condie, D. Knudson, "In-Pile Thermal Conductivity Measurement Method for Nuclear Fuels," Thermal Conductivity 30/Thermal Expansion 18, Daniela S. Gaal and Peter S. Gaal (Editor), DEStech Publications Inc., p 886, October 2010.

120. B. Fox, H. Ban, J. Daw, K. Condie, D.Knudson, and J. Rempe, Evaluation of Candidate In-Pile Thermal Conductivity Techniques, INL/EXT-09-16039, May 2009.

121. B. Fox, H. Ban, J. Rempe, J. Daw, K. Condie, and D. Knudson, "In-Pile Thermal Conductivity Measurement Method for Nuclear Fuels," *30th International Thermal Conductivity Conference and 18th International Thermal Expansion Symposium,* Pittsburgh, PA, August 29-September 2, 2009.

122. J. Daw, J. Rempe, K. Condie, D. Knudson, S. C. Wilkins, B. Fox, and H. Ban, "Hot Wire Needle Probe for In-Pile Thermal Conductivity Detection," *7th International Topical Meeting on Nuclear Plant Instrumentation, Control, and Human Machine Interface Technologies (NPIC&HMIT 2010)*, Las Vegas, NV, November 7-11, 2010.

123. I. Cohen, B. Lustman, and J. D. Eichenberg, "Measurement of the Thermal Conductivity of Metal-Clad URanium Oxide Rods during Irradiation," *Journal of Nuclear Material*s, **3**, No 3 (1961), pp 331-353.

124. "Needle Probe for In-Pile Thermal Conductivity Detection," Patent filed by DOE on October 10, 2012 (ID 13648502, Application S-122190). Inventors: Keith G. Condie, Joy L. Rempe, Darrell L. Knudson, Joshua E. Daw, S. Curtis Wilkins, Brandon S. Fox, and Heng Ban.

125. A. L. E. F. Schleirmacher, Vher die Warmeleitungder gase, *Weidemann Ann. Phys.* 34, p. 625, 1988.

126. W.N. Beck and R. J. Fousek, "Fission Gas Release and Thermal Conductivity Measurements on U-5 wt% F Irradiated in CP-5," *Trans. American Nuclear Society*, 30, 528, 1978.

127. P. R. Betten, "In-Core Measurements of Uranium-5 wt% Fissium Alloy Thermal Conductivity," *Transactions of the American Nuclear Society*, **50**, pp. 239-240, November 1985.

128. Standard Test Method for Determination of Thermal Conductivity of Soil and Soft Rock by Thermal Needle Probe Procedure, ASTM D 5334-05, May 27, 2008.

129. M. S. Baghe-Khandan, Y. Choi, and M. R. Okos, "Improved Line Heat Source Thermal Conductivity Probe," *Journal of Food Science,* 45, p 1430-1432, 1981.

130. J.J. Healy, J. J. de Groot, and J. Kestin, "The Theory of the Transient Hot-Wire Method for Measuring Thermal Conductivity," *Physica*, 82C, pp 392-408, 1976.

131. X-G Liang, "The Boundary Induced Error on the Measurement of Thermal Conductivity by Transient Hot Wire Method," Measurement Science Technology, 6, pp 467-471, 1995.

132. K.Manohar, D. W. Yarbrough, and J. R. Booth, "Measurement of Apparent Thermal Conductivity by the Thermal Probe Method," Journal of Testing and Evaluation, September 2000.

133. P. Prelovsek and B. Uran, "Generalized Hot Wire Method for Thermal Conductivity Measurements," J. Phs. E: Sci. Instrum., 17, 1984.

134. M. Ichikawa, M. Uchida, K Yanagisawa, J. Nakamura and T. Nakajima, "Irradiation Studies of JAERI's Fuel at Halden Reactor," *Journal of Nuclear Science and Technology*, **25** [8], pp.609-614, August 1988.

135. M. Ichikawa, T. Fujishiro and S. Kawasaki, "LWR Fuel Safety Research with Particular Emphasis on RIA/LOCA and Other Conditions," *Journal of Nuclear Science and Technology,* **26**(1), pp. 118~125 (January 1989).

136. B. G. Kim, J. Rempe, D. Knudson, K. Condie, and B. Sencer, "An In-situ Creep Testing Capability for the Advanced Test Reactor," *submitted to Nuclear Technology*, MS 10-58, accepted October 24, 2011.

137. B. G. Kim, J. L. Rempe, D. L. Knudson, K. G. Condie, and B. H. Sencer, "Development of an In-situ Creep Testing Capability for the Advanced Test Reactor," *7th International Topical Meeting on Nuclear Plant Instrumentation, Control, and Human Machine Interface Technologies (NPIC&HMIT 2010),* Las Vegas, NV, November 7-11, 2010.

138. D. L. Knudson and J. L. Rempe, "LVDT Evaluations for ATR Irradiations," *Proceedings of the ANS NPIC HMIT 2009 Topical Meeting on Nuclear Plant Instrumentation, Controls, and Human Machine Interface Technology*, Knoxville, TN, April 2009.

139. D. Knudson and J. Rempe, "Recommendations for use of LVDTs in ATR High Temperature Irradiation Testing," *7th International Topical Meeting on Nuclear Plant Instrumentation, Control, and Human Machine Interface Technologies (NPIC&HMIT 2010)*, Las Vegas, NV, November 7-11, 2010.

140. D. L. Knudson and J. L. Rempe, "LVDT-Based Elongation Measurements in Advanced Test Reactor High Temperature Irradiation Testing," *Measurement Science and Technology,* accepted November 28, 2011.

141. D.L. Knudson, K.L. Davis, K.G. Condie, and J.L. Rempe, "Qualification of an LVDT-Based Creep Test Rig for Use in ATR Loop 2A," INL/LTD-12-26173, Idaho National Laboratory, August 2012

142. to://www.americanpiezo.com/

143. Toacsan, M. I., Ioachim, A., Nedelcu, L. and Alexandru, H. V., "Accelerated ageing of PZT-type ceramics," *Progress in Solid State Chemistry* **35**, 531-537 (2007).

144. Broomfield, G. H., "The effect of low-fluence neutron irradiation on silver-electrode lead-zirconate-titanante piezoelectric ceramics," *J of Nuclear Materials* 91, 23-34 (1980).

145. R. Bratton, "AGC-1 Irradiation Experiment Test Plan," INL/EXT-06-11102, May 2006.

146. K. Totsu, Y. Haga and M. Esashi, "Ultra-miniature fiber-optic pressure sensor using white light interferometry," *J. Micromech. Microeng*. **15** (2005) 71-75.

147. R. Schley, J. Rempe, and D. Knudson, "Fiber Optic Elongation/Displacement Sensor," Idaho National Laboratory Invention Disclosure Record BA-725, 2219, Rev. 1, submitted February 29, 2012.

148. R. B. Firestone, V. S. Shirley, C. M. Baglin, S.Y. F. Chu, and J. Zipkin, *The 8th edition of the Table of Isotopes*, Book and CD-ROM, Published by John Wiley & Sons, Inc., 1996.

149. Standard Test Method for Measuring Neutron Fluence Rates by Radioactivation of Cobalt and Silver, ASTM E481-03, February 2003.

150. M.F. Ohmes, D.S. McGregor, J.K. Shultis, P.M. Whaley, A.S.M. Sabbir Ahmed, C.C. Bolinger, T.C. Pinsent, "Development of Micro-Pocket Fission Detectors (MPFD) for Near-Core and In-Core Neutron Flux Monitoring," *Proc. SPIE*, Vol. 5198 (2003) pp. 234-242.

151. D.S. McGregor, J.K. Shultis, M.F. Ohmes, A.S.M.S. Ahmed, R. Ortiz, K Hoffert, "Micro-Pocket Fission Detectors (MPFD) for Near-Core and In-Core Neutron Flux Monitoring," *ANS 4th Topical Meeting NPIC & HMIT*, Columus, Ohio, September 19-22, 2004.

152. D.S. McGregor, M.F. Ohmes, R.E. Ortiz, A.S.M.S. Ahmed, and J.K. Shultis, "Micro-Pocket Fission Detectors (MPFD) for In-Core Neutron Flux Monitoring," *Nuclear Instruments and Methods,* A554 (2005) pp. 494-499.

153. M.F. Ohmes, D.S. McGregor, J.K. Shultis, A.S.M.S. Ahmed, R. Ortiz, R.W.Olsen, "Recent Results and Fabrication of Micro-Pocket Fission Detectors," *Proc. SPIE*, 6319 (2006) pp. 1P1 - 1P9.

154. D.S. McGregor, "Near-Core and In-Core Neutron Radiation Monitors for Real Time Neutron Flux Monitoring and Reactor Power Levels Measurements," NERI Final Report 2002-174, 2006

155. M. F. Ohmes, J. K. Shultis, D. S. McGregor, "3D Real-Time in-Core Neutron Flux Mapping with Micro-Pocket Fission Detectors (MPFD)," *IEEE Nuclear Science Symposium*, Waikiki, Hawaii, Oct. 28-Nov. 3, 2007.

156. C. Jammes, P. Filliatre, B. Geslot, L. Oriol, F. Berhouet, J.-F. Villard, et L. Vermeeren, "Research Activities in Fission Chamber Modeling in Support of the Nuclear Energy Industry," *IEEE Transactions on Nuclear Science,* 2010.

157. B. Geslot, F. Berhouet, L. Oriol, S. Bréaud, C. Jammes, P. Filliatre, et J.F. Villard, "Development and manufacturing of special fission chambers for in-core measurement requirements in nuclear reactors," *Advancements in Nuclear Instrumentation Measurement Methods and their Applications (ANIMMA)*, 2009.

158. N. Tsoulfanidis, *Measurement and Detection of Radiation*, 2nd Ed. Taylor & Francis, Washington, D.C., 1993.

159. Kansas State University, "Electronics Design Laboratory" http://www.k-state.edu/ksuedl/, Accessed August 15, 2012.

160. Kansas State University, "TRIGA Mark II Reactor Facility" http://www.mne.ksu.edu/research/centers/reactor/, Accessed August 15, 2012.

161. Kansas State University, "SMART Laboratory" http://www.mne.ksu.edu/research/centers/SMART-lab/mission, Accessed August 15, 2012.

162. R.H. Leyse and R.D. Smith, "Gamma Thermometers for Light Water Reactors," *IEEE Transactions on Nuclear Science*, NS-26, pp.934-943, February 1979.

163. R. Van Nieuwenhove, IFE/HRP, personal communication with J. Rempe, INL, Halden, Norway, August 2012.

164. D. Ensminger, and L. J. Bond, *Ultrasonics: Fundamentals, Technologies, and Applications,* CRC Press, 2012.

165. K. Phani, et. al, "Estimation of Elastic Properties of Nuclear Fuel Material Using Longitudinal Ultrasonic Velocity - A New Approach," *J. Nucl. Mat.*, 366, 2007, pp. 129-136.

166. J. F. Villard, et. al.,"Acoustic Sensor for In-Pile Fuel Rod Fission Gas Release Measurement," *IEEE Transactions on Nuclear Science*, 58, 2011, pp. 151-155.

167. L.C. Lynnworth, "Ultrasonic Measurements for Process Control: Theory, Techniques, and Applications," Academic Press, 1989.

168. *MITR Users Guide Rev. 3 July 2012,* Massachusetts Institute of Technology (2012).

169. K. E. Holbert, S. Sankaranarayanan, S. S. McCready, "Response of Lead Metaniobate Acoustic Emission Sensors to Gamma Irradiation," I*EEE Transactions on Nuclear Science*, vol. 52, no. 6, 2005, pp. 2583-2590.

170. Kulikov, et al., "Computer simulation of ferroelectric property changes in PLZT ceramics under neutron irradiation," *Proceedings of SPIE*, 4348, 2001, pp. 264-269.

171. H. Shea, "Radiation sensitivity of microelectromechanical system devices," *J. Micro/Nanolith.,* 8, 2009, pp. 1-11.

172. Wittels & Sherrill, "Fast Neutron Effects in Tetragonal Barium Titanate," J*ournal of Applied Physics*, 28 [5], 1957, pp. 606-609.

173. W. Primak, T. Anderson, "Metamimictization of Lithium Niobate by Thermal Neutrons," *Nuclear Technology*, 23, 1975, pp. 235.

174. T.K. Bierney, "Instrumentation for the Measurement of Vibration in Severe Environments Such as Nuclear Reactors," Endevco Technical Paper 272, 1976, pp. 1-8.

175. D.A. Parks, B. R. Tittmann. "Ultrasonic NDE in a Reactor Core," *Presented at Review of Progress in Quantitative Nondestructive Evaluation*, July 17-22, Burlington, VT, 2011.

176. R.N. Ord, R.W. Smith, "Ultrasonic Under-Sodium Viewing System Development for the FFTF," HEDL-SA-335. Westinghouse Hanford Co., Richland, Washington, 1972.

177. R. Kazys, V. Voleisis, R. Sliteris, B. Voleisiene, L. Mazeika, and H. Abderrahim, "Research and Development of Radiation Resistant Ultrasonic Sensors for Quasi-Image Forming Systems in a Liquid Lead-Bismuth," *Ultragarsas (Ultrasound)*, 62(3),2006, pp. 7-15.

178. N. D. Patel and P. S. Nicholson, "High Frequency - High Temperature Ultrasonic Transducers," *NDT International*, pp. 262-266, 1990.

179. D. Stubbs, and R. Dutton, "High-Temperature Ultrasonic Sensor for in Situ Monitoring of Hot Isostatic Processing," *SPIE*, 1996, pp. 164-172.

180. K. Trachenko, "Understanding resistance to amorphization by radiation damage," *Journal of Physics: Condensed Matter*, 16(49), 2004, pp. R1491-R1515.

181. T. Yano, K. Inokuchi, M. Shikama, and J. Ukai, "Neutron irradiation effects on isotope tailored aluminum nitride ceramics by a fast reactor up to $2 \cdot 10^{26}$ n/m^2," *Journal of Nuclear Materials*, 2004, pp. 1471-1475.

182. Y. Ito, et al., "Radiation Damage of Materials Due to High Energy Ion Irradiation," *Nuclear Instruments and Methods in Physics Research*, 530, 2002.

183. Y. P. Meleshko, S. G. Karpechko, G. K. Leont'ev, V. I. Nalivaev, A. D. Nikiforov, and V. M. Smirnov, "Radiation Resistance of the Piezoelectric Ceramics TrsTS-21 and TNV-I," Translated from *Atomnaya Energiya*, 1986, pp. 50-52.

184. K. Trachenko, "Understanding resistance to Amorphization by Radiation Damage," *Journal of Physics Condensed Matter*, 16(49), 2004, pp. R1491-R1515.

185. Arnokrome 3 Datasheet Rev. 01-11-11,www.arnoldmagnetics.com/WorkArea/DownloadAsset.aspx?id=5262, Accessed 08/09/2012.

186. Arnokrome 4 Specification Rev. 1/11/11,www.arnoldmagnetics.com/WorkArea/DownloadAsset.aspx?id=5263, Accessed 08/09/2012.

187. Arnokrome 5 Specification Rev. 2/24/11,www.arnoldmagnetics.com/WorkArea/DownloadAsset.aspx?id=5328, Accessed 08/09/2012.

188. “What is Galfenol?”, Etrema Products, Inc., http://www.etrema-usa.com/core/galfenol/, Accessed 08/09/2012.

189. R.S. Sery, et al., “Radiation Damage Thresholds for Permanent Magnets,” NOLTR 61-45, 1961.

190. Liu, et al., “Thermal Stability and Radiation Resistance of Sm-Co Based Permanent Magnets,” Paper 2036, Proceedings of Space Nuclear Conference, 2007.

191. K.L Telschow, D.L. Cottle, and R.S. Schley, INL Letter Report on LDRD, completed 2005.

192. K.L. Stinson-Bagby and R.S. Fielder, “Fiber Bragg Gratings for High-Temperature Thermal Characterization,” *Proc. ICAPP '04,* Pittsburgh, PA, Paper 4299, June 2004.